CHARACTERIZATION OF THE CELLULOSIC FIBER OBTAINED FROM NEPALESE LOKTA BUSHES AND EXPLORE ITS NOVEL APPLICATIONS

A THESIS SUBMITTED TO THE

CENTRAL DEPARTMENT OF CHEMISTRY

INSTITUTE OF SCIENCE AND TECHNOLOGY

TRIBHUVAN UNIVERSITY

NEPAL

FOR THE AWARD OF

DOCTOR OF PHILOSOPHY

IN CHEMISTRY

BY

GIRJA MANI ARYAL

MAY, 2024

CHARACTERIZATION OF THE CELLULOSIC FIBER OBTAINED FROM NEPALESE LOKTA BUSHES AND EXPLORE ITS NOVEL APPLICATIONS

A THESIS SUBMITTED TO THE

CENTRAL DEPARTMENT OF CHEMISTRY

INSTITUTE OF SCIENCE AND TECHNOLOGY

TRIBHUVAN UNIVERSITY

NEPAL

FOR THE AWARD OF

DOCTOR OF PHILOSOPHY

IN CHEMISTRY

BY

GIRJA MANI ARYAL

MAY, 2024

DECLARATION

The thesis entitled **"Characterization of the Cellulosic Fiber Obtained from Nepalese Lokta Bushes and Explore its Novel Applications** is being submitted to the Central Department of Chemistry, Institute of Science and Technology (IOST), Tribhuvan University, Nepal for the award of the degree of Doctor of Philosophy (Ph.D.), is a research work carried out by me under the supervision of Dr. Bhanu Bhakta Neupane of Central Department of Chemistry, Tribhuvan University and co-supervised by Dr. Mahesh Kumar Joshi of Central Department of Chemistry, Tribhuvan University and Dr. Bhoj Raj Gautam of Department of Chemistry, Physics and Materials Science, Fayetteville State University, Fayetteville, North Carolina, USA.

This research is original and has not been submitted earlier in part or full in this or any other form to any university or institute, here or elsewhere, for the award of any degree.

.....

Girja Mani Aryal

RECOMMENDATION

This is to recommend that **Girja Mani Aryal** has carried out research entitled **"Characterization of the Cellulosic Fiber Obtained from Nepalese Lokta Bushes and Explore its Novel Applications"** for the award of Doctor of Philosophy (Ph.D.) in **Chemistry** under our supervision. To our knowledge, this work has not been submitted for any other degree.

He has fulfilled all the requirements laid down by the Institute of Science and Technology (IOST), Tribhuvan University, Kirtipur, Kathmandu for the submission of the thesis for the award of a Ph.D. degree.

Dr. Bhanu Bhakta Neupane

Supervisor

(Assistant Professor)

Central Department of Chemistry

Tribhuvan University

Kirtipur, Kathmandu, Nepal

Dr. Mahesh Kumar Joshi

Co-Supervisor

(Associate Professor)

Central Department of Chemistry

Tribhuvan University

Kirtipur, Kathmandu, Nepal

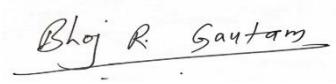

Dr. Bhoj Raj Gautam

Co-Supervisor

(Associate Professor)

Department of Chemistry, Physics and Material Science,

Fayetteville State University

Fayetteville, North Carolina, USA

May, 2024

LETTER OF APPROVAL

May, 2024

On the recommendation of **Dr. Bhanu Bhakta Neupane, Dr. Mahesh Kumar Joshi and Dr. Bhoj Raj Gautam**, this Ph. D. thesis submitted by **Girja Mani Aryal,** entitled "**Characterization of the Cellulosic Fiber Obtained from Nepalese Lokta Bushes and Explore its Novel Applications"** is forwarded by Central Department Research Committee (CDRC) to the Dean, IOST, T.U.

Dr. Jagadeesh Bhattarai
Professor
Head
Central Department of Chemistry
Tribhuvan University
Kirtipur, Kathmandu, Nepal

ACKNOWLEDGEMENTS

I am thankful to my supervisor Dr. Bhanu Bhakta Neupane, CDC, TU for guiding the PhD work. I similarly acknowledge my co-supervisors Dr. Mahesh Kumar Joshi at CDC and Dr. Bhoj Raj Gautam at Fayetteville State University, USA.

I also acknowledge HoD of CDC Prof. Dr. Jagadeesh Bhattarai for cooperating while carrying out research and in administrative works. Similarly, I am thankful to the director of RECAST Prof. Dr. Ram Nath Prasad Yadav for providing scientific support.

I also acknowledge all the support staffs at CDC and RECAST. I am thankful to Prof. Rameshwor Adhikari and Dr. Khage Raj Sharma for supporting in FTIR measurement and Prof. Dr. Hem Raj Pant (IOE, Pulchowk, TU) for supporting in UV-Visible measurement. I also acknowledge all the CDRC members and IoST for fruitful scientific comments and feedback and technical support. I am thankful to Mr. Bhawani Prasad Adhikari, NBSM, Nepal for the tensile strength measurement.

I am also thankful to my friends Dr. Netra Lal Bhandari, Hari Paudyal, Dr. Kedar Nath Dhakal, Dr. Shankar Prasad Khatiwada, Dr. Chandra Kanta Subedi, Dr. Bijaya Raj Subedi. Special thanks to Yukti Acharya for supporting in data analysis. Lately, I am indebted to my parents and family members for supporting me morally throughout my PhD work.

Girja Mani Aryal

May, 2024

शोधसार

नेपालमा विभिन्न प्रकारका बोटबिरूवा बाट प्राप्तहुने रेशादार जैविकपदार्थहरू प्रयोग गरी कागज तयार गर्ने परम्परागत प्रविधि रहेको पाइन्छ । विशेषगरी लोक्ता नामक विरूवाबाट प्राप्तहुने जैविक पदार्थलाई वातावरणमैत्री विधि अपनाएर तयार गरिने कागजलाई लोक्ता वा नेपालीकागज भनिन्छ । उक्त कागज नेपालका ग्रामीण जनताहरूको लागि आर्थिक उपार्जनको एक महत्वपूर्ण माध्यमको रूपमा समेत रहेको छ । टिकाउ, बलियो तथा किटाणु प्रतिरोधी क्षमता जस्ता विशिष्ट गुणहरूको कारण यो कागज प्रसिद्ध रहेको छ । यद्यपि भौतिक तथा रासायनिक गुणहरूको वैज्ञानिक अध्ययन/अनुसन्धान गरी प्रकाशन भएको पाइँदैन । त्यसकारण, यो शोधकार्यको प्रमुख उद्देश्य लोक्ता कागज र यसका रेशाहरूको वैज्ञानिक अध्ययन गरी उक्त कागजमा जिङ्कअक्साइड/ चाँदी (ZnO/Ag) तथा तामाका नानो-कणहरू (Nano particles) प्रयोग गरी तयार गरिएको नानो कम्पोजिट म्याट (Nano composite mat) को सूक्ष्म जिवाणु प्रतिरोधात्मक क्षमताको परीक्षण गर्नु रहेको थियो ।

उक्त उद्देश्य अनुरूप स्थानीय बजारबाट सङ्कलित दशवटा नमुनाहरू माथि अध्ययन अनुसार लोक्ता कागजको चमक अन्यकागजहरू भन्दा कम, हल्का तौल, मोटाइमा भिन्नता र मध्यमदेखि उच्च मानको यान्त्रिक क्षमता रहेको पाइएको छ । इलेक्ट्रोन दर्शन क्षमताको सूक्ष्म दर्शक यन्त्र (Electron microscope) द्वारा माइक्रो-फाइब्रिलहरूको अध्ययन गर्दा समानान्तर रूपमा रहेको तन्तुहरूको अखण्ड सञ्जाल देखिएको छ । यसकारण लोक्ता बलियो र टिकाउ रहेको पाइएको छ । साथै मध्यम तापक्रममा क्षारीय माध्यममा प्रशोधित लोक्ताका रेशाहरूको अध्ययनगर्दा तिनीहरूको अवस्थिति लिग्निन र हेमिसेलुलोजको मात्रा र तिनीहरूको चौडाइमा कमी आयोभने तिनीहरूको मणिभीकरणको सुचाङ्क (Crystalline index), यान्त्रिक सबलता (Mechanical strength) र तापबहन क्षमता (Thermal stability) मा वृद्धि भएको पाइयो । यी परिणामहरूको आधारमा क्षारीय प्रशोधन विधिलाई लोक्ता रेशाहरूका गुणहरू अभिवृद्धि गरी उच्च श्रेणीको कागज तयार गर्ने विधिको रूपमा सुझाउनु सकिन्छ ।

यही निष्कर्षका आधारमा प्रयोगशालामा लोक्ता प्रयोग गरी तयार गरिएको हाते कागज र बजारमा उपलब्ध कागजको भौतिक तथा रासायनिक गुणहरूको तुलनात्मक अध्ययन गरियो । साथै उक्त कागजमा विभिन्न रासायनिक विधि मार्फत जिङ्कअक्साइड/चाँदी (ZnO/Ag) तथा तामाका नानो कणहरू विकास गरी नानो कम्पोजिट म्याट (Nano composite mat) तयार गरियो । उक्त म्याटले इ.कोली (*E. coli*), वेसिलस सब्टीलिस (*Baillus subtilis*) जस्ता ब्याक्टेरियाहरू र क्यान्डीडा एल्वीकान्स (*Candida albicans*) नामक ढुसीका प्रजाति विरूद्ध प्रभावकारी प्रतिरोधात्मक क्षमता प्रस्तुत गऱ्यो । परिणाम स्वरूप लोक्ता कागजको यस प्रकारको म्याटलाई सूक्ष्म जिवाणु प्रतिरोधी प्याकेजिङ्ग सामाग्रीका रूपमा प्रयोग गर्न सकिने सम्भावना सम्भाव्यता रहेको देखिन्छ ।

शब्दकुञ्जी:- हाते कागज, लोक्ता रेशा, न्यानो कम्पोजिट म्याट, प्याकेजिङ्ग सामाग्री, लीग्नीन

ABSTRACT

In Nepal, Handmade papers (HPs) are made from fibrous biomass of several plant species. Paper fabricated from fibrous biomass obtained from Lokta bushes following the traditional eco-friendly method is called Lokta paper or Nepal Kagaj. Handmade paper fabricated from Lokta bushes is being used to fabricate value-added products. The paper is traditionally believed to be durable and bug and mold-resistant. However, a systematic study on the material properties of this paper is not reported yet. Additionally, material properties of Lokta fiber retted under different conditions; which help to understand the performance of Lokta fiber-derived products is not mentioned in the literature. To increase, trade value it is also equally important to find next generation applications of the Lokta paper. This dissertation work was aimed at understanding the material properties of Lokta paper and fiber, and the fabrication of Lokta paper-derived nanocomposite mat for antimicrobial application.

It was found that the mean caliper, apparent density, Cobb 60, grammage, brightness, opacity equilibrium moisture content, tensile strength, and tensile index values in the paper samples collected from local enterprises (n=10) ranged from ~90–700µm, 0.2–0.4 g/cm^3, 50–150 g/m^2, 4–7%, 50–400 g/m^2, 56–67 %, 83–98 %, 30–2900 N/m, and 1–27 Nm/g; in that order. These data recommended that Lokta paper is a light weight paper having intermediate to high strength, high caliper variation and relatively low brightness. All paper samples exhibited considerably increased tensile strength across the length axis ($p<0.05$). Distinctive characteristics of hemi–cellulose, cellulose, and lignin were spotted in the FTIR spectra of all the samples. The amorphous and crystalline cellulosic segments were detected in X–ray diffraction (XRD) data. Most importantly, electron microscopic showed a properly cross-linked web of entire fibers organizing a parallel layout of microfibrils. These morphological qualities could be responsible for delivering strength and durability to the paper samples.

A comprehensive analysis of material properties of Lokta fiber subjected to 1-9% NaOH (w/v) concentrations at ambient temperature was also performed. The alkali resulted in significant shrinkage of lignin and hemicellulose; thereby increasing the cellulose content. On alkali treatment, fiber width and equilibrium moisture content decreased whilst fiber density, crystallinity index, tensile strength, and thermal stability increased. These changes can be assigned to the deduction of cementing materials from

fiber bundles. These findings suggested that processing conditions greatly affect the fiber properties and to get Lokta paper of optical performance fiber chemistry needs to be properly tailored.

Finally, Lokta paper-making process was mimicked in laboratory settings and the physico-chemical properties of lab-made Loka paper were compared with commercially available paper. The Ag/ZnO and Cu nanoparticles were doped in the Lokta paper following hydrothermal and chemical reduction methods. The Lokta paper nanocomposite mat showed promising antimicrobial activity contrary to two bacteria (*Escherichia coli* and *Bacillus subtilis*) and a fungal strain (*Candida Albicans*). These observations suggested that the Lokta paper-derived nanocomposite mat can find potential applications as an antimicrobial packaging material.

Keywords: Handmade paper, Lokta fiber, Nanocomposite mat, Packaging material, Lignin

LIST OF ACRONYMS AND ABBREVIATIONS

ATR	: Attenuated Total Reflection
EDX	: Energy-dispersive X-ray Spectroscopy
CI	: Confidence Interval
DP	: Degree of Polymerization
DTG	: Derivative Thermogravimetry
GSM	: Grams per Square Meter
HP	: Handmade Paper
ISO	: International Organization for Standardization
MB	: Methyl Blue
NPs	: Nanoparticles
RBA	: Relative Bonding Area
RH	: Relative Humidity
SEM	: Scanning Electron Microscopy
TGA	: Thermogravimetry Analysis
UV-Vis	: Ultraviolet-visible Spectroscopy
XRD	: X-ray Diffraction

LIST OF SYMBOLS

Å	: Ångstrom
λ	: Lambda
θ	: Theta
ε	: Epsilon
E	: Elongation
H	: Hours
°C	: Degree Celsius
%	: Percentage
µg	: Microgram
µS	: Microsiemens
kV	: Kilovolt
a.u.	: Arbitrary Unit

LIST OF TABLES

LIST OF FIGURES

TABLE OF CONTENTS

CHAPTER 1

INTRODUCTION

1.1 Introduction

In a broad sense, fiber is a thin and thread-like material of natural, semi-synthetic, and of synthetic origin. Fibers obtained naturally from natural resources such as plants are said to be natural fibers while synthetic fibers are made from synthetic materials by using various chemical process (Shahinur *et al*., 2022). Semi-synthetic fiber is cellulose regenerated fiber synthesized by polymerization reaction (Kauffman, 1993).

Natural fibers can be achieved from bast, stem, seed leaf, and other components of plant. Such fibers are reported to have intermediate to elevated elastic modulus, elevated moisture absorption, high strength, and low density contrasted to non-natural fibers (Morton & Hearle, 2008; Pritchard *et al*., 2000). Non-toxic nature, low cost, and biodegradability are further noticeable benefits of natural fibers (Mohanty *et al*., 2001). However, when used in composites, they also have significant disadvantages that can cause and encourage material flaws (Cantero *et al*., 2003; Fernandes *et al*., 2013). Natural fiber obtained from plants is classified into several types on the basis of their origin as shown in **figure 1** (Jayaramudu *et al*., 2014; Khoathane *et al*., 2015).

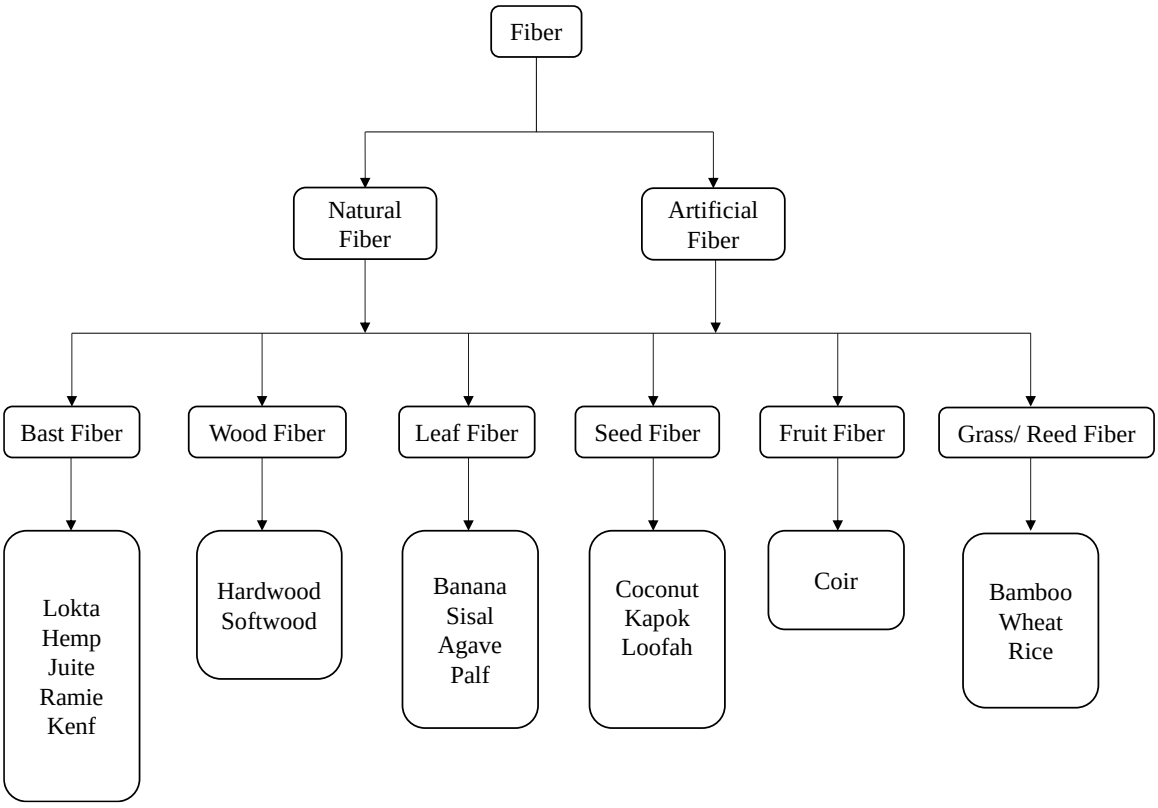

Figure 1: A schematics to show the classification of natural fibers

1.2 Types of Plant fibers

1.2.1 Bast fiber

Bast fiber is a kind of natural fiber that is obtained from the inner bark or phloem of dicotyledonous plants. Soft fiber, commonly referred to as bast fiber, is recognized by its fineness and flexibility. The fibers are situated in between the internal core and the epidermis, or bark surface of the plant. Bast fibers are longer than wood fibers and have reduced lignin content. Flax, hemp, jute, kenaf, and ramie, are some of the most common bast fibers (Gleba & Harris, 2019; Madsen & Gamstedt, 2013).

1.2.2 Wood fiber

Wood fibers are obtained from trees of lignin-rich, woody trunks and utilized to create a variety of products, including paper. Wood fibers are processed by blending them with other chemicals, which causes the fibers to break down into a spongy mass known as pulp. The network of small fibers in the pulp is then treated, flattened, and made into paper. Softwoods and hardwoods are the two major wood types from which wood fibers can be obtained. Wood fibers obtained from these two types can be comparable in terms of their

chemical and physical characteristics. Wood fibers are durable, affordable, recyclable, and adaptable, thus wood fiber-based paper products are frequently employed in packaging applications around the globe (Bledzki *et al*., 2002; Jones *et al*., 2017).

1.2.3 Leaf fiber

Leaf fibers, sometimes also recognized as hard fibers, a plant fiber that have higher lignin content in comparison to wood fibers. Leaf fibers are made up of phloem, xylem, and any other vascular sheathing tissues that can be found in the vascular bundles of monocot plant leaves. The fibers are usually obtained from the leaves by mechanical processing. These fibers are rougher or harsh in texture than the bast fibers. Leaf fibers are being used in making rope, mats, and other useful products (Smole, M.S., *et al*., 2013).

1.2.4 Seed fiber

Seed fibers are the type of fiber that are obtained from the seeds of plants. The best example of this type of fiber is obtained from seed of cotton plant. This type of fiber grows within a pod or boll from developing seeds. It is the soft, fluffy fiber which is most commonly used in cloth industries to manufacture varieties of cotton clothes (Möller & Popescu, 2012).

1.2.5 Grass/ Reed fiber

Grass fibers can be derived from different plant parts, especially from the leaves, stems and vascular tissues. Bamboo, switch grass and elephant grass are the common grass species from which these fibers can be extracted. Bamboo is the most widely used of the several grass varieties. The grass fiber has an exceptional strength-to-weight ratio (Jones *et al*., 2017)

1.3 Properties of Lignocellulose fiber

Lignocellulose fiber is one of the abundant resources. It mainly contains hemicellulose, lignin, cellulose, and other impurities. The lignin content of the fibers influences their morphological and structural characteristics. The place of origin, climatic conditions, various methods of extraction, and age of the fiber plant are related to their differences in structural parameters and properties. The fiber properties are also determined by its chemical makeup, internal organization, and cellular configuration (Bledzki & Gassan, 1999). The geometrical characteristics of these fibers, particularly their length, are largely dependent on where they are situated in the plant body. Leaf and stem fibers are much

longer as compared to seed and fruit fibers. The lignocellulose biomass is found in plant cell walls. If a plant cell is viewed closely primary and secondary cell walls is observed; as illustrated in **figure 2** (John & Thomas, 2008).

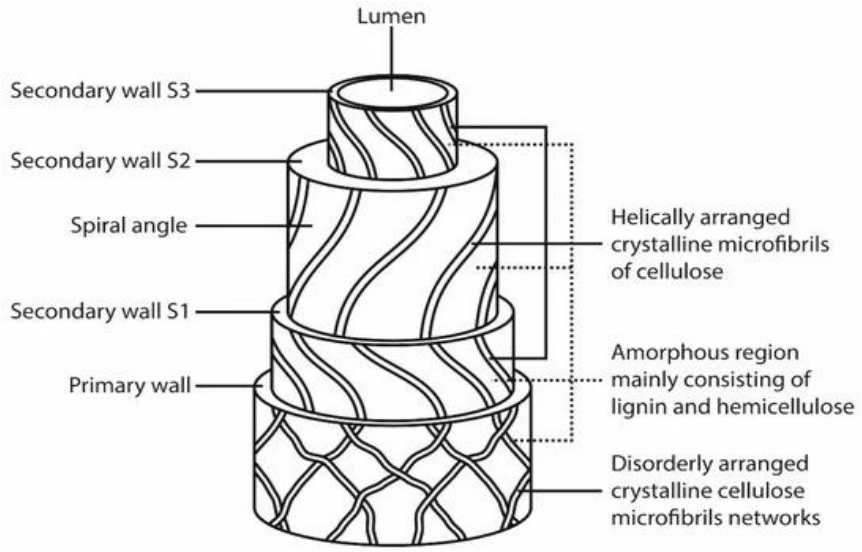

Figure 2: Cross section view of cell wall (*John & Thomas, 2008*)

The primary cell wall is formed earlier during the cell growth in which crystalline cellulose microfibrils are arranged in random orientation. The secondary cell wall then forms within the primary wall, and this comprises three different layers: S1, S2, and S3, which are the outer, middle as well as inner layer, respectively in which the cellulose microfibrils are amorphous and have helical orientations (**Figure 2**). Within the secondary cell wall, a hollow tube called the lumen is present that contain water and nutrients required for plants (Ali *et al*., 2018; Truss, 2011).

1.4 Lignocellulose biomass

Cellulose, hemicellulose, and lignin in lignocellulosic biomass are joined together by hydrogen bonding, van der Waals' bonding and various intermolecular bridges forming a complex structure insoluble in water. The plant cell wall is majorly composed of these three components which make it a compact, resistant, and very rigid structure (Chen, 2014). Among three of the major components, hemicellulose and cellulose are made of carbohydrate molecules whereas lignin is an aromatic-rich polymer (**Figures 3** and **4**).

Cellulose molecules are arranged regularly into bundles, or irregularly forming amorphous structures. The polymers of cellulose are joined together by Van der Waals' and hydrogen bonds and stay protected by hemicellulose and lignin. It occupies about 40-55% of the dry weight of lignocellulose biomass (Yousuf *et al*., 2020). Hemicellulose is the second major component that is composed of repeated polymers of pentose and hexose sugars. It is located in between both the macro and the microfibrils of cellulose and consists of about 20-30% of lignocellulose biomass (Iqbal *et al*., 2013). Lignin is another important component of lignocellulose biomass containing aromatic alcohols that bind together cellulose and hemicellulose. There exists hydrogen bonding as well as chemical bonding between lignin and hemicellulose, which produces an isolated form of lignin molecules. Lignin is the second richest natural polymeric component next to cellulose, contributing 10-35% of total biomass (Chen, 2014; De Lima *et al*., 2016). However, the composition of the three major components in lignocellulose biomass is variable depending upon the type of plant, source and habitat, whether it is obtained from the grasses, softwood, or hardwood (Sun & Cheng, 2002). The lignocellulose biomass composition varies depending on the source of origin (**Table 1)**.

Table 1: Lignocellulose biomass composition of selected sources.

Lignocellulosic components	Lignin (%)	Hemicellulose (%)	Cellulose (%)	References
Hardwood	18-25	24-40	45-55	(Betts *et al*., 1991; McKendry, 2002; Shahzadi *et al*., 2014; Sun & Cheng, 2002)
Softwood	25-30	25-35	45-50	
Grass	10-30	35-50	25-40	
Sugarcane	20-42	19-25	42-48	(M. Kim & Day, 2011; Saini *et al*., 2015)
Corn cobs	14-15	35-39	42-45	(Kuhad & Singh, 1993; Shahzadi *et al*., 2014)
Rice straw	12-14	23-28	28-36	

Lignocellulose biomass has gained increased popularity so far for different novel applications due to their bio-availability and bio-renewability. Lignocellulosic biomass such as forest products (hardwood and softwood), agricultural residues, crops, and grass are becoming a potent source for generating valuable products (Anwar *et al*., 2014). Utilizing lignocellulosic materials offers a sustainable alternative for waste management while assisting in reducing over-reliance on petroleum resources (Okolie *et al.*, 2021). Lignocellulose biomass have found its great potential and application in paper and pulp industries. Similarly, other industrial applications of lignocellulose biomass include biofuel and biochemical production, bioplastics, biomedical, pharmaceuticals and cosmeceuticals, and manufacturing of other environment-friendly bioproducts (Haq *et al*., 2020; Okolie *et al*., 2021).

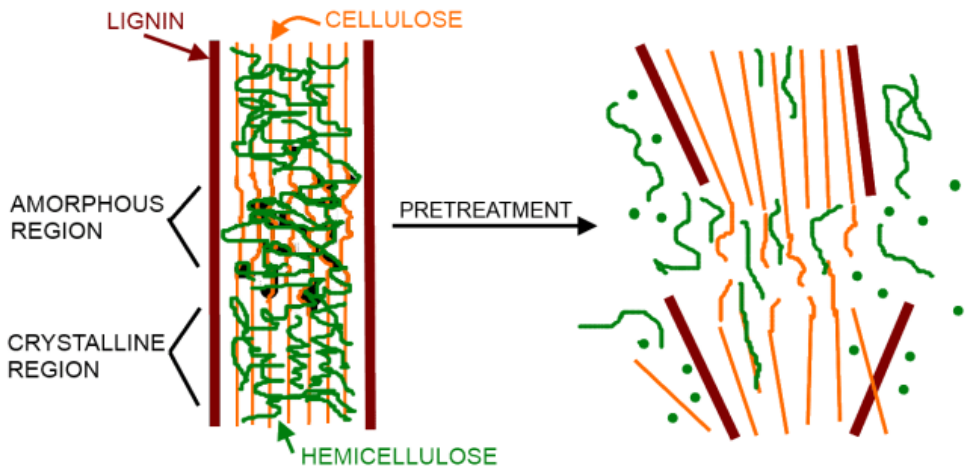

Figure 3: Schematic of breakdown of Lignocellulose after pre-treatment (*Mosier, 2005)*

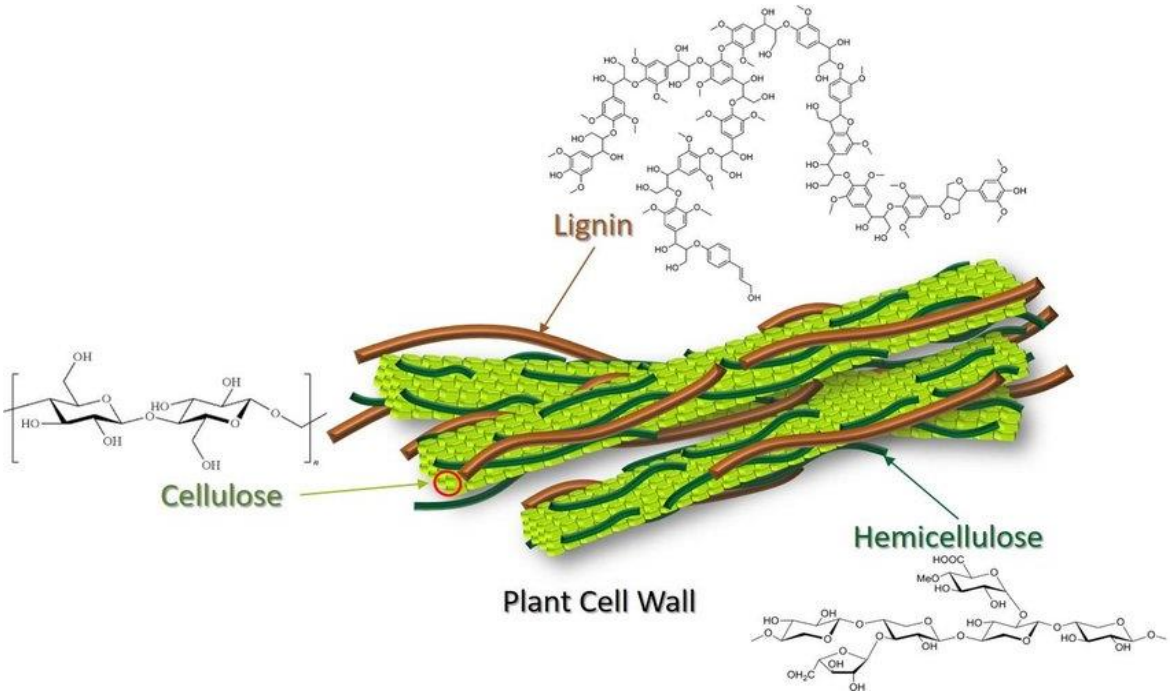

Figure 4: Molecular structure of lignin, hemicellulose and cellulose (*Jensen et al., 2017)*

1.4.1 Cellulose

It is the chief constituent of the primary cell wall in higher plants. It is also found in algae, fungi, and bacteria. In plants, cellulose is synthesized in the plasma membrane by CESA (Cellulose Synthase) proteins (Kimura *et al*., 1999). Naturally, cellulose is a tasteless, odorless, biodegradable, hydrophilic polymer (Klemm *et al*., 2005). Cellulose cannot dissolve in diluted alkaline and acidic solutions, including water at normal temperatures. However, the rise in temperature increases its solubility, as the generated energy reaches a level where it is adequate to disrupt the hydrogen bonds within the crystalline structure. (P. Harmsen *et al*., n.d.). The cellulose is abbreviated as $(C_6H_{10}O_5)_n$ where n is the polymerization chain length representing the number of glucose molecules linked by glycosidic bonds (**Figure 5**). The cellulose polymer is an unbranched chain rectilinear polymer having greater ability to create intra- and inter-molecular H-bond by OH units on its linear chain (Tayeb et al., 2018). The polymerization degree of cellulose chains varies between 10,000-15,000 glucopyranose units (Chen, 2014). These repeating units unite together to make microfibrils, which in turn aggregate together to form cellulose fibrils. A

fibril is a small, stretching unit consisting of approximately 60-80 glucose molecules. Cellulose fibrils are arranged in a polysaccharide matrix giving strength to plant cells (Robak & Balcerek, 2018). The polymeric chain of cellulose contains both amorphous and crystalline regions. The crystalline forms exist in I, II, III, and IV forms. Cellulose I is a naturally occurring, native and highly stable polymer. It undergoes additional hydrolysis to create cellulose II, III, or IV. Cellulose types II, III, and IV are variants synthesized through artificial processing methods. At temperatures beyond 320°C, cellulose undergoes amorphous form which makes it susceptible to hydrolysis (Quiroz Castañeda & Folch-Mallol, 2013; Zhang & Zhang, 2013). Cellulosic biomass is extensively used in cardboard, pulp, and paper industries. Similarly, this eco-friendly raw material can be harnessed for the manufacture of bio-ethanol and bio-fuels.

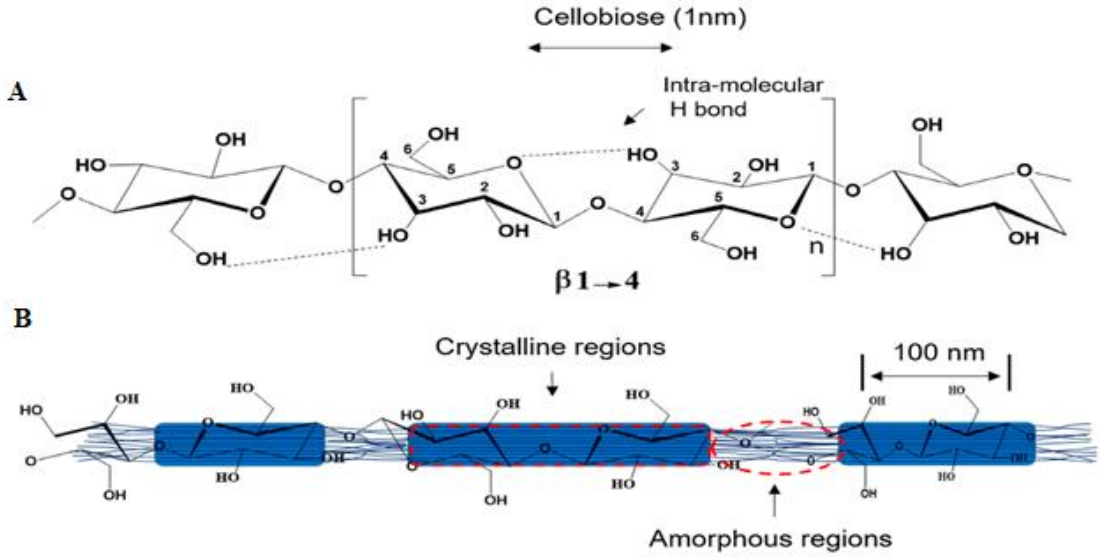

Figure 5: (A) Cellulose molecular structure showing intramolecular hydrogen bonding. (B) Amorphous and crystalline regions (*Tayeb et al., 2018)*.

1.4.2 Hemicellulose

A branched, short lateral chain heteropolymer, hemicellulose consists large number of different molecules of pentose sugar together with hexose sugar, acetylated sugars and most abundantly polymers of Xylans. The presence of short lateral chains makes it

susceptible to easy hydrolysis by alkali treatment (Lu *et al*., 2021). This copolymer composed of large amounts of different saccharide molecules was named Hemicellulose by Schulz in 1891 (Chen, 2014). Hemicellulose is a structurally diverse biomass that cross-links with either cellulose or lignin providing rigidity and strength to plant cell walls. It is linked with cellulose through hydrogen bonds and to lignin through ether and ester linkages (covalent bonds). It is a polymer with low molecular weight and a polymerization length extending from 80 to 200 with the general formulas $(C_6H_{10}O_5)_n$ and $(C_5H_8O_4)_n$ for hexosans and pentosans. Hexosans and Pentosans are polysaccharides containing hexose and pentose sugars respectively. (Wang *et al*., 2015). The backbone of hemicellulose contains tiny branches linked mostly by β-(1,4) and infrequently β-(1,3)-glycosidic bonds (**Figure 6**) (Bajpai, 2016). Hemicelluloses are amorphous in nature which is attributed to the existence of acetyl group and their extremely branched structure. Just like cellulose, its solubility increases with the increase in temperature. In addition, side-chain substitution enhances the solubility; the more side-chain substitutions, the more will be the solubility of hemicellulose in water.(Gatenholm & Tenkanen, 2003).

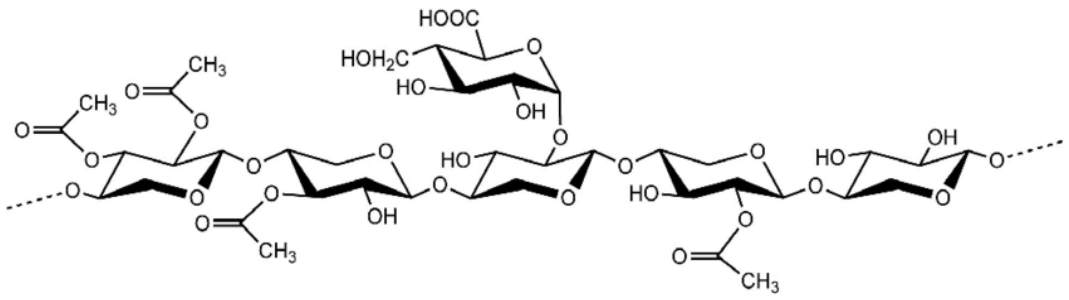

Figure 6: Structure of hemicellulose (reproduced from the permission from reference *Hu et al., 2020)*)

Xylans, mannans, glucans, and xylogucans are the four classes of hemicellulose based on structural variations (Ebringerová *et al*., 2005). Xylan is the predominant polysaccharide in hemicellulose excessively present in hardwoods and can be further classified into heteroxylans and homoxylans. Mannan, another class of hemicellulose, is a biopolymer of mannose majorly present in softwoods. It is further sub-divided into linear mannan, glucomannan, galactomannan, and galactoglucomanan (**Figure 7**).

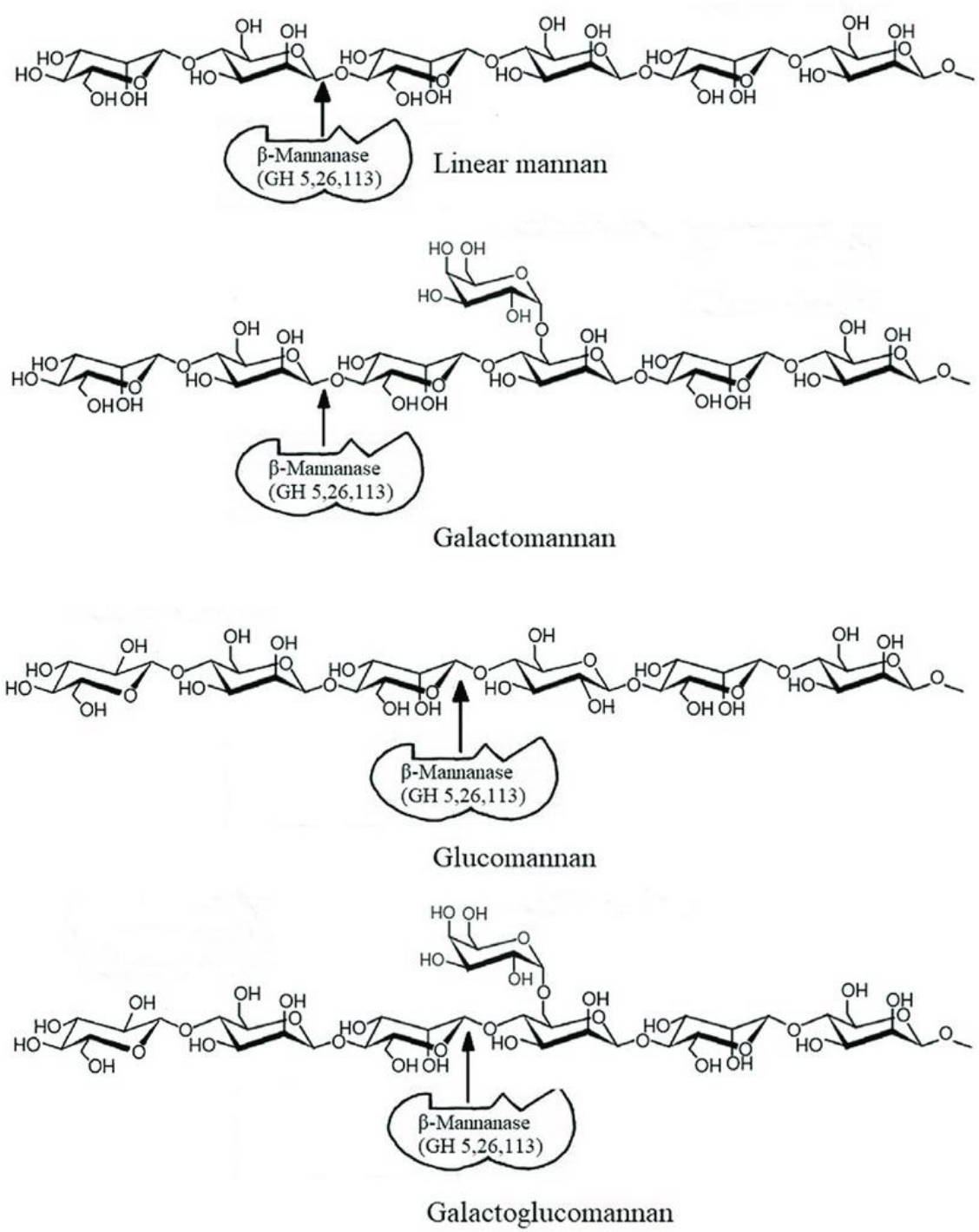

Figure 7: Molecular structure of types of Mannans. The degradation sites by Mannanze enzyme is shown by vertical arrows (*Dawood & Ma, 2020)*

1.4.3 Lignin

Lignin is a polymer of phenolic components that come up with three aromatic structural monomers: syringyl monomer (S type) obtained from sinapyl alcohol, H type p-phenyl monomer as of coumaryl alcohol, and G type guaiacyl monomer from coniferyl alcohol. Lignin molecules are made by phenyl units attached by aryl glycerol-“-aryl-(“-O-4) ether bonds. It is highly hydrophobic and water-insoluble at acidic or neutral pH but easily soluble in alkaline solutions at both low and high temperatures (P. F. H. Harmsen *et al*., 2010; Sharma & Kumar, 2020).

Alkaline treatment of Lignin results in cleavage of ether bond and aromatic ring separation. Furthermore, the addition of hydrogen sulfide enhances the bond cleavage (**Figure 8**). The bond cleavage reaction under alkaline and hydrogen sulfide treatment is shown in the reaction given below (P. F. H. Harmsen *et al*., 2010).

If lignin is removed, the brightness of the paper and also the bug resistance increases.

Lignin has a highly complex branched configuration which makes it non-crystalline in nature. In plants, lignin provides rigidity and protection to the cell from microbial attack due to linear chain molecules and the presence of several types of chemical bonds (Mäki-Arvela *et al*., 2012). The molecular weight of native lignin remains ambiguous because the separation process and environmental factors affect its molecular weight. The distribution of its molecular can span from several hundred to several million (Bajpai, 2016).

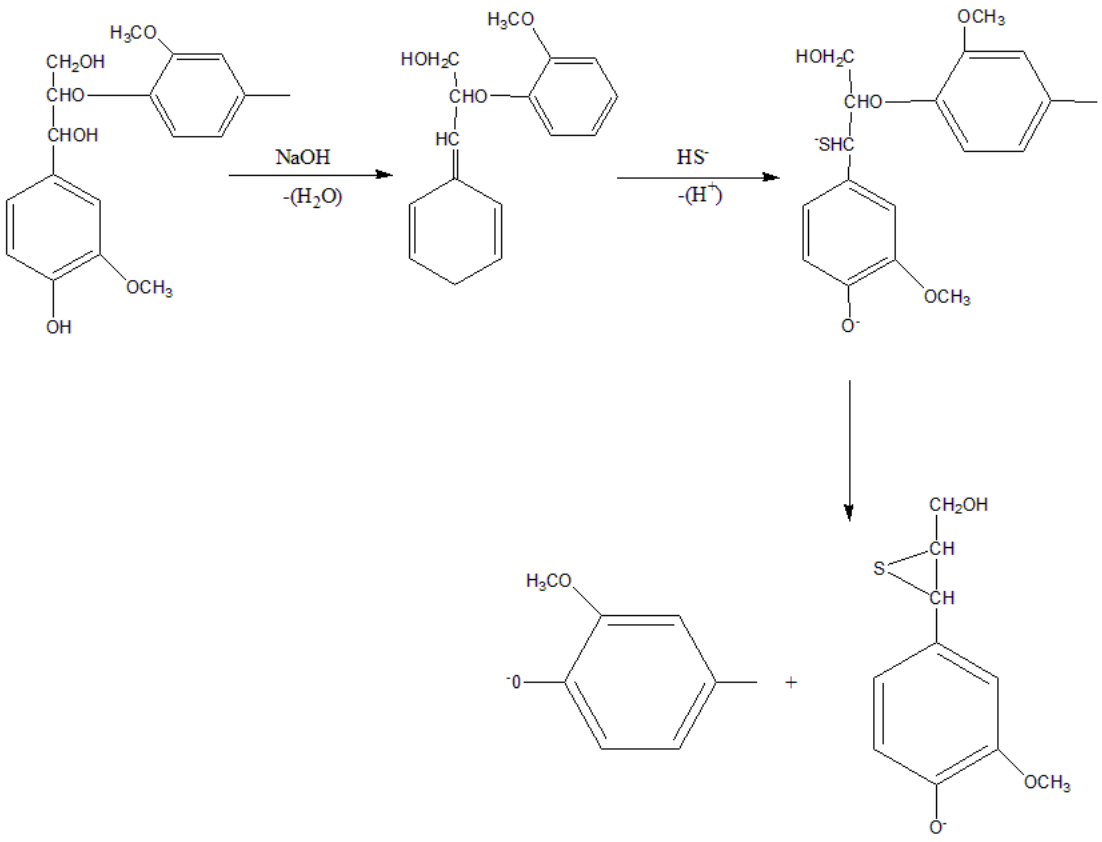

Figure 8: Mechanism of alkaline mediated cleavage of lignin

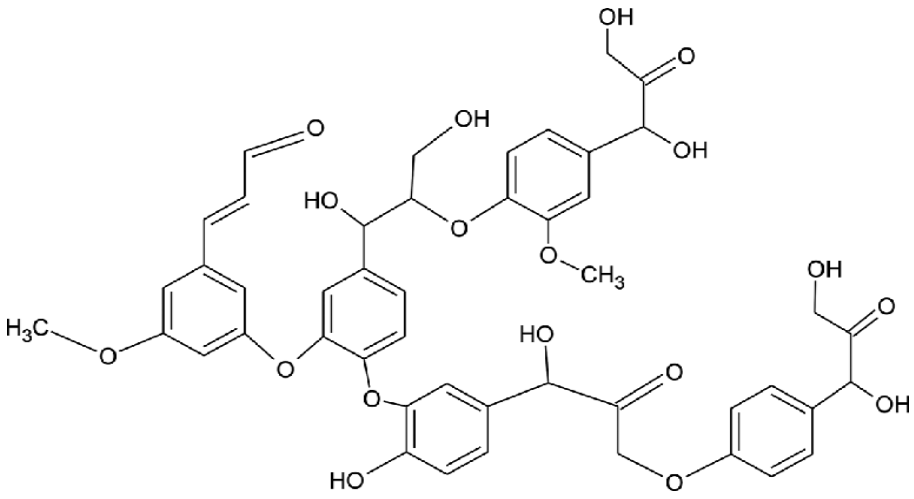

Figure 9: Structure of Lignin

Guaiacyl lignin, syringyl lignin and hydroxy-phenyl lignin are the three types of lignin molecules (**Figure 10**). Guaiacyl (G) lignin is predominatly found in gymnosperms, guaiacyl-syringyl (GS) in dicotyledons, and guaiacyl-syringyl-hydroxy-phenyl (GSH) lignin in monocotyledons (Chen, 2014). Generally, hardwoods and softwoods have the highest lignin contents, whereas herbaceous plants like grasses have the lowest. Hardwood encompasses both guaiacyl and syringyl lignins while softwood predominantly contains guaiacyl lignin. (Hendriks & Zeeman, 2009).

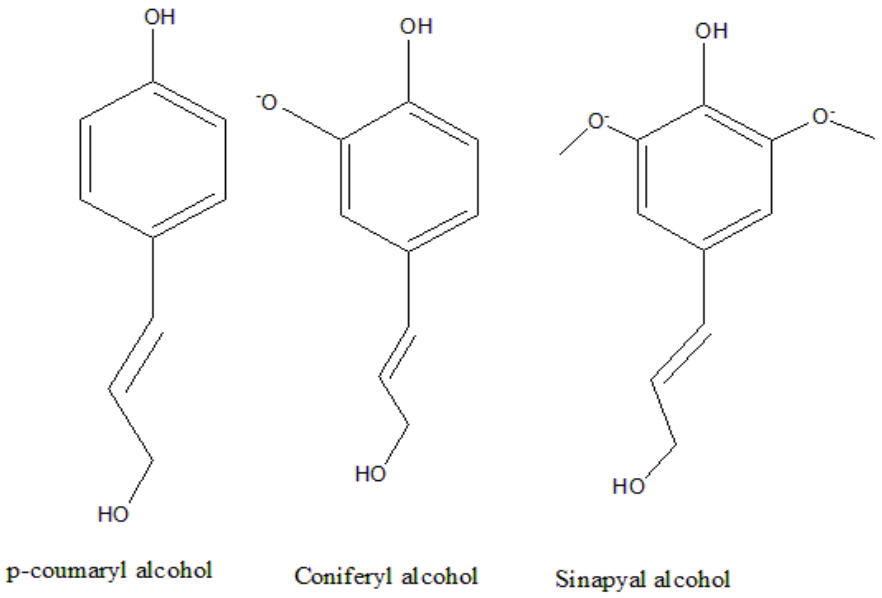

Figure 10: Components of Lignin

1.5 Retting of Natural Fibre

Retting is also called degumming as it helps in the separation of fiber bundles by removing non-cellulosic components such as pectin, lignin, hemicellulose, waxes, and other impurities. This process separates the natural fiber from lignocellulosic biomass without damaging the fiber cellulose by removing the bonds between fiber bundles and stem. Retting is especially done by using an alkali such as sodium hydroxide (NaOH) at a differing concentration at 1–25% by weight to remove non-cellulosic components. This

process is known as alkali retting. Retting must be done carefully if high-grade fiber is to be obtained. Under-retted and over-retted fiber may cause ineffective fiber separation and weakening, respectively (Preisner *et al*., 2014). Various retting techniques are in use and among them physical, chemical retting, microbial retting are most commonly used.

1.5.1 Physical retting

Some of the physical methods that separate natural fiber bundles from the plant materials are given below:

1.5.1.1 Plasma Treatment

In this method, thermal and non-thermal plasma is often utilized to extract the natural fibers in industries (Zille *et al*., 2015). Plasma treatment removes surface impurities from the fiber, which causes surface quality changes such as flammability, dyeability and wettability. This process can make the surface rough which will improve the mechanical binding and adhesion of the polymers an interface within fiber matrix. In addition, the plasma can create free radicals that can interact with gases such as oxygen to form surfaces with varying hydrophobic or hydrophilic properties (Skundric *et al*., 2007).

1.5.1.2 Steam explosion

It is one of the most prevalent and cost-effective techniques, exhibiting remarkable versatility and minimizing the need for excessive energy for the processing of various fibers. This process employs saturated steam at high pressure and abrupt decompression, which breaks down the lignocellulosic structure and causes the hemicellulose fraction and lignin components to hydrolyze and depolymerize; respectively. This results in fiber bundle separation while retaining its cellulosic component. The optimal temperature and pressure required for this method is 160–260 °C and 0.7–4.83 MPa, respectively for variable time scale. Hemp and banana fiber have both been processed using this method with effectiveness (Sheng *et al*., 2014; Thomsen *et al*., 2006).

1.5.2 Chemical retting

Chemical retting involves chemical reactions for the separation and modification of natural fibers. In this process plant section is submerged in heated tanks with different chemical solutions such as sodium or potassium hydroxide to dissolve non-cellulosic components. Several chemical methods that facilitate extraction and improvement of fiber

characteristics include alkali treatment (mercerization), ammonia treatment, acidic retting, and peroxide treatment. The time required for chemical retting is 60-75 minutes depending on the type of chemical used.

1.5.2.1 Alkali Treatment

Alkali treatment also called as mercerization and is the most extensively studied method for producing flexible, stronger, and less brittle fibers. This method involves treating plant material in an alkaline solution, usually sodium hydroxide (NaOH) at a differing concentration at 1–25% by weight to remove non-cellulosic components (Oushabi *et al*., 2017). Alkali treatment changes the thermal, mechanical, and water absorption properties of fiber (Fiore *et al*., 2015b). A typical reaction involved in alkali treatment is:

$$\text{Fiber–OH} + \text{NaOH} \rightarrow \text{Fiber–O}^{-}\ \text{Na}^{+} + \text{H}_2\text{O}$$

A combination of NaOH, Na_2CO_3, and Na_2S in retting not only effectively diminishes retting time but also improves mechanical properties such as flexural rigidity, linear density, and diameter (Basu *et al*., 2015). Furthermore, alkali treatment has demonstrated an increased mechanical integrity by enhancing the surface roughness of the fiber (Gurunathan *et al*., 2015).

1.5.2.2 Treatment with peroxides and other oxidizing agents

Hydrogen peroxides and other oxidizing agents have demonstrated an influence on the delignification of fibers. Hydrogen peroxide works better at removing waxes and fatty acids from fiber surfaces, enabling efficient and high-quality fiber extraction. Bleaching the fibers with alkaline hydrogen peroxide is relatively a safe process of removing lignin content and color from the fiber. It was noted that the brightness of fiber increased with peroxide treatment (Kandel, *et al*., 2022a). Under alkaline conditions, H_2O_2 decomposes into HOO^{-}. This decomposition is attributed to delignification of fibers (More *et al*., 2021). HOO- reacts with phenyl propanol, propiophenone, and quinone as well as the double bonds and carbonyl side chains structures in lignin, promoting its fragmentation and solubility.

The mechanism of delignification under alkaline hydrogen peroxide treatment is shown in the reaction as:

$$H_2O_2 + HOO^- \rightarrow HO + O_2^- + H_2O$$

$$HO + O_2^- \rightarrow O_2 + OH^-$$

$$\text{Lignin} + O_2/\ HOO^- \rightarrow \text{delignification}$$

Additionally, Hydrogen peroxide improves the thermal stability of harvested fibers. Furthermore, treatment with other oxidizing agents such as NaOCl and NaOH is effective in the deduction of part of the lignin and hemicellulose that interconnects the cellulose fibrils (Brígida *et al*., 2010).

1.5.2.3 Acidic retting

This retting technique treats lignocellulosic materials for the entire cellulose hydrolysis by using concentrated strong acids like hydrochloric acid and sulfuric acid (Sun & Cheng, 2002). Moreover, the diluted form of these acids possesses enhanced reaction rates and improves the rate of hydrolysis of cellulose at high temperature (Esteghlalian *et al*., 1997). Organic acids such as fumaric and maleic acids can also be utilized for alkali pretreatment (Kootstra *et al*., 2009). Due to the significant danger of the cellulosic fraction degrading and the complexity of managing the processing waste, only a few studies have described this technique, and such methodology is not widely used.

1.5.3 Mechanical retting

This technique uses mechanical force to separate fibers from the plant materials. Although this process is automated nowadays, the basic steps in mechanical retting include breaking, scutching and hackling for the processing of fibers. One of the most popular methods for the mechanical retting of fibre is decortication. Decortication is the process of removing outer layers of plants such as barks or husks. This process efficiently separates the fibers from the innermost part of the plant stalk. The inner core is the by product which can be removed by further processing to obtain core free fiber. Depending upon the quality, quantity and the application, different types of decorticators can be used. Among several different types, hammer mills and roller mills are the two most common decorticators that have shown their effectiveness in fiber processing. While the hammer mill has a higher throughput capacity, the roller mill offers considerably improved length control, which results in intact and long fibers (Sadrmanesh & Chen, 2019).

1.5.4 Enzymatic retting

Enzymatic retting is an eco-friendly alternative process for the extraction of plant fiber. It is also known as bio-scouring. This cost-effective, convenient method takes 8-24 hours for the completion of retting (Tahir *et al*., 2011). In this retting process, microbiological enzymes play crucial role for the degradation of lignin, pectin, and hemicellulose, present in plant. Some of these microbial enzymes includes pectinase, hemicellulose, xylanase, etc (George *et al*., 2014). Among the several enzymes, pectinase is the most easily available and commonly used enzyme in majority of studies related to retting in natural plant such as knef, juite, hemf, flax and ramie (Jayani *et al*., 2005). While extracting bast fiber, this enzyme dissolves the non-cellulosic components that bind with plant fiber in a complex orientation. It mainly hydrolyze the low-methylated pectins within the middle lamella section for the separation of fiber bundles (Manian *et al*., 2021). One of the most utilized fungi in the manufacturing of pectinolytic enzymes is *Aspergillus niger*. This enzyme is able to produce high-strength renewable fiber for use in various composites (Jayani et al., 2005). Various studies suggest that the addition of ethylene diamine tetra acetic acid (EDTA); a chelating agent in pectin-rich enzyme mixtures increases the retting efficiency of natural fibers in plants (Adamsen *et al*., 2002). Novozymes, one of the global biotechnology companies has been producing industrial enzymes such as Viscozyme® L, Pectinex® Ultra SP-L, Scourzyme® L, Flaxzyme®, etc. These commercial enzymes contain mixture of pectinase, hemicellulose, and cellulase that effectively degrades the non-cellulosic components without compromising fiber quantity and quantity (Sisti *et al*., 2018).

1.5.5 Microbiological retting

Microbial retting is the indigenous method that utilizes microorganisms such as bacteria and fungi. These microorganisms secret enzymes for the removal of gummy substances such as pectin, and facilitates the extraction of fiber from plant tissue. Microbial retting is further categorized into two types: Water retting and Dew retting.

1.5.5.1 Water retting

The simplest technique, called water retting, takes place in an aqueous environment. This method is also known as steep retting in which anaerobic Pectinolytic bacteria cause the decomposition of pectic materials and subsequent release of fibers. The steam or outer bark

of the plant is soaked in fresh water in large tanks for 7-14 days during which water leads to the breakdown of the outermost layer increasing moisture absorption and the formation of pectinolytic bacterial colonies. One of the approaches is utilizing aerobic microorganisms that consume most of the dissolved oxygen making oxygen-deficient condition favorable for the growth of anaerobic microorganisms (Sisti *et al*., 2018). Water retting results in long and strong fibers. However, the retting process is slow. Water retting produces several pollutants and the water should be cleaned before being released into lakes, streams, and groundwater since it causes contamination (van der Werf & Turunen, 2008). Warm water retting is thought to be more effective and comparatively faster than normal water retting as the process requires 3-4 days for the formation of microbial community (Jain *et al*., 2017).

1.5.5.2 Dew retting

The main microorganism that plays a crucial role in dew retting is soil fungi that colonize to the stem or bast of plants and cause degradation of non-cellulosic components by releasing polygalacturonase as by-product (Tahir *et al*., 2011). The most favorable conditions for dew retting is moderate humidity and warmth (Lewin & Pearce, 1998). This process is also recognized as field retting. In this course, thin layers of harvested bast of the plant is spread in the field for about 2-10 weeks during which filamentous fungi act on to remove the non-cellulosic components without destroying cellulosic fiber. These fungi exhibited an increased pectinase action and the ability to invade the cuticular exterior of the stem (Sisti *et al*., 2018). The most noticeable disadvantage of this technique is darker and poor-quality fiber as compared to another process, although this process is one of the choices of many farmers due to cheap and low labor cost (Jain *et al*., 2017).

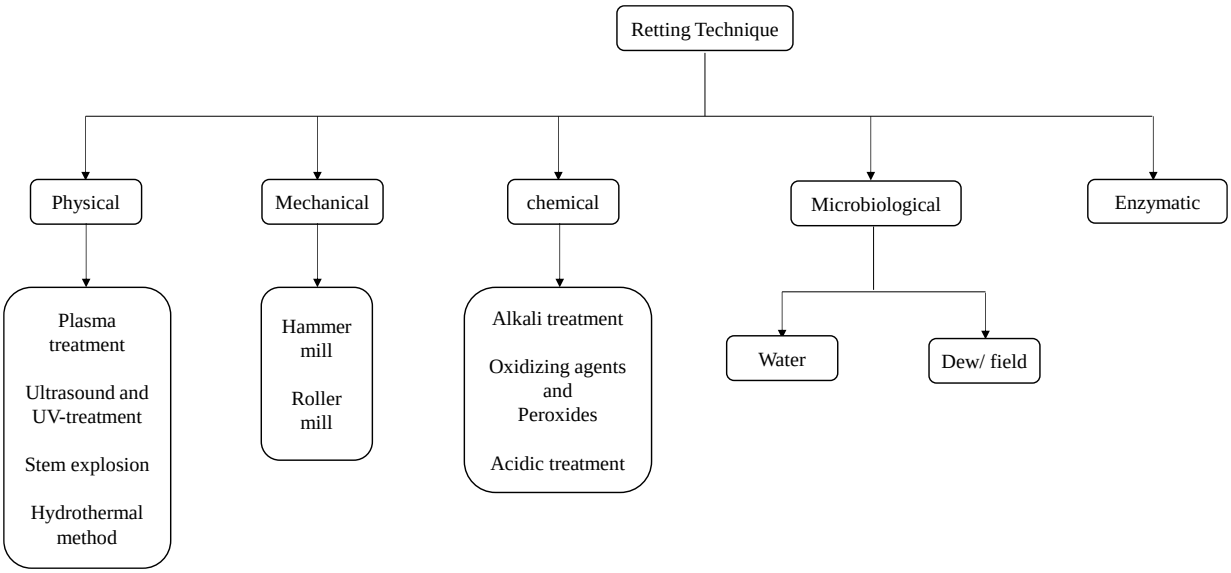

Figure 11: Classification of retting techniques

1.6 Handmade Loka paper in Nepal

The handmade paper in Nepal is mostly obtained from the fibrous inner barks of the Lokta plant and other plant species. Lokta paper is believed to have unique properties and is being used for a wide range of applications. This paper is commonly referred to as Nepali Kagaz and is highly valued for its distinct rough texture, toughness, and exceptional durability. In Nepal, Lokta paper serves crucial official functions, being used to maintain important government records. In addition, it holds immense significance in religious and sacred contexts, where it is employed for preserving ancient texts and scriptures. One of the most remarkable qualities of Lokta paper lies in its strength and resilience. It can withstand in various unfavorable conditions, moisture, tearing, and fungal growth (Biggs & Messerschmidt, 2005b). In addition, it is resistant to insects like silverfish and paper crawlers, ensuring the preservation of the content written on it for surprisingly a long time. Remarkably, texts written on Lokta paper can remain legible for up to three millennia, spanning a period of 2000 to 3000 years. The paper does not change over time and has a unique feel and texture. This exceptional property makes Lokta paper an effective medium for preserving knowledge and history. Today, these papers are widely utilized for many

purposes such as in wallpaper, menus at restaurants, phone books, wrapping paper, paper lamps, and other contemporary goods (Subedi *et al*., 2006).

1.6.1 History of handmade Lokta paper in Nepal

The history of Handmade Lokta paper in Nepal is very old. The earliest form of Lokta paper emerged as the sacred Buddhist text, the Karanya Buha Sutra. The existence of this document in Nepal is from Lichchhavi period and it can be found in the National Archives of Nepal in Kathmandu (DOF & UNICEF, 1984). In the seventh century, Tibet learned from the people of Nepal how to make paper. Handmade Lokta paper production is believed to have started in Baglung district of Nepal around the 12^{th} century AD (Banjara, G., 2007). However, by the early 20th century, imports of paper from Tibet and India reduced the demand for Lokta paper. In the 1960s, the handmade paper sector in Nepal was also overtaken by Indian paper.

In the 1970s, a conservation effort and the establishment of national parks and animal shelters led to the revival of Lokta paper production. The funding agency UNICEF played a key role in introducing Lokta paper to the global market, building a manufacturing facility in Bhaktapur and concentrating production in Baglung and Myagdi districts in the early 1980s. The UNICEF approach also highlighted the sustainability of Lokta paper, as it had been responsibly harvested by locals in Baglung and Myagdi for over 35 years without harming the environment (Messerschmidt, 1988). In the early 1990s, businessmen and environmentalists established trade routes, leading to increased popularity and growth of Lokta paper. Historical records revealed that Nepal has been producing handmade paper for commercial purposes since the eleventh century, providing employment opportunities for traditional families of Nepal. The exceptional qualities of Lokta paper, such as its strength, softness, longevity, and resistance to insects, make it a preferred choice for legal and religious documents (Subedi *et al*., 2006).

1.6.2 Lokta paper making process in Nepal

The process of manufacturing Lokta paper is simple and does not require a lot of labor, time, or equipment. Although a small number of people are needed to carry out the process, the procedure has been significantly improved to meet the demands of the modern world.

There are two methods for producing Lokta paper in Nepal: the traditional method and the improved method (Biggs & Messerschmidt, 2005b; FORWARD Nepal, 2016; ITC, 2017).

1.6.2.1 Traditional method

The traditional approach is the most widespread and favored among Nepalese people because it is simple to implement and offers a steady source of income to many rural communities in Nepal. The conventional method for producing Lokta paper involves a number of steps.

To begin the process, the Lokta plant stem is first chopped, the bark is removed and washed several times to remove impurities.

After cooking the bark in boiling water, it needs to be quickly soaked under cold running water to remove any oily and water-soluble organic matter, as well as any dirt or other objects. This process disconnects fiber bundles and neutralizes toxins. For best results, the bark can be cooked in water that has been filtered through fire ashes for six to eight hours. Boiling can also be done using sodium hydroxide (NaOH), or a mixture of calcium carbonate ($CaCO_3$) and sodium carbonate (Na_2CO_3) (Marella *et al*., 2014). To reduce the amount of fuel wood consumption, caustic soda (NaOH) can replace wood ash, typically 5-20% by weight, depending on the initial cleanliness of the raw material. This technique effectively softens the bark (Kandel, Menuka Adhikari, *et al*., 2022a).

In the third step, the softened bark is turned into pulp by hitting it with a stone pestle or wooden hammers. Then, the resulting pulp is placed in another vessel containing pure water and stirred until it becomes smooth. The pulp is spread out uniformly on the frame plates. Beater machines are now commonly used to make the pulp, reducing labor costs and improving the paper quality.

Finally, the pulp is dried on the frame and is gently and carefully removed from the frame once it has dried. In addition, a number of new methods aid in giving the paper its shape and color (Bajpai, 2018a).

1.6.2.2 Modern method

The Department of cottage and village industries collaborated with Japanese experts to enhance the paper manufacturing process (Herman, 1956). To prepare Lokta bast for paper-making, it is soaked in cold water for a few hours to remove any organic debris and foreign

objects. Additional hand cleaning and scraping can also be done. Next, the bast is boiled for 2 to 4 hours in a 5–15% solution of NaOH along with the bark to separate the cellulose fibers from non-cellulose organic debris. This method can reduce the amount of fuel wood needed by up to one-third.

After boiling, the bark is washed in running water or fresh water to remove residual NaOH. The bark is then reduced in size by being hammered in a wooden or stone mortar for 15 to 30 minutes before being placed in a manual or hydraulic Hollander-type beating machine to obtain homogeneous pulp. Beating helps to give the fibers desired properties like flexibility, plasticity, and viscosity. Homogeneous pulp is then used to create sheets of paper.

The paper can be made in different thicknesses by either sun-drying or using the layering method, where the frame is dipped into the pulp and raised horizontally while a mucilage solution is added. Once the sheet is formed, it is then pressed using a stone-weighted lever press, a screw press, a jack press or a hydraulic press. Finally, the wet sheets are dried using different methods such as air-drying, sun-drying, or fire-drying. After drying, the sheets are sorted, trimmed, and polished before being graded and trimmed to the desired size.

1.7 Description of Lokta plant

Two species of Lokta plant viz. *Daphne Bhoula* and *Daphne Papyracea* are reported. It is an indigenous plant that regenerates spontaneously and matures 4 to 5 years after the first cutting, as a result, it has no negative effects on the forest ecosystem. This regenerative property makes it an excellent source of raw materials for the paper (Chikanbanjar *et al*., 2020).

The Lokta plant, however, begins to dry out and decompose if the stem is not cut off once it reaches maturity. Therefore, to use it as a raw material, the stem must be removed during the harvesting season. In the high-elevation Himalayan forests, evergreen Lokta bushes can be seen in open clusters or colonies. Furthermore, this amazing plant only grows in moist places between an altitude of 1600-4000 m above sea level. These small, woody Lokta shrubs, also known as Baruwa or Kaagte Paat, can grow as tall as 7 feet. Overall, Lokta is a wonderful resource for Nepal, with a wide range of applications (Biggs & Messerschmidt, 2005b)**.**

1.8 Nanocomposite

Nanocomposite is a new class of reinforced material formed by the dispersion of nanoparticles throughout a polymer matrix. It consists of two phases, an organic polymer matrix embedded with inorganic particles in the nanometer range (size typically in the range from 1-100 nm). Nanoparticles are composed of a broad range of components such as polymers, metals, and metal oxides and have captured significant attention due to their diverse applications across physics, chemistry, biology, pharmacy, and material science driven by their ability to produce novel nanocomposites. Nanocomposites have superior properties compared to their components, including increased strength, toughness, and conductivity, as well as improved resistance to corrosion (Vinyas *et al*., 2019).

Recently, the idea of using natural cellulosic fibers as a substrate to fabricate nanocomposite materials has gotten much attention due to the increased applications in several fields including biomedical and bio-engineering. The use of natural cellulosic fibers in nanocomposite fabrication possesses several advantages because these manufactured nanocomposites are biodegradable, renewable, and less toxic. Nanocomposite materials can be fabricated utilizing several metals (silver, zinc, and copper) and their metal oxides (zinc oxides, silver oxides, and copper oxides) nanoparticles. In the metal category, Silver (Ag) nanoparticles are mostly studied and utilized components with a wide range of applications. Among metal oxide nanoparticles, Zinc oxide nanoparticles are extensively studied nanoparticles due to their improved stability, self-life, and promising antibacterial activity. Several studies have shown that ZnO-Ag coated nanocomposite materials fabricated by combining Ag nanoparticles with ZnO nanostructures can exhibit enhanced synergistic antimicrobial properties (Mohapatra *et al*., 2023; Saravanadevi *et al*., 2022).

Many efforts have been made for the fabrication of nanocomposite material using cellulose fibre as a starting material. Cellulose fibers can be utilized for the manufacture of cellulose mat or paper which acts as a scaffold for the attachment of nanoparticles in it. This supporting material provides mechanical support, a biodegradable environment and porosity to the nanocomposite. Furthermore, the use of cellulosic matrix mat in the synthesis of ZnO-Ag nanocomposite provides a novel alternative to the traditional synthetic approach. Nanocomposite can be fabricated by soaking paper or cellulosic mat in a solution of silver nitrate and zinc nitrate followed by heating as a result of which ZnO-

Ag nanoparticles are incorporated on the surface of cellulosic mat. In this research, high-strength fiber from the tradition Lokta plant (*Daphne bholua*) has been utilized for the fabrication of cellulosic mat which is later dropped into the solutions of silver nitrate and zinc oxide in the synthesis of Ag-ZnO / cellulose nanocomposite material.

1.9 Rationale

Synthetic plastic/fiber-based materials either degrade very slowly and remain in the environment for a long time (i.e. persistent material). In this respect, these materials cause environmental pollution at different levels. There is a need to find an alternate material that is easily available (abundant), can be processed easily, and is environmentally friendly.

From a material standpoint, a natural fiber obtained from Lokta bushes is the least studied material. The proposed research aims to extract and characterize the physical and mechanical properties of fibers, optimize the Lokta paper-making process, and explore novel applications of cellulosic fiber.

The research will help to find the best processing parameters for Lokta paper making. This will help to boost the quality of Lokta paper and its trade value. Additionally, this research will help to find new applications of Lokta fiber which will eventually increase the trade value. In these respects, the findings of this research will directly or indirectly help to promote the Local Lokta paper-making industries.

1.10 Research questions

- How the mechanical properties of cellulosic fiber obtained from lokta bushes is different as compare to other commonly studied counterparts (for example jute fiber)?
- How do the processing parameters change the quality of cellulosic fiber?
- How a Lokta paper having optimal properties (high mechanical strength, low water absorbency and low density) can be prepared?
- Will the nano-composite mat fabricated from Lokta fiber biomass show antimicrobial properties?

1.11 Objectives

The *broad objectives* of the research were to study the material properties of Lokta paper sheets and alkali-retted Lokta fiber, and explore next-generation applications of the Lokta paper.

The *specific objectives* were as listed.

- To measure the physical and chemical properties of the Lokta paper samples gathered from the local enterprises.
- To explore the microscopic details of Lokta paper samples to understand observed differences in several properties.
- To explore the material properties of alkali-retted Lokta fiber.
- To fabricate Lokta paper in laboratory settings and measure its major properties.
- To fabricate Lokta paper-derived nanocomposite mat by hydrothermal doping of ZnO-Ag and Cu nanoparticles.
- To study the antimicrobial properties of the nanocomposite mat.

1.12 Organization of the thesis

This dissertation contains five chapters (I-V), ruling out references and appendices. The chapter I explains the contexts, rationale, research questions, objectives, and thesis organization. Chapters II-IV show the major achievements of this dissertation and is arranged as an introduction, materials and methods, result and discussions.

Chapter II reports the detail study on the material properties of Lokta paper samples gathered for local firms. Chapter III reports material properties of alkali retted Lokta fiber, and chapter IV reports the material properties of Lokta paper fabricated in laboratory settings and the fabrication of nanocomposite mat.

The findings of all the study with some of the important future recommendation is provided in chapter V.

CHAPTER 2

Material Properties of Traditional Handmade Paper Samples Fabricated from Cellulosic Fiber of Lokta Bushes

2.1 Introduction

The history of handmade papermaking is very old as it has been practiced around the world since 105 A.D. utilizing locally available bushes (Hubbe & Bowden, 2009). In Nepal, traditional handmade papermaking is believed to have emerged from the western district of Baglung in the 12th century A.D. This traditional craft making is still popular with families in Baglung and the nearby Parbat district (Biggs & Messerschmidt, 2005b). The handmade paper (HNP) of Nepal is known as Lokta paper, commonly known as *Nepali kagaj*. The fibrous biomass of plants like Argeli (*Edgeworthia gardneri*) and Lokta (*Daphne bholua* and *Daphne Papyracea*) or their mixtures are used to make Lokta paper. This evergreen plant species is found at an altitude of 1600–4000 m from the sea level (Banjara, G., 2007; ITC, 2017; Poudyal, 2004). HNP is mostly used in holy literature and for keeping official records since it is considered a strong, mold- and bug-resistant paper. Furthermore, HNP is used to manufacture a variety of high-value items, including paper jewelry, gift bags and boxes, photo albums, and notebooks. The manufacture of handmade paper has been able to open up employment opportunities to approximately 5,000 families as many small and medium-sized paper-making enterprises started producing paper and paper-based products in Nepal with annual sell value of ~$2.5 to ~ 5.5 million (ITC, 2017). Handmade papermaking begins with harvesting the suitable plant stalks and manually removing the outer scaly bark followed by chopping the long fibrous biomass into small pieces. The waste remains are washed out after the pieces are soaked in cold water for about 6-12 hours. Next, the biomass necessary for making the paper is boiled in water or ash solution for around 5−10 hours which makes it soft and spongy. The weakened fiber biomass is beaten into pulp and mixed with water to obtain a slurry. Finally, a paper sheet is obtained after the slurry is drained and air-dried in a standard wooden frame. In recent years, literature has shown that 4-5% hot alkali treatment for 3-5 hours gives better promising results than ash solution or traditional hot water digestion in paper making. Additional stages like chemical bleaching and machine glazing are carried out according

on the needs of the customer. If necessary, the paper can be dyed with conventional plant-based or synthetic dyes. When compared to the procedure used to make commercial paper, traditional HNP production uses little to no chemicals and consumes less energy (Banjara, G., 2007; ITC, 2017).

Paper sheets and other paper-based materials are made from plant components that are both woody and non-woody using a mechanical and chemical and combination of both procedures. The strength of the paper sheet is affected by parameters, including the length and strength of individual fiber and their aspect ratio, the degree of crosslinking and bonding, the degree of fibrillation, and the level of fines and crill content in the paper. Longer fibers can create more contact points than shorter fibers, ultimately resulting in stronger paper. However, Long fibers increase the likelihood of fiber entanglement and floc formation (Beghello, 1998; Hubbe, 1999). Furthermore, fiber aspect ratio, surface morphology, and chemical composition of fiber also change paper properties (Johansson, 2011). Therefore, it is crucial to know about the material properties at sub-microscopic levels so that it can determine the final characteristics of a paper sheet.

Understanding HNP's material qualities at microscopic to submicroscopic scales is crucial for enhancing the product's quality and developing fresh novel applications. Although HNP synthesized from Lokta bushes is thought to be long-lasting and unaffected by molds and bugs, the literature lacks information about material properties in this paper. In this study, the mechanical, chemical, physical, and optical properties of ten handmade paper samples gathered from Nepalese paper industries were systematically investigated. The results are compared with those from other sorts of publications, and a correlation between various parameters is shown. Finally, a few recommendations and strategies are proposed in this paper to improve the quality of hand-made paper.

2.2 Materials and Methods

Ten different handmade Nepali paper samples were gathered directly from local paper manufacturers. The papers were indicated as P1–P10. From these ten different paper samples, a total of 20 different paper samples (60×100 cm) were prepared and kept in the dark in closed container without access to atmospheric air until experiments were conducted.

The inner fibrous bark of Lokta plants was harvested from the Baglung District of Nepal and used to make raw lokta fiber. The biomass of the Lokta fiber was air-dried and utilized for further research after the exterior scaly bark had been manually removed. We purchased all the chemicals for the investigation from Thermo Fisher Scientific India Pvt. Ltd, and they were all used with no additional refinement. Double distilled water having pH = 7.1 ± 0.1 and conductivity 5 ± 1 μS was used for making all the reagents used in the experiments.

2.2.1 Measurement of physical properties

A high-precision digital thickness micrometer (Hans Schmidt, D2000C) was used to determine the thickness (caliper) of a paper sheet (TAPPI, 1997). Six separate measurements were taken in different spots on the paper sheet. The TAPPI-410 method (TAPPI, 2012a) was used to resolve the basic weight, or grammage of the Lokta paper samples at 23 °C temperature and 50% relative humidity (RH) under standard conditions. In brief, a 500 cm^2 piece of paper was made circular by cutting it with a circular cutter, and its weight (0.001g) was measured to obtain the grammage (g/m^2). Each sample underwent six separate measurements. Grammage (g/m^2) was divided by thickness (m) to get apparent density (g/cm^3).

About 2.000 g of Lokta paper sample, conditioned at 23°C and 50% RH, was kept in an oven (105±2^{o}C) for 24 hours to determine the moisture content under ambient conditions. The sample was weighed after cooling in a non-hygroscopic desiccator.

Using the standard Cobb size tester, the Cobb 60 value was determined for non-bibulous paper using the TAPPI-T441 method (TAPPI, 2012b). By rolling the hand roller (10 kg) one forward and one backward without applying further pressure, more water from the wet specimen was eliminated. Cobb 60 value was evaluated by taking the difference between the weight of the paper after and before wetting.

A standard brightness-opacity tester (UEC1018, India) was used to measure the paper's opacity and brightness (ISO brightness). To determine the optical characteristics, five paper specimens with a 5 mm by 5 mm size were cut and placed in the tester.

A tensile strength was measured at 23 °C and 50% relative humidity. About 10 different paper specimens were obtained and cut at 15×25 mm size for each paper. A ratio of the

paper's tensile strength (measured in N/m) and its basic weight or grammage (measured in g/m^2) gave its the tensile index (Nm/g).

2.2.2 Determination of chemical composition

For the quantification of cellulose, Lignin, hemicellulose, and ash composition of the Lokta paper samples, the Gravimetric method following standard procedure was used (Ayeni *et al*., 2015; Boopathi *et al*., 2012b; Das *et al*., 2014b; Kandel, Menuka Adhikari, *et al*., 2022a). 1.000 g of cellulose that had been oven-dried at 105°C for four hours and kept in a non-hygroscopic desiccator was reacted with 5% NaOH (w/v) for five hours (fiber to solution w/w ratio: 1:30). After cooling the product was neutralized with 10% H_2SO_4. The leftover biomass was washed repeatedly several times and dried at 105°C to achieve constant weight. The cellulose content was determined by taking the weight differences.

Lignin content was determined by treating 1.000 g of extractive-free paper sample for two hours with 72% H_2SO_4 (sample to acid ratio 1:12.5 w/v) with careful shaking. After repeated dilutions and washing, the top content was eliminated and the residue was filtered. Filtered residue was then dehydrated at around one hundred degrees to achieve consistent weight.

For the determination of hemicellulose, 1.000 g of an extractive-free paper sample was boiled for 4 hours in 0.5 M NaOH solution. After multiple washing with distilled water, the content was neutralized, and dried at around one hundred degrees until a constant weight was achieved.

Ash content was calculated in percentage by taking the weight difference. For the calculation, 1.000 g of moisture-free paper sample was kept in an electric muffle furnace and burnt at 550±10 °C.

2.2.3 XRD, SEM, and FTIR measurement

An X-ray diffractometer (Rigaku, UK) was used to acquire X-ray diffraction (XRD) data in the 2θ range of 5–40^o at the scan rate of 0.25^o/sec and step size of 0.05^o.

A field emission microscope (JEOL, FESEM) was used to gather scanning electron microscopic (SEM) pictures. 4–6 SEM pictures were taken at 100–5000X magnifications for each sample. A free program (ImageJ, NIH, USA) was used to measure the fiber width. FTIR spectra were collected in ATR mode in the range of 4000-400 cm^{-1}.

The conceptual framework or basic idea of this research is summarized in **Figure 12.**

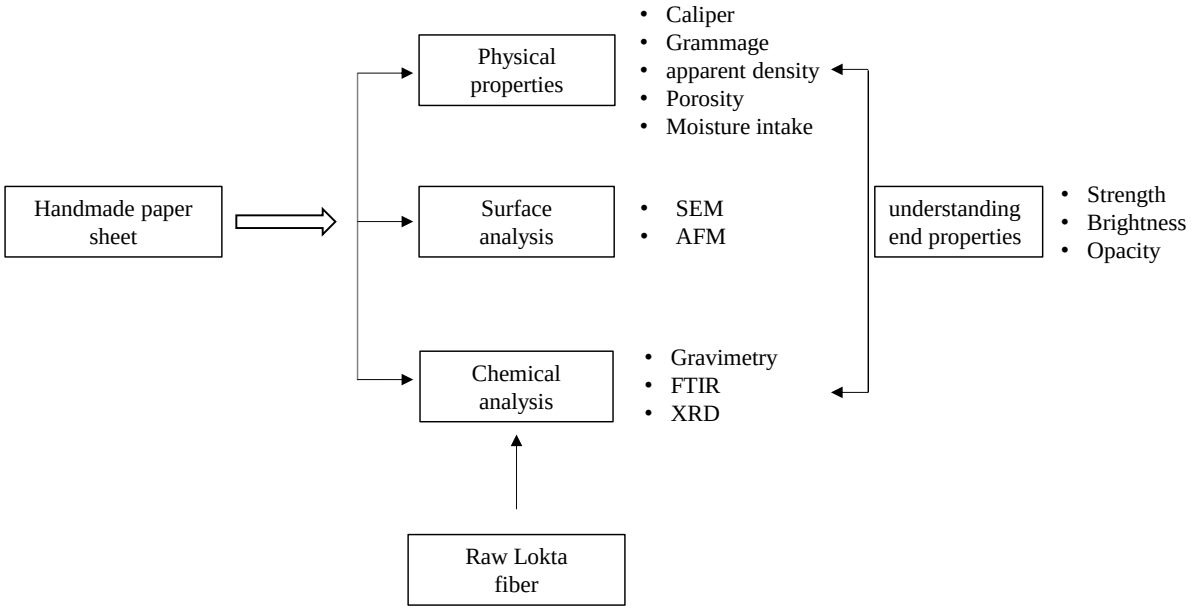

Figure 12: Schematic diagram showing the conceptual workflow of this research

2.3 Results and Discussion

2.3.1 Basic physical properties

Table 2 contains the list of all the fundamental physical characteristics of HNP samples. The mean thickness value (caliper) of paper samples varied in the range from ~90 µm (P9) to 675 µm (P8). Grammage varied similarly, from 20 g/m^2 (P9) to 150 (P3). These two metrics indicate a strong positive correlation (r=0.83). The vast variation of grammage indicates that these papers are designed for many purposes. Typically, paper sheets with a grammage of 50 or less are used for printing, and higher grammage paper is used to construct various value-added items.

Table 2: Different physical Properties of Lokta Paper Samples

paper	porosity (ε %)	caliper (μm), n = 6	apparent density (g/cm^3)	Cobb 60 (g/m^2), n = 5	moisture content (%), n = 3	grammage (g/m^2), n = 6
P1	83.5 ± 2.3	207.2 ± 26.4	0.25 ± 0.03	114.9 ± 14.0	4.3 ± 0.1	50.2 ± 2.4
P2	74.4 ± 1.9	196.5 ± 11.1	0.38 ± 0.03	154.2 ± 20.1	4.7 ± 0.3	74.7 ± 4.7
P3	77.1 ± 4.5	462.5 ± 55.1	0.34 ± 0.07	351.2 ± 14.0	5.3 ± 0.0	155.0 ± 11.7
P4	77.6 ± 0.8	143.2 ± 2.8	0.33 ± 0.01	96.4 ± 5.9	6.7 ± 0.8	47.7 ± 1.5
P5	88.8 ± 1.1	158.0 ± 10.7	0.17 ± 0.01	92.0 ± 9.1	5.8 ± 0.3	26.3 ± 1.9
P6	77.7 ± 3.8	166.0 ± 13.2	0.33 ± 0.02	128.5 ± 9.6	5.6 ± 1.2	54.6 ± 5.0
P7	68.4 ± 3.2	274.8 ± 24.2	0.47 ± 0.06	221.4 ± 10.4	6.±0.6	128.7 ± 5.3
P8	86.9 ± 1.8	674.0 ± 110.7	0.19 ± 0.05	411.4 ± 26.6	7.3 ± 0.4	128.9 ± 7.8
P9	86.8 ± 2.8	91.8 ± 11.4	0.20 ± 0.04	52.3 ± 4.6	5.9 ± 0.8	17.7 ± 2.4
P10	84.2 ± 0.7	122.3 ± 8.3	0.24 ± 0.01	63.1 ± 6.3	4.9 ± 0.5	28.7 ± 1.3

A digital micrometer with a 10 μm resolution was used to measure the caliper. The thickness of sample P1 varied from 180 to 254 μm (mean: 207.2±26.4μm). Since the paper thickness varies greatly, it can be inferred that HP samples have non-uniform thicknesses. Various chemical-mechanical methods are used for the processing of fiber, which primarily yields long fiber (<1 mm), typically used to create handmade paper samples. During the papermaking process, the long fibers have a high propensity to create flocs, which results in deviation in fiber thickness (Beghello, 1998; Lundell *et al*., 2011)

Additionally, we determined the apparent density (g/cm^3) of each sample of paper by dividing the grammage (g/m^2) by the thickness (μm). The volume of air or free space existing within the paper is included in the apparent density of the paper. As a result, apparent density is always less than true density. As shown in (Table 2), the apparent density of Lokta paper samples varied from ∼0.20 (P8 and P9) to 0.50 (P7) g/cm^3. According to reports, the apparent density of commercially accessible and machine-made paper sheets is greater (0.5–0.8 g/cm^3) in comparison to Lokta sheets (Bajpai, 2018b; ITC, 2017). HPs appear to be a lightweight paper based on their low apparent density.

From the known density of the paper network and cellulose, the apparent porosity associated with paper can be calculated (Henriksson *et al*., 2008; Sampson, 2004;

Tanpichai et al., 2012b, 2019b). The equation given below was used to calculate the paper's apparent porosity.

$$\varepsilon(\%) = \left[1 - \frac{\rho_{adp}}{\rho_{cf}}\right] \times 100 \quad \text{……………………………….. (1)}$$

Where, ρ_{cf} and ρ_{adp} are the density of cellulose fiber and the apparent density of paper network, respectively. For the calculation, 1.49 g/cm^3 was used as the density of cellulose fiber (Ehrnrooth, 1984). The apparent porosity ranged from 69% (P7) to 89% (P5). An ideal negative correlation (r = −1) was seen between apparent density and porosity. Low apparent density (high porosity) in paper is caused by long, stiff fibers, inadequate refining, a lack of fillers and fines, inadequate calendaring, and their combinations which may account for the low apparent density of handmade papers. A low apparent density, in the range 0.2 to 0.5 g/cm^3 was also noted in the lab-made handmade paper samples (Bajpai, 2018b; Marrakchi *et al*., 2011; Mejouyo *et al*., 2020; Obi Reddy *et al*., 2014a).

Table 3: Different mechanical and optical properties of all Lokta paper samples

	tensile index, Nm/g		tensile strength, KN/m				
Samples	CD	LD	CD	LD	Opacity	RBA	Brightness
P1	8.4±1.3	12.7±1.6	0.4±0.1	0.6±0.1	92.9±0.5	0.028	66.8±0.4
P2	25.4±0.5	27.4±1.1	1.9±0.0	2.05±0.1	97.1±0.4	0.069	61.9±0.7
P3	10.8±0.8	13.0±2.8	1.7±0.1	2.02±0.4	97.7±0.2	0.052	65.1±0.3
P4	12.1±1.6	15.9±0.5	0.6±0.1	0.7±0.0	95.3±0.4	0.054	62.7±0.5
P5	0.7±0.1	1.2±0.4	0.02±0.0	0.03±0.0	86.4±2.2	0.013	61.8±0.1
P6	16.9±0.9	18.3±1.2	1.08±0.1	1.2±0.1	95.4±0.4	0.052	63.8±0.7
P7	21.1±1.0	22.4±0.3	2.69±0.1	2.9±0.0	97.5±0.3	0.103	61.4±0.7
P8	9.7±0.9	11.7±0.4	1.25±0.1	1.5±0.0	97.8±0.4	0.017	55.6±0.3
P9	12.2±0.9	14.3±1.2	0.22±0.0	0.3±0.0	79.5±3.4	0.019	59.6±0.5
P10	11.4±0.8	15.2±1.1	0.34±0.0	0.4±0.0	87.4±1.7	0.027	66.9±0.4

The equilibrium moisture content (EMC) of experimental handmade paper samples ranged from approximately 4.3% (P1) to 7.3% (P8). (Bajpai, 2018b) reported similar moisture content levels for cellulose-based paper sheets. The parameter that is most frequently used to assess the capability of paper sheets to absorb water is the Cobb 60 value. Cobb 60

measures the weight or amount of water that one square meter of paper submerged in one centimeter of water can absorb in 60 seconds. The chemical composition of the fiber, its shape and structure, and its caliper all affect the Cobb value. The Cobb sizing examined in the paper samples ranged from ~50 (P9) to 410 g/m^2. Chemical compositions (given in **Table 4**) of paper samples and a slight variation in fiber organization and morphology (seen in SEM images in Figure 15) may be the causes of the wide variety in Cobb 60. A significant positive correlation exists with the thickness (r = +0.97) and grammage (r = +0.92) for a Cobb 60 value of HNP. It is probable that in an experiment, mechanical pressing with a 10 Kg roller would also be difficult for a paper that has greater thickness and porosity to remove retained water, resulting in a high Cobb 60 value.

Table 4: Chemical Composition Data for Raw Fiber and the Paper Samples

Samples	Hemicellulose (%)	Lignin (%)	Cellulose (%)	Ash (%)
P1	23.5 ± 4.0	3.9 ± 0.5	66 ± 1.7	7.8 ± 0.0
P2	25.9 ± 0.4	5.7 ± 0.2	67.4 ± 7.2	4.5 ± 0.7
P3	11.4 ± 3.0	2 ± 0.5	83.6 ± 6.5	3.5 ± 0.6
P4	11.3 ± 4.0	2 ± 0.7	81.7 ± 4.4	3.6 ± 0.5
P5	19.5 ± 1.4	9.8 ± 0.3	73.1 ± 2.8	7.7 ± 0.1
P6	12.1 ± 2.2	5.4 ± 0.5	80.4 ± 3.9	6.6 ± 0.4
P7	14.1 ± 1.7	7.5 ± 0.7	75.7 ± 3.8	3.5 ± 0.4
P8	20.8 ± 0.3	9.3 ± 1.5	71.4 ± 1.1	3.6 ± 0.1
P9	18.2 ± 1.0	7.4 ± 0.5	76.2 ± 1.8	7.1 ± 0.5
P10	13.7 ± 2.1	7.9 ± 1.3	75.7 ± 1.1	3.5 ± 0.6
Raw fiber	44 ± 1.0	19.2 ± 1.0	36.8 ± 1.0	2.6 ± 0.2

2.3.2 Optical properties

The two most crucial optical characteristics of paper are brightness and opacity. A yellowish piece of paper absorbs more light or reflects less light when illuminated with blue light. Therefore, more brightness is a sign of less yellowness in the paper. The degree of bleaching and surface smoothness affect the brightness of the paper sample. It has been reported that commercial printing paper can have ISO brightness levels as high as 100%

(Bajpai, 2018b). **Table 3** shows that the paper samples ranged from 56% (P8) to 67% (P1 and P10) in terms of brightness.

The amount of coloring impurities and lignin content, as well as tiny surface structures, are some of the factors that affect the brightness of paper and pulp samples (Bajpai, 2018b). HNP samples with somewhat lower brightness values may be the result of the pulping process using lower-quality water and chemicals, unbleached pulp, or both. A quite significant negative correlation (r = -0.51) was found between the lignin content and brightness data for the paper samples in **Tables 3** and **4**.

For double-sided printing, it is necessary to use high-opacity paper in order to study the texts on the front page without getting diverted by the presence of graphics or characters on the other side of the paper. High opacity results from small air gaps or pores in thick paper sheets reflecting more blue light (Bajpai, 2018b). The paper samples in our investigation ranged in opacity from ~83% (P9) to 98% (P2, P7, and P8) (**Table 3**). A moderately positive correlation (r = +0.68) between apparent density and opacity was discovered for our HNP sample.

2.3.3 Mechanical properties

The tensile index and tensile strength of paper samples were evaluated in two directions: across and along the length of the paper molds or wooden frame. These directions were labeled as CD and LD for easier comparison. In machine-made paper, these directions are known as cross direction (CD) and machine direction (MD). The tensile strength of paper samples varied from 0.02 to 2.7 kN/m across the CD and from 0.03 (P5) to 2.9 (P7) kN/m along the LD (as shown in **Table 3**). In the process of manufacturing handmade paper, the pulp is introduced to a rectangular wooden frame/ mesh of paper molds size 40 cm × 60 cm, placed over a pool of water, and the slurry is slowly disseminated by shaking the wooden frame along its length. This explains the observed strength differential in the two directions.

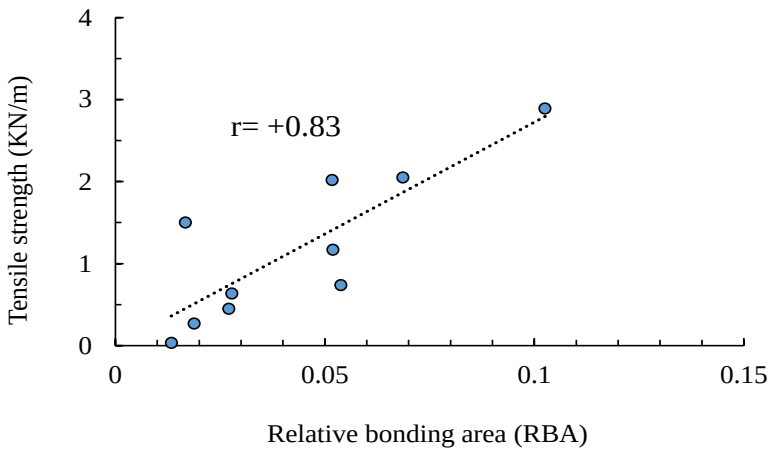

Figure 13: Tensile strength versus relative bonding area plot. The dotted line indicates the linear fit to the measured data

The maximum stress exerted per unit width (N/m or kN/m) of paper to break the paper strip is referred to as tensile strength. A paper sheet can be subjected to varying degrees of stress during printing and other uses such as the manufacture of gummed paper tape. In such instances, a paper with poor tensile strength can cause web-breaking (Bajpai, 2018b). HNP samples examined here have comparatively high tensile strength, indicating that web breakage is less likely to occur during printing.

The tensile strength index i.e., grammage normalized tensile strength, was also measured along the CD and LD axes. The tensile index of the paper samples ranged from 0.7 (P5) to 25.4 (P2) Nm/g and 1.2 (P5) to 27.5 (P2) Nm/g along the CD and LD, respectively (Table 3). The LD values are considerably greater than the CD values ($p < 0.05$) in all samples, with a mean CD: LD ratio of 2 (P7):1.1 (P7). This suggests that the fiber orientation is varied in two directions. In machine-made paper, an MD/CD ratio of ∼1.5−5 is observed (Bajpai, 2018b). According to this observation, fiber orientation in handmade paper is lower than in machine-made paper.

The tensile strength of paper crafts is affected by several parameters, including individual fiber length, fiber strength, and fiber-to-fiber bonding and contact. When a paper sheet is considered as a multi-layered composite structure comprising two-dimensional fibrous networks that are not interwound between layers, the relative bonding area (RBA) of a

paper sheet can be used to determine the degree of contact between layers (Sampson, 2004; Soszyński, 1995). RBA can be established using the data on fractional porosity (ε) and the number of fiber layers (*n*), which is the ratio of caliper to fiber diameter (Sampson, 2004). In order to estimate RBA, a fiber with a diameter of 10 μm was employed. **Table 3** contains the RBA values for each paper sample. In order to estimate RBA, a fiber with a diameter of 10 μm was employed.

The tensile strength of a fiber sheet shows a direct relation with relative bonding area for fibers with the same cross-section perimeter, coarseness, length, and bonding strength (Page, 1969; Tao & Liu, 2011). The fact that the fiber morphology (length, width, and coarseness) is identical in the paper samples examined here is supported by the microscopy photographs displayed in the later section. Surprisingly, In **Table 3**, RBA values and measured tensile strength indicated a quite strong positive correlation (r = +0.83, shown in **Figure 13**). The highest and lowest tensile strength readings for P7 and P5, might be attributed to the highest and lowest RBA values respectively, taking into account the discussion from above. The variation in fiber-to-fiber bonding strength may be caused by the different chemical compositions (**Table 4**).

2.3.4 Chemical analysis

The cellulose, hemicellulose, lignin, and ash content mean values (n = 3) ranged from ~66 to 84, 11 to 26, 2 to 10, and 3 to 8%; respectively. Raw Lokta fiber indicated a considerably higher quantity of cellulose (~37%), lignin (~19%), and hemicellulose (~44%), as compared to paper samples. Lignin and hemicellulose are partially eliminated during the processing of fibers, which increases the amount of cellulose content (Hashim *et al.*, 2017b; Kandel, Menuka Adhikari, *et al*., 2022a). This explains the reason behind higher cellulose content while less lignin and hemicellulose content in the paper samples. The variations in fiber processing or the usage of various fiber types in the paper samples could also be the reason for the differences in chemical makeup.

2.3.5 FTIR and XRD study

Figure 14A displays the FTIR data for both paper samples and the Lokta fiber. The spectra have a similar shape but have somewhat different relative peak intensities. We assigned the spectral bands based on information from the literature (Åkerholm *et al*., 2004; Kondo

& Sawatari, 1996; Poletto *et al*., 2014b; Tanpichai *et al*., 2019b; Xu *et al*., 2013). The O-H stretching of cellulose is responsible for the broad peak in the region of 3000–3600 cm^{-1} (with three weak peaks/shoulders). The aliphatic C-H stretching vibration in hemicellulose and cellulose is the source of the faint peak at ~2900 cm^{-1} (Poletto *et al*., 2014b). The ester C=O or acetyl or groups of lignin or hemicellulose give rise to the peak at 1735 cm^{-1} and the peak at 1630 cm^{-1} results from the conjugated lignin with C=O stretching vibration (Haque *et al*., 2009b; Tanpichai *et al*., 2019b). The raw Lokta fiber has these peaks at a significantly higher strength. This finding indicated that hemicellulose and lignin are partially eliminated during pulping. The weak peak at 1250 cm^{-1} is caused by acetyl groups in cellulose and hemicellulose being stretched along the C-O axis (Sinha & Rout, 2008b). The peak is weaker in paper samples, indicating that hemicellulose has been eliminated during fiber processing to make paper. These findings match with the chemical analysis results shown in Table 4.

Interestingly, in all paper samples and raw fiber the distinctive peaks of amorphous cellulose (weak peak ~660 cm^{-1} and a weak broad shoulder ~3420 cm^{-1}), and crystalline cellulose I_β (weak peaks at ~710 and 3270 cm^{-1}) are observed (Åkerholm *et al*., 2004; Kondo & Sawatari, 1996; Sassi *et al*., 2000; Sugiyama *et al*., 1991). The distinctive features for I_α, claimed to be ~3240 and 750 cm^{-1}, were not present in all of the samples (Sassi *et al*., 2000). I_α and I_β forms of cellulose are compositionally reported to be species-dependent and I_α could change to I_β form during pulping due to its meta-stability. The latter possibility could be ruled out because I_α peaks aren't present in the raw fiber.

In order to determine the hydrogen bond intensity (HBI) in samples made of cellulose, the absorption intensity ratio of several IR bands is used (Kljun *et al*., 2011; Oh *et al.*, 2005; Poletto *et al*., 2012; Xiao *et al*., 2014). Water content and structural flexibility are both correlated with hydrogen bond intensity. In fact, increase in HBI decreases crystallinity (Kljun *et al*., 2011). HBI was determined by taking the absorption ratio of bands at ~1320 and 3336 cm^{-1} (A3336/A1320) (Oh *et al*., 2005; Poletto *et al.*, 2012).

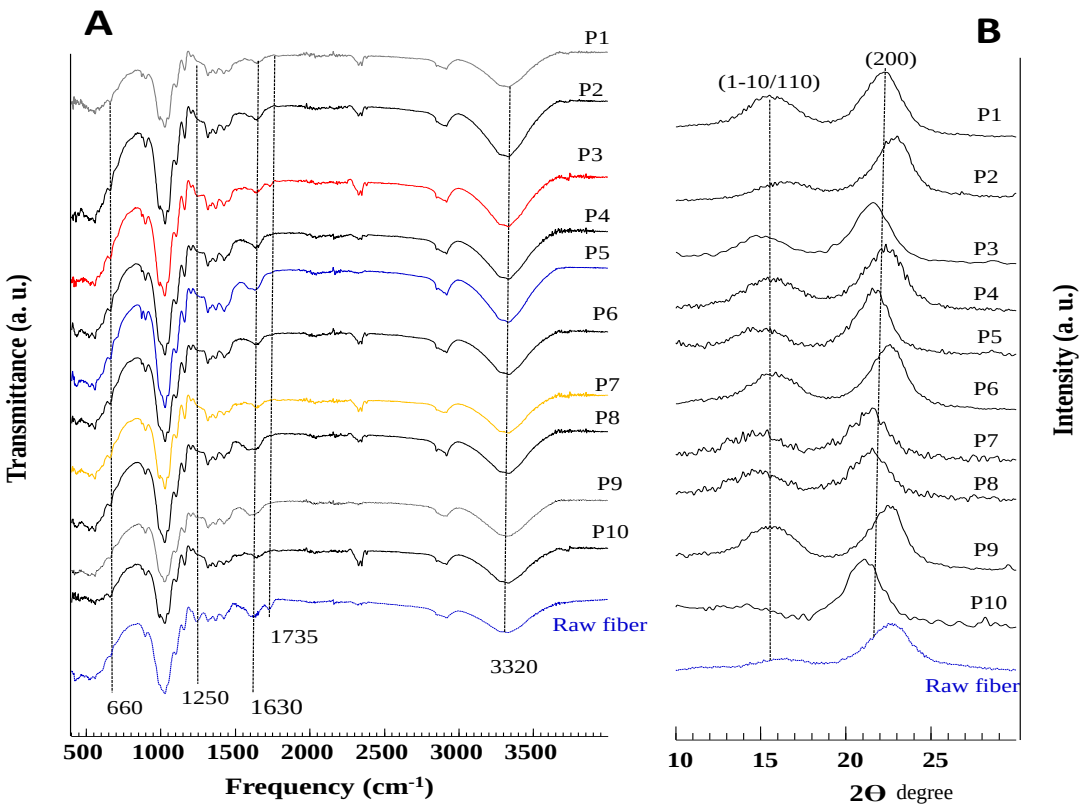

Figure 14: FTIR and XRD data. (A) FTIR data of paper samples measured as P1−P10 and raw fiber. For easy comparison, spectra are vertically overlaid. The dotted vertical lines indicate important peaks. (B) XRD data of ten paper samples. Reflection planes at 2θ values of ~15.5 and 21.5° are indicated in parenthesis. Spectra are vertically overlaid vertically for easy comparison.

In **Table 5**, the data range for HBI can be observed. The nature of fiber and the fiber-processing parameters affect HBI. The observed variations in HBI in the samples are therefore not unexpected. For several cellulose samples, HBI in the range of 1.4–1.8 has been recorded.

All of the paper samples and raw fiber were also subjected to XRD measurements (**Figure 14B**). The peak at 2θ values of ~15.5° and ~21.5 originates from (1−10/110) and (200) planes of crystalline phase cellulose I, respectively. (Park *et al*., 2010b; Saha *et al.*, 2010b). The amorphous phase is responsible for the broad background that lies behind the peaks (Park *et al*., 2010b; Segal *et al*., 1959). On the basis of equation given below, we also calculated the crystallinity index (CI) from XRD data.

$$CI = \left(\frac{A_t - A_{am}}{A_t} \right) \times 100 \ldots\ldots\ldots\ldots\ldots\ldots\ldots\ldots (2)$$

Where A_{am} is the intensity of amorphous phases only and A_t is the integrated intensity of both crystalline and amorphous phases. Gaussian fitting in the 2θ range of 10−30° was done to calculate *At*, A_{am}, and CI. The CI in the paper samples ranged from ~62 to 85% whereas it was found to be 58.5% for the raw fiber sample (**Table 5**). The variations seen in samples P1–P10 are explained by the CI, which relies on the resource of the cellulose biomass and the processing settings. When a fiber is exposed to alkali during the paper-making process, lignin gets removed from the interfibrillar region, which causes the cellulose chain to reorganize and improves the crystallinity index (Park *et al*., 2010b; Saha *et al*., 2010b).This clarifies that all paper samples have greater crystallinity indices than raw fiber. For reference, in several cellulosic samples, CI is achieved in the range of 20–97% (Kljun *et al*., 2011; Oh *et al*., 2005; Poletto *et al*., 2012). Additionally, we discovered a strong negative connection (r = -0.83) between HBI and CI. This finding is consistent with the literature review (Kljun *et al*., 2011).

Table 5: CI and Hydrogen Bonding Intensity (HBI) of the Paper Samples

Parameters	P1	P2	P3	P4	P5	P6	P7	P8	P9	P10
CI	70.7	65.4	72.9	62.4	83.8	72.6	62.2	70.2	83.6	84.5
HBI	1.48	1.52	1.33	1.38	1.21	1.5	1.52	1.34	1.22	1.19

2.3.6 SEM imaging of the paper samples

Figure 16A-J shows representative SEM images of the Lokta paper samples. In the photographs, individual fibers are randomly positioned to create interwoven networks. A strong paper sheet can be obtained in the presence of long and interconnected fibers. Images of paper samples P1, P2, and P10 (**Figures 16A**, **B**, and **J**) reveal a few fibers that are fibrillated, damaged, and curled, obtained due to the chemical and mechanical \ forces during fiber processing and paper making.

Fiber width is a crucial indicator to measure the strength and integrity of a paper sheet. A paper sheet with a significant portion of collapsed fibers is supposed to be weaker (Bajpai,

2018b; Johansson, 2011). In each of our samples, the fiber width was assessed. The mean, lowest, and highest fiber width values were determined to be in the range of 9 and 11, 4 and 6, and 18 and 26 μm, respectively, based on 100 measurements in each sample. In all of the samples, the average width distribution of fiber was statistically insignificant ($p < 0.05$). For instance, **Figure 15A** shows the distribution of fiber width in sample P3. Some fibers may experience lumen or cell wall collapse during fiber processing. Such fibers can have a higher apparent width (Aryal, *et al*., 2021; Hubbe, 1999). Additionally, some of the fibers might not be dispersed or can stay connected forming a bundle, which could have a high apparent breadth. This reasoning helps to explain the enormous apparent width (≥20 μm) that was obtained in some of the fibers.

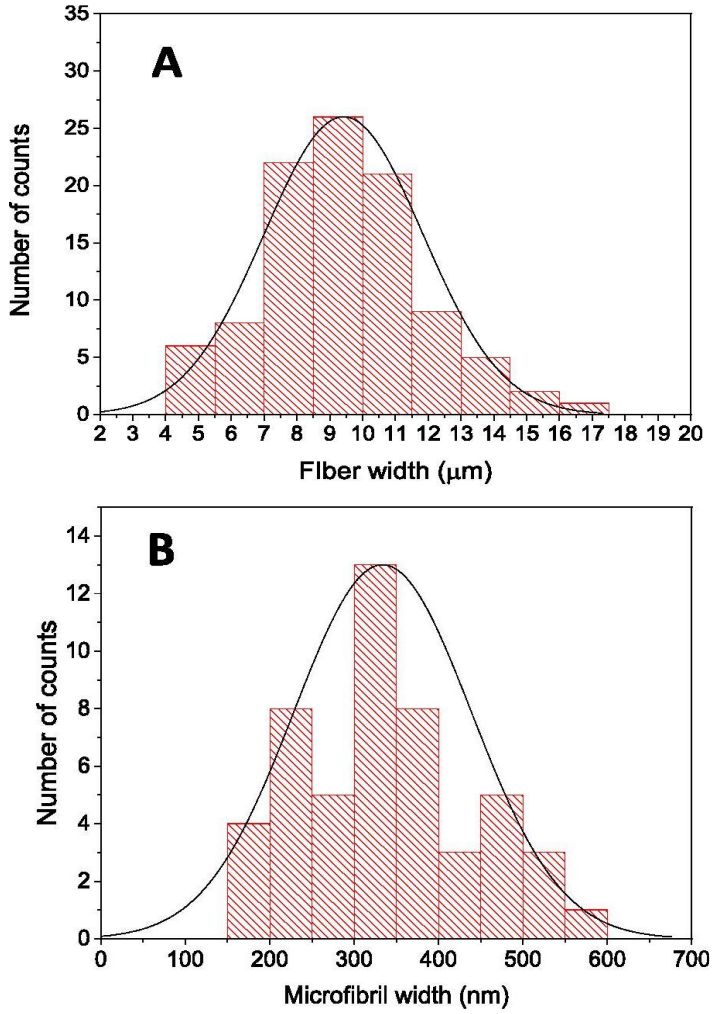

Figure 15: Distribution of fiber and microfibril width (A) Fiber width (n = 100) and (B) microfibril width distribution in P3 (n = 50). In both figures, normal distribution curve is shown in solid lines.

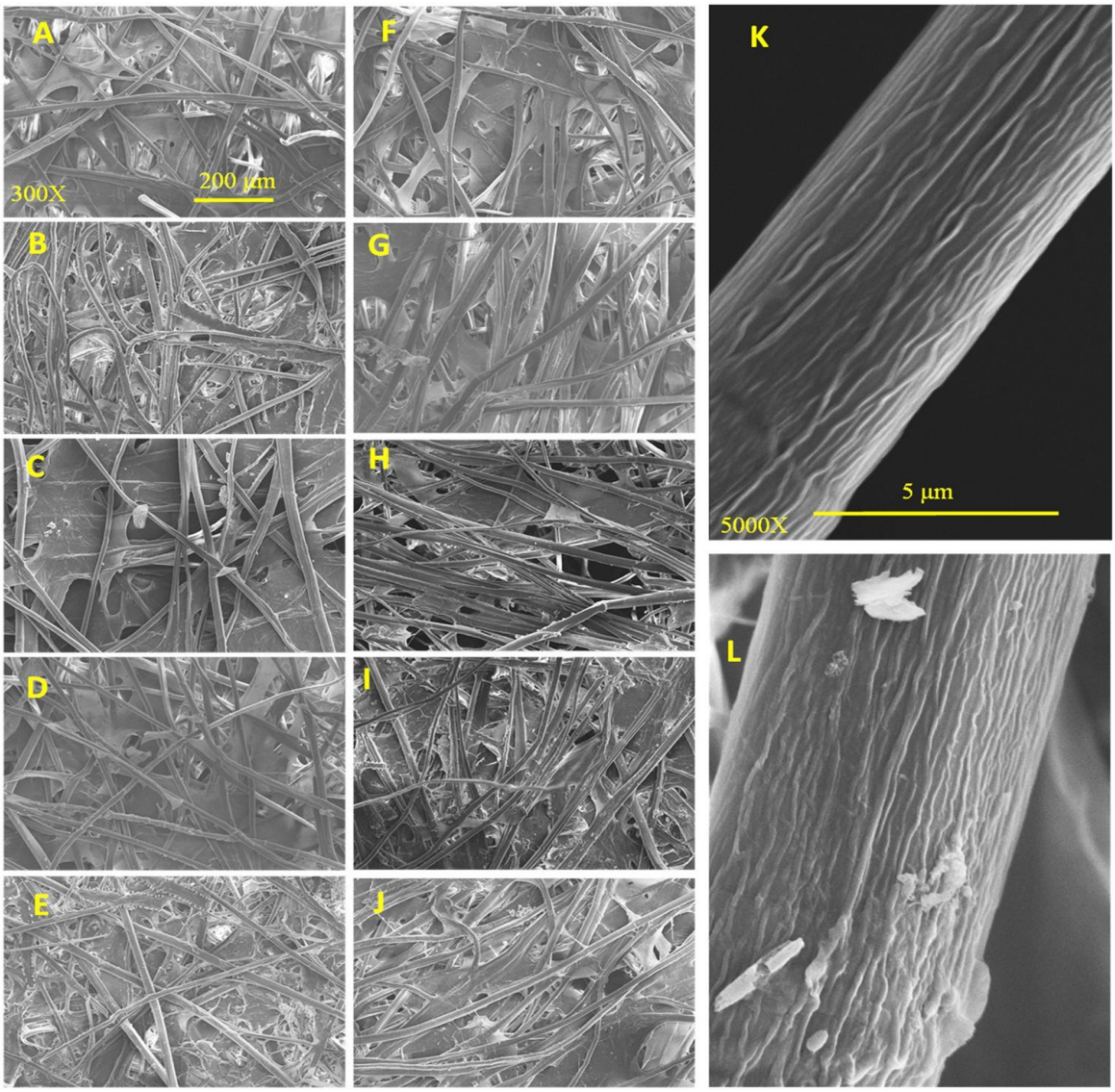

Figure 16: SEM images of the P1-P10 (fames A-J) paper samples measured at 300X magnification. K and L are the Images of individual fibers taken at 5000X magnification.

In **Figure 16K, L**, a zoomed-in view of a single fiber is shown. It's fascinating to observe individual microfibrils that are almost parallel to the lengths of fiber. We observed that the samples have mean microfibril widths ranging from 250 to 450 nm (n = 50). For instance, **Figure 15B** indicates the width distribution profile of sample P3. The sticky substances like hemicellulose and lignin, washed out from the exterior of fiber during fiber processing have left the microfibrils visible. The microfibrils are arranged almost parallelly in **Figure 16K, L**, which gives both the fiber web and individual fibers great strength.

The roughness of the fiber surface influences the tensile strength of the paper sheet. The increased fiber−fiber bonding and strength can be attributed to microscopic or even sub-microscopic structures and roughness found at the individual fiber level (Johansson, 2011). We performed AFM imaging on a specifically selected specimen, the thinnest sample, known as "P9" (as shown in **Figure 17A-D**), for our better understanding. The images clearly revealed surface roughness and microfibrils, with a roughness of around ±700 nm (**Figure 17D**). The height profile was obtained from the scale given in the figures. It is contact mode. These structures could possibly contribute to the strength of the paper.

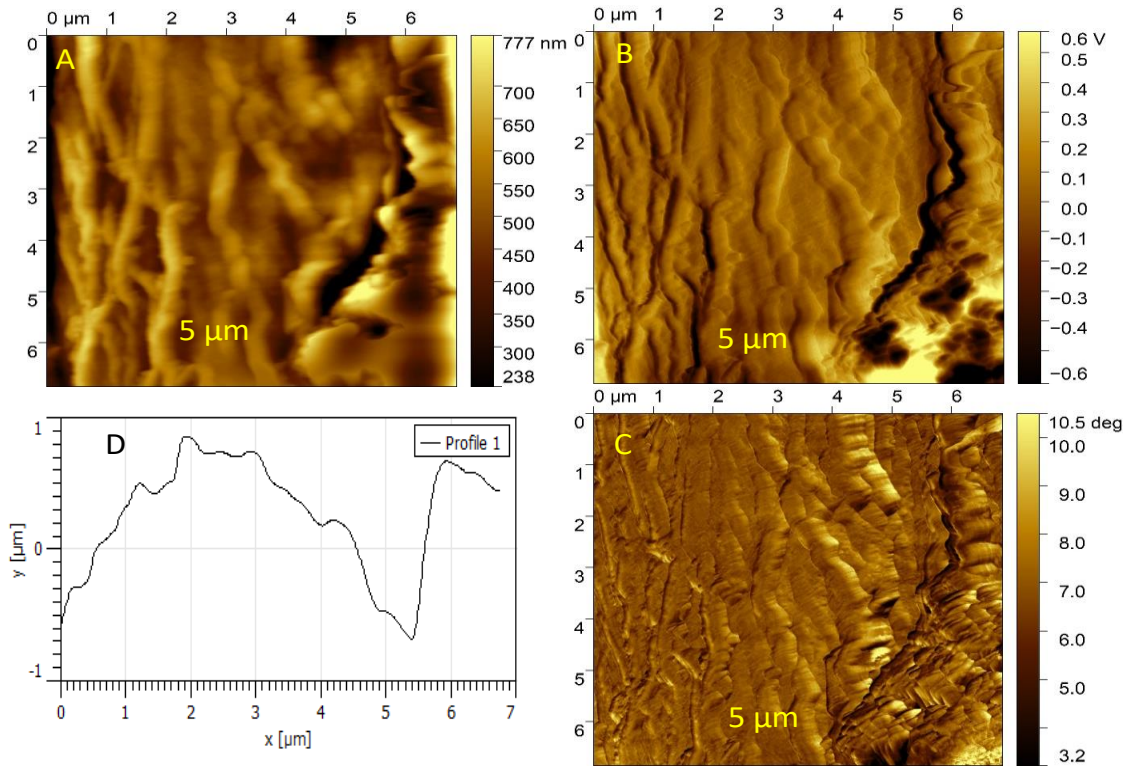

Figure 17: AFM topography (A), amplitude (B), and phase phase (C) images of small regions with a cellulose fiber and profile (D) along the line labeled in (A)

2.3.7 Further Implications of the Research

This study is largely focused on exploring the material properties of Handmade Papers at the sub-microscopic level and understanding how these properties influence the differences observed in mechanical and optical characteristics. The Lokta paper samples exhibited varying thickness, low apparent density (high porosity), and low brightness. To enhance these properties for handmade paper industries, eco-friendly and cost-effective approaches can be explored. Using locally isolated microbial cultures for enzymatic bleaching could increase brightness. Additionally, employing a locally designed handmade machine for calendaring the paper sheet can address issues of high porosity and thickness variation.

In the future, Lokta fiber-derived handmade paper could be the basis for creating valuable nanomaterials, like nano cellulose, antimicrobial cellulose film, and micro/ Nano-composites for chemical sensing and filtering applications (Abral *et al*., 2020; Beckermann & Pickering, 2008; Dufresne, 2008b; Ilyas *et al*., 2017, 2018, 2019; Samy *et al*., 2022).

2.4 Conclusion

In summary, we analyzed 10 Nepali handmade paper samples and studied their physical and chemical properties. These papers had a mean caliper of 90 to 700 μm, grammage of 50 to 150 g/m^2, and apparent density of 0.2 to 0.4 g/cm^3. The tensile strength, tensile index, and optical brightness varied from 30 to 2900 N/m, 1 to 27 Nm/g, and 56 to 67%, respectively. The paper showed higher tensile strength along the length direction compared to the cross direction indicating that Handmade Paper possesses the characteristics of lightweight paper, having medium to high tensile strength but intermediate yellowness. The handmade paper exhibited characteristics of both amorphous and crystalline cellulose phase which is depicted in XRD and FTIR data. SEM micrographs displayed interconnected networks of long cellulose fibers, with microfibrils arranged almost parallel on the fiber surfaces.

CHAPTER 3

Material Properties of Alkali Treated Lokta Fiber

3.1 Introduction

In the past few decades, there has been increasing curiosity in harnessing plant-based lignocellulose biomass derived from various natural sources as a workable substitute to synthetic fibers. The shift toward these natural source-based materials is driven by several compelling advantages compared to synthetic ones, including being lightweight, flexible, greater specific strength, biodegradable, and readily available in abundance. Natural fiber-reinforced materials are under intense investigation as a highly promising alternative to traditional materials in various industries, including healthcare, textiles, agriculture, and the automobile sector (Amara *et al*., 2021; Camargo *et al*., 2009; Chandrasekar *et al*., 2017a; Dufresne, 2008a; Jagadeesh *et al*., 2022; W. Liu *et al*., 2020; Lobo *et al*., 2021; Sanjay *et al*., 2018; Shavandi *et al*., 2020; Vinod *et al*., 2020). In plant cell walls, semi-crystalline cellulose microfibrils are enclosed strongly in a matrix of hemicellulose and lignin with varying compositions (Bismarck *et al*., 2005a; Kandel, *et al*., 2022b; Ververis *et al*., 2004). Thus, the raw fiber is a crucial component in composite material.

The source from where fiber is obtained and several processing methodologies utilized, influence the quality of fiber. Various factors in the processing stage play a vital role. These factors involve the type of chemicals used in retting and their concentrations, the temperature at which processing occurs, and the duration of treatment. When it comes to assessing the quality of a fiber bundle, several key parameters come into play. These include the size of microfibrils (tiny structural units within the fibre), the angles or orientation of these microfibrils, crystallinity, and the chemical composition (Fu & Lauke, 1996; Park *et al*., 2010a; Tanpichai *et al*., 2012a).

When fiber undergoes alkali treatment, it eliminates cementing materials like lignin and hemicellulose. This process leads to the partial or complete separation of fiber bundles, reducing their width while increasing their aspect ratio which in turn makes pulping easier for materials like paper, cardboard and composites. Under optimized processing conditions, fibers undergo significant enhancements in their end properties, including improved water resistance, thermal stability, and mechanical strength. For instance, NaOH

retting is reported to increase the tensile strength and thermal stability of *Neuropeltis acuminates* liana, *Megaphrynium macrostachyum*, Kenaf, Alfa, and banana fibers (Betené *et al*., 2023; Borchani *et al*., 2015a; Hashim *et al*., 2017c; Obame *et al*., 2022; Vardhini *et al*., 2019). When natural fiber is intended to be utilized for a cellulose-polymer composite, treating it with alkali or mercerization results in the creation of mercerized cellulose structure. This alteration, like changing fiber-OH to fiber-ONa^+, enhances the binding capability with polymer (Chandrasekar *et al*., 2017b).

There has been active investigation of natural fibers obtained from different plant and bacterial species by the global research community (Km. Arafat *et al*., 2018; Aryal, Ware, *et al*., 2021; Aryal *et al*., 2022; Elanthikkal *et al*., 2010; Haque *et al*., 2009a; Harwood *et al*., 2004; Kandel, *et al*., 2022a; W. Liu *et al*., 2020; Obi Reddy *et al*., 2014b; Tanpichai *et al*., 2019a). The study primarily revolves around four key areas: extraction methods, physio-chemical properties, physio-mechanical characteristics, and thermo-mechanical processes. Moreover, there is growing interest in harnessing these fibers, particularly in the creation of eco-friendly composite materials, aiming to create sustainable solutions across several sectors. (Bismarck *et al*., 2005b; Camargo *et al*., 2009; Jabbari *et al*., 2022; Sitotaw *et al*., 2021; Tanpichai et al., 2022; Torres *et al*., 2019).

Only a few studies have been done on natural fibers that come from plants species like *Daphne bholua* and *Daphne papyracea*, locally as "Lokta bushes." These bushes can be found in different districts of Nepal and other parts of Asia, typically thriving at altitudes between 1600 and 4000 meters. In Nepal, bast fibers obtained from Lokta bushes serve multiple practical purposes from crafting handmade Lokta paper to the creation of packaging and wrapping materials. The handmade Lokta paper, in particular, has a rich history and finds its way into several important applications. Additionally, Lokta paper is trusted for official documents, stationery, greeting cards, and decorative products, where its natural and rustic charm is highly appreciated (Aryal *et al*., 2022; Banjara, 2007; Biggs & Messerschmidt, 2005a; GoN, 2017). To increase understanding into the potential uses of materials derived from Lokta fiber, it is fundamental to inspect how the properties of the fiber are altered through various processing conditions.

This research involved the utilization of raw fibrous biomass obtained from Lokta bushes, subjecting it to treatments with sodium hydroxide (NaOH) solutions ranging from 1-9%.

The goal was to carefully assess how this treatment affects fiber quality. A systematic approach was employed to measure and document these changes.

Additionally, the critical material characteristics of both the untreated and alkali-retted samples were investigated encompassing parameters such as the effective width of fiber bundles, crystallinity levels, and thermal stability. To achieve this, a combination of techniques was used.

Furthermore, the variation in end properties of the fiber such as tensile strength, thermal stability, and water absorptivity under varying retting conditions were examined and the findings were systematically compared with existing data on other types of fibers documented in the literature.

3.2 Materials and Methods

3.2.1 Extraction and alkaline treatment of fibers

A fully matured stem of the Lokta plant measuring ~45 cm long and 1.5 cm diameter, sourced from Annapurna municipality, Myagdi, Nepal, was cut and brought to the laboratory (**Figures 18A** and **B**). The stems were soaked in distilled water for 60 minutes. The raw form of fiber bundles from Lokta bush was obtained by mechanically peeling the bark region of the stem (area b, **Figure 18C)** and removing both the outer cuticular layer (area a, **Figure 18C**) using a stainless-steel knife. The fiber bundles underwent a washing process with distilled water to wash out the surface dirt and were subsequently sun-dried to eliminate moisture (**Figure 18D**).

Subsequently, the extracted raw Lokta fiber (4-5cm long and 0.5-1.5mm wide) underwent treatment with sodium hydroxide (NaOH) solutions at different concentrations: 1%, 3%, 6%, and 9% (w/v) at room temperature (24±1 °C) for a fixed duration of 1 hour. After the treatment process, the biomass was thoroughly cleaned by tap water, typically requiring 2-3 wash cycles. Neutralization was achieved using diluted hydrochloric acid (HCl) solution at a concentration of 0.1 N. The residual chemicals present were removed by rinsing 4 to 5 times with distilled water. Subsequently, the treated material was dehydrated in a hot air oven set at 90±2°C for a period of 24 hours. The effectiveness of the retting process was assessed by calculating the % weight loss or the retting efficiency (ε) using the equation:

$$\varepsilon = \left(\frac{W_1 - W_2}{W_1}\right) * 100 \qquad \ldots\ldots\ldots\ldots\ldots\ldots\ldots\ldots (3).$$

where, W1 and W2 are the initial and final mass of the fiber, respectively.

3.2.2 Determination of biomass composition and water absorption

The percentage of cellulose, lignin, hemicellulose, extractives, and ash composition were determined in both water-retted and alkali-retted fibers based on procedures reported in existing literature, with minor modifications to suit the study (Adeeyo *et al*., 2015a; Boopathi *et al*., 2012a; Das *et al*., 2014a; Kandel, *et al*., 2022a). For each of the components, triplicate measurements were made and the mean and standard deviations (mean ± SD) were calculated. The percentage composition (χ) of each individual component was as:

$$\chi = \left(\frac{a - b}{a}\right) * 100 \qquad \ldots\ldots\ldots\ldots\ldots\ldots\ldots\ldots (4).$$

where a and b are the initial and final dry weights of the biomass; respectively.

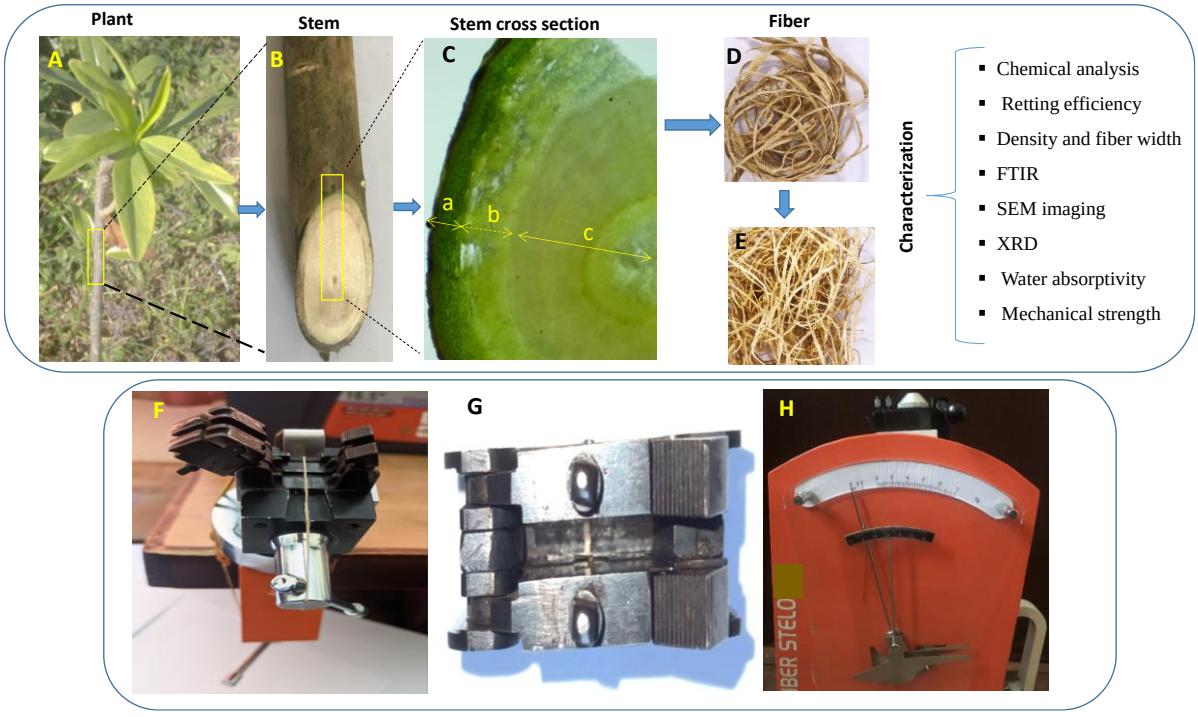

Figure 18: Experimental flow chart showing mechanical strength testing setup. (A) Lokta plant; (B) freshly chopped stem; (C) cross section of stem taken with a stereomicroscope: a= cuticular layer, b= bark region, c=woody region; (D) untreated fiber; (E) alkali treated fiber. (F) A thin fiber bundle ready to be placed in Pressley jaw, (G) fiber mounted in Pressley jaw, (H) front view of fiber bundle strength tester showing the % elongation (lower) and load (upper) scales.

3.2.3 Determination of extractives

2 grams of oven-dried raw fiber was kept in a Soxhlet extraction apparatus and mixed with 200 mL of 190-proof ethyl alcohol (95%). This mixture was then subjected to reflux for a period of 6 hours. The extracted solid material was separated and dried and its weight was noted.

3.2.4 Determination of cellulose

To determine cellulose content, the process began with 1.00 grams of oven-dried fiber, at around 90±2°C for 4 hours. The sample was then allowed to cool in a non-hygroscopic desiccator and treated by immersing in 5% NaOH (w/v) solution for the duration of 5 hours. During this step, a fiber-to-NaOH ratio of 1:30 (w/v) was maintained. The mixture was then cooled and neutralized using a ten percent (v/v) H_2SO_4 solution. The remaining biomass was thoroughly washed multiple times and then dried at ~ 90±2°C until consistent. The cellulose content was assessed using the initial and final weights.

3.2.5 Determination of Hemicellulose

To begin the process, an extractive-free fiber sample of weight 1.00 g was taken and boiled in 0.5 M NaOH for 4 hours. The boiled mixture was cleaned and neutralized repeatedly with distilled water to maintain contamination-free conditions. The sample was then dried at ~ 90±2 °C and weight was taken.

3.2.6 Determination of lignin

Acid insoluble lignin (Klason lignin) content was determined following the procedure as described in the literature (Adeeyo *et al*., 2015b; Boopathi *et al*., 2012c; Das *et al*., 2014c; Kandel, *et al*., 2022a).To begin the process, oven oven-dried and extractive free fiber sample (40-50 micron mesh size) of weight 1.00 grams was taken in a flask and subjected to digestion with 15 ml of 72% H_2SO_4. The content was stirred carefully for 3 hours at room temperature, and followed by boiling for 2 hours after adding approximately 200 ml distilled water. The content was carefully subjected to a crucible after it was cooled to room temperature. The residue underwent multiple washing until it became acid-free which is verified with litmus paper. Finally, the residue was dried in an oven at a temperature of 105 °C, until a constant weight was obtained. Both fibers and residual weight were used to obtain percentage lignin content.

3.2.7 Determination of equilibrium moisture content

In order to assess moisture content, 2.00 g of fiber sample, initially conditioned at approximately 23°C and 50% relative humidity, were put in an oven set to 90±2 °C for 24 hours. The fiber sample was then allowed to cool in a non-hygroscopic desiccator, and weight was measured. The moisture content was estimated based on the weight difference before and after drying.

3.2.8 Determination of water absorptivity

A constant weight of fiber bundle was submerged in 50 mL distilled water at room temperature (24±1 °C). The fiber was taken out at certain intervals and weight was measured. The process was repeated for the intended time period (0-12 days), and percentage weight gain was calculated from the weight difference (Espert *et al*., 2004; Kandel *et al*., 2023).

3.2.9 Determination of fiber density and width

The density of cellulose fiber was determined using the liquid Pyknometer method, also known as gravimetric method (Beakou *et al*., 2008; Truong *et al*., 2009). To prepare the fiber sample, it was first dried in a non-hygroscopic desiccator with $CaCl_2$ as a desiccant for 48 hours. The sample was then soaked in toluene for about 2 hours to remove the presence of any micro-bubbles, this process is known as impregnation. The fiber samples used to place in the pyknometer were cut into 5 mm lengths, and the density was subsequently calculated as (Beakou *et al*., 2008; Truong *et al*., 2009):

$$\rho = \frac{(m_2 - m_1)\rho_T}{(m_3 - m_1) - (m_4 - m_1)} \quad \text{..... (5)}$$

where, m_1, m_2, m_3, and m_4 are the weight of the unfilled pycnometer (in grams), pyknometer with fibers, pyknometer filled with toluene, and pyknometer filled with fiber and toluene solution; respectively, and ρ_T is density of toluene.

For the fiber width measurement, optical microscope images of fiber bundles were taken at 40X magnification using the Olympus SZ61 microscope. To ensure accuracy, the field of view was calibrated using a linear calibration grid with a high precision and a minimum division of 10 μm. Image analysis software (ImageJ, NIH, USA) was used to convert pixel

sizes to micrometers, providing data on fiber width. About thirty fiber samples were measured based on which mean width and other statistical parameters were reported.

3.2.10 Determination of Fiber Strength

In order to determine strength, Lokta fiber samples underwent preconditioning at a temperature of 23±2 °C and 65% RH and for 24 hours, following the ASTM test method (ASTM, 2004). For measuring the fiber bundle strength, a fiber bundle strength tester (TSI instrument) with the highest load capacity of 7 Kg was utilized. To maintain consistent measurement conditions, fiber bundles obtained from the identical region of the stem, ensuring uniform width (300–350 μm, as verified under a microscope) were loaded into Pressley Jaw apparatus of gauze length 15 mm. This assembly was then loaded to the tester and subjected to a constant loading speed of 1 Kg/sec until the fiber disintegrated into pieces. This arrangement was then inserted into the tester and subjected to a steady loading rate of 1 Kg/sec until the fiber fragmented into splits. The load at which the fiber bundles break and the corresponding percentage elongation were noted. Breaking tenacity (cN/tex) was calculated from the obtained quantities of fracturing load and bundle weight (0.0001g). Furthermore, tensile strength or stress was determined using **equation (6)** (Elmogahzy & Farag, 2018). Fifteen independent measurements were done and the data are reported as the mean values.

$$S = 10.d.T \quad \text{..... (6)}$$

Here, T is the tenacity (cN/tex), S is the tensile strength (MPa), and d is the material density in g cm^{-3}.

3.2.11 FTIR, XRD, SEM, TGA measurements

XRD data were calculated in the range of 5–50^{o} at the movement size of 0.02^{o} and a scan rate of 0.25^{o}/sec. The measurement was finished using a Rigaku X-ray diffractometer in the UK, utilizing Cu Kα line (λ=1.540A°) as the X-ray source.

Scanning electron microscope (SEM) images were taken at various magnifications via a JEOL JSM-6510LV scanning emission microscope. Before performing the SEM analysis, the samples were sputter-coated with gold (thickness ~ 5 nm).

IR spectra were recorded in ATR mode using an ABB Bomen Fourier transform infrared spectrometer (MB100, Canada). The spectral resolution, scan range, and number of scans were 4 cm^{-1}, 4000-400 cm^{-1}, and 100 scans, respectively.

Thermo gravimetric analysis (TGA) data were collected under a nitrogen atmosphere using a Perkin Elmer TGA-7 analyzer. The fiber size was ~ 3 mm long and 500 μm wide and the sample weight was ~ 10 mg. The analysis spanned a temperature range of 25-600 °C, with a heating range of 10°C/min. Balance accuracy and temperature precision were 0.1 μg and ± 2 °C respectively.

3.2.12 Statistical analysis

The collected data were entered into an Excel spreadsheet for analysis and the descriptive statistical parameters including mean, maximum, minimum, and standard deviations were calculated. In order to assess the significance of mean differences, a paired t-test was conducted at a 95% confidence interval, resulting in the calculation of p-values.

3.3 Results and Discussion

3.3.1 Weight loss and chemical composition

Retting efficiency ascertains the weight loss in lignocellulose biomass during alkali treatment. It varies with biomass type and retting conditions, including alkali concentration, treatment duration, and temperature (Hashim *et al*., 2017a; Kandel, *et al*., 2022a; Saha *et al*., 2010a). As anticipated, higher alkali concentrations correspond to increased % weight loss (**Figure 19A**). A strong positive correlation, as indicated by the Pearson correlation coefficient r = + 0.93 was found between % weight loss and alkali concentration. Alkali retting of fiber with 9% NaOH showed a maximum weight loss of 27.0±1.6%.

The elimination of non-cellulosic and binding materials from the lignocellulose biomass during alkali treatment results in weight loss of fiber. Considering this fact, extractive, Kalson lignin, hemicellulose, and cellulose content was measured in all dry or moisture-free samples.

Notably, a substantial loss in extractive content was evident in alkali-treated samples (**Figure 19B**). For instance, the 9% alkali treatment led to approximately 65% extractive loss, decreasing from 8.9±0.1% to 3.1±0.0%. In the alkali-treated samples, an extensive

decline in lignin and hemicellulose content (**Figures 19B** and **C**) was also observed. In 9% alkali-treated fiber, there was approximately a 51.2% reduction in lignin (from 14.3 to 7.0%) and a 32% reduction in hemicellulose (from 44% to 30%) content. The cellulose content in untreated samples and those treated with 1%, 3%, 6%, and 9% alkali solutions was determined to be 36.8 ± 1.0, 49.0 ± 1.0, 53.7 ± 1.0, 61.0 ± 1.0, and 61.0 ± 1.0, respectively. This indicates a notable rise in cellulose composition on alkali treatment (**Figure 19C**). The overall rise in cellulose content is credited to the combined reduction of hemicellulose, extractives, and lignin.

Similar trends of lignin and hemicellulose loss with the rise in NaOH strength and a corresponding increase in cellulose content have been reported in Alfa stem fiber (Borchani *et al*., 2015b), *M. oleifera* fruit fiber (Bharath *et al*., 2020), *Carica papaya* bark fibres (Saravanakumaar *et al*., 2018a), water hyacinth fiber (Sumrith *et al.*, 2020), and Sterculia fiber (Kandel, *et al*., 2022b) . This loss may be attributed to the disruption of specific bonds, such as hydrogen bonding between cellulose, hemicellulose, and lignin, resulting in partial solubility and subsequent removal of these components (Mwaikambo & Ansell, 2002).

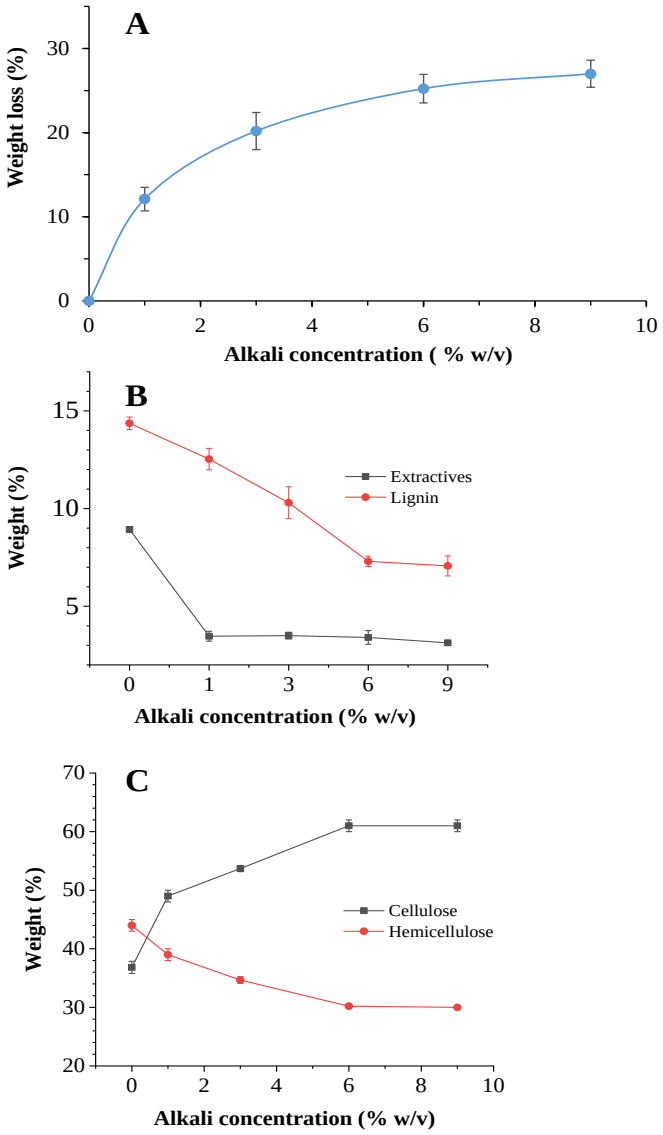

Figure 19: Chemical composition and retting efficiency. (A) Retting efficiency as a function of % weight and alkali concentration. (B) Extractive and lignin content measured as function of % weight and alkali concentration (C) Cellulose and hemicellulose content measured as function of % weight and alkali concentration

3.3.2 Moisture content, density, fiber width, and water absorptivity

Another notable change resulting from alkali treatment is the reduction in equilibrium moisture content. It was found that the increase in alkali concentration decreased the equilibrium moisture content (**Table 5**). There was approximately a 25% decrease in equilibrium moisture content (from 13.3% to 9.8%) with 9% NaOH treatment. This decline in wetness could be qualified to the removal of more hydrophilic components alike extractives and lignin from the fiber bundle. Other studies have also reported a noteworthy reduction in moisture content on alkali treatment. For instance, a 16.4% decrease (from 13.4% to 11.2%) was reported for banana fiber which was treated for 3 hours with 10% NaOH (Vardhini *et al*., 2019). Similarly, a ~40% decrease (from 9.7% to 5.8%) was observed in *Carica papaya* bark fibers cured with 5% NaOH for 1 hour (Saravanakumaar *et al*., 2018a).

There was a slight, gradual increment in the density of fiber with the intensification in alkali concentration (r= +0.96). For instance, in 9% alkali-treated sample, there was about 24% increase in density (from 1.11 to 1.38 g cm^{-3}) as shown in **Table 5**. Studies have reported that density tends to increase or decrease depending on alkali concentration and fiber type. One study on Kenaf and hemp fiber treated with alkali at or below 10% (w/v), reported an increase in density while another reported a decrease in density at alkali concentration below 10% (w/v) (Aziz & Ansell, 2004; Hashim *et al*., 2017a; Modibbo *et al*., 2009). In banana fiber treated with 10 and 15% alkali, an increase in density (~7-9%) was noticeable (Vardhini *et al*., 2019). The increment in density may be attributed to a decrease in low-density non-cellulosic components or the densification of cell walls. Conversely, density decrement could result from cell wall rupture leading to the depolymerization of cellulose chains (Hashim *et al*., 2017a; Vardhini *et al*., 2019). In this study, the increase in fiber density could be the result of loss of non-cellulosic components from Lokta fiber.

Table 5: Fiber width, density, and Moisture content

Sample type	Decrease in fiber Width (%)	Density (g/cm3)	Moisture content
9% treated	30.6±5.9	1.38±0.01	9.8±0.5
6% treated	25.8±5.2	1.23±0.01	10.4±0.4
3% treated	22.7±6.2	1.20±0.01	10.9±0.6
1% treated	18.6±3.9	1.17±0.01	11.2±0.1
untreated	-	1.11±0.00	13.3±0.2

Alkali treatment further causes a significant decrease in the effective fiber bundle width, primarily by reason of the loss of non-cellulosic factors from the fiber surface. (Hashim *et al*., 2017a; Kandel, *et al*., 2022a; Vardhini *et al.*, 2019). Alkali-treated Lokta fiber samples showed a significant reduction in fiber width (**Table 5**). The reduction of fiber width for 9%, 6%, 3%, and 1%, alkali-treated samples at 95% confidence interval was found to be 30.6±5.9%, 25.8±5.2%, 22.7±6.2%, and 18.6±3.9%; respectively.

The water absorptivity, expressed as a percentage weight gain, varied across different treatment conditions. For untreated, 9%, 6%, 3%, and 1% NaOH-treated fibers, it was found to be 506.2 ± 64.1%, 295.7 ± 42.9%, 296.0 ± 20.5%, 338.7 ± 25.4%, and 380.8 ± 32.8%, respectively (**Figure 20A**). When a cellulose fiber is dipped in water, the hydrogen bonds within the fiber chain break and new hydrogen bonds get formed involving the -OH groups in water molecules, causing a substantial increase in weight. However, alkali treatment removes the more hydrophilic components, leading to enhanced water resistance or reduced water absorptivity (Chandrasekar *et al*., 2017b). Remarkably, the data on % weight loss (shown in **Figure 19A**) and % weight gain (depicted in **Figure 20A**) exhibited a strong negative correlation, with a correlation coefficient r = -0.98. To provide a comprehensive view, water uptake kinetics curves for selected samples are shown in **Figure 20B**. These curves, typical for natural fibers, depict both rapid absorption (at short

immersion times) and slower water uptake (at longer immersion times) in all the samples (Beakou *et al*., 2008; Gouanvé *et al*., 2007; Kandel *et al*., 2023).

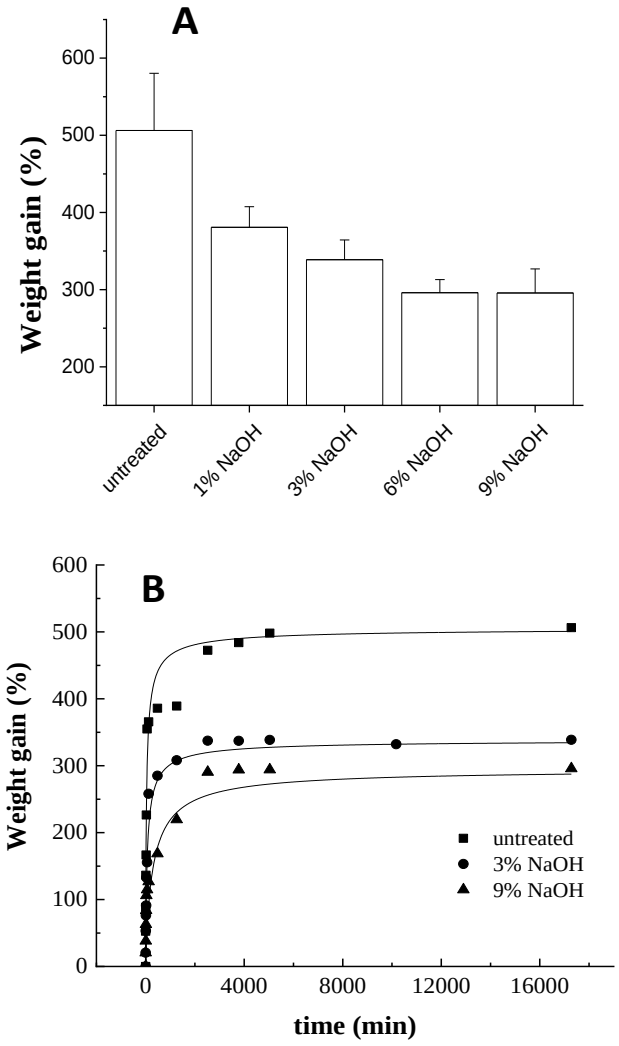

Figure 20: Equilibrium water absorption. (A) % weight gain for different samples measured after 12 days. The error bar denotes the standard deviation obtained from three independent samples. (B) Water absorption kinetics plot for 9%, and 3% NaOH- treated, and untreated samples.

Several studies have shown that water absorption, measured as % weight gain, is affected by chemical components of the fiber, the origin (plant source and fiber location), treatment conditions, and water composition. In the majority of studies, samples treated with alkali are reported to exhibit decreased weight gain or enhanced water resistance (Beakou *et al*.,

2008; Gouanvé *et al*., 2007; Kandel *et al*., 2023; Ramadevi *et al*., 2012). For instance, 2.5 times decrease in % weight gain (from 160% to 65%) was observed in 5% treated *Sterculia* fiber (Kandel *et al*., 2023), 1.3 times decrease (from approximately 850% to 630%) in 6% NaOH-treated Areca fiber (Begum *et al*., 2021), and 1.4 times decrease (from 200% to 140%) in 10% NaOH-treated abaca fiber (Ramadevi *et al*., 2012). Surprisingly, increased water absorption is also found in alkali-treated fibers. For instance, 6% NaOH-treated cotton exhibited a substantial 23 times increase (from 50% in untreated to 1160% in treated), and a 1.5 times increase was reported in pineapple fiber (from 200% in untreated to 300% in treated). The rationale behind this is that NaOH treatment causes the loss of a hydrophobic waxy layer, resulting in an increase in water uptake (Begum *et al*., 2021).

3.3.3 FTIR Study

The FTIR spectra of samples exhibited striking similarities, with minor variations in peak position, peak intensity, and shape (**Figure 21**). The hydrogen-bonded networks within cellulose and hemicellulose chains of fiber is responsible for the broad peaks with O-H stretching frequency in the range of 3000-36000 cm^{-1} (Saha *et al*., 2010a; Sinha & Rout, 2008a). In the alkali-treated samples, this band appears more symmetrical and narrower. This alteration may arise due to the disruption of hydrogen bonding between O-H groups in hemicellulose and cellulose, resulting from the partial loss of hemicellulose.

In FTIR spectra, a faint peak at 1730 cm^{-1} corresponds to ester or acetyl -C=O groups found in (non-conjugated) hemicellulose or lignin (Haque et al., 2009a; Tanpichai *et al.*, 2019a). Meanwhile, a distinctive peak at approximately 1260 cm^{-1} indicates C-O stretching related to the acetyl group present in hemicellulose and cellulose (Sinha & Rout, 2008a). These peaks exhibit reduced intensity in alkali-treated samples due to the loss of hemicellulose and lignin. As reported earlier, these spectral changes are consistent with weight loss data. Notably, a characteristic peak at around 1430 cm^{-1}, associated with $–CH_2$ bending vibration, remains unchanged in alkali-treated samples. The mechanical strength in alkali-treated fiber could be preserved due to the presence of intact cellulose content in the fiber (Saha *et al.*, 2010a; Sui *et al*., 2009).

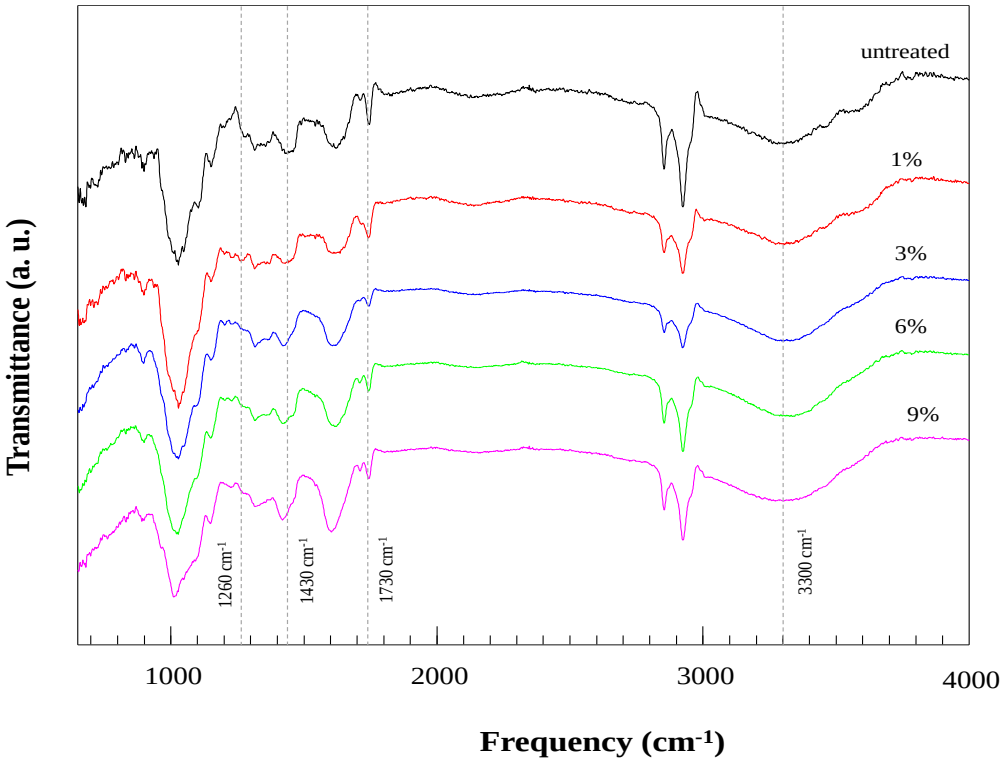

Figure 21: FTIR spectra of the Lokta fiber samples. Spectra are overlaid vertically for easy compassion. Peak positions of important frequency are represented in the dotted lines.

3.3.4 SEM imaging

The surface of untreated fiber samples appears to contain additional substances deposited on it (**Figure 22A**). These additional deposits likely consist of non-cellulosic materials such as hemicellulose, pectin, inorganic minerals, wax, and lignin. Surprisingly, in the alkali-treated samples, these surface impurities are effectively removed, leading to the effortless separation of individual fiber from fiber bundles. This kind of transformation aligns with weight loss observed in the retting study, the reduction in effective fiber bundle width, and the weakening of specific lignin and hemicellulose peaks observed in the FTIR spectra. Similar changes have been reported in the alkali retting of other fibers, including Hemp (H. Liu *et al.*, 2013), *Sterculia* (Kandel, *et al.*, 2022a), *Bauhinia* (Kandel *et al.*, 2023), Kenaf (Fiore *et al.*, 2015a), *M. oleifera* (Bharath *et al.*, 2020) fruit fibers, *Carica papaya* (Saravanakumaar *et al.*, 2018a) bark fibers (5% NaOH), and water hyacinth (Sumrith *et al.*, 2020) plant fiber. For instance, in case of 9% alkali-treated samples, the

mean width of individual fibers was found to be 15.4±6 µm, with a width range ranging from 4.8 to 31.5 µm. (**Figure 22E**) shows fiber width distribution in a histogram plot.

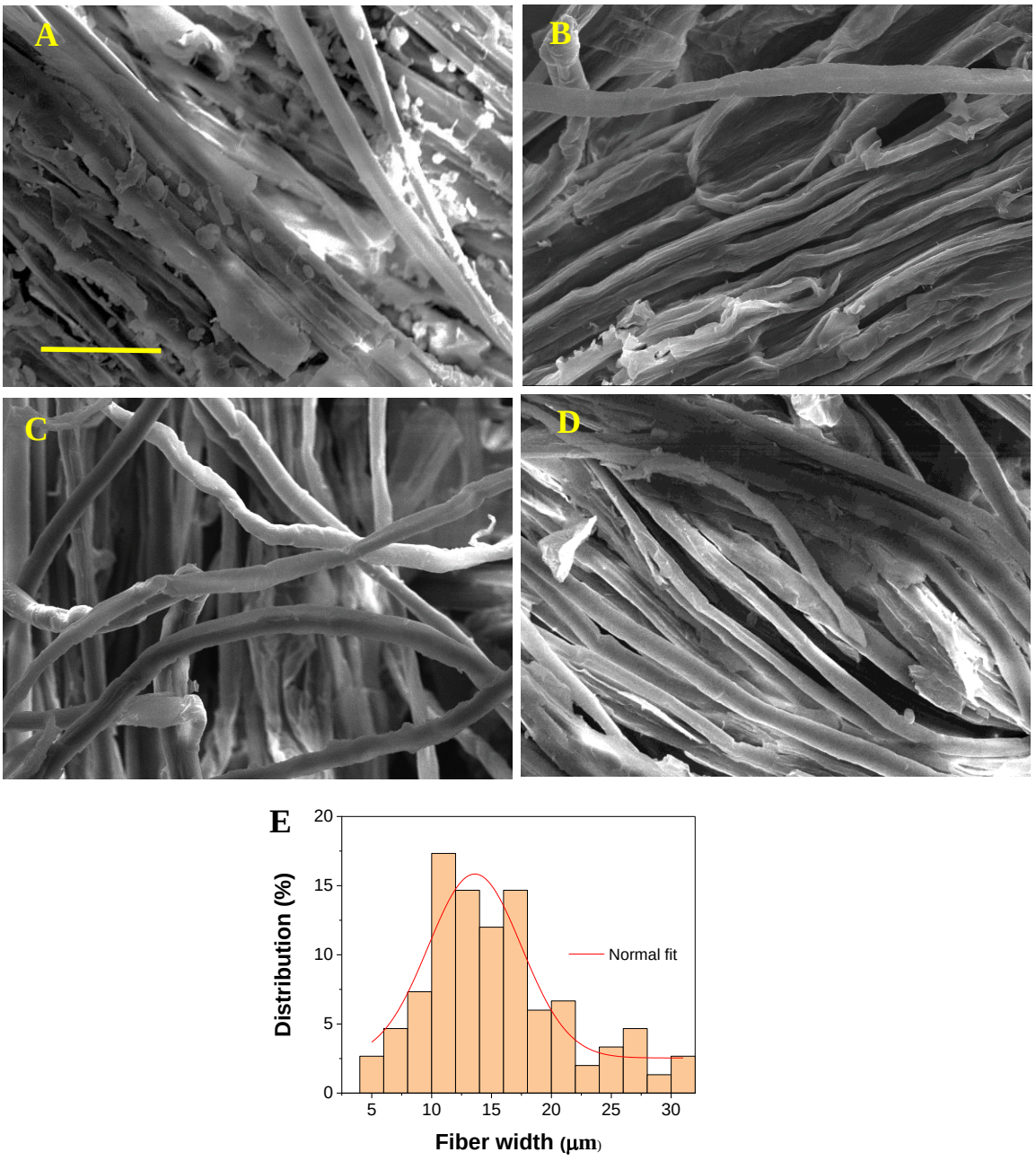

Figure 22: SEM images and data. (A), (B), (C), and (D) are representative SEM images for untreated, 3%, 6% and 9% treated fiber samples; respectively. A scale bar of 50 µm shown in A also applies for B, C, and D. (E) A histogram plot (n=150 and bin size 2 µm) with a Gaussian distribution fit (solid line) shows the fiber width distribution.

3.3.5 XRD study

The shape of XRD profiles of all fiber samples exhibits a characteristic pattern resembling typical lignocellulose fiber (**Figure 23**). Natural cellulose fibers inherently possess both crystalline and amorphous domains (French, 2020; Park *et al*., 2010a; Yao *et al*., 2020). Within the XRD profile, the diffraction peaks observed at 2θ value at ~16^o and ~13^o arise from crystalline planes (110) and (1-10), respectively. The most prominent peak at around 22.5^o originates from the (200) plane, while a less pronounced peak at approximately 35^o arises from the (004) planes of crystalline cellulose phase-I. In order to gain preliminary insights into the change in crystallinity resulting from alkali retting, Segal's Crystallinity index (CI) was calculated using **equation 7**.

$$CI = \left(\frac{I_{200}}{I_{200} + I_{am}} \right) \times 100 \quad \ldots\ldots\ldots\ldots\ldots\ldots\ldots\ldots \quad (7)$$

where, I_{am} and I_{200} are the intensities of the major amorphous profile and crystalline peak measured at 2θ values of ~18.2^o and ~22.5^o, respectively.

The Segal's crystallinity index (CI) was determined to be 73%, 76.2%, 78.5%, and 75.2% for untreated, 3%, 6%, and 9% alkali-treated samples respectively. This increase in CI can be attributed to the loss of amorphous components, particularly lignin and hemicellulose, primarily from the inter-fibrillar regions (Boopathi *et al*., 2012a, 2012a; Kandel, *et al*., 2022a; Park *et al*., 2010a; Saha *et al*., 2010a). The same reasoning can elucidate the increase in crystallinity index (CI) observed in alkali-treated samples. This phenomenon has been reported in various fiber types, including *Moringa oleifera* fruit fibers (Bharath *et al*., 2020), *Carica papaya* bark fibers (Saravanakumaar *et al*., 2018a), water hyacinth fiber (Sumrith *et al*., 2020), and *Sterculia* fiber (Kandel, *et al*., 2022b). The alkali treatment likely alters the fiber structure, removing impurities or modifying the fiber surface, thereby increasing the crystallinity index.

The crystallite size (D, nm) was determined using the Scherrer equation given below, utilizing the full width at half maximum parameter (β, in radians) associated with the most intense peak corresponding to the (200) plane (Cullity, 1978).

$$D = \frac{\kappa\lambda}{\beta\cos\theta} \quad \ldots\ldots\ldots\ldots\ldots\ldots\ldots\ldots \quad (8)$$

The calculation employed a κ factor of 0.94 and a wavelength (λ) of 0.154 nm. The results indicate that the crystallite size increased in both 3% and 6% by approximately 22%, and in 9% alkali treated samples by 14%.

The crystallite size generally increases with an increase in alkali treatment due to the removal of amorphous components (**Table 6**).

In addition, the inter-planar spacing (d_{200}) in the fiber samples was obtained by further analyzing the XRD data.

$$n\lambda = 2d200\ \sin\theta \quad \text{(9)}$$

In the calculation, θ was obtained from the peak position of d 200 (from XRD data), n = 1 (first-order diffraction), and λ of 0.154 nm was used. A slight expansion in inter-planar spacing (d_{200}) was observed in the alkali-treated samples, potentially attributed to the micro-strain present on the crystallite surface (Ioelovich, 2018; Sinha & Rout, 2008a).

Table 6: XRD parameters for Lokta fiber samples at different treatment conditions

Sample type	D (nm)	d_{200} (nm)	CI (%)	β (º)	2Θ (º)
9% treated	2.79	0.395	75.25	2.9	22.5
6% treated	3	0.396	78.5	2.7	22.4
3% treated	3	0.398	76.2	2.7	22.3
untreated	2.45	0.39	73	3.3	22.8

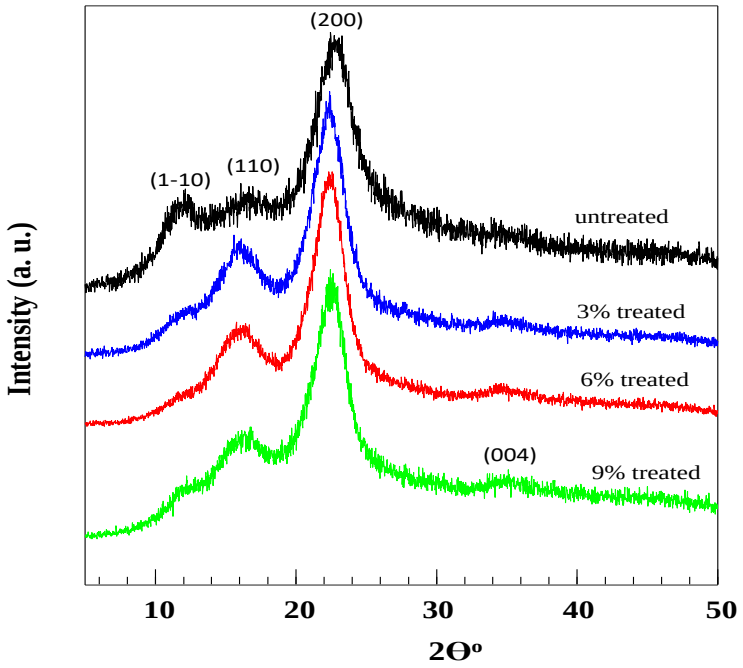

Figure 23: XRD data of untreated and alkali treated samples. For easy composition, data are overlaid vertically. The number within parentheses indicate the crystalline planes

3.3.6 Mechanical strength

The tensile strength (MPa) data for the fiber samples is visually presented in the form of a Box and Whisker plot (**Figure 24**). The tensile strength values for 9%, 6%, and 3% alkali treated and untreated samples were determined to be 249.3±32.2 MPa, 227.3±23.3 MPa, 305.5±44.0 MPa, and 219.9±24.2 MPa, respectively. The corresponding % elongation was found to be 8.0 ± 1.1, 8.0 ± 1.0, 7.0 ± 1.0, and 8.5 ± 1.4, respectively. This data clearly demonstrates a significant increase in tensile strength on alkali treatment ($p<0.01$). Studies have shown that the tensile strength on alkali-treated samples increases or decrease depending on treatment parameters and fiber type (Chandrasekar *et al.*, 2017a; Hashim *et al*., 2017a; H. Liu *et al*., 2013; Saha *et al*., 2010a).

The increase in tensile strength observed during alkali treatment can be attributed to the removal of hemicellulose and lignin from the inter-fibrillar regions which reduces the internal constrains within the cellulose chains, ultimately leading to higher tensile strength. This reasoning provides a plausible explanation for increased tensile strength as observed

in Lokta fiber. Furthermore, a slight decrease in tensile strength at higher alkali concentrations may be due to the formation of surface defects on the fiber.

Table 7: Comparison of mechanical properties

Fiber	Treatment conditions	Tensile strength (MPa)	Elongation (%)
Lokta fiber (This study)	9% NaOH, RT, 1 hour	249.3±32.2	6-9
Jute fiber (Saha *et al*., 2010a)	8% NaOH, RT, 1 hour	350±32.2	1-4
Carica papaya bark fibers (Saravanakumaar *et al*., 2018b)	5% NaOH, RT, 1 hour	548 ± 14.6	1.83 ± 0.04
Borassus fruit fiber (Boopathi *et al*., 2012a)	10% NaOH, RT, 0.5 hour	160	34
Prosopis juliflora bark fiber (Saravanakumar *et al*., 2013a)	Raw fiber	558± 13.4	1.77± 0.04
Cotton fiber (Seki *et al*., 2012)	variable	200-400	6-8
Coir (Seki *et al*., 2012)	variable	95-175	13.7-41
Flax (Seki *et al*., 2012)	-	500-1500	2.7-3.2
Bamboo fiber (Wong *et al*., 2010)	5% NaOH, RT, 24 hours	222± 14.6	15.2± 0.04

The mechanical properties of plant fibers depend on several parameters. However, not all studies provide detailed measurement parameters such as testing speed, fiber diameter or width, gauge length, and environmental conditions like temperature and humidity. In **Table 7**, a comparison is presented with a few selected studies that report very similar treatment conditions to the current study.

It is proposed that the percentage elongation increases with the microfibril angle (MFA) in fibers (Reddy & Yang, 2005; Saravanakumar *et al.*, 2013b). The MFA of natural fibers typically ranges from 3 to 50 degrees. For instance, cotton is reported to have an MFA of 20–30 degrees, resulting in a higher percentage elongation (6–8%) compared to flax fiber,

which has an elongation percentage of approximately 3% with an MFA of 10 degrees. Lokta fiber exhibits a very similar percentage elongation to cotton fiber, suggesting that its MFA could be similar as well.

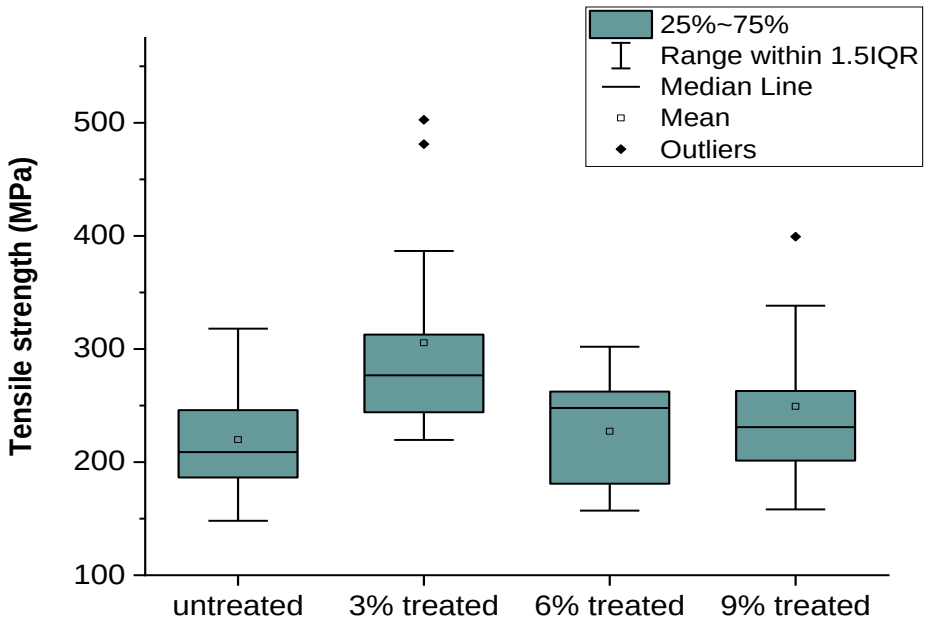

Figure 24: Tensile strength data for the Lokta fiber samples. Mean, inter-quartile range, and median values along with few outliers are shown as a box and Whisker plot for easy comparison.

3.3.7 Thermal analysis

The TGA (Thermo Gravimetric Analysis) data for the selected fiber samples are depicted in **Figure 25**, with the corresponding DTG (Differential Thermogravimetry) data shown in insets. In the TGA data, three distinct weight loss regions, one below 100°C, another between 175 °C and 400 °C and a third above 400 °C were observed as reported in lignocellulose biomass (Bharath *et al*., 2020; Poletto *et al*., 2014a; Saravanakumaar *et al*., 2018a; Sumrith *et al*., 2020). For easy comparison, **Table 8** represents the percentage weight loss data within various temperature ranges. In all samples, the initial weight loss occurring at temperatures below 100 °C can be attributed to the evaporation of volatile impurities and moisture. Minor variations in weight loss within this region may be

influenced by changes in crystallinity, disparities in chemical composition, and differences in equilibrium moisture content.

The weight in the range of 200-300 °C primarily results from hemicellulose degradation (Poletto *et al*., 2014a). This region is notably evident in the DTG plot, marked by the shoulder around 260 °C (**Figure 25** inset). Interestingly, this shoulder is sufficiently strong in the untreated lokta samples, indicating a higher hemicellulose content. This observation aligns with the findings from FTIR, SEM, and chemical analysis data reported in previous sections. The degradation of hemicellulose as compared to cellulose could be linked to its amorphous nature (H. Yang *et al*., 2006).

In the temperature range of 300-400 °C, the weight loss primarily results from the cleavage of glycosidic linkages in cellulose, appearing as a sharp peak in the DTG plot (H. Yang *et al*., 2006). The enhanced thermal stability of cellulose is attributed to its well-organized, long polymeric units. The maximum degradation temperatures were measured to be 325 °C for untreated samples, 343 °C for 6% treated samples, and 347 °C for 9% NaOH treated samples (**Table 8**). This indicates an increase in thermal stability linked to increased crystallinity and grain size resulting from the alkali treatment. An increase in thermal stability upon alkali treatment has been documented in various studies. For instance, an increase from 321.1 to 346.6 °C was observed in *Carica papaya* bark fibers (Saravanakumaar *et al*., 2018a) treated with 5% alkali for 1 hour at room temperature, and an increase from 321 to 332 °C was noted in 5% NaOH-treated *Sterculia* fibers (Kandel, *et al*., 2022a) subjected to 4 hours of treatment at 80 °C. These findings suggest that alkali-treated samples possess high thermal stability, making them suitable for use in composite materials.

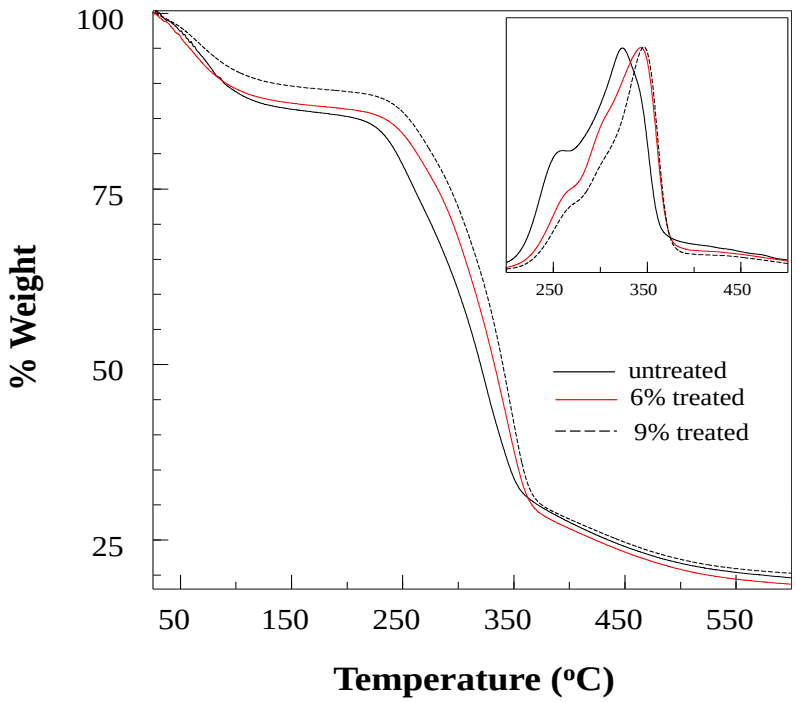

Figure 25: Thermal analysis data. The main frame shows the TGA data for untreated, 6% and 9% NaOH treated samples. The inset shows the corresponding DTG data

The degradation of lignin is reported to occur over a broad temperature range spanning from 200-600 °C. The wide range is due to the high molecular weight and cross-linked structure of lignin (Kim *et al*., 2006). Notably, the increased weight loss observed in the temperature range from 475-650°C in the untreated sample may be attributed to its excess lignin content.

The slight variance in residual mass left after heating could stem from differences in chemical composition and the presence of impurities, such as inorganic minerals. It has been observed that the residual mass at 600°C might increase or decrease after the alkali treatment. This phenomenon might be due to the loss of hemicellulose, allowing for the formation of a highly stable lignin–cellulose complex, which could lead to increased residual char in the alkali-treated sample (Ray *et al*., 2002). For instance, there has been observed a rise in residual char from 18.9% in the untreated sample to 19.7% in the 9% NaOH-treated sample. Residual mass around 600°C has been reported to vary across different fiber types. For example, around 40% was found in both alkali-treated and raw *Acacia planifrons* bark fibers (Senthamaraikannan *et al*., 2019), 30–40% in *Carica papaya*

bark fibers (Saravanakumaar *et al*., 2018a), 25–28% in *Sterculia* fiber (Kandel, *et al*., 2022b), 15–22% in jute fibers (Ray *et al*., 2002), 20–22% in Alfa stem fiber (Borchani et al., 2015a), and 30–32% in water hyacinth fibers (Sumrith *et al*., 2020). The decreased residual mass observed in Lokta fiber suggests it has minimal mineral impurities, indicating that the biomass may be easily processed for making biocomposite materials and paper materials.

Table 8: A summary of TGA data

Sample type	ΔT, ˚C	Mass loss, %	Degradation temperature, ˚C	Residual mass at 650 ˚C, %
Untreated	26-100	11	325	18.9
	100-275	20		
	275-375	40		
	375-650	11.3		
6% treated	26-100	10	343	18.0
	100-275	12.6		
	275-375	47.5		
	375-650	10.7		
9% treated	26-100	8	347	19.7
	100-275	9.5		
	275-375	50.2		
	375-650	9.8		

3.4 Conclusions

In summary, various material properties of 9%, 6%, 3%, and 1% NaOH-treated as well as untreated Lokta fiber samples were systematically investigated. Alkali treatment led to a significant reduction in lignin, extractives, and hemicellulose content, accompanied by a notable rise in cellulose content (from approximately 37% to 61% in the 9% NaOH-treated sample). The effective fiber width and equilibrium moisture content decreased significantly, while the fiber crystallinity index, thermal stability, and density, increased upon alkali treatment. These alterations were attributed to the loss of hemicellulose and lignin from the fiber bundle, as supported by evidence from SEM images and FTIR data. The tensile strength of treated and untreated was measured, revealing significant increases upon alkali treatment ($p<0.01$). Moreover, the maximum degradation temperature (T_{max}) increased from 325 °C in untreated samples to 343°C and 347°C in 6% and 9% NaOH-treated samples, respectively, indicating enhanced thermal stability. These findings hold significant implications for optimizing and understanding the characteristics of Lokta fiber-based composite materials and papers. Further insights into the mechanical properties of the fibers could be gained through experimental determination of tensile curves and fracture analysis. Additionally, future research could entail a systematic exploration of the material properties of Lokta fiber-derived paper and composite materials.

CHAPTER 4

Lokta fiber-derived nanocomposite mat for antimicrobial application

4.1 Introduction

A reinforced material composed by mixing tiny nanoparticles into a polymeric matrix is known as a nanocomposite. Nanoparticles are inorganic particles having dimensions in the nanometer range. Typically, nanoparticles have sizes ranging from 1 nm to 100 nm. A variety of materials are being used in manufacturing nanoparticles. The ability of nanomaterials to synthesize novel nanocomposite materials is the subject of interest nowadays due to increasing applications in the fields of physical, chemical, biological/biomedical, and material science.

The knowledge of nanomaterials for the improvement of human life and the environment is not new because evidence can be found that links between human life and nanotechnology in ancient Ayurvedic medicine. It can be predicted that even before the term "nanotechnology" was coined, Ayurveda, the one and only system of traditional medicine, had some understanding of the production of nanomedicines and their effects (Nazeruddin *et al*., 2014; Prasad *et al*., 2021). The plant fibers, mainly bast and leaf fibers were studied as potential reinforcement materials for the nanocomposite fabrication due to their high unique properties, renewability, accessibility, and biodegradable nature. Furthermore, certain plants such as Kenf, Cotton, Sisal and Lokta contain natural biopolymers and biomolecules having anti-microbial, anti-bacterial, and anti-proliferative properties. The utilization of extracted fibers from such plants for nanocomposite materials possesses synergistic advantages (Zamora-Mendoza *et al*., 2023).

Silver, Zinc oxide, and Copper nanoparticles are among the most generally utilized nanoparticles for the production of nanocomposites. In addition to silver and zinc, studies have revealed that copper, manganese, nickel, and their respective metal oxides are also frequently employed in the synthesis of nanocomposites. Ag-doped ZnO and CuO nanomaterials is reported to have high surface area, low toxicity, and easy synthesis. Because of these properties, these materials are being explored for antimicrobial and dye degradation applications. Studies have indicated that the effectiveness of nanoparticles in fighting bacteria is determined by their size, with smaller particles proving more effective

in their antimicrobial abilities. The primary mechanism behind the antibacterial properties of these nanoparticles is believed to be oxidative stress (Mohapatra *et al*., 2023).

Various nanocomposites, such as ZnO, Ag/ZnO, CuO, and Ag/CuO, have been discovered to restrict the survival and growth of a wide range of microbes, making them fascinating discoveries in the world of nanotechnology. Studies have shown that ZnO-Ag-coated nanocomposite cotton material exhibited enhanced antimicrobial potency (El-Nahhal *et al.*, 2020). (Ghasemi *et al*., 2017) synthesized Ag and CuO nanoparticles, then used them to create an Ag/CuO nanocomposite which was tested for antibacterial activity. Studies have shown that silver-zinc oxide nanocomposites can improve the photocatalytic degradation of harmful chemicals like methylene blue. Researchers have experimented with varying amounts of silver doping to the ZnO compound, resulting in promising results (Azmina *et al*., 2017). Another study found that using Ag-ZnO/cellulose nanocomposites can break down methyl orange dye with increased photocatalytic activity, improved catalyst stability, and multiple reuses (Shi *et al*., 2021).

Metallic nanoparticles like silver, zinc oxide, and copper oxide are being studied for their potential use in the food industry. Incorporating such nanoparticles into bionanocomposite materials can enhance their mechanical and barrier properties and environmental stability. Ultimately, this can lead to improved product stability during transportation and storage (Kumar *et al*., 2021; Youssef & El-Sayed, 2018). A food packaging film was made using a bio-nanocomposite reinforced with ZnO nanoparticles (Arifin *et al.*, 2022). Bacterial cellulose-ZnO has been studied for its effective antibacterial properties and potential use in biomedical treatment of wound (Azizan *et al.*, 2023).

A cellulose mat can be used as a substrate to synthesize nanocomposites. This mat provides mechanical support and serves as a porous, biodegradable scaffold for nanocomposite development. To create the Ag-ZnO nanocomposite, the cellulose mat can be impregnated with a solution of zinc nitrate and silver nitrate. The mat can then be dried and annealed to form ZnO and silver nanoparticles on the cellulose fibers. The Ag-ZnO nanocomposite can be utilized for various applications, including antimicrobial coatings, sensors, and catalysis. The silver nanoparticles provide antimicrobial properties, while the ZnO nanoparticles offer photocatalytic activity. Synthesizing Ag-ZnO nanocomposite within a

matrix of cellulose mat provides an eco-friendly and more biodegradable alternative to traditional synthetic materials.

The fiber for the fabrication of cellulose mat is obtained from a traditional plant known as Lokta. Scientifically, this plant is also known as "*Daphne bhoula*" or "*Daphne papyracea.* The fibers obtained from this plant is supposed to have exceptional strength and resistance properties. The cellulosic mat from Lokta fibers can be used as the matrix for synthesizing Ag-ZnO/cellulose nanocomposite material which could be useful in dye degradation and antimicrobial activity. In this study, a cellulose mat was prepared using the fiber obtained from this plant's species. Physico-chemical properties of the mats were systematically investigated. The mat was then doped with ZnO and Ag and Cu particles and antimicrobial activities were measured.

4.2 Materials and Methods

4.2.1 Materials

The Lokta fiber stems were collected from the Gandaki province, Nagi, Annapurna Rural Municipality, Myagdi, Nepal. All reagents used in this study were of analytical grade.

4.2.2 Extraction of fiber and pulping

The outer cuticular layer was removed mechanically, and then washed multiple times in regular tap water and once in distilled water. A two-stage process was to extract pulp from Lokta fiber (**Figure 33**). The raw fiber mass was delignified using 15% sodium hydroxide at 100°C for four hours under normal atmospheric pressure (Fiber: NaOH solution ratio of 1:30). After treatment multiple washing with distilled water was performed to neutralize the biomass. Secondly, fibers were treated with 2% hydrogen peroxide solution prepared in a $NaHCO_3$–Na_2CO_3 buffer system of pH 9 for 5 hours at room temperature. This process isolated the cellulose from the hemicelluloses in the delignified fibers. A mixer grinder was used to grind these fibers into a fine powder. The fine cellulose fiber is called pulp.

4.2.3 Fabrication of paper sheet

Handmade paper sheets were formed from the dried pulp using a 23×30 cm^2 sheet former (homemade equivalent to Hand Sheet Former - UEC-2005). 4.5 g of the pulp was added and distributed in 1 L of water. It was transferred to sheet former. After 10 seconds, water was drained through the wire screen at a 45^o angle, and the paper sheet was sun-dried for 4 hours. The paper sheet was mechanically compressed using a 10 Kg steel roller to get the

final paper. The samples were stored in polyethylene bag in the dark for future measurement.

4.2.4 Measurement of Basic Properties

The TAPPI-410 method was used to calculate the basis weight of the paper. The test conditions temperature of 23±1˚C and 50±2% relative humidity. Using a GSM cutter, a 100 cm^2 paper sheet was weighed (0.001 g). The grammage of a sheet of paper was determined by dividing its total mass (g) by its total area (m^2).

The Cobb 60 value was estimated following the TAPPI-T441 method. The paper's opacity and brightness (ISO brightness) were assessed by means of a standard opacity-brightness instrument (UEC1018, India). The optical characteristics of the paper were determined by cutting five 5×5 mm^2 samples and placing them in the tester. Tensile strength was measured with a 550-kilogram load on a tensile machine (UEC1005B, India) at 23 °C and 50% relative humidity. Paper samples measuring 15 mm to 25 mm were cut from each sheet. The tensile index (Nm/g) was estimated as the ratio of tensile strength (in N/m) and grammage (in g/m^2). Five independent measurements were made for each physical property and data are reported as mean ± standard deviation.

4.2.5 Preparation of Ag/ZnO and Cu nanocomposite

Ag/ZnO composite sheet was prepared by following Kim *et al*. (2015) with some modifications. 30 ml of 1.7% hexamethylene tetraamine, 30 ml of 2.5% zinc nitrate hexahydrate, and 10 ml of 30 parts per million $AgNO_3$ solutions were prepared in distilled water. The solutions of zinc nitrate and hexamethylene tetraamine were combined and agitated for 30 minutes. A slurry was made, and then the $AgNO_3$ solutions were transferred to it. This solution was transferred to a Teflon crucible and a 4×4 cm^2 paper mat was dipped in the solution. The content was heated in a hydrothermal autoclave at 140^o for four hours. The paper mat was cleaned several times with distilled water followed by C_2H_5OH. The mat was then oven-dried for five hours. For further testing, the mat was wrapped in aluminum foil in a zip-lock bag.

For Cu nanoparticle doping, a 4×4 cm^2 sheet was soaked for 2 days in freshly prepared alkaline copper hydroxide solution. The solution was made by mixing 1 molar NaOH and 0.32 molar $CuSO_4$ solution followed by dissolving the gelatinous content in ten molar castic soda solution. To reduce copper ions adsorbed in the fiber, the Lokta sheet was

immersed in 10% ascorbic acid for 30 minutes. The samples were washed with water, oven-dried, and stored in a zip-lock back in the dark for further testing.

4.2.6 Antimicrobial test preparation and Determination of antibacterial efficiency

The nanocomposite paper sheets were investigated for their antimicrobial activities versus different strains by the disk diffusion technique (Ericsson *et al*., 1960; Biemer, 1973; Sedighi *et al*., 2014). This procedure is often referred to as the 'Kirby–Bauer method'. The method consisted of employing 6 mm paper disks with antimicrobial agents (E. coli ATCC 8739 (gram -ve), Bacillus subtilis ATCC 6051 (Gram +ve), Candida Albicans ATCC 2091on a lawn of bacteria/ fungus) scattered on the surface of an agar medium. The Petri plates were incubated for 24 hours at thirty-seven degree Celsius.

4.2.7 UV-Vis, XRD, and SEM measurements

The UV-Vis spectra were measured in a UV-visible spectrometer (Scimadzu, UV 1900i). The optical resolution and the number of scans were 1 nm and 100; respectively.

XRD data on the paper and nanocomposite mats were measured using an X-ray diffractometer (Rigaku, Minflex 600). The data were measured at 30 kV, and the step size, scanning range, and scanning speed were 0.05^{o}, $10–80^{o,}$ and 0.25^{o}/sec; respectively. Scanning electron microscopic (SEM) images of the paper and nanocomposite mats were measured using a field emission microscope (FESEM, JEISS) at various magnifications. A basic outline of the work conducted in **Figure 26**.

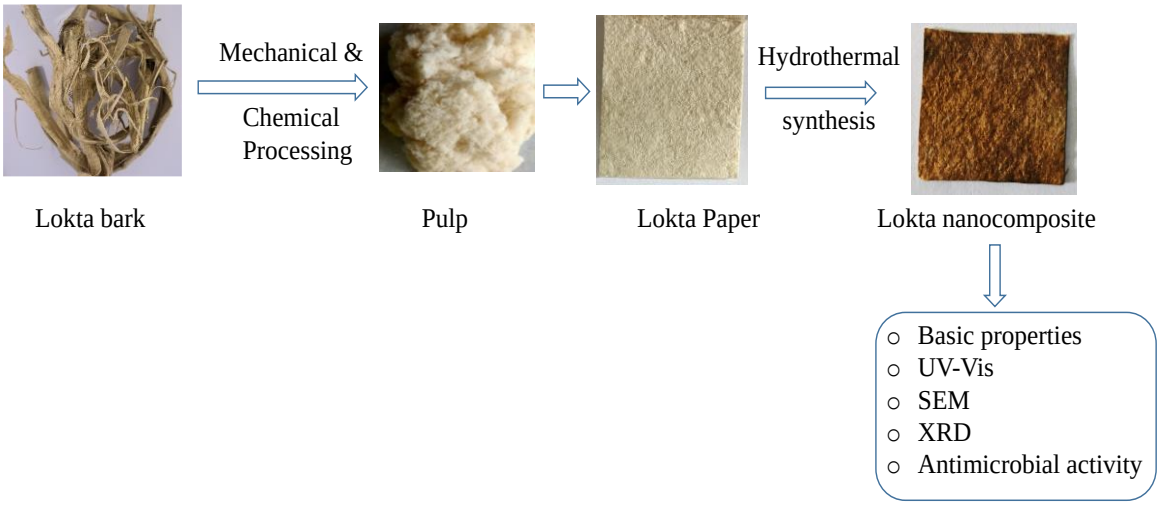

Figure 26: Schematic outline to show the major steps involved in this research.

4.3 Results and Discussion

4.3.1 Characterization of Lokta paper

4.3.1.1 Basic physical properties

The mean caliper and grammage for the paper samples were found to be 208.6±43.8 µm and 93.4±12.9 µm; respectively (**Table 9**). The variation in the measured values, as indicated by high standard deviation, suggests that the handmade paper (HP) samples aren't uniformly thicker. The chemo-mechanical method of fiber processing can form longer fiber and such fiber has a high tendency to floc formation, leading to inconsistent thickness (Beghello, 1998; Lundell *et al.*, 2011).

Table 9: Physical properties of Lokta paper

Basic properties	Mean	SD
Thickness, μm	208.6	43.8
GSM, g/m^2	93.4	12.9
Cobb 60, g/m^2	224.2	38.5
Apparent density, g/cm^3	0.5	0.2
Apparent porosity, %	62	14.6
Optical properties		
Brightness, %	66.0	3.4
Opacity, %	95.0	0.7
Mechanical properties		
Tensile strength, kN/m	1.6	0.5
Tensile index, Nm/g	17.0	5.2
% Elongation	1.5	0.5
Breaking length, km	1.7	0.5

The apparent density (g/cm^3) of the paper samples was found to be 0.47±0.16 g/cm^3. The volume of air or empty space within a sheet of paper is included in its apparent density. This means that apparent density always falls short of true density. The apparent density of the Handmade papers is reported to be in the 0.3-0.7 g/cm^3.

The paper samples had Cobb 60 sizing of 224.2±38.4 g/m^2. The high SD could be due to slight variations in fiber shape and organization. The Grammage and Cobb 60 values showed should strong positive correlation (r= +0.9).

Lokta paper appears to be lightweight paper based on its low apparent density. The known densities of the paper network and cellulose can be used to evaluate the apparent porosity of paper. The apparent porosity of the paper samples was found to be 62±14.6% (**Table 10**). Specifically, it was found that apparent density and porosity are perfectly inversely related to one another (r =-1). Some possible causes of the high porosity (low apparent density) of the handmade papers include the use of long and inflexible fibers, not enough refining, and the lack of fillers and fines (Bajpai, 2018b). Samples of laboratory-made

handmade paper have also been found to have a low apparent density, in the extent of 0.2 to 0.5 g/cm^3.

4.3.1.2 Optical Properties

The brightness of paper sheets was found to be 66.0±3.4 %. Handmade paper made in local industries is reported to have a brightness of 60-65% (Aryal *et al*., 2022). Paper and pulp samples vary in brightness based on factors including lignin and coloring impurity levels and microscopic surface features (Bajpai, 2018a).

The capacity of paper to conceal an item on the other side of the sheet is measured by its opacity. A high-opacity paper is needed for double-sided printing so that the front page can be read without being distracted by the letters or graphics on the reverse and the strikethrough is not visible. High opacity is caused by the scattering of blue light by tiny air gaps or pores in thick paper sheets (Bajpai, 2018a). The Lokta paper sheets had a mean opacity of 95.0±0.7 % (**Table 9**). It is possible that the papers' low apparent density and/or high porosity contribute to their greater opacity. Handmade paper made in local industries is reported to have an opacity of 80-98% (Aryal *et al*., 2022).

4.3.1.3 Mechanical properties

The paper samples were tested for tensile strength and the tensile index throughout the length of the paper molds or the wooden frame. Tensile strength was found to be 1.5±0.5 kN/m. The tensile strength index, also known as tensile strength adjusted for weight, was also determined. The tensile index was found to be 17.0±5.2 Nm/g. The majority of Lokta paper samples made in local enterprise enterprises is reported to have tensile strength and index of 0.03-1.5 kN/m and 8-27 Nm/g (Aryal *et al*., 2022).

Several variables affect the TS of paper-based materials, including fiber length, fiber strength, and fiber-to-fiber connection and bonding. The degree of contact connecting two layers may be characterized in terms of relative bonding area (RBA) by observing a paper sheet as multiple layers of fabric composite assembly comprising two-dimensional fibrous setups that are not interwinding between layers (Soszynski, 1995; Henriksson *et al.*, 2008). RBA may be roughly estimated from the values of fractional porosity (ε) and the number of fiber layers (n), where n is the ratio of thickness to fiber diameter (Sampson, 2004).

$$RBA = \frac{n}{n-1}(1-\varepsilon)^2 \quad \ldots\ldots\ldots\ldots\ldots\ldots \quad (10)$$

where, n= defined as caliper/fiber diameter is the number of fiber layers and ε is fractional porosity. The RBA for the paper samples ranged from 0.05-0.42; much higher than observed for paper samples collected from local enterprises (0.01-0.1). This explains the relatively higher strength of Lokta paper samples in this study as compared to paper samples made in local industries or enterprises (Aryal *et al*., 2022).

4.3.2 Characterization of nanocomposite mat

4.3.2.1 UV-Vis study

A preliminary confirmation on the doping of Cu and Ag/ZnO nanoparticles can be obtained from the color change of the Lokta paper (**Figures 27A, B**, and **C**). The UV-Vis spectra of the mat show more definitive information on the nanoparticle incorporation. The UV-Vis spectra of Cu-nanocomposites show bands at ~300 nm, 450 nm, and 750 nm (**Figure 27D**, **curve a**). The first two features can be attributed to copper oxide nanoparticle (Berra *et al*., n.d.), resulting from the oxidation of Cu nanoparticles and 750 nm broadband to the Cu nanoparticles agglomerates. The UV-Vis spectra of Ag/ZnO-nanocomposites show a shoulder around 300 nm and a distinct peak around 450 nm. The shoulder 300 nm can be attributed to ZnO nanoparticles (Talam *et al*., 2012). The 450 nm peak is the surface plasmon band of Ag nanoparticles. This observation suggested Ag/ZnO and Cu nanoparticles are incorporated in the Lokta paper resulting in the composite mat.

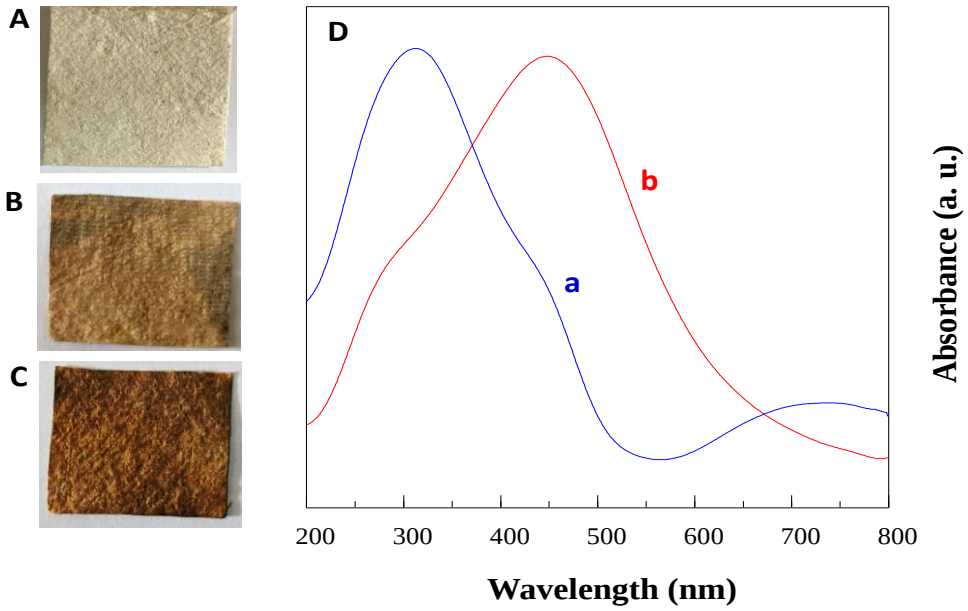

Figure 27: Photographs and UV-Vis spectra. A, B, and C are photographs of Lokta paper, Ag/ZnO- and Cu-nanocomposite mat. The curves 'a' and 'b' in D show the optical spectra for Cu- and Ag/ZnO nanocomposite mats; respectively.

4.3.2.2 SEM imaging

Figure 28 shows SEM images of the paper sample and Ag/ZnO- and Cu-nanocomposite mats. The paper sample (**Figure 28A**) is long and intertwined passing from one end to another. This could be attributed to the strength of paper samples. The nanocomposite mat surface (**Figure 28B** and **C**) shows nanoparticles on the surface. Alkali-treated lignocellulose fiber surface is reported to have nanoscale porosity (Maneerung *et al.*, 2008). The hydroxyl of the cellulose interacts with electro-positive metal. The porous structures along with cellulose-nanoparticle interaction help nanoparticles anchor firmly on the mat (Ali *et al.*, 2016).

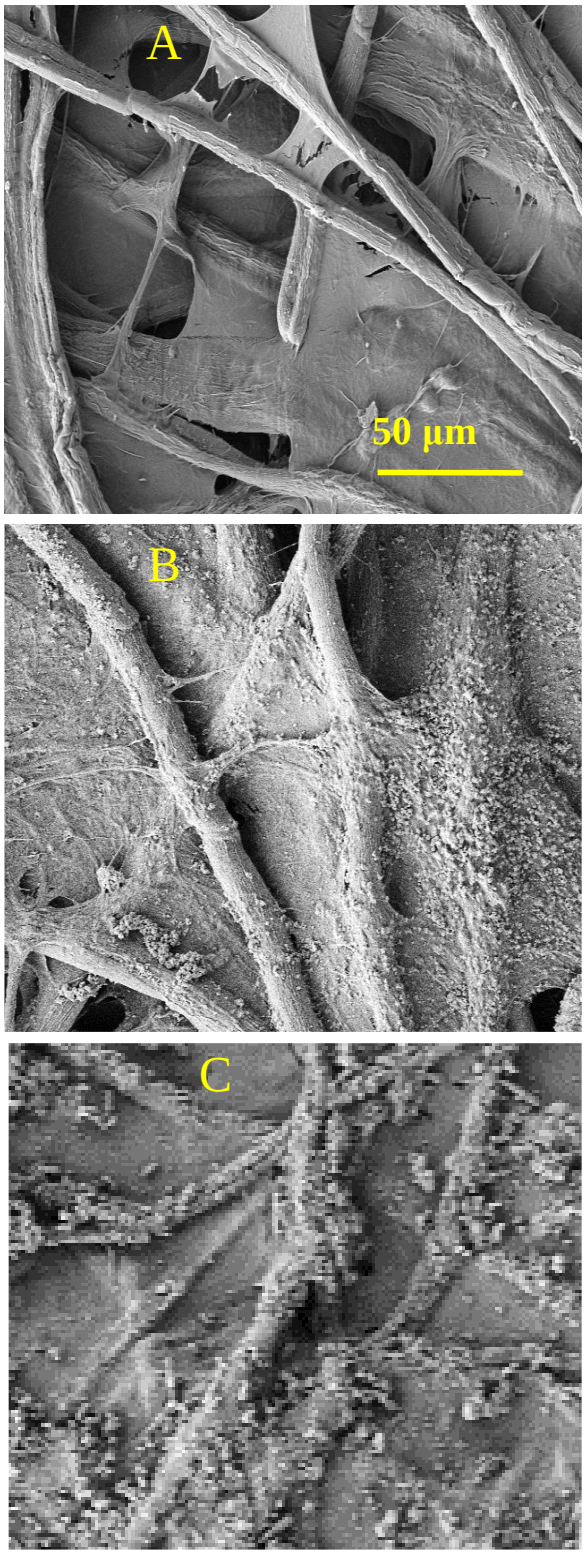

Figure 28: SEM image. A) Lokta paper, B) Ag/Zno-Nanocomposite mat, c) Cu-Nanocomposite mat.

4.3.2.3 XRD study

The broad peak observed at 2θ values of 21.5 and 15.5° in Lokta paper (**curve a**, **Figure 29**) and in Ag/Zno-nanocomposite mat (**curve c**, **Figure 4**) is due to (200) and (110/110) planes of the cellulose I crystalline phase (Park *et al.*, 2010a; Saha *et al.*, 2010). These features are shifted to lower 2θ values in the Cu-nanocomposite mat (**curve b**, **Figure 4**) most likely due phase change of crystalline cellulose. The nanocomposite mat (**curves b and c**) shows additional peaks at 2θ>30º. This is due incorporation of nanoparticles in the cellulose surface.

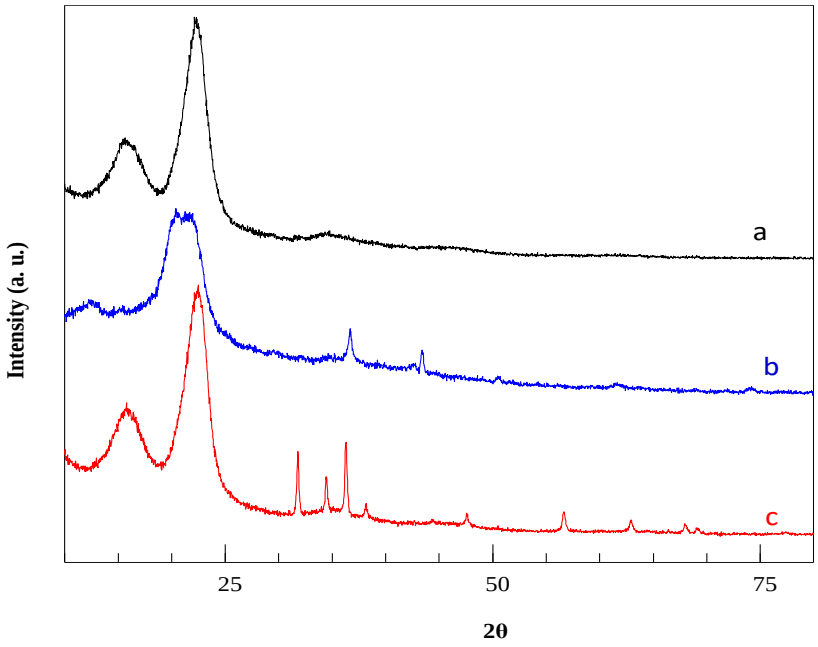

Figure 29: XRD data. Curves a belong to lokta, b to Cu-nanocomposite mat, c to Ag/Zno-nanocomposite.

In the XRD of Cu-nanocomposite mat, peaks at 2θ values of 43.6, 50.5, and 74.4 correspond to the (111), (200), and (220) planes of cubic crystals of Cu nanoparticles (Theivasanthi & Alagar, n.d.). The peaks at 36.7, 42.6, and 41.6 to the (111), (200) and (220) planes of cubic crystal of Cu_2O nanoparticles (Berra et al., n.d.). In the XRD data of Ag/ZnO-nanocomposite mat, peaks at 2θ values of 31.77, 34.3, 36.4, 47.6, 56.6, 62.9, and 68.9 correspond to the (100), (002), (101), (102), (103), (110), and (112) planes of

hexagonal wurtzite ZnO crystal structure. The peaks at 2θ values of 38.1, 67.5, and 77.4 correspond to (111), (220), and (311) planes of cubic crystal of Ag nanoparticles (Zhou *et al.*, 2013; Ibănescu *et al.*, 2014; Al Abdullah *et al*., 2017; Zhou *et al*., 2007).

A rough estimate of mean particle size as determined from the Scherrer equation using the most intense peaks for Ag, Cu/Cu_2O, and ZnO nanoparticles was found to be 28.1 nm, 23.2 nm, and 36.1 nm; respectively.

4.3.3 Antimicrobial activity

The antimicrobial activity of synthesized Ag-ZnO/cellulose and Cu/Cellulose nanocomposite is shown in **Table 10** and **Figures 30A-F**. The zone inhibition was used to assess their antibacterial performance. *Escherichia coli* (*E. coli*) ATCC 8739 (Gram -ve) shows the least response to the ZnO-Ag/cellulose nanocomposite prepared. *Bacillus subtilis* ATCC 6051 (Gram +ve) and *Candida albicans* ATCC 2091 show better antimicrobial activity. Cu/cellulose nanoparticle paper mat showed better performance with tested microbes.

Table 10: Zone of inhibition microbial test

Strains	**Zone of inhibition (cm)**					
	Ag/ZnO-mat	C^-	C^+	Cu-mat	C^-	C^+
Escherichia coli	0	0	1.0	0.7	0	1.2
Bacillus subtilis	0.5	0	1.0	0.6	0	1.2
Candida Albicans	0.5	0`	1.0	1.1	0`	1.2

C^- = negative control, C^+ = positive (neomycin) control

According to Yamamoto (2001), ZnO particles suppress bacterial growth by creating hydrogen peroxide; nevertheless, their antibacterial efficacy appeared to be lower than that of AgNPs. Even though the mechanism of antimicrobial activeness of nanoparticles is unfamiliar, it is suggested that Ag and Cu NPs can have bactericidal effects by leaking biological material and interrupting DNA replication caused by reactive oxygen species directly through a bacterial cell's membrane (Yamamoto, 2001). The findings of this study

also support the additional evidence that the Ag/ZnO- and Cu-cellulose nanocomposites show increased antibacterial activity (Chatterjee, Chakraborty, and Basu, 2014).

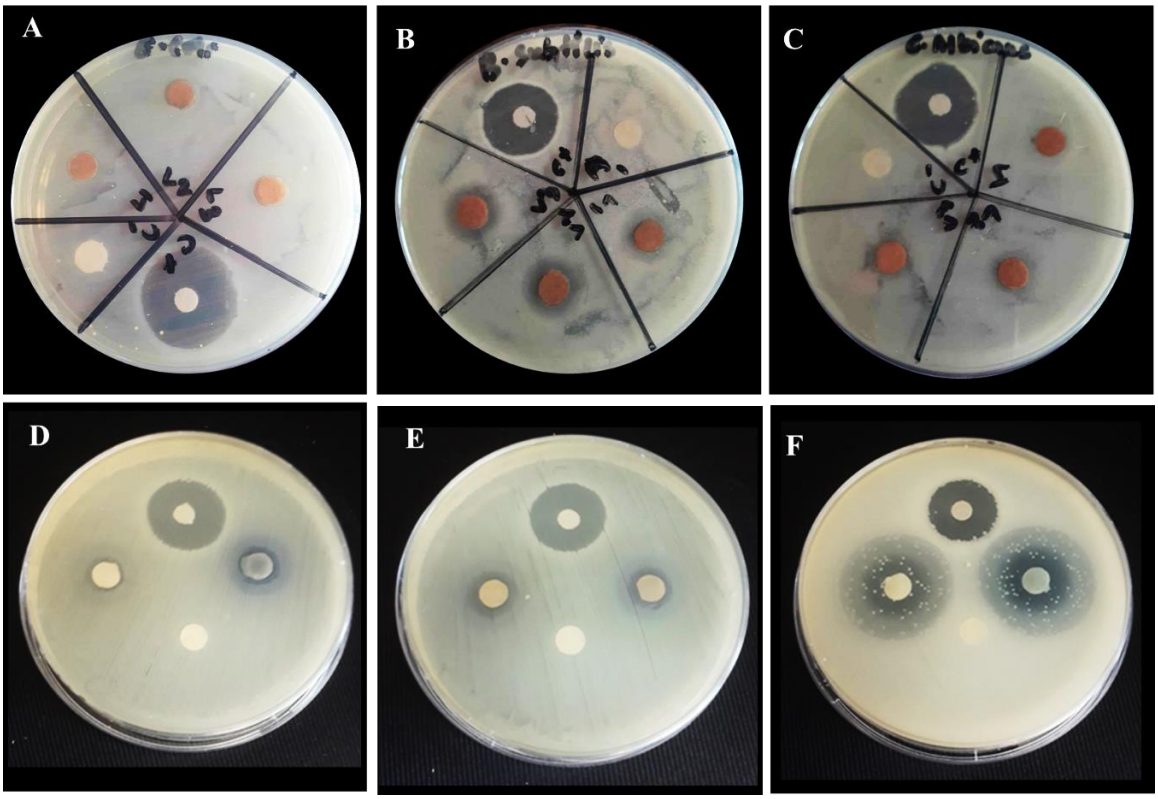

Figure 30: Antimicrobial activity of Ag/ZnO nanocomposite paper-mat for A*) Escherichia coli* B) *Bacillus subtilis* C) *Candida albicans* and Cu-nanocomposite for D) *Escherichia coli* E) *Bacillus subtilis* F) *Candida albicans*

4.4 Conclusions

In conclusion, hydrothermal treatment was employed to create a stable Ag-doped ZnO/cellulose composite, and copper nanoparticles were generated using a chemical reduction approach. The hydrothermal treatment results in the deposition of Ag and ZnO NPs from their precursor solution onto the enormous surface area of cellulose, with no NP aggregation. In experimental conditions, the Ag-ZnO/cellulose and Cu/cellulose nanocomposite showed remarkable antibacterial properties and durability, indicating that it might be used to remove contaminants. The antibacterial properties of the Ag-ZnO particles put on the surface of the cellulose mat fibers demonstrate that the noble nanocomposite mat may be used as an inexpensive and environment-friendly material.

CHAPTER 5

CONCLUSIONS AND RECOMMENDATIONS

5.1 Conclusions

In the first phase of the studies, various physical and chemical factors of ten diverse Lokta paper samples gathered from local industries and enterprises were systematically explored. These papers had a mean caliper of 90 to 700 μm, grammage of 50 to 150 g/m^2, and apparent density of 0.2 to 0.4 g/cm^3. The tensile strength, tensile index, and optical brightness of paper samples varied from 30 to 2900 N/m, 1 to 27 Nm/g, and 56 to 67%; respectively. As compared to the cross direction, the paper showed higher tensile strength along the length direction. These findings indicated that Lokta paper possesses the characteristics of lightweight paper, having intermediate to high tensile strength but intermediate yellowness. The paper exhibited characteristics of both amorphous and crystalline cellulose phases in XRD and FTIR data. SEM micrographs displayed interconnected networks of long cellulose fibers, with microfibrils arranged almost parallel on the fiber surfaces. These observations explain the moderate to high strength observed for the Lokta paper.

In the second phase of the study, a comprehensive analysis of material properties of Lokta fiber subjected to 1-9% NaOH (w/v) concentrations at ambient temperature was conducted. The alkali retting process led to a gradual reduction in extractives, lignin, and hemicellulose content with an increase in alkali concentration. Simultaneously, significant changes were observed in other key properties. A decrease in equilibrium moisture content and effective fiber width while an increase in fiber density, crystallinity index, and thermal stability, all attributed to alkali treatment. These changes can be due to the loss of cementing materials from fiber bundles, supported by the results obtained from Fe-SEM images and FTIR data. Interestingly, alkali treatment also led to an enhanced tensile strength and thermal properties further underscoring its impact on fiber properties. These findings hold significance for optimizing and comprehending the ultimate properties of Lokta fiber-based paper and composite materials.

In the subsequent study, it was found that Lokta paper having improved optical and mechanical properties can be fabricated in a laboratory. The Ag/ZnO and Cu nanoparticles were doped in the Lokta paper using hydrothermal and chemical reduction methods. The

Lokta paper nanocomposite mat showed promising antimicrobial activity against two bacteria (*Escherichia coli* and *Bacillus subtilis*) and a fungal strain (*Candida albicans*). These observations suggested that the Lokta paper-derived nanocomposite mat can find potential applications as an antimicrobial packaging material.

5.2 Recommendation

One of the major objectives of this study was to explore the material properties of Handmade paper at the sub-microscopic level and understand how these properties influence the differences observed in optical and mechanical characteristics. The paper samples exhibited low apparent density (high porosity), varying thickness, and low brightness. To enhance these properties for handmade paper industries, eco-friendly and cost-effective approaches can be explored. The locally isolated microbial cultures for enzymatic bleaching or chemical bleaching could be used to increase brightness. Additionally, employing a locally designed handmade machine for calendaring the paper sheet can address issues of high thickness variation and porosity.

In the future, Lokta fiber or Lokta paper could be the basis for creating valuable nanomaterials, like nano cellulose, antimicrobial cellulose film, and micro/nano-composites for filtering and chemical sensing applications (Abral *et al*., 2020; Beckermann & Pickering, 2008; Dufresne, 2008b; Ilyas *et al.*, 2017, 2018, 2019; Samy *et al*., 2022). Also, strategies to make Lokta paper hydrophobic for water-resistant packaging and oil/water separation could be explored in the future.

As demonstrated in this study, Lokta fiber on alkali treatment leads to decreased water absorptivity and increased mechanical strength. In the future, experimental measurement of tensile curves and microscopic imaging of fiber subjected to different levels of tension could be explored to enhance the better understanding of the mechanical properties of the fibers. Furthermore, a systematic study on the material properties of Lokta fiber paper and composite materials could be investigated further.

Lokta paper-derived nanocomposite mat had promising antimicrobial properties. It would be interesting to explore the stability of nanocomposite mat and self-life study of a food product packaged with the mat.

REFERENCES

Abral, H., Ariksa, J., Mahardika, M., Handayani, D., Aminah, I., Sandrawati, N., Pratama, A. B., Fajri, N., Sapuan, S. M., & Ilyas, R. A. (2020). Transparent and Antimicrobial Cellulose Film from Ginger Nanofiber. *Food Hydrocolloids*, **98:** 105266. https://doi.org/10.1016/j.foodhyd.2019.105266

Adamsen, A. P. S., Akin, D. E., & Rigsby, L. L. (2002). Chelating Agents and Enzyme Retting of Flax. *Textile Research Journal*, **72**(4)**:** 296–302. https://doi.org/10.1177/004051750207200404

Adeeyo, O. A., Oresegun, O. M., & Oladimeji, T. E. (2015a). Compositional Analysis of Lignocellulosic Materials: Evaluation of an Economically Viable Method Suitable for Woody and Non-Woody Biomass. *American Journal of Engineering Research (AJER)*, **4**(4)**:** 14–19.

Adeeyo, O. A., Oresegun, O. M., & Oladimeji, T. E. (2015b). Compositional Analysis of Lignocellulosic Materials: Evaluation of an Economically Viable Method Suitable for Woody and Non-Woody Biomass. *American Journal of Engineering Research (AJER)*, **4**(4)**:** 14–19.

Åkerholm, M., Hinterstoisser, B., & Salmén, L. (2004). Characterization of the Crystalline Structure of Cellulose Using Static and Dynamic FT-IR Spectroscopy. *Carbohydrate Research*, **339**(3)**:** 569–578. https://doi.org/10.1016/j.carres.2003.11.012

Al Abdullah, K., Awad, S., Zaraket, J., & Salame, C. (2017). Synthesis of ZnO Nanopowders by Using Sol-Gel and Studying Their Structural and Electrical Properties at Different Temperature. *Energy Procedia*, **119:** 565–570. https://doi.org/10.1016/j.egypro.2017.07.080

Ali, A., Shaker, K., Nawab, Y., Jabbar, M., Hussain, T., Militky, J., & Baheti, V. (2018). Hydrophobic Treatment of Natural Fibers and Their Composites—A Review. *Journal of Industrial Textiles*, **47**(8)**:** 2153–2183. https://doi.org/10.1177/1528083716654468

Amara, C., El Mahdi, A., Medimagh, R., & Khwaldia, K. (2021). Nanocellulose-Based Composites for Packaging Applications. *Current Opinion in Green and Sustainable Chemistry*, **31:** 100512.

Anwar, Z., Gulfraz, M., & Irshad, M. (2014). Agro-Industrial Lignocellulosic Biomass a Key to Unlock the Future Bio-energy: A Brief Review. *Journal of Radiation Research and Applied Sciences*, **7**(2)**:** 163–173. https://doi.org/10.1016/j.jrras.2014.02.003

Arafat, K., Nayeem, J., Quadery, A., Quaiyyum, M., & Jahan, M. S. (2018). Handmade Paper From Waste Banana Fibre. *Bangladesh Journal of Scientific and Industrial Research*, **53**(2)**:** 83–88. https://doi.org/10.3329/bjsir.v53i2.36668

Arafat, Km., Nayeem, J., Quadery, A. H., Quaiyyum, M. A., & Jahan, M. S. (2018). Handmade Paper From Waste Banana Fibre. *Bangladesh Journal of Scientific and Industrial Research*, **53**(2)**:** 83–88.

Arifin, H. R., Djali, M., Nurhadi, B., Azlin-Hasim, S., Masruchin, N., Vania, P. A., & Hilmi, A. (2022). Corn Starch-Based Bionanocomposite Film Reinforced With ZnO Nanoparticles and Different Types of Plasticizers. *Frontiers in Sustainable Food Systems*, **6:** https://www.frontiersin.org/articles/10.3389/fsufs.2022.886219

Aryal, G. M., Aryal, B., Kandel, K. P., & Neupane, B. B. (2021). Cellulose-Based Micro-Fibrous Materials Imaged With a Home-Built Smartphone Microscope. *Microscopy Research and Technique*, **84**(8)**:** 1794–1801. https://doi.org/10.1002/jemt.23736

Aryal, G. M., Kandel, K. P., Bhattarai, R. K., Giri, B., Adhikari, M., Ware, A., Han, S., George, G., Luo, Z., & Gautam, B. R. (2022). Material Properties of Traditional Handmade Paper Samples Fabricated from Cellulosic Fiber of Lokta Bushes. *ACS Omega*, **7**(36)**:** 32717–32726.

Aryal, G. M., Ware, W., Han, S., George, G., Luo, Z., Kandel, K. P., Gautam, B., & Neupane, B. (2021). Microscopic Characterization of Eco-friendly Lokta Paper. *Microscopy and Microanalysis*, **27**(S1)**:** 720–721.

ASTM. (2004). *ASTM D1776–04, Standard Practice for Conditioning and Testing Textiles. American Society for Testing and Materials, West Conshohocken, Pennsylvania, USA.*

Ayeni, A. O., Adeeyo, O. A., Oresegun, O. M., & Oladimeji, E. (2015). Compositional Analysis of Lignocellulosic Materials: Evaluation of an Economically Viable Method Suitable for Woody and Non-Woody Biomass. *American Journal of Engineering Research*.

Aziz, S. H., & Ansell, M. P. (2004). The Effect of Alkalization and Fibre Alignment on the Mechanical and Thermal Properties of Kenaf and Hemp Bast Fibre Composites: Part 1–Polyester Resin Matrix. *Composites Science and Technology*, **64**(9)**:** 1219–1230.

Azizan, A., Samsudin, A. A., Shamshul Baharin, M. B., Dzulkiflee, M. H., Rosli, N. R., Abu Bakar, N. F., & Adlim, M. (2023). Cellulosic Fiber Nanocomposite Application Review With Zinc Oxide Antimicrobial Agent Nanoparticle: An Opt for COVID-19 Purpose. *Environmental Science and Pollution Research International*, **30**(7)**:** 16779–16796. https://doi.org/10.1007/s11356-022-18515-5

Azmina, M., Md Nor, R., Ahmad Rafaie, H., Razak, N., Abdul Sani, S. F., & Osman, Z. (2017). Enhanced Photocatalytic Activity of ZnO Nanoparticles Grown on Porous Silica Microparticles. *Applied Nanoscience*. https://doi.org/10.1007/s13204-017-0626-3

Babu, A. T., & Antony, R. (2019). Green Synthesis of Silver Doped Nano Metal Oxides of Zinc & Copper for Antibacterial Properties, Adsorption, Catalytic Hydrogenation & Photodegradation of Aromatics. *Journal of Environmental Chemical Engineering*, **7**(1)**:** 102840. https://doi.org/10.1016/j.jece.2018.102840

Bajpai, P. (2016). Structure of Lignocellulosic Biomass. In P. Bajpai, *Pretreatment of Lignocellulosic Biomass for Biofuel Production*, 7–12. Springer Singapore. https://doi.org/10.1007/978-981-10-0687-6_2

Bajpai, P. (2018a). Brief Description of the Pulp and Papermaking Process. In P. Bajpai, *Biotechnology for Pulp and Paper Processing*, 9–26. Springer Singapore. https://doi.org/10.1007/978-981-10-7853-8_2

Bajpai, P. (2018b). Paper and Its Properties. In *Biermann's Handbook of Pulp and Paper* **2:** 35–63. Elsevier.

Banjara, G. (2007). Handmade Paper in Nepal: Upgrading with Value Chain Approach. GTZ/PSP-RUFIN.

Basu, G., Mishra, L., Jose, S., & Samanta, A. K. (2015). Accelerated Retting Cum Softening of Coconut Fibe. *Industrial Crops and Products*, **77:** 66–73. https://doi.org/10.1016/j.indcrop.2015.08.012

Beakou, A., Ntenga, R., Lepetit, J., Ateba, J. A., & Ayina, L. O. (2008). Physico-Chemical and Microstructural Characterization of "*Rhectophyllum camerunense*" Plant Fiber. *Composites Part A: Applied Science and Manufacturing*, **39**(1)**:** 67–74.

Beckermann, G. W., & Pickering, K. L. (2008). Engineering and Evaluation of Hemp Fibre Reinforced Polypropylene Composites: Fibre Treatment and Matrix Modification. *Composites Part A: Applied Science and Manufacturing*, **39**(6)**:** 979–988. https://doi.org/10.1016/j.compositesa.2008.03.010

Beghello, L. (1998). Some Factors That Influence Fiber Flocculation. *Nordic Pulp & Paper Research Journal*, **13**(4)**:** 274–279. https://doi.org/10.3183/npprj-1998-13-04-p274-279

Begum, H. A., Tanni, T. R., & Shahid, M. A. (2021). Analysis of Water Absorption of Different Natural Fibers. *Journal of Textile Science and Technology*, **7**(4)**:** 152–160. https://doi.org/10.4236/jtst.2021.74013

Benedetto, R. M. D., Gelfuso, M. V., & Thomazini, D. (2015). Influence of UV Radiation on the Physical-chemical and Mechanical Properties of Banana Fiber. *Materials Research*, **18:** 265–272. https://doi.org/10.1590/1516-1439.371414

Betené, A. D. O., Batoum, C. S., Ndoumou Belinga, R. L., Betené Ebanda, F., Tamba, J. G., Atangana, A., Moukené, R., Tcheudjo, G. K., & Nyembè, A. (2023). Extraction and Characterization of a Novel Tropical Fibre *Megaphrynium macrostachyum* as a Biosourced Reinforcement for Gypsum-Based Biocomposites. *Journal of Composite Materials*, **57**(16)**:** 2543–2562. https://doi.org/10.1177/00219983231174682

Betts, W. B., Dart, R. K., Ball, A. S., & Pedlar, S. L. (1991). Biosynthesis and Structure of Lignocellulose. In W. B. Betts (Ed.), *Biodegradation* 139–155. Springer London. https://doi.org/10.1007/978-1-4471-3470-1_7

Bharath, K. N., Madhu, P., Gowda, T. G. Y., Sanjay, M. R., Kushvaha, V., & Siengchin, S. (2020). Alkaline Effect on Characterization of Discarded Waste of *Moringa oleifera* Fiber as a Potential Eco-friendly Reinforcement for Biocomposites. *Journal of Polymers and the Environment*, **28**(11)**:** 2823–2836. https://doi.org/10.1007/s10924-020-01818-4

Biggs, S., & Messerschmidt, D. (2005a). Social Responsibility in the Growing Handmade Paper Industry of Nepal. *World Development*, **33**(11)**:** 1821–1843.

Biggs, S., & Messerschmidt, D. (2005b). Social Responsibility in the Growing Handmade Paper Industry of Nepal. *World Development*, **33**(11)**:** 1821–1843. https://doi.org/10.1016/j.worlddev.2005.06.002

Bismarck, A., Mishra, S., & Lampke, T. (2005a). Plant Fibers as Reinforcement for Green Composites. In *Natural fibers, biopolymers, and biocomposites* 52–128. CRC Press.

Bismarck, A., Mishra, S., & Lampke, T. (2005b). Plant Fibers as Reinforcement for Green Composites. In *Natural fibers, biopolymers, and biocomposites* 52–128. CRC Press.

Bledzki, A. K., & Gassan, J. (1999). Composites Reinforced with Cellulose Based Fibres. *Progress in Polymer Science*, **24**(2)**:** 221–274. https://doi.org/10.1016/S0079-6700(98)00018-5

Bledzki, A. K., Sperber, V. E., & Faruk, O. (2002). *Natural and Wood Fibre Reinforcement in Polymers*. iSmithers Rapra Publishing. Google-Books-ID: XoZa5t3_ogAC

Boopathi, L., Sampath, P. S., & Mylsamy, K. (2012a). Investigation of Physical, Chemical and Mechanical Properties of Raw and Alkali Treated Borassus Fruit Fiber. *Composites Part B: Engineering*, **43**(8)**:** 3044–3052.

Boopathi, L., Sampath, P. S., & Mylsamy, K. (2012b). Investigation of Physical, Chemical and Mechanical Properties of Raw and Alkali Treated Borassus Fruit fiber. *Composites Part B: Engineering*, **43**(8)**:** 3044–3052. https://doi.org/10.1016/j.compositesb.2012.05.002

Boopathi, L., Sampath, P. S., & Mylsamy, K. (2012c). Investigation of Physical, Chemical and Mechanical Properties of Raw and Alkali Treated Borassus Fruit Fiber. *Composites Part B: Engineering*, **43**(8)**:** 3044–3052. https://doi.org/10.1016/j.compositesb.2012.05.002

Borchani, K. E., Carrot, C., & Jaziri, M. (2015a). Untreated and Alkali Treated Fibers From Alfa Stem: Effect of Alkali Treatment on Structural, Morphological and Thermal Features. *Cellulose*, **22:** 1577–1589.

Borchani, K. E., Carrot, C., & Jaziri, M. (2015b). Untreated and Alkali Treated Fibers From Alfa Stem: Effect of Alkali Treatment on Structural, Morphological and Thermal Features. *Cellulose*, **22:** 1577–1589.

Boufi, S., González, I., Delgado-Aguilar, M., Tarrès, Q., Pèlach, M. À., & Mutjé, P. (2016). Nanofibrillated Cellulose as an Additive In Papermaking Process: A Review. *Carbohydrate Polymers*, **154:** 151–166. https://doi.org/10.1016/j.carbpol.2016.07.117

Brígida, A. I. S., Calado, V. M. A., Gonçalves, L. R. B., & Coelho, M. A. Z. (2010). Effect of Chemical Treatments on Properties of Green Coconut Fiber. *CarbohydratePolymers*, **79**(4)**:** 832–838. https://doi.org/10.1016/j.carbpol.2009.10.005

Camargo, P. H. C., Satyanarayana, K. G., & Wypych, F. (2009). Nanocomposites: Synthesis, Structure, Properties and New Application Opportunities. *Materials Research*, **12**(1)**:** Article 1. https://doi.org/10.1590/S1516-14392009000100002

Cantero, G., Arbelaiz, A., Llano-Ponte, R., & Mondragon, I. (2003). Effects of Fibre Treatment on Wettability and Mechanical Behaviour of Flax/Polypropylene Composites. *Composites Science and Technology*, **63**(9)**:** 1247–1254. https://doi.org/10.1016/S0266-3538(03)00094-0

Chandrasekar, M., Ishak, M. R., Sapuan, S. M., Leman, Z., & Jawaid, M. (2017a). A Review on The Characterisation of Natural Fibres and Their Composites After Alkali Treatment and Water Absorption. *Plastics, Rubber and Composites*, **46**(3)**:** 119–136.

Chandrasekar, M., Ishak, M. R., Sapuan, S. M., Leman, Z., & Jawaid, M. (2017b). A Review on The Characterisation of Natural Fibres and Their Composites After Alkali Treatment and Water Absorption. *Plastics, Rubber and Composites*, **46**(3)**:** 119–136.

Chatterjee, S., Sharma, S., Prasad, R. K., Datta, S., Dubey, D., Meghvansi, M. K., Vairale, M. G., & Veer, V. (2016). Cellulase Enzyme Based Biodegradation of Cellulosic Materials: An Overview. *South Asian Journal of Experimental Biology*, **5**(6)**:** 271–282. https://doi.org/10.38150/sajeb.5(6).p271-282

Chen, H. (2014). Chemical Composition and Structure of Natural Lignocellulose. In H. Chen, *Biotechnology of Lignocellulose*, 25–71. Springer Netherlands. https://doi.org/10.1007/978-94-007-6898-7_2

Chikanbanjar, R., Baniya, B., & Dhamala, M. K. (2020). An Assessment of Forest Structure, Regeneration Status and the Impact of Human Disturbance in Panchase Protected Forest, *Nepal*. **17**.

Das, A. M., Ali, A. A., & Hazarika, M. P. (2014a). Synthesis and Characterization of Cellulose Acetate From Rice Husk: Eco-Friendly Condition. *Carbohydrate Polymers*, **112:** 342–349.

Das, A. M., Ali, A. A., & Hazarika, M. P. (2014b). Synthesis and Characterization of Cellulose Acetate From Rice Husk: Eco-Friendly Condition. *Carbohydrate Polymers*, **112:** 342–349. https://doi.org/10.1016/j.carbpol.2014.06.006

Das, A. M., Ali, A. A., & Hazarika, M. P. (2014c). Synthesis and Characterization of Cellulose Acetate From Rice Husk: Eco-Friendly Condition. *Carbohydrate Polymers*, **112:** 342–349. https://doi.org/10.1016/j.carbpol.2014.06.006

Dawood, A., & Ma, K. (2020). Applications of Microbial β-Mannanases. *Frontiers in Bioengineering and Biotechnology*, **8:** 598630. https://doi.org/10.3389/fbioe.2020.598630

De Lima, D. R., Silveira, M. H. L., Del Rio, L., & Ramos, L. P. (2016). Pretreatment Processes for Cellulosic Ethanol Production: Processes Integration and Modeling for the Utilization of Lignocellulosics Such as Sugarcane Straw. In C. R. Soccol, S. K. Brar, C. Faulds, & L. P. Ramos (Eds.), *Green Fuels Technology*, 107–131. Springer International Publishing. https://doi.org/10.1007/978-3-319-30205-8_5

Djafari Petroudy, S. R. (2017). 3 - Physical and Mechanical Properties of Natural Fibers. In M. Fan & F. Fu (Eds.), *Advanced High Strength Natural Fibre Composites in Construction*, 59–83. Woodhead Publishing. https://doi.org/10.1016/B978-0-08-100411-1.00003-0

DOF & UNICEF. (1984). Lokta (Daphne) and Craft Paper-Making In Nepal. A Series of Papers Presented at The HMGN Department of Forest and UNICEF Lokta (Daphne) Forestry Policy and Planning Workshop-Seminar. *Kathmandu: Department of Forest and UNICEF*.

Donaghy, J. A., Levett, P. N., & Haylock, R. W. (1990). Changes In Microbial Populations During Anaerobic Flax Retting. *Journal of Applied Bacteriology*, **69**(5)**:** 634–641. https://doi.org/10.1111/j.1365-2672.1990.tb01556.x

Dufresne, A. (2008a). Cellulose-Based Composites and Nanocomposites. In *Monomers, polymers and composites from renewable resources*, 401–418. Elsevier.

Dufresne, A. (2008b). Cellulose-Based Composites and Nanocomposites. In M. N. Belgacem & A. Gandini (Eds.), *Monomers, Polymers and Composites from Renewable Resources*, 401–418. Elsevier. https://doi.org/10.1016/B978-0-08-045316-3.00019-3

Ebringerová, A., Hromádková, Z., & Heinze, T. (2005). Hemicellulose. In T. Heinze (Ed.), *Polysaccharides I: Structure, Characterization and Use*, 1–67. Springer. https://doi.org/10.1007/b136816

Ehrnrooth, E. M. L. (1984). Change in Pulp Fibre Density With Acid-Chlorite Delignification. *Journal of Wood Chemistry and Technology*, **4**(1)**:** 91–109. https://doi.org/10.1080/02773818408062285

Elanthikkal, S., Gopalakrishnapanicker, U., Varghese, S., & Guthrie, J. T. (2010). Cellulose Microfibres Produced From Banana Plant Wastes: Isolation and Characterization. *Carbohydrate Polymers*, **80**(3)**:** 852–859.

Elmogahzy, Y., & Farag, R. (2018). Tensile Properties of Cotton Fibers: Importance, Research, and Limitations. In *Handbook of properties of textile and technical fibres*, 223–273. Elsevier.

El-Nahhal, I. M., Salem, J., Anbar, R., Kodeh, F. S., & Elmanama, A. (2020). Preparation and Antimicrobial Activity of Zno-Nps Coated Cotton/Starch and Their Functionalized Zno-Ag/Cotton And Zn(II) Curcumin/Cotton Materials. *Scientific Reports*, **10**(1)**:** Article 1. https://doi.org/10.1038/s41598-020-61306-6

Espert, A., Vilaplana, F., & Karlsson, S. (2004). Comparison of Water Absorption In Natural Cellulosic Fibres From Wood and One-Year Crops In Polypropylene Composites and Its Influence on Their Mechanical Properties. *Composites Part A: Applied Science and Manufacturing*, **35**(11)**:** 1267–1276. https://doi.org/10.1016/j.compositesa.2004.04.004

Esteghlalian, A., Hashimoto, A. G., Fenske, J. J., & Penner, M. H. (1997). Modeling and Optimization of The Dilute-Sulfuric-Acid Pretreatment of Corn Stover, Poplar and Switchgrass. *Bioresource Technology*, **59**(2–3)**:** 129–136. https://doi.org/10.1016/S0960-8524(97)81606-9

Fernandes, E. M., Mano, J. F., & Reis, R. L. (2013). Hybrid Cork–Polymer Composites Containing Sisal Fibre: Morphology, Effect of The Fibre Treatment on The Mechanical Properties and Tensile Failure Prediction. *Composite Structures*, **105:** 153–162. https://doi.org/10.1016/j.compstruct.2013.05.012

Fiore, V., Di Bella, G., & Valenza, A. (2015a). The Effect of Alkaline Treatment on Mechanical Properties of Kenaf Fibers And Their Epoxy Composites. *Composites Part B: Engineering*, **68:** 14–21.

Fiore, V., Di Bella, G., & Valenza, A. (2015b). The Effect of Alkaline Treatment on Mechanical Properties Of Kenaf Fibers And Their Epoxy Composites. *Composites PartB: Engineering*, **68:** 14–21. https://doi.org/10.1016/j.compositesb.2014.08.025

Fischer, W. J., Mayr, M., Spirk, S., Reishofer, D., Jagiello, L. A., Schmiedt, R., Colson, J., Zankel, A., & Bauer, W. (2017). Pulp Fines-Characterization, Sheet Formation, And Comparison to Microfibrillated Cellulose. *Polymers*, **9**(8)**:** 366. https://doi.org/10.3390/polym9080366

FORWARD Nepal. (2016). Implementation of Forest-Based Enterprise Promotion Programme in Bajura and Doti.

French, A. D. (2020). Increment In Evolution of Cellulose Crystallinity Analysis. In *Cellulose* **27**(10)**:** 5445–5448. Springer.

FRY, S. C. (1989). The Structure and Functions of Xyloglucan. *Journal of Experimental Botany*, **40**(1)**:** 1–11. https://doi.org/10.1093/jxb/40.1.1

Fu, S.-Y., & Lauke, B. (1996). Effects of Fiber Length And Fiber Orientation Distributions on The Tensile Strength of Short-Fiber-Reinforced Polymers. *Composites Science and Technology*, **56**(10)**:** 1179–1190.

Gatenholm, P., & Tenkanen, M. (2003). Hemicellulose And Their Derivatives. In *Hemicelluloses: Science and Technology*. Americal Chemical society.

George, M., Mussone, P. G., & Bressler, D. C. (2014). Surface And Thermal Characterization of Natural Fibres Treated with Enzymes. *Industrial Crops and Products*, **53:** 365–373. https://doi.org/10.1016/j.indcrop.2013.12.037

Ghasemi, N., Jamali-Sheini, F., & Zekavati, R. (2017). Cuo and Ag/Cuo Nanoparticles: Biosynthesis and Antibacterial Properties. *Materials Letters*, **196:** 78–82. https://doi.org/10.1016/j.matlet.2017.02.111

Gleba, M., & Harris, S. (2019). The First Plant Bast Fibre Technology: Identifying Splicing in Archaeological Textiles. *Archaeological and Anthropological Sciences*, **11**(5)**:** 2329–2346. https://doi.org/10.1007/s12520-018-0677-8

GoN, I. (2017). *Nepal National Center Export Strategy: Handmade Paper and Paper Products 2017-2021,* 1–124. International Trade Center, Government of Nepal.

Gouanvé, F., Marais, S., Bessadok, A., Langevin, D., & Métayer, M. (2007). Kinetics of Water Sorption in Flax and PET Fibers. *European Polymer Journal*, **43**(2)**:** 586–598. https://doi.org/10.1016/j.eurpolymj.2006.10.023

Gurunathan, T., Mohanty, S., & Nayak, S. K. (2015). A Review of The Recent Developments in Biocomposites Based on Natural Fibres and Their Application Perspectives. *Composites Part A: Applied Science and Manufacturing*, **77:** 1–25. https://doi.org/10.1016/j.compositesa.2015.06.007

Haq, I., Mazumder, P., & Kalamdhad, A. S. (2020). Recent Advances in Removal of Lignin From Paper Industry Wastewater and Its Industrial Applications – A Review. *Bioresource Technology*, **312:** 123636. https://doi.org/10.1016/j.biortech.2020.123636

Haque, M. M., Hasan, M., Islam, M. S., & Ali, M. E. (2009a). Physico-Mechanical Properties of Chemically Treated Palm and Coir Fiber Reinforced Polypropylene composites. *Bioresource Technology*, **100**(20)**:** 4903–4906.

Haque, Md. M., Hasan, M., Islam, Md. S., & Ali, Md. E. (2009b). Physico-Mechanical Properties of Chemically Treated Palm and Coir Fiber Reinforced Polypropylene Composites. *Bioresource Technology*, **100**(20)**:** 4903–4906. https://doi.org/10.1016/j.biortech.2009.04.072

Harmsen, P. F. H., Huijgen, W., Bermudez, L., & Bakker, R. (2010). Literature Review of Physical and Chemical Pretreatment Processes for Lignocellulosic Biomass. *Wageningen UR - Food & Biobased Research.* https://library.wur.nl/WebQuery/wurpubs/396201

Harmsen, P. F., Huijgen, W., Bermudez, L., & Bakker, R. (2010). *Literature review of physical and chemical pretreatment processes for lignocellulosic biomass* (No. 1184). Wageningen UR-Food & Biobased Research.

Booth, I., Goodman, A. M., Grishanov, S. A., & Harwood, R. J. (2004). A mechanical investigation of the retting process in dew-retted hemp (Cannabis sativa). *Annals of applied biology*, **145**(1)**:** 51-58.

Hashim, M. Y., Amin, A. M., Marwah, O. M. F., Othman, M. H., Yunus, M. R. M., & Huat, N. C. (2017a). The Effect of Alkali Treatment Under Various Conditions on Physical Properties of Kenaf Fiber. *Journal of Physics: Conference Series*, **914**(1)**:** 012030.

Hashim, M. Y., Amin, A. M., Marwah, O. M. F., Othman, M. H., Yunus, M. R. M., & Huat, N. C. (2017b). The Effect of Alkali Treatment Under Various Conditions on Physical Properties of Kenaf Fiber. *Journal of Physics: Conference Series*, **914**(1)**:** 012030. https://doi.org/10.1088/1742-6596/914/1/012030

Hashim, M. Y., Amin, A. M., Marwah, O. M. F., Othman, M. H., Yunus, M. R. M., & Huat, N. C. (2017c). The Effect of Alkali Treatment Under Various Conditions on Physical Properties of Kenaf Fiber. *Journal of Physics: Conference Series*, **914**(1)**:** 012030. https://doi.org/10.1088/1742-6596/914/1/012030

Hendriks, A. T. W. M., & Zeeman, G. (2009). Pretreatments To Enhance the Digestibility of Lignocellulosic Biomass. *Bioresource Technology*, **100**(1)**:** 10–18. https://doi.org/10.1016/j.biortech.2008.05.027

Henriksson, M., Berglund, L. A., Isaksson, P., Lindström, T., & Nishino, T. (2008). Cellulose Nanopaper Structures of High Toughness. *Biomacromolecules*, **9**(6)**:** 1579–1585. https://doi.org/10.1021/bm800038n

Herman, T. (1956). The Role of Cottage and Small-Scale Industries in Asian Economic Development. *Economic Development and Cultural Change*, **4**(4)**:** 356–370. JSTOR.

Hu, L., Fang, X., Du, M., Luo, F., & Guo, S. (2020). Hemicellulose-Based Polymers Processing and Application. *American Journal of Plant Sciences*, **11**(12)**:** 2066–2079. https://doi.org/10.4236/ajps.2020.1112146

Hubbe, M. A. (1999). Difficult Furnishes. *Proc. TAPPI*, ***99*:** 1353–1367.

Hubbe, M. A., & Bowden, C. (2009). Handmade Paper: A Review of Its History, Craft, and Science. *BioResources*, ***4*:** 1736–1792.

Ilyas, R. A., Sapuan, S. M., & Ishak, M. R. (2018). Isolation and Characterization of Nanocrystalline Cellulose from Sugar Palm Fibres (*Arenga pinnata*). *Carbohydrate Polymers*, **181:** 1038–1051. https://doi.org/10.1016/j.carbpol.2017.11.045

Ilyas, R. A., Sapuan, S. M., Ishak, M. R., & Zainudin, E. S. (2017). Effect of Delignification on the Physical, Thermal, Chemical, and Structural Properties of Sugar Palm Fibre. *BioResources*, **12**(4)**:** Article 4.

Ilyas, R. A., Sapuan, S. M., Ishak, M. R., & Zainudin, E. S. (2019). Sugar Palm Nanofibrillated Cellulose (*Arenga pinnata* (Wurmb.) Merr): Effect of Cycles on Their Yield, Physic-Chemical, Morphological and Thermal Behavior. *International Journal of Biological Macromolecules*, **123:** 379–388. https://doi.org/10.1016/j.ijbiomac.2018.11.124

Ioelovich, M. (2018). Determination of Distortions and Sizes af Cellulose Nanocrystallites. *Res. J. Nanosci. Eng*, **2**(1)**:** 1–5.

Iqbal, H. M. N., Kyazze, G., & Keshavarz, T. (2013). Advances in the Valorization of Lignocellulosic Materials by Biotechnology: An Overview. *BioResources*, **8**(2)**:** 3157–3176. https://doi.org/10.15376/biores.8.2.3157-3176

Ishaq, A. R., Jabeen, F., Manzoor, M., Younis, T., Noor, A., & Noor, F. (2020). *Current Status of Microalgae to Produce Biogas Through Pretreatment of Lignocellulosic Waste in the Era of 21-Century* [Preprint]. BIOLOGY. https://doi.org/10.20944/preprints202008.0233.v1

ITC. (2017). *Nepal National Center Export Strategy: Handmade Paper and Paper Products 2017-2021*. Government of Nepal.

Jabbari, F., Babaeipour, V., & Bakhtiari, S. (2022). Bacterial Cellulose-Based Composites for Nerve Tissue Engineering. *International Journal of Biological Macromolecules*.

Jagadeesh, P., Puttegowda, M., Thyavihalli Girijappa, Y. G., Rangappa, S. M., & Siengchin, S. (2022). Effect of Natural Filler Materials on Fiber Reinforced Hybrid Polymer Composites: An Overview. *Journal of Natural Fibers*, **19**(11)**:** 4132–4147. https://doi.org/10.1080/15440478.2020.1854145

Jain, A., Rastogi, D., & Chanana, B. (2017). Processing and Application of Ligno-Cellulosic Fibres. *International Journal of Current Research*, ***9***

Jayani, R. S., Saxena, S., & Gupta, R. (2005). Microbial Pectinolytic Enzymes: A Review. *Process Biochemistry*, **40**(9)**:** 2931–2944. https://doi.org/10.1016/j.procbio.2005.03.026

Jayaramudu, J., Reddy, G. S. M., Varaprasad, K., Sadiku, E. R., Ray, S. S., & Rajulu, A. V. (2014). Mechanical Properties of Uniaxial Natural Fabric *Grewia tilifolia* Reinforced Epoxy Based Composites: Effects of Chemical Treatment. *Fibers and Polymers*, **15**(7)**:** 1462–1468. https://doi.org/10.1007/s12221-014-1462-7

Jensen, C. U., Rodriguez Guerrero, J. K., Karatzos, S., Olofsson, G., & Iversen, S. B. (2017). Fundamentals of Hydrofaction^{TM}: Renewable Crude Oil from Woody Biomass. *Biomass Conversion and Biorefinery*, **7**(4)**:** 495–509. https://doi.org/10.1007/s13399-017-0248-8

Jobe, M. C., Mthiyane, D. M. N., Mwanza, M., & Onwudiwe, D. C. (2022). Biosynthesis of Zinc Oxide and Silver/Zinc Oxide Nanoparticles from *Urginea epigea* for Antibacterial and Antioxidant Applications. *Heliyon*, **8**(12)**:** e12243. https://doi.org/10.1016/j.heliyon.2022.e12243

John, M., & Thomas, S. (2008). Biofibres and Biocomposites. *Carbohydrate Polymers*, **71**(3)**:** 343–364. https://doi.org/10.1016/j.carbpol.2007.05.040

Jones, D., Ormondroyd, G. O., Curling, S. F., Popescu, C.-M., & Popescu, M.-C. (2017). Chemical Compositions of Natural Fibres. In *Advanced High Strength Natural Fibre Composites in Construction*, 23–58. Elsevier. https://doi.org/10.1016/B978-0-08-100411-1.00002-9

Kandel, K. P., Adhikari, M., Kharel, M., Aryal, G. M., Pandeya, S., Joshi, M. K., Dahal, B., Gautam, B., & Neupane, B. B. (2022a). Comparative Study on Material Properties of Wood-Ash Alkali and Commercial Alkali Treated Sterculia Fiber. *Cellulose*, 1–10.

Kandel, K. P., Adhikari, M., Kharel, M., Aryal, G. M., Pandeya, S., Joshi, M. K., Dahal, B., Gautam, B., & Neupane, B. B. (2022b). Comparative Study on Material Properties of Wood-Ash Alkali and Commercial Alkali Treated Sterculia Fiber. *Cellulose*, 1–10.

Kandel, K. P., Aryal, G. M., & Neupane, B. B. (2023). Kinetics of Water Sorption in Single Sterculia and Bauhinia Fibers at Ambient Temperature. *Results in Chemistry*, **5:** 100872.

Kandel, K. P., Menuka Adhikari, Madhav Kharel, Girja Mani Aryal, Shiva Pandeya, Mahesh Kumar Joshi, Bipeen Dahal, Bhoj Gautam, & Bhanu Bhakta Neupane. (2022a). Comparative Study on Material Properties of Wood-Ash Alkali and Commercial Alkali Treated Sterculia Fiber. *Cellulose*, **29**(10)**:** 5913–5922. https://doi.org/10.1007/s10570-022-04610-w

Kandel, K. P., Menuka Adhikari, Madhav Kharel, Girja Mani Aryal, Shiva Pandeya, Mahesh Kumar Joshi, Bipeen Dahal, Bhoj Gautam, & Bhanu Bhakta Neupane. (2022b). Comparative Study on Material Properties of Wood-Ash Alkali and Commercial Alkali Treated Sterculia Fiber. *Cellulose*, **29**(10)**:** 5913–5922. https://doi.org/10.1007/s10570-022-04610-w

Kauffman, G. B. (1993). Rayon: The First Semi-Synthetic Fiber Product. *Journal of Chemical Education*, **70**(11)**:** 887. https://doi.org/10.1021/ed070p887

Khoathane, M. C., Sadiku, E. R., & Agwuncha, C. S. (2015). Surface Modification of Natural Fiber Composites and Their Potential Applications. In *Surface Modification of Biopolymers*, 370–400. John Wiley & Sons, Ltd. https://doi.org/10.1002/9781119044901.ch14

Kim, H.-S., Kim, S., Kim, H.-J., & Yang, H.-S. (2006). Thermal Properties of Bio-Flour-Filled Polyolefin Composites With Different Compatibilizing Agent Type and Content. *Thermochimica Acta*, **451**(1–2)**:** 181–188.

Kimura, S., Laosinchai, W., Itoh, T., Cui, X., Linder, C. R., & Brown, R. M., Jr. (1999). Immunogold Labeling of Rosette Terminal Cellulose-Synthesizing Complexes in the Vascular Plant Vigna Angularis. *The Plant Cell*, **11**(11)**:** 2075–2085. https://doi.org/10.1105/tpc.11.11.2075

Klemm, D., Heublein, B., Fink, H.-P., & Bohn, A. (2005). Cellulose: Fascinating Biopolymer and Sustainable Raw Material. *Angewandte Chemie International Edition*, **44**(22)**:** 3358–3393. https://doi.org/10.1002/anie.200460587

Kljun, A., Benians, T. A., Goubet, F., Meulewaeter, F., Knox, J. P., & Blackburn, R. S. (2011). Comparative Analysis of Crystallinity Changes in Cellulose I Polymers Using ATR-FTIR, X-ray Diffraction, and Carbohydrate-Binding Module Probes | Biomacromolecules. *Biomacromolecules*, **12:** 4121−4126.

Kondo, T., & Sawatari, C. (1996). A Fourier Transform Infra-Red Spectroscopic Analysis of the Character of Hydrogen Bonds in Amorphous Cellulose. *Polymer*, **37**(3)**:** 393–399. https://doi.org/10.1016/0032-3861(96)82908-9

Kootstra, A. M. J., Beeftink, H. H., Scott, E. L., & Sanders, J. P. M. (2009). Comparison of Dilute Mineral and Organic Acid Pretreatment for Enzymatic Hydrolysis of Wheat Straw. *Biochemical Engineering Journal*, **46**(2)**:** 126–131. https://doi.org/10.1016/j.bej.2009.04.020

Kumar, A., Choudhary, A., Kaur, H., Mehta, S., & Husen, A. (2021). Metal-Based Nanoparticles, Sensors, and Their Multifaceted Application in Food Packaging. *Journal of Nanobiotechnology*, **19**(1)**:** 256. https://doi.org/10.1186/s12951-021-00996-0

Kumar, A., Singh, B., Jain, R., & Sharma, A. (2013). Banana Fibre (*Musa sapientum*): "A Suitable Raw Material for Handmade Paper Industry via Enzymatic Refining ". *International Journal of Engineering Research and Technology*. **8**

Larsson, P. T., Lindström, T., Carlsson, L. A., & Fellers, C. (2018). Fiber Length and Bonding Effects on Tensile Strength and Toughness of Kraft Paper. *Journal of Materials Science*, **53**(4)**:** 3006–3015.

Lewin, M., & Pearce, E. M. (1998). *Handbook of Fiber Chemistry, Second Edition, Revised and Expanded*. CRC Press. Google-Books-ID: rsieide7lUkC

Li, Q., Lin, T., & Wang, X. (2012). Effects of Ultrasonic Treatment on Wool Fibre and Fabric Properties. *Journal of the Textile Institute*, **103**(6)**:** 662–668. https://doi.org/10.1080/00405000.2011.597569

Li, X., Tabil, L. G., & Panigrahi, S. (2007). Chemical Treatments of Natural Fiber for Use in Natural Fiber-Reinforced Composites: A Review. *Journal of Polymers and the Environment*, **15**(1)**:** 25–33. https://doi.org/10.1007/s10924-006-0042-3

Liu, H., You, L., Jin, H., & Yu, W. (2013). Influence of Alkali Treatment on the Structure and Properties of Hemp Fibers. *Fibers and Polymers*, **14**(3)**:** 389–395.

Liu, W., Du, H., Zhang, M., Liu, K., Liu, H., Xie, H., Zhang, X., & Si, C. (2020). Bacterial Cellulose-Based Composite Scaffolds for Biomedical Applications: A Review. *ACS Sustainable Chemistry & Engineering*, **8**(20)**:** 7536–7562.

Lobo, F. C., Franco, A. R., Fernandes, E. M., & Reis, R. L. (2021). An Overview of the Antimicrobial Properties of Lignocellulosic Materials. *Molecules*, **26**(6)**:** 1749.

Lorenci Woiciechowski, A., Dalmas Neto, C. J., Porto De Souza Vandenberghe, L., De Carvalho Neto, D. P., Novak Sydney, A. C., Letti, L. A. J., Karp, S. G., Zevallos Torres, L. A., & Soccol, C. R. (2020). Lignocellulosic Biomass: Acid and Alkaline Pretreatments and Their Effects on Biomass Recalcitrance – Conventional Processing and Recent Advances. *Bioresource Technology*, ***304*****:** 122848. https://doi.org/10.1016/j.biortech.2020.122848

Lu, Y., He, Q., Fan, G., Cheng, Q., & Song, G. (2021). Extraction and Modification of Hemicellulose from Lignocellulosic Biomass: A Review. *Green Processing and Synthesis*, **10**(1)**:** 779–804. https://doi.org/10.1515/gps-2021-0065

Lundberg, M., Norgren, M., & Edlund, H. (2018). Validation of Crill Measurements in A High-Yield Pulp Refining Process for Improved Fines Material Control. *Nordic Pulp & Paper Research Journal*, **33**(2)**:** 200–209.

Lundell, F., Söderberg, L. D., & Alfredsson, P. H. (2011). Fluid Mechanics of Papermaking. *Annual Review of Fluid Mechanics*, **43:** 195–217.

Madsen, B., & Gamstedt, E. K. (2013). Wood Versus Plant Fibers: Similarities and Differences in Composite Applications. *Advances in Materials Science and Engineering*, **2013:** e564346. https://doi.org/10.1155/2013/564346

Mahzan, S., Fitri, M., & Zaleha, M. (2017). UV Radiation Effect Towards Mechanical Properties of Natural Fibre Reinforced Composite Material: A Review. *IOP Conference Series: Materials Science and Engineering*, **165**(1)**:** 012021. https://doi.org/10.1088/1757-899X/165/1/012021

Mäki-Arvela, P., Salminen, E., Riittonen, T., Virtanen, P., Kumar, N., & Mikkola, J.-P. (2012). The Challenge of Efficient Synthesis of Biofuels from Lignocellulose for Future Renewable Transportation Fuels. *International Journal of Chemical Engineering*, **2012:** e674761. https://doi.org/10.1155/2012/674761

Manian, A. P., Cordin, M., & Pham, T. (2021). Extraction of Cellulose Fibers from Flax and Hemp: A Review. *Cellulose*, **28** (13)**:** 8275–8294. https://doi.org/10.1007/s10570-021-04051-x

Marella, J. B. R., Madireddy, S., & Maripi, A. N. (2014). Production of Pulp from Banana Pseudo Stem for Grease Proof Paper. **2**(1)**:**

Marrakchi, Z., Khiari, R., Oueslati, H., Mauret, E., & Mhenni, F. (2011). Pulping and Papermaking Properties of Tunisian Alfa Stems (*Stipa tenacissima*)—Effects of Refining Process. *Industrial Crops and Products*, **34**(3)**:** 1572.

McKendry, P. (2002). Energy Production from Biomass (Part 1): Overview of Biomass. *Bioresource Technology*, **83**(1)**:** 37–46. https://doi.org/10.1016/S0960-8524(01)00118-3

Mejouyo, P. W. H., Nkemaja, E. D., Beching, O. R., Tagne, N. R. S., Kana'a, T., & Njeugna, E. (2020). Physical and Tensile Properties of Handmade *Sida rhombifolia* Paper. *International Journal of Biomaterials*, **2020:** 3967641. https://doi.org/10.1155/2020/3967641

Messerschmidt, D. A. (1988). Success in Small Farmer Development: Paper Making at Pang and Nanglibang, Nepal. *World Development*, **16**(6)**:** 733–750. https://doi.org/10.1016/0305-750X(88)90179-9

Modibbo, U. U., Aliyu, B. A., & Nkafamiya, I. I. (2009). The Effect of Mercerization Media on the Physical Properties of Local Plant Bast Fibres. *International Journal of Physical Sciences*, **4**(11)**:** 698–704.

Mohanty, A., Misra, M., & Drzal, L. (2001). Surface Modifications of Natural Fibers and Performance of the Resulting Biocomposites: An Overview. *Composite Interfaces*, ***8*:** 313–343.

Mohapatra, B., Mohapatra, S., & Sharma, N. (2023). Biosynthesized Ag–Zno Nanohybrids Exhibit Strong Antibacterial Activity by Inducing Oxidative Stress. *Ceramics International*, **49**(12)**:** 20218–20233. https://doi.org/10.1016/j.ceramint.2023.03.146

Möller, M., & Popescu, C. (2012). Natural Fibers. In *Polymer Science: A Comprehensive Reference*, 267–280. Elsevier. https://doi.org/10.1016/B978-0-444-53349-4.00266-1

More, A., Elder, T., & Jiang, Z. (2021). A Review of Lignin Hydrogen Peroxide Oxidation Chemistry with Emphasis on Aromatic Aldehydes and Acids. *Holzforschung*, **75**(9)**:** 806–823. https://doi.org/10.1515/hf-2020-0165

Moreira, L. R. S., & Filho, E. X. F. (2008). An Overview of Mannan Structure and Mannan-Degrading Enzyme Systems. *Applied Microbiology and Biotechnology*, **79**(2)**:** 165–178. https://doi.org/10.1007/s00253-008-1423-4

Morton, W., & Hearle, J. (2008). An Introduction to Fibre Structure. In *In: Physical properties of textile fibres*. Woodhead Publishing Limited.

Mosier, N. (2005). Features of Promising Technologies for Pretreatment of Lignocellulosic Biomass. *Bioresource Technology*, **96**(6)**:** 673–686. https://doi.org/10.1016/j.biortech.2004.06.025

Motamedian, H. R., Halilovic, A. E., & Kulachenko, A. (2019). Mechanisms of Strength and Stiffness Improvement of Paper After PFI Refining with a Focus on the Effect of Fines. *Cellulose*, **26**(6)**:** 4099–4124. https://doi.org/10.1007/s10570-019-02349-5

Mwaikambo, L. Y., & Ansell, M. P. (2002). Chemical Modification of Hemp, Sisal, Jute, and Kapok Fibers by Alkalization. *Journal of Applied Polymer Science*, **84**(12)**:** 2222–2234.

Nazeruddin, G. M., Prasad, N. R., Prasad, S. R., Shaikh, Y. I., Waghmare, S. R., & Adhyapak, P. (2014). Coriandrum Sativum Seed Extract Assisted In Situ Green Synthesis of Silver Nanoparticle and Its Anti-Microbial Activity. *Industrial Crops and Products*, **60:** 212–216. https://doi.org/10.1016/j.indcrop.2014.05.040

Nechita, P., Mirela, R., & Ciolacu, F. (2021). Xylan Hemicellulose: A Renewable Material with Potential Properties for Food Packaging Applications. *Sustainability*, **13**(24)**:** Article 24. https://doi.org/10.3390/su132413504

Obame, S. V., Betené, A. D. O., Naoh, P. M., Betené, F. E., & Atangana, A. (2022). Characterization of the Neuropeltis Acuminatas Liana Fiber Treated as Composite Reinforcement. *Results in Materials*, **16:** 100327. https://doi.org/10.1016/j.rinma.2022.100327

Obi Reddy, K., Uma Maheswari, C., Shukla, M., & Muzenda, E. (2014a). Preparation, Chemical Composition, Characterization, and Properties of Napier Grass Paper Sheets. *Separation Science and Technology*, **49**(10)**:** 1527–1534. https://doi.org/10.1080/01496395.2014.893358

Obi Reddy, K., Uma Maheswari, C., Shukla, M., & Muzenda, E. (2014b). Preparation, Chemical Composition, Characterization, and Properties of Napier Grass Paper sheets. *Separation Science and Technology*, **49**(10)**:** 1527–1534.

Oh, S. Y., Yoo, D. I., Shin, Y., & Seo, G. (2005). FTIR Analysis of Cellulose Treated with Sodium Hydroxide and Carbon Dioxide. *Carbohydrate Research*, **340**(3)**:** 417–428. https://doi.org/10.1016/j.carres.2004.11.027

Okolie, J. A., Nanda, S., Dalai, A. K., & Kozinski, J. A. (2021). Chemistry and Specialty Industrial Applications of Lignocellulosic Biomass. *Waste and Biomass Valorization*, **12**(5)**:** 2145–2169. https://doi.org/10.1007/s12649-020-01123-0

Oushabi, A., Sair, S., Oudrhiri, H. F., Abboud, Y., Tanane, O., & El, B. A. (2017). The Effect of Alkali Treatment on Mechanical, Morphological and Thermal Properties af Date Palm Fibers (Dpfs): Study of the Interface of Dpfepolyurethane Composite. *South African Journal of Chemical Engineering*, **23**(1)**:** 116–123. https://doi.org/10.1016/j.sajce.2017.04.005

Page, D. H. (1969). A Theory for the Tensile Strength of Paper. *Tappi*, **52:** 674–681.

Panchal, P., Sharma, R., Sudharshan Reddy, A., Nehra, K., Sharma, A., & Nehra, S. P. (2023). Eco-Friendly Synthesis of Ag-Doped Zno/Mgo as a Potential Photocatalyst for Antimicrobial and Dye Degradation Applications. *Coordination Chemistry Reviews*, **493:** 215283. https://doi.org/10.1016/j.ccr.2023.215283

Park, S., Baker, J. O., Himmel, M. E., Parilla, P. A., & Johnson, D. K. (2010a). Cellulose Crystallinity Index: Measurement Techniques and Their Impact on Interpreting Cellulase Performance. *Biotechnology for Biofuels*, **3**(1)**:** 1–10.

Park, S., Baker, J. O., Himmel, M. E., Parilla, P. A., & Johnson, D. K. (2010b). Cellulose Crystallinity Index: Measurement Techniques and Their Impact on Interpreting Cellulase Performance. *Biotechnology for Biofuels*, **3**(1)**:** 10. https://doi.org/10.1186/1754-6834-3-10

Piqué, N., Gómez-Guillén, M. del C., & Montero, M. P. (2018). Xyloglucan, A Plant Polymer with Barrier Protective Properties Over the Mucous Membranes: An Overview. *International Journal of Molecular Sciences*, **19**(3)**:** 673. https://doi.org/10.3390/ijms19030673

Poletto, M., Ornaghi, H. L., & Zattera, A. J. (2014a). Native Cellulose: Structure, Characterization and Thermal Properties. *Materials*, **7**(9)**:** 6105–6119.

Poletto, M., Ornaghi, H. L., & Zattera, A. J. (2014b). Native Cellulose: Structure, Characterization and Thermal Properties. *Materials*, **7**(9)**:** Article 9. https://doi.org/10.3390/ma7096105

Poletto, M., Pistor, V., Santana, R. M. C., & Zattera, A. J. (2012). Materials Produced from Plant Biomass: Part II: Evaluation of Crystallinity and Degradation Kinetics of Cellulose. *Mater. Res.*, **15:** 421−427.

Poudyal, A. (2004). Sustainability of Local Hand-made Paper (Nepali Kagat) Enterprises: A Case Study of Dolakha District. *Journal of Forest and Livelihood*, **4:** 64–69.

Prasad, R. D., Charmode, N., Shrivastav, O. P., Prasad, S. R., Moghe, A., AnantSamant, Sarvalkar, P. D., & Prasad, N. R. (2021). A Review on Concept of Nanotechnology in Veterinary Medicine. *ES Food & Agroforestry*, **4**(0)**:** 28–60.

Preisner, M., Kulma, A., Zebrowski, J., Dymińska, L., Hanuza, J., Arendt, M., Starzycki, M., & Szopa, J. (2014). Manipulating Cinnamyl Alcohol Dehydrogenase (CAD) Expression in Flax Affects Fibre Composition and Properties. *BMC Plant Biology*, **14**(1)**:** 50. https://doi.org/10.1186/1471-2229-14-50

Pritchard, M., Sarsby, R. W., & Anand, S. C. (2000). 14 - Textiles In Civil Engineering. Part 2 – Natural Fibre Geotextiles. In A. R. Horrocks & S. C. Anand (Eds.), *Handbook of Technical Textiles*, 372–406. Woodhead Publishing. https://doi.org/10.1533/9781855738966.372

Quiroz Castañeda, R., & Folch-Mallol, J. (2013). *Degradation of Lignocellulosic Biomass - Techniques, Applications and Commercialization Sustainable Degradation of Lignocellulosic Biomass - Techniques, Applications and Commercialization* 275.

Ramadevi, P., Sampathkumar, D., Srinivasa, C. V., & Bennehalli, B. (2012). Effect of Alkali Treatment on Water Absorption of Single Cellulosic Abaca Fiber. *BioResources*, **7**(3)**:** 3515–3524. https://doi.org/10.15376/biores.7.3.3515-3524

Ray, D., Sarkar, B. K., Basak, R. K., & Rana, A. K. (2002). Study of the Thermal Behavior of Alkali-Treated Jute Fibers. *Journal of Applied Polymer Science*, **85**(12)**:** 2594–2599. https://doi.org/10.1002/app.10934

Reddy, N., & Yang, Y. (2005). Structure and Properties of High Quality Natural Cellulose Fibers from Cornstalks. *Polymer*, **46**(15)**:** 5494–5500. https://doi.org/10.1016/j.polymer.2005.04.073

Robak, K., & Balcerek, M. (2018). Review of Second Generation Bioethanol Production from Residual Biomass. *Food Technology and Biotechnology*, **56**(2)**:** 174–187. https://doi.org/10.17113/ftb.56.02.18.5428

Sadrmanesh, V., & Chen, Y. (2019). Bast Fibres: Structure, Processing, Properties, and Applications. *International Materials Reviews*, **64**(7)**:** 381–406. https://doi.org/10.1080/09506608.2018.1501171

Saha, P., Manna, S., Chowdhury, S. R., Sen, R., Roy, D., & Adhikari, B. (2010a). Enhancement of Tensile Strength of Lignocellulosic Jute Fibers By Alkali-Steam Treatment. *Bioresource Technology*, **101**(9)**:** 3182–3187.

Saha, P., Manna, S., Chowdhury, S. R., Sen, R., Roy, D., & Adhikari, B. (2010b). Enhancement of Tensile Strength of Lignocellulosic Jute Fibers By Alkali-Steam Treatment. *Bioresource Technology*, **101**(9)**:** 3182–3187. https://doi.org/10.1016/j.biortech.2009.12.010

Sampson, W. W. (2004). A Model for Fibre Contacts in Planar Random Fibre Networks. *Journal of Materials Science*, **39**(8)**:** 2775–2781. https://doi.org/10.1023/B:JMSC.0000021453.00080.5a

Samy, M. M., Mohamed, M. G., Mansoure, T. H., Meng, T. S., Khan, M. A. R., Liaw, C.-C., & Kuo, S.-W. (2022). Solid State Chemical Transformations Through Ring-Opening Polymerization of Ferrocene-Based Conjugated Microporous Polymers in Host–Guest Complexes with Benzoxazine-Linked Cyclodextrin. *Journal of the Taiwan Institute of Chemical Engineers*, **132:** 104110. https://doi.org/10.1016/j.jtice.2021.10.010

Sanjay, M. R., Madhu, P., Jawaid, M., Senthamaraikannan, P., Senthil, S., & Pradeep, S. (2018). Characterization and Properties of Natural Fiber Polymer Composites: A Comprehensive Review. *Journal of Cleaner Production*, **172:** 566–581. https://doi.org/10.1016/j.jclepro.2017.10.101

Saravanadevi, K., Kavitha, M., Karpagavinayagam, P., Saminathan, K., & Vedhi, C. (2022). Biosynthesis of ZnO and Ag doped ZnO nanoparticles from Vitis vinifera leaf for antibacterial, photocatalytic application. *Materials Today: Proceedings*, **48:** 352–356. https://doi.org/10.1016/j.matpr.2020.07.707

Saravanakumaar, A., Senthilkumar, A., Saravanakumar, S. S., Sanjay, M. R., & Khan, A. (2018a). Impact of Alkali Treatment on Physico-Chemical, Thermal, Structural and Tensile Properties of Carica Papaya Bark Fibers. *International Journal of Polymer Analysis and Characterization*, **23**(6)**:** 529–536. https://doi.org/10.1080/1023666X.2018.1501931

Saravanakumaar, A., Senthilkumar, A., Saravanakumar, S. S., Sanjay, M. R., & Khan, A. (2018b). Impact of Alkali Treatment on Physico-Chemical, Thermal, Structural and Tensile Properties of *Carica Papaya* Bark Fibers. *International Journal of Polymer Analysis and Characterization*, **23**(6)**:** 529–536. https://doi.org/10.1080/1023666X.2018.1501931

Saravanakumar, S. S., Kumaravel, A., Nagarajan, T., Sudhakar, P., & Baskaran, R. (2013a). Characterization of A Novel Natural Cellulosic Fiber From Prosopis Juliflora Bark. *Carbohydrate Polymers*, **92**(2)**:** 1928–1933.

Saravanakumar, S. S., Kumaravel, A., Nagarajan, T., Sudhakar, P., & Baskaran, R. (2013b). Characterization of A Novel Natural Cellulosic Fiber From Prosopis Juliflora Bark. *Carbohydrate Polymers*, **92**(2)**:** 1928–1933. https://doi.org/10.1016/j.carbpol.2012.11.064

Sassi, J.-F., Tekely, P., & Chanzy, H. (2000). Relative Susceptibility of the Iα And Iβ Phases of Cellulose Towards Acetylation. *Cellulose*, **7**(2)**:** 119–132. https://doi.org/10.1023/A:1009224008802

Segal, L., Creely, J. J., Martin, A. E., & Conrad, C. M. (1959). An Empirical Method for Estimating the Degree of Crystallinity of Native Cellulose Using the X-Ray Diffractometer. *Text. Res. J.*, **29:** 786− 794.

Seki, Y., Sever, K., Erden, S., Sarikanat, M., Neser, G., & Ozes, C. (2012). Characterization of *Luffa cylindrica* Fibers and the Effect of Water Aging on the Mechanical Properties of its Composite with Polyester. *Journal of Applied Polymer Science*, **123**(4)**:** 2330–2337. https://doi.org/10.1002/app.34744

Senthamaraikannan, P., Saravanakumar, S. S., Sanjay, M. R., Jawaid, M., & Siengchin, S. (2019). Physico-Chemical and Thermal Properties of Untreated and Treated *Acacia planifrons* Bark Fibers for Composite Reinforcement. *Materials Letters*, **240:** 221–224. https://doi.org/10.1016/j.matlet.2019.01.024

Shahinur, S., Sayeed, M. M. A., Hasan, M., Sayem, A. S. M., Haider, J., & Ura, S. (2022). Current Development and Future Perspective on Natural Jute Fibers and Their Biocomposites. *Polymers*, **14**(7)**:** 1445. https://doi.org/10.3390/polym14071445

Shahzadi, T., Mehmood, S., Irshad, M., Anwar, Z., Afroz, A., Zeeshan, N., Rashid, U., & Sughra, K. (2014). Advances In Lignocellulosic Biotechnology: A Brief Review on Lignocellulosic Biomass and Cellulases. *Advances in Bioscience and Biotechnology*, **5**(3)**:** 246–251. https://doi.org/10.4236/abb.2014.53031

Sharma, S., & Kumar, A. (2020). Lignin: Biosynthesis and Transformation for Industrial Applications. *Springer International Publishing*. https://doi.org/10.1007/978-3-030-40663-9

Shavandi, A., Hosseini, S., Okoro, O. V., Nie, L., Eghbali Babadi, F., & Melchels, F. (2020). 3D Bioprinting of Lignocellulosic Biomaterials. *Advanced Healthcare Materials,* **9**(24)**:** 2001472.

Sheng, Z., Gao, J., Jin, Z., Dai, H., Zheng, L., & Wang, B. (2014). Effect of Steam Explosion on Degumming Efficiency and Physicochemical Characteristics of Banana Fiber. *Journal of Applied Polymer Science*, **131**(16)**:** https://doi.org/10.1002/app.40598

Shi, C., Zhang, L., Bian, H., Shi, Z., Ma, J., & Wang, Z. (2021). Construction of Ag–Zno/Cellulose Nanocomposites via Tunable Cellulose Size for Improving Photocatalytic Performance. *Journal of Cleaner Production*, **288:** 125089. https://doi.org/10.1016/j.jclepro.2020.125089

Sinha, E., & Rout, S. K. (2008a). Influence of Fibre-Surface Treatment on Structural, Thermal and Mechanical Properties of Jute. *Journal of Materials Science*, **43**(8)**:** 2590–2601.

Sinha, E., & Rout, S. K. (2008b). Influence of Fibre-Surface Treatment on Structural, Thermal and Mechanical Properties of Jute. *Journal of Materials Science*, **43**(8)**:** 2590–2601. https://doi.org/10.1007/s10853-008-2478-4

Sisti, L., Totaro, G., Vannini, M., & Celli, A. (2018). Retting Process as a Pretreatment of Natural Fibers for the Development of Polymer Composites. In S. Kalia (Ed.), *Lignocellulosic Composite Materials,* 97–135. Springer International Publishing. https://doi.org/10.1007/978-3-319-68696-7_2

Sitotaw, Y. W., Habtu, N. G., Gebreyohannes, A. Y., Nunes, S. P., & Van Gerven, T. (2021). Ball Milling as an Important Pretreatment Technique in Lignocellulose Biorefineries: A Review. *Biomass Conversion and Biorefinery*, 1–24.

Skundric, P., Kostic, M., Medovic, A., Pejic, B., Kuraica, M., Vuckovic, A., Obradovic, B., Mitrakovic, D., & Puric, J. (2007). Wetting Properties of Hemp Fibres Modified by Plasma Treatment. *Journal of Natural Fibers*, **4**(1)**:** 25–33. https://doi.org/10.1300/J395v04n01_03

Smole, M.S., Hribernik, S., Kleinschek, K.S., & Kreze, T.,. (2013). Plant Fibres for Textile and Technical Applications. In *Advances in Agrophysical Research*.

Soszyński, R. M. (1995). Relative Bonded Area - A Different Approach. *Nordic Pulp & Paper Research Journal*, **10**(2)**:** 150–151. https://doi.org/10.3183/npprj-1995-10-02-p150-151

Sottile, F., Modica, A., Rosselli, S., Catania, C. A., Cavallaro, G., Lazzara, G., & Bruno, M. (2021). Hand-Made Paper Obtained by Green Procedure of Cladode Waste of *Opuntia ficus Indica* (L.) Mill. From Sicily. *Natural Product Research*, **35**(3)**:** 359–368. https://doi.org/10.1080/14786419.2019.1631820

Stamboulis, A. (2000). Environmental Durability of Flax Fibres and Their Composites Based on Polypropylene Matrix. *Applied Composite Materials*, **7**(5/6)**:** 273–294. https://doi.org/10.1023/A:1026581922221

Subedi, B. P., Binayee, S., & Gyawali, S. (2006). *Handmade Paper Value-Chain of Nepal: Prospects and Challenges in Growth, Distributional Equity and Conservation*.

Sugiyama, J., Persson, J., & Chanzy, H. (1991). Combined Infrared and Electron Diffraction Study of the Polymorphism of Native Celluloses. *Macromolecules*, **24:** 2461−2466. https://doi.org/10.1021/ma00009a050

Sui, G., Fuqua, M. A., Ulven, C. A., & Zhong, W. H. (2009). A Plant Fiber Reinforced Polymer Composite Prepared by a Twin-Screw Extruder. *Bioresource Technology*, **100**(3)**:** 1246–1251.

Sumrith, N., Techawinyutham, L., Sanjay, M. R., Dangtungee, R., & Siengchin, S. (2020). Characterization of Alkaline and Silane Treated Fibers of 'Water Hyacinth Plants' and Reinforcement of 'Water Hyacinth Fibers' with Bioepoxy to Develop Fully Biobased Sustainable Ecofriendly Composites. *Journal of Polymers and the Environment*, **28**(10)**:** 2749–2760. https://doi.org/10.1007/s10924-020-01810-y

Sun, Y., & Cheng, J. (2002). Hydrolysis of Lignocellulosic Materials for Ethanol Production: A Review. *Bioresource Technology*, **83**(1)**:** 1–11. https://doi.org/10.1016/S0960-8524(01)00212-7

Synytsya, A., & Novak, M. (2014). Structural Analysis of Glucans. *Annals of Translational Medicine*, **2**(2)**:** 17. https://doi.org/10.3978/j.issn.2305-5839.2014.02.07

Tahir, P., Ahmed, A. B., SaifulAzry, S. O. A., & Ahmed, Z. (2011). Retting Process of Some Bast Plant Fibres and its Effect on Fibre Quality: A Review.

Talam, S., Karumuri, S. R., & Gunnam, N. (2012). Synthesis, Characterization, and Spectroscopic Properties of ZnO Nanoparticles. *ISRN Nanotechnology*, **2012:** 1–6. https://doi.org/10.5402/2012/372505

Tanpichai, S., Boonmahitthisud, A., Soykeabkaew, N., & Ongthip, L. (2022). Review of the Recent Developments in All-Cellulose Nanocomposites: Properties and Applications. *Carbohydrate Polymers*, **286:** 119192.

Tanpichai, S., Sampson, W. W., & Eichhorn, S. J. (2012a). Stress-Transfer in Microfibrillated Cellulose Reinforced Poly (Lactic Acid) Composites Using Raman Spectroscopy. *Composites Part A: Applied Science and Manufacturing*, **43**(7)**:** 1145–1152.

Tanpichai, S., Sampson, W. W., & Eichhorn, S. J. (2012b). Stress-Transfer in Microfibrillated Cellulose Reinforced Poly (Lactic Acid) Composites Using Raman Spectroscopy. *Composites Part A: Applied Science and Manufacturing*, **43**(7)**:** 1145–1152. https://doi.org/10.1016/j.compositesa.2012.02.006

Tanpichai, S., Witayakran, S., Srimarut, Y., Woraprayote, W., & Malila, Y. (2019a). Porosity, Density and Mechanical Properties of the Paper of Steam Exploded Bamboo Microfibers Controlled by Nanofibrillated Cellulose. *Journal of Materials Research and Technology*, **8**(4)**:** 3612–3622.

Tanpichai, S., Witayakran, S., Srimarut, Y., Woraprayote, W., & Malila, Y. (2019b). Porosity, Density and Mechanical Properties of the Paper of Steam Exploded Bamboo Microfibers Controlled by Nanofibrillated Cellulose. *Journal of Materials Research and Technology*, **8**(4)**:** 3612–3622. https://doi.org/10.1016/j.jmrt.2019.05.024

Tao, J., & Liu, H. (2011). A Method to Determine Sheet Relative Bonded Area Using the Fiber Flexiblity Index. *Instrumentation Science & Technology*, **39**(2)**:** 161–172. https://doi.org/10.1080/10739149.2010.545849

TAPPI. (1997). Thickness (Caliper) of Paper, Paperboard and Combined Board. *T411 Om-97*.

TAPPI. (2012a). Grammage of Paper and Paperboard (Weight Per Unit Area). *T410 Om-08*.

TAPPI. (2012b). Water Absorptiveness of Sized (Non-Bibulous) Paper, Paperboard, and Corrugated Fiberboard (Cobb Test). *T441 Om-09*.

Tayeb, A. H., Amini, E., Ghasemi, S., & Tajvidi, M. (2018). Cellulose Nanomaterials—Binding Properties and Applications: A Review. *Molecules*, **23**(10)**:** Article 10. https://doi.org/10.3390/molecules23102684

Thomsen, A. B., Thygesen, A., Bohn, V., Nielsen, K. V., Pallesen, B., & Jørgensen, M. S. (2006). Effects of Chemical–Physical Pre-Treatment Processes on Hemp Fibres for Reinforcement of Composites and for Textiles. *Industrial Crops and Products*, **24**(2)**:** 113–118. https://doi.org/10.1016/j.indcrop.2005.10.003

Torres, F. G., Arroyo, J. J., & Troncoso, O. P. (2019). Bacterial Cellulose Nanocomposites: An All-Nano Type of Material. *Materials Science and Engineering: C*, **98:** 1277–1293.

Truong, M., Zhong, W., Boyko, S., & Alcock, M. (2009). A Comparative Study on Natural Fibre Density Measurement. *The Journal of the Textile Institute*, **100**(6)**:** 525–529.

Truss, R. W. (2011). Natural Fibers for Biocomposites. *MRS Bulletin*, **36**(9)**:** 711–715. https://doi.org/10.1557/mrs.2011.207

van der Werf, H. M. G., & Turunen, L. (2008). The Environmental Impacts of the Production of Hemp and Flax Textile Yarn. *Industrial Crops and Products*, **27**(1)**:** 1–10. https://doi.org/10.1016/j.indcrop.2007.05.003

Vardhini, K. J., Murugan, R., & Rathinamoorthy, R. (2019). Effect of Alkali Treatment on Physical Properties of Banana Fibre. *Indian Journal of Fibre & Textile Research (IJFTR)*, **44**(4)**:** 459–465.

Ververis, C., Georghiou, K., Christodoulakis, N., Santas, P., & Santas, R. (2004). Fiber Dimensions, Lignin and Cellulose Content of Various Plant Materials and Their Suitability for Paper Production. *Industrial Crops and Products*, **19**(3)**:** 245–254.

Vinod, A., Sanjay, M. R., Suchart, S., & Jyotishkumar, P. (2020). Renewable and Sustainable Biobased Materials: An Assessment on Biofibers, Biofilms, Biopolymers and Biocomposites. *Journal of Cleaner Production*, **258:** 120978. https://doi.org/10.1016/j.jclepro.2020.120978

Vinyas, M., Athul, S. J., Harursampath, D., Loja, M., & Thoi, T. N. (2019). A Comprehensive Review on Analysis of Nanocomposites: from Manufacturing to Properties Characterization. *Materials Research Express*, **6**(9)**:** 092002. https://doi.org/10.1088/2053-1591/ab3175

Wang, F.-Y., Li, H.-Y., Liu, H.-M., & Liu, Y.-L. (2015). Fractional Isolation and Structural Characterization of Hemicelluloses from Soybean Hull. *BioResources*, **10**(3)**:** 5256–5266. https://doi.org/10.15376/biores.10.3.5256-5266

Wong, K. J., Yousif, B. F., & Low, K. O. (2010). The Effects of Alkali Treatment on the Interfacial Adhesion of Bamboo Fibres. *Proceedings of the Institution of Mechanical Engineers, Part L: Journal of Materials: Design and Applications*, **224**(3)**:** 139–148. https://doi.org/10.1243/14644207JMDA304

Xiao, L.-P., Lin, Z., Peng, W.-X., Yuan, T.-Q., Xu, F., Li, N.-C., Tao, Q.-S., Xiang, H., & Sun, R.-C. (2014). Unraveling The Structural Characteristics of Lignin in Hydrothermal Pretreated Fibers and Manufactured Binderless Boards from *Eucalyptus grandis*. *Sustainable Chemical Processes*, **2**(1)**:** 9. https://doi.org/10.1186/2043-7129-2-9

Xu, F., Yu, J., Tesso, T., Dowell, F., & Wang, D. (2013). Qualitative and Quantitative Analysis of Lignocellulosic Biomass Using Infrared Techniques: A Mini-Review. *Applied Energy*, **104:** 801–809. https://doi.org/10.1016/j.apenergy.2012.12.019

Yang, H., Yan, R., Chen, H., Zheng, C., Lee, D. H., & Liang, D. T. (2006). In-Depth Investigation of Biomass Pyrolysis Based on Three Major Components: Hemicellulose, Cellulose and Lignin. *Energy & Fuels*, **20**(1)**:** 388–393.

Yao, W., Weng, Y., & Catchmark, J. M. (2020). Improved Cellulose X-Ray Diffraction Analysis Using Fourier Series Modeling. *Cellulose*, **27:** 5563–5579.

Yeganeh-Faal, A., Bordbar, M., Negahdar, N., & Nasrollahzadeh, M. (2017). Green Synthesis of the Ag/Zno Nanocomposite Using Valeriana Officinalis L. Root Extract: Application as a Reusable Catalyst for the Reduction of Organic Dyes an a Very Short Time. *IET Nanobiotechnology*, **11**(6)**:** 669–676. https://doi.org/10.1049/iet-nbt.2016.0198

Youssef, A. M., & El-Sayed, Samah. M. (2018). Bionanocomposites Materials for Food Packaging Applications: Concepts and Future Outlook. *Carbohydrate Polymers*, **193:** 19–27. https://doi.org/10.1016/j.carbpol.2018.03.088

Yousuf, A., Pirozzi, D., & Sannino, F. (2020). Fundamentals of Lignocellulosic Biomass. In *Lignocellulosic Biomass to Liquid Biofuels*, 1–15. Elsevier. https://doi.org/10.1016/B978-0-12-815936-1.00001-0

Zamora-Mendoza, L., Gushque, F., Yanez, S., Jara, N., Álvarez-Barreto, J. F., Zamora-Ledezma, C., Dahoumane, S. A., & Alexis, F. (2023). Plant Fibers as Composite Reinforcements for Biomedical Applications. *Bioengineering*, **10**(7)**:** 7. https://doi.org/10.3390/bioengineering10070804

Zhang, X.-Z., & Zhang, Y.-H. P. (2013). Cellulases: Characteristics, Sources, Production, and Applications. In S.-T. Yang, H. A. El-Enshasy, & N. Thongchul (Eds.), *Bioprocessing Technologies in Biorefinery for Sustainable Production of Fuels, Chemicals, and Polymers*, 131–146. John Wiley & Sons, Inc. https://doi.org/10.1002/9781118642047.ch8

Zhou, J., Zhao, F., Wang, Y., Zhang, Y., & Yang, L. (2007). Size-Controlled Synthesis of Zno Nanoparticles and Their Photoluminescence Properties. *Journal of Luminescence*, **122–123:** 195–197. https://doi.org/10.1016/j.jlumin.2006.01.089

Zille, A., Oliveira, F. R., & Souto, A. P. (2015). Plasma Treatment in Textile Industry: Plasma Treatment in Textile Industry. *Plasma Processes and Polymers*, **12**(2)**:** 98–131. https://doi.org/10.1002/ppap.201400052

APPENDIX

Publications

First Authorship

Aryal, G. M., Kandel, K. P., Bhattarai, R. K., Giri, B., Adhikari, M., Ware, A., Han, S.,George, G., Luo, Z., Gautam, B. R., & Neupane, B. B. (2022). Material Properties of Traditional Handmade Paper Samples Fabricated from Cellulosic Fiber of Lokta Bushes. *ACS Omega*, **7**(36)**:** 32717–32726. https://doi.org/10.1021/acsomega.2c04398

Aryal, G. M., Ware, W., Han, S., George, G., Luo, Z., Kandel, K. P., Gautam, B & Neupane, B. (2021). Microscopic Characterization of Eco-friendly Lokta Paper. *Microscopy and Microanalysis*, **27**(S1)**:** 720-721. doi:10.1017/S1431927621002932

Aryal, G. M., Aryal, B., Kandel, K. P., & Neupane, B. B. (2021). Cellulose-basedMicro-fibrous Materials Imaged with a Home-built Smartphone Microscope. *Microscopy Research and Technique*, **84**(8)**:** 1794-1801. DOI: 10.1002/jemt.23736

Aryal, G. M., Kandel, K. P., Adhikari, M., Evans, J., Dangol, H., Poudel, M., Pokharel, S., Shrestha, R., Gautam, B., & Neupane, B. B. (2024). Understanding the Material Properties of Alkali-Treated Lignocellulose Fiber Obtained from High-Altitude Lokta Bushes. *Biomass Conversion and Biorefinery*. https://doi.org/10.1007/s13399-024-05278-x

Contributing Authorship

Kandel, K. P., Aryal, G. M., KC, S. A., Joshi, M. K., Dahal, B., & Neupane, B. B. (2023). A Systematic Study on Material Properties of Water Retted Sterculia and Bauhinia Fiber. *BIBECHANA*, **20**(1)**:** 27–35.

Kandel, K. P., Aryal, G. M., & Neupane, B. B. (2023). Kinetics of Water Sorption in Single Sterculia and Bauhinia Fibers at Ambient Temperature. *Results in Chemistry*, 5, 100872. https://doi.org/10.1016/j.rechem.2023.100872

Kandel, K. P., Adhikari, M., Kharel, M., Aryal, G. M., Pandeya, S., Joshi, M. K., Dahal, B., Gautam, B., & Neupane, B. B. (2022). Comparative Study on Material Properties of Wood-ash Alkali and Commercial Alkali Treated Sterculia Fiber. *Cellulose*, **29**(10)**:** 5913–5922. https://doi.org/10.1007/s10570-022-04610-w

Paudel, R., Karn, G., Aryal, G., Giri, J., Adhikari, R., & Sharma, M. L. (2022). Synthesis, Characterization, Biological Study of Synthesized Lauha Bhasma. *Journal of Nepal Chemical Society*, **43:** 4–15. https://doi.org/10.3126/jncs.v43i1.47031

Dhakal, K. N., Aryal, G. M., Adhikari, H. S., & Adhikari, R. (2021). Facile Synthesis of Nanosized Magnesium-Aluminium Layered Double Hydroxides. *Journal of Nepal Chemical Society*, **42**(1)**:** 39-44 https://doi.org/10.3126/jncs.v42i1.35327

Rauniyaar, J., Aryal, G. M., & Neupane, B. B. (2019). Morphological Study on Particulate Matter of Kathmandu Valley. *BIBECHANA*, **16:** 41-46. http://dx.doi.org/10.3126/bibechana.v16i0.19190

List of Presentations and Participations

1. **Poster Presentation:** Understanding the Material Properties of Nepali Kagaj Fabricated from Lignocellulose Biomass of Himalayan Fibrous Plant, *National Conference on Advance in Polymer Materials (APM)-2023, April 25-26, 2023, Pantanagar, Uttarakhand, India.*

G. B. Pant University of Agriculture and Technology, Pantnagar, Uttarakhand, India

National Conference on
Advances in Polymer Materials

APM-2023

April 25 - 26, 2023

Department of Chemistry, College of Basic Sciences and Humanities

Supported by
Defence Research & Development Organization, India

Certificate

This is to certify that GIRJA MANI ARYAL
From RECAST, TRIBHUVAN UNIVERSITY, NEPAL
Presented/delivered/participated POSTER
in the two days National Conference, APM-2023 held from at GBPUA&T Pantnagar.

Dr. Sameena Mehtab
Convener

Dr. M.G.H. Zaidi
Convener

Dr. Sandeep Arora
Coordinator & Dean, CBS&H

2. **Poster Presentation:** Investigation of Physical, Chemical and Mechanical Properties of Raw and Alkali Treated Lokta Fibers, *Kathmandu Humboldt-Kolleg-2022, October 16-19, 2022*.

काठमाडौं हुम्बोल्ड सम्मेलन
KATHMANDU HUMBOLDT-KOLLEG 2022
Interdisciplinary Collaboration for Strengthening Science and Culture
October 16-19, 2022, Kathmandu, Nepal

Unterstützt von / Supported by
Alexander von Humboldt
Stiftung/Foundation

Certificate of Appreciation

is hereby awarded to Dr. / Mr. / Ms.

Girja Mani Aryal

for **Poster Presentation** in the international scientific conference "**Kathmandu Humboldt-Kolleg 2022**" organized by **Humboldt Club Nepal** generously supported by **Alexander von Humboldt Foundation, Germany.**

PROF. DR. RAMESHWAR ADHIKARI
Coordinator
Kathmandu Humboldt-Kolleg 2022
Humboldt Club Nepal

DR. JUDITH SCHILDT
Sponsorship and Network Department,
Alexander von Humboldt Foundation,
Germany

3. **Poster Presentation:** Understanding the Material Properties of Nepali Kagaj Fabricated from Lignocellulose Biomass of Himalayan Fibrous Plants, *4th International Conference on Bioscience & Biotechnology (ICBB)-2022, March 3-6, 2022*.

CERTIFICATE

OF PARTICIPATION

THIS IS TO CERTIFY THAT

Mr. Girja Mani Aryal

HAS PARTICIPATED AS A **POSTER PRESENTER** IN
4th INTERNATIONAL CONFERENCE ON BIOSCIENCE & BIOTECHNOLOGY
(ICBB – 2022)
Sauraha, Nepal | March 3-6, 2022

Prajwal Rajbhandari
Chair, ICBB - 2022
Research Institute for Bioscience and Biotechnology (RIBB), Nepal

Suvechhya Bastola
Secretary, ICBB - 2022
Research Institute for Bioscience and Biotechnology (RIBB), Nepal

Biomass Conversion and Biorefinery
https://doi.org/10.1007/s13399-024-05278-x

ORIGINAL ARTICLE

Understanding the material properties of alkali-treated lignocellulose fiber obtained from high-altitude Lokta bushes

Girja Mani Aryal[1] · Krisha Prasad Kandel[1] · Menuka Adhikari[2] · Jianna Evans[2] · Hisila Dangol[1] · Madan Poudel[1] · Sushil Pokharel[1] · Ramdeep Shrestha[1] · Bhoj Gautam[2] · Bhanu Bhakta Neupane[1]

Received: 3 October 2023 / Revised: 27 December 2023 / Accepted: 1 January 2024
© The Author(s), under exclusive licence to Springer-Verlag GmbH Germany, part of Springer Nature 2024

Abstract

Lignocellulose fiber obtained from high-altitude plant species *Daphne bholua* and *Daphne papyracea*, locally named Lokta bushes, is used in Asian regions to fabricate high-quality handmade paper sheets, packaging materials, composites, and paper bills. A systematic study on the material properties of the fiber to explain the performance of Lokta fiber–based materials has not been reported yet. In this study, the physio-chemical properties of untreated and 1%, 3%, 6%, and 9% NaOH (w/v)-treated Lokta fiber were systematically investigated at ambient temperature. The retting efficiency and cellulose content increased with alkali concentration followed by a decrease in lignin, hemicellulose, and extractives. This observation was consistent with the reduction of lignin and hemicellulose characteristics peaks in the FTIR, a reduction of effective fiber bundle width, and an increase in fiber density. High-resolution scanning electron microscope (SEM) images showed that alkali treatment results in significant loss of cementing materials and separation of fiber bundles. Alkali retting also increased the crystallinity index, tensile strength, and thermal stability. The degradation temperature for untreated, 6% NaOH treated, and 9% NaOH treated samples was found to be 325 °C, 343 °C, and 347 °C; respectively. The findings of this study will be important to optimize the end properties of the Lokta fiber–based paper and composite materials.

Keywords Lignocellulose biomass · Cellulose · Retting efficiency · Mechanical strength · Fiber density

1 Introduction

In recent decades, lignocellulose fibrous biomass obtained from different natural sources has been explored as an alternative material to synthetic fibers. As compared to synthetic fibrous materials, the biomass-based materials offer unique advantages such as lightweight, high specific strength, flexibility, biodegradability, and abundance. Because of these advantages, the natural fiber–reinforced materials are being explored as an alternative material in several sectors, such as health care, textiles, agro-products, and the automobile industry [1–10].

✉ Bhoj Gautam
bgautam@uncfsu.edu

✉ Bhanu Bhakta Neupane
newbhanu@gmail.com

[1] Central Department of Chemistry, Tribhuvan University, Kathmandu 44613, Nepal

[2] Department of Chemistry, Physics and Materials Science, Fayetteville State University, Fayetteville, NC 28301, USA

The fibrous biomass can be obtained from various parts of plants, such as roots, bark, leaf, and fruit. The major chemical components in natural fiber are cellulose, hemicellulose, lignin, and pectin. These chemical constituents are found in the primary cell walls of plants. In plant cell walls, semi-crystalline cellulose microfibrils are embedded in a hemicellulose-lignin matrix of varying composition [11–13]. Therefore, raw fiber is considered a composite material.

The quality of the fiber not only depends on the source but also on the processing parameters such as nature of retting agent and concentration, temperature and treatment time, etc. The size of microfibrils, microfibrils angles or orientation, degree of crystallinity, and the chemical composition are the major parameters that determine the overall quality of the fiber bundle [14–16]. On alkali treatment, the cementing materials such as lignin and hemicellulose are removed from the fiber resulting in partial or complete separation of fiber bundles, reduction of width, and increase in aspect ratio. This makes pulping easier for the intended materials such as papers, cardboards, and composites. Under optimized processing conditions, the end properties of fiber

Published online: 15 January 2024

such as water resistance, thermal and mechanical strength are significantly improved. For example, increase in tensile strength and thermal stability on alkali treatment was reported in *Neuropeltis acuminatas* liana fiber [17], *Megaphrynium macrostachyum* fiber [18], Kenaf fiber [19], Alfa fiber [20], and banana fiber [21]. If natural fiber is intended for cellulose-polymer composite, alkalization or mercerization leads to the formation of mercerized cellulose structure (for example, fiber-OH to fiber-ONa^{+}) so that bonding with polymer increases [3].

Natural fiber obtained from different plant species and bacteria is actively investigated by several researchers throughout the world [5, 12, 22–29]. Most of the studies are focused on extraction, physicochemical, physicomechanical, and thermomechanical characterization. Applications of these fibers in the fabrication of green composite materials are also being explored [2, 11, 30–33]. From a material point perspective, the natural fiber obtained from *Daphne bholua* and *Daphne papyracea*, locally named Lokta bushes, is one of the least studied plant species. The Lokta bushes are distributed in different districts of Nepal and other Asian countries at an altitude of 1600 to 4000 m. In Nepal, bast fiber obtained from Lokta bushes is being used to make handmade Lokta paper, packaging materials, and gifts. Handmade paper is being used in religious books and documents, official documents, packaging, stationary, greeting cards, decorative products, etc. [24, 34–36]. To understand the end applications of materials made from Lokta fiber, it is important to explore fiber properties processed under different conditions. The motivation of this study was to explore several materials properties of raw and alkali-treated Lokta fiber down to microscopic level and explain the observed differences in water absorptivity, thermal, and mechanical properties.

In this study, raw fibrous biomass obtained from Lokta bushes was treated with 1–9% NaOH solution. The change in chemical composition and weight loss was systematically measured. Several important material properties of the untreated and alkali treated samples such as effective fiber bundle width, crystallinity, and thermal stability were explored using optical microscopic, XRD, SEM, and TGA techniques. Finally, variation on end properties such as water absorptivity, thermal stability, and tensile strength with change in alkali concentration were systematically explored and compared with other fiber types.

2 Materials and methods

2.1 Extraction and alkaline treatment of fibers

Fully matured stems (~45 cm long and 1.5 cm diameter) were cut from Lokta bushes from Annapurna municipality, Myagdi, Nepal (Fig. 1A and B). The stems were brought to the lab and soaked in distilled water for 60 min. The bark region of the stem (area b, Fig. 1C) was mechanically peeled, and the outer cuticular layer (area a, Fig. 1C) was removed with a stainless steel knife. The fiber bundles were washed with distilled water to remove the surface impurities and sun dried to remove the moisture (Fig. 1D).

The extracted raw Lokta fiber (4–5 cm long and 0.5–1.5 mm wide) was treated with 1%, 3%, 6%, and 9% (w/v) sodium hydroxide solution at room temperature (24 ± 1 °C) for 1 h. The biomass after treatment was washed with tap water 2–3 times, washed with 0.1N HCl to neutralize residual NaOH on the surface of the fibers [37, 38], rinsed 4–5 times with distilled water, and oven-dried (90 ± 2 °C) for 24 h. The % weight loss or retting efficiency (ε) was calculated as:

$$\varepsilon = 100\left(\frac{W_1 - W_2}{W_1}\right) \tag{1}$$

where, W_1 and W_2 are the initial and final mass of the fiber, respectively.

2.2 Determination of biomass composition and water absorption

The percentage of extractives, cellulose, hemicellulose, lignin, and ash content both in untreated and retted and alkali-treated fiber samples was determined following the literature reported gravimetric methods [12, 37, 39, 40]. The % composition (χ) of each component was calculated as:

$$\chi = 100\left(\frac{a - b}{a}\right) \tag{2}$$

where, a and b are initial and final dry weights of the fibrous biomass, respectively.

Three independent measurements were made for each component, and mean and standard deviation (mean ± SD) were reported.

2.2.1 Determination of extractives

The 2.000 g of oven dried raw fiber along with 200 mL of 190 proof ethyl alcohol (95%) was added to a Soxhlet extraction apparatus. The content was refluxed for 6 h. The extracted solid was filtered through filter paper, dried, and weighed. The initial and final weights of fiber were used extractive content using Eq. 2.

2.2.2 Determination of cellulose

To determine cellulose, 1.000 g of extractive-free fiber was oven-dried at ~90 ± 2 °C for 4 h and cooled in non-hygroscopic desiccator, and the sample was treated with 5% NaOH (w/v) for 5 h while keeping fiber mass to alkali solution ratio of 1:30 (w/v). The content was cooled and neutralized with

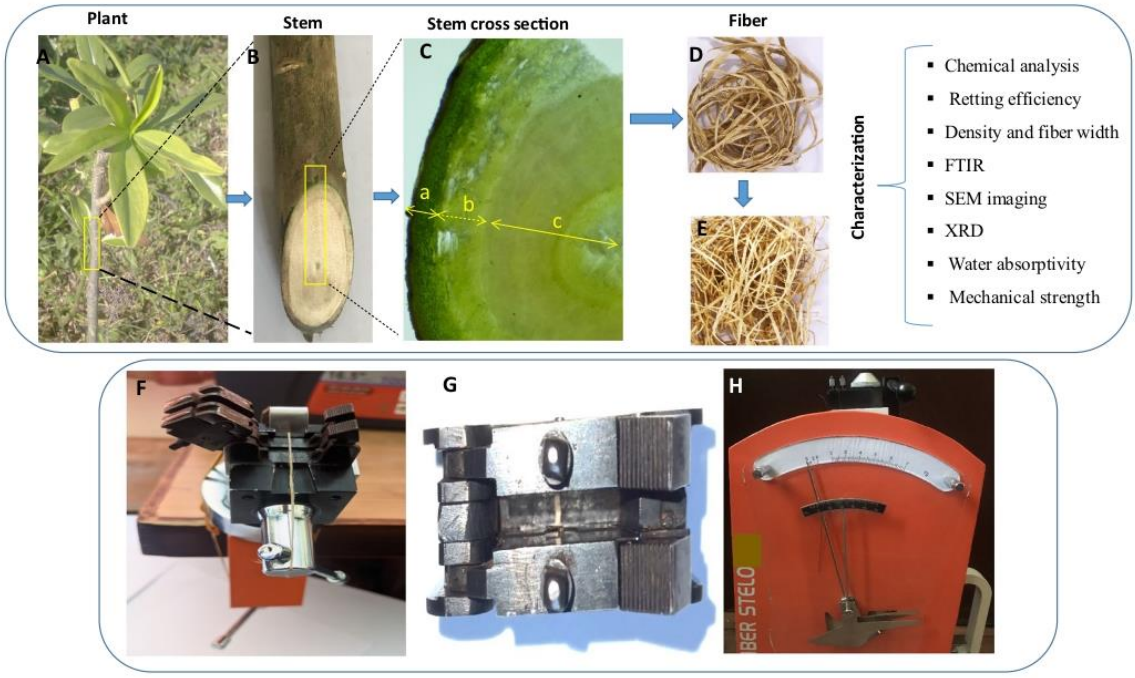

Fig. 1 Experimental flow chart and mechanical strength testing setup. **A** Lokta plant; **B** freshly cut stem; **C** stem cross section taken with a stereomicroscope: a = cuticular layer, b = bark region, c = woody region; **D** untreated fiber; **E** alkali-treated fiber; **F** A thin fiber bundle ready to mount in Pressley jaw; **G** fiber mounted in Pressley jaw; **H** front view of fiber bundle strength tester showing the load (upper) and % elongation (lower) scales

10% H_2SO_4. The residual biomass was washed several times with distilled water and then dried at 90 ± 2 °C until constant weight was obtained. The final and initial weights were used to calculate the cellulose content using Eq. (2).

2.2.3 Determination of hemicellulose

To determine the hemicellulose, 1.000 g of extractive free and oven dried sample was boiled in 0.5 M NaOH for 4 h. The content was neutralized after several washings with distilled water, and dried at 90 ± 2 °C till constant weight was obtained. The final and initial weights were used to calculate hemicellulose content.

2.2.4 Determination of lignin

Acid insoluble lignin (Klason lignin) was determined following literature reported method [12, 37, 39, 40]. To determine the lignin, 1.000 g of extractive free and oven dried sample (40–50 micron mesh size) was taken in a flask and digested with 15 mL of 72% H_2SO_4. The content was carefully stirred 3 h at room temperature, and then around 200 mL of distilled water added and boiled 2 h. The content was cooled to room temperature, and the residue was carefully transferred to a crucible. The residue was washed several times till it becomes acid free (checked with litmus paper). The residue was oven dried at 105 °C till a constant weight was achieved. The fiber and residue were used to get % lignin content.

2.2.5 Determination of equilibrium moisture content

To measure the moisture content at ambient condition, 2.000 g of fiber sample was conditioned was oven dried at 90 ± 2 °C for 24 h. The sample was cooled in a non-hygroscopic desiccator and weighed. The difference in the weights before and after drying was used to calculate the moisture content in the fiber. Three independent measurements were made for each sample.

2.2.6 Determination of water absorptivity

Fixed weight of fiber bundle was submerged in 50 mL distilled water at room temperature (24 ± 1 °C). The fiber was

taken out at certain time period and weighed. The process was repeated for the intended time period (0–12 days), and % weight gain was calculated from the weight difference [41, 42].

2.2.7 Determination of fiber density and width

The density of cellulose fiber was measured gravimetrically following liquid pyknometer method [43, 44]. Fibers were cut to ~ 5 mm length and dried for 48 h in a non-hygroscopic desiccator ($CaCl_2$ as a desiccant) and impregnated in toluene for around 2 h to remove any microbubbles. The density was then calculated as [43, 44]:

$$\rho = \frac{(m_2 - m_1)\rho_T}{(m_3 - m_1) - (m_4 - m_1)} \quad (3)$$

where, ρ_T is the density of toluene and m_1, m_2, m_3, and m_4 are the weight (in grams) of the empty pyknometer, pyknometer with fibers, pyknometer filled with toluene, and pyknometer filled with fiber and toluene solution, respectively.

To determine the fiber width, the fiber bundles were imaged with an optical microscope at magnification of 40 × (Olympus, SZ61, USA). The field of view was calibrated using a high- precision linear calibration grid having least count of 10 µm. The pixel size was converted to a micrometer using image analysis software (ImageJ, NIH, USA) to get fiber width information. Data were reported as the mean values obtained from thirty independent measurements.

2.3 Determination of fiber strength

The Lokta fiber samples were preconditioned at 65% RH at 23 ± 2 °C for 24 h following the ASTM test method [45]. To ensure the control measurement condition, fiber bundle obtained from the same region of stem having uniform width (300–350 µm; as examined under microscope) was mounted to the Pressley Jaw assembly gauge length 15 mm (Fig. 1F and G), loaded to the fiber bundle strength tester (Fig. 1H) (TSI instruments, max load 7 kg) and pulled at a constant loading speed of 1 kg/s. The load at which the fiber bundle breaks and the corresponding % elongation was noted. From measured values for breaking load and broken bundle weight (measured at nearest accuracy of 0.0001 g), breaking tenacity (cN/tex) was calculated. The tenacity was converted to ultimate tensile strength or stress using Eq. (4) [46]. Data were reported as the mean values obtained from fifteen independent measurements.

$$S = 10.d.T \quad (4)$$

here, S is the tensile strength (MPa), d is the material density in g cm^{-3}, and T is the tenacity (cN/tex).

2.4 FTIR, XRD, SEM, and TGA measurements

XRD data were measured in the range of 5–50° at the step size of 0.02° and scan rate of 0.25°/s using an X-ray diffractometer (Rigaku, UK). The X-ray source originating from Cu Kα line (λ = 1.540A°) was used in the measurement.

Scanning electron microscopic images were measured at different magnifications using JEOL JSM-6510LV scanning electron microscope (SEM). The samples were sputter coated with gold (thickness ~ 5 nm) before doing SEM.

The IR spectra were measured in attenuated total reflection (ATR) mode using a Fourier transform infrared spectrometer (ABB Bomen, MB100, Canada). The scan range, spectral resolution, and number of scans were 4000–400 cm^{-1}, 4 cm^{-1}, and 100, respectively.

The thermo gravimetric analysis (TGA) data were collected using a TG/DTA simultaneous measuring instrument (Shimadzu DTG-60 series) under a nitrogen atmosphere. The sample weight was ~ 10 mg, and fiber size was ~ 3 mm long and 500 µm wide. The temperature range, heating rate, temperature precision, and balance accuracy were 25 to 600 °C, 10 °C/min, ± 2 °C, and 0.1 µg, respectively.

2.5 Statistical analysis

The as-measured data were entered and analyzed in Excel spreadsheet to get descriptive statistical parameters such as mean and standard deviation. To find if the mean difference in the mechanical properties is significant, a paired t test at 95% confidence interval was performed and p value was calculated. The level of correlation between two variables was determined from Pearson correlation coefficient (r).

3 Results and discussion

3.1 Weight loss and chemical composition

The % weight loss is a measure of retting efficiency from the lignocellulose biomass on alkali treatment. It depends on the nature of biomass and retting conditions such as concentration of alkali, treatment time, and temperature [12, 19, 47]. As expected, % weight loss increases with alkali concentration (Fig. 2A). Indeed, a strong positive correlation between alkali concentration and % weight loss was found, as indicated by the Pearson correlation coefficient $r = +0.93$. A maximum weight loss of 27.0 ± 1.6% was achieved on 9% alkali treatment.

The weight loss on alkali treatment results from the removal of non-cellulosic and cementing materials from the biomass. To explore this extractive, Klason lignin,

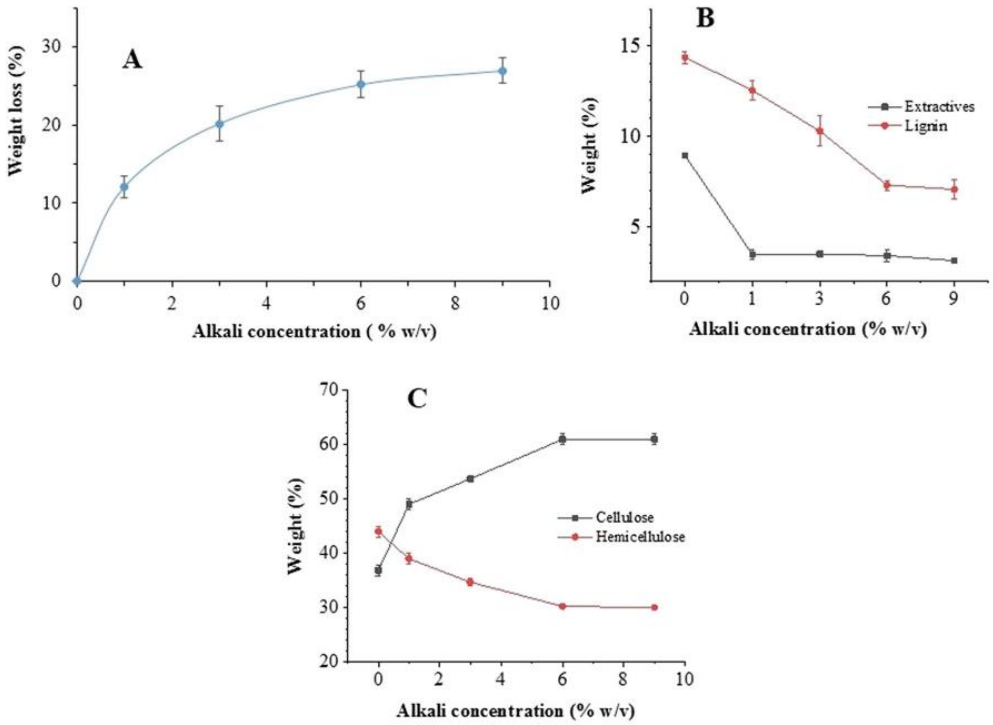

Fig. 2 The weight loss and chemical composition. **A** Weight loss (%) as a function of alkali concentration. **B** Extractive and lignin content measured as function and alkali concentration. **C** Cellulose and hemicellulose content measured as function and alkali concentration. The error bars in all figures, represent the standard deviation obtained from three independent fiber samples ($n = 3$)

hemicellulose, and cellulose were measured in dry or moisture free samples.

A significant loss in extractive content was observed in alkali-treated samples (Fig. 2B). For example, in a 9% alkali-treated sample ~ 65% extractive loss was found (8.9 ± 0.1 to 3.1 ± 0.0%). Loss of lignin and hemicellulose was also observed in the alkali-treated samples (Fig. 2B and C). In 9% alkali-treated sample, ~ 51.2% lignin loss (14.3 to 7.0%) and 32% hemicellulose loss (44 to 30%) were observed. The cellulose content in untreated, 1%, 3%, 6%, and 9% treated samples was found to be 36.8 ± 1.0, 49.0 ± 1.0, 53.7 ± 1.0, 61.0 ± 1.0, and 61.0 ± 1.0, respectively, suggesting a significant increase in cellulose content on alkali treatment (Fig. 2C). The net increase in cellulose content is due to collective loss of extractive, lignin, and hemicellulose.

Loss of lignin and hemicellulose with increased alkali concentration and the corresponding increase in cellulose content was also reported in Alfa stem fiber [20], *M. oleifera* fruit fibers [48], *Carica papaya* bark fibers [49], and water hyacinth fiber [50], and *Sterculia* fiber [12]. The loss of lignin and hemicellulose could be due to the disruption of specific bonds, for example, hydrogen bonding between cellulose, hemicellulose, and lignin, resulting in partial solubility and washing of the components [51].

Table 1 Moisture content, density, and fiber width

Sample type	Moisture content (%)	Density (g cm^{-3})	% decrease in fiber width
Untreated	13.3 ± 0.2	1.11 ± 0.00	-
1% treated	11.2 ± 0.1	1.17 ± 0.01	18.6 ± 3.9
3% treated	10.9 ± 0.6	1.20 ± 0.01	22.7 ± 6.2
6% treated	10.4 ± 0.4	1.23 ± 0.01	25.8 ± 5.2
9% treated	9.8 ± 0.5	1.38 ± 0.01	30.6 ± 5.9

3.2 Moisture content, density, fiber width, and water absorptivity

Another change in alkali treatment is the decrease in equilibrium moisture content with the increase on alkali concentration (Table 1). For example, in 9% NaOH-treated fiber the equilibrium moisture content decreased by ~ 25% (13.3 to 9.8%). The decreased moisture content could be due to the loss of more hydrophilic components such as extractives and

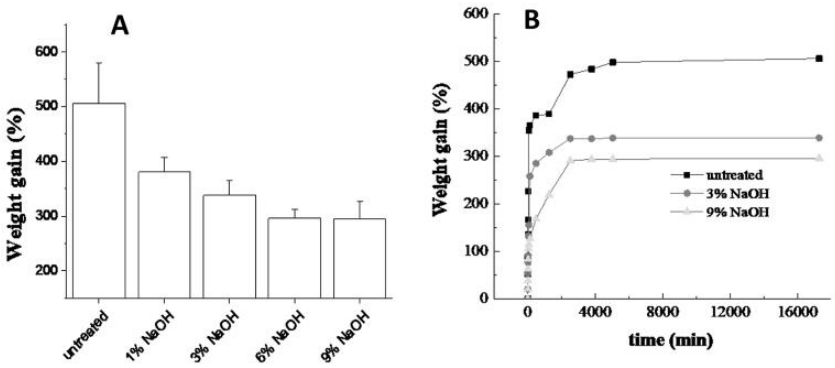

Fig. 3 Equilibrium water absorption. **A** % weight gain for different samples measured after 12 days. The error bar represents the standard deviation obtained from three independent samples. **B** A typical water absorption kinetics plot for untreated, 3% and 9% NaOH-treated samples

lignin from the fiber bundle. Significant decrease in moisture content on alkali treatment is also reported in other studies; for example, 16.4% decrease (13.4 to 11.2%) is reported for banana fiber treated for 3 h in 10% NaOH [21], ~ 40% decrease (9.7 to 5.8%) in *Carica papaya* bark fibers treated 1 in 5% NaOH [49].

A small but gradual increment in density was observed with an increase in alkali concentration. In fact, density showed strong positive correlation ($r = +0.96$) with alkali concentration. In the 9% alkali-treated sample, a ~ 24% increase in density (1.11 to 1.38 g cm^{-3}) was observed (Table 1). In literature studies, depending on alkali concentration and fiber type, density is reported to increase or decrease. An increase in density (by ~ 2.5%) was reported for Kenaf and Hemp fiber treated at or below 10% (w/v), whereas the decrease in density was observed at concentration > 10% [19, 52, 53]. In banana fiber, an increase in density (~ 7–9%) was observed in fiber treated to 10 and 15% alkali [21]. The density increase can be due to the loss of low-density non-cellulosic components or cell wall densification, whereas density decrease could originate due to the cell wall rupture leading to de-polymerization of cellulose chains [19, 21]. In this study, relatively high increase in fiber density could be due to a significant loss of non-cellulosic components from the Lokta fiber.

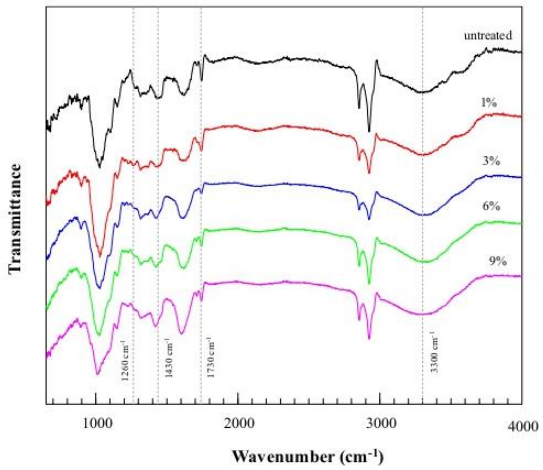

Fig. 4 FTIR spectra of the fiber samples. For easy compassion, spectra are overlaid vertically. The dotted lines are to indicate the peak position of important frequencies

Another change reported on alkali treatment is a significant decrease in effective fiber bundle width [12, 19, 21]. This is mainly attributed to the loss of non-cellulosic components from the bundle surface. In Lokta fiber, a significant reduction in fiber width was observed in alkali-treated samples (Table 1). The reduction in fiber width on 1%, 3%, 6%, and 9% NaOH treated samples at 95% confidence interval was found to be 18.6 ± 3.9%, 22.7 ± 6.2%, 25.8 ± 5.2%, and 30.6 ± 5.9%; respectively.

The water absroptivity measured in terms of % weight gain in untreated, and 1%, 3%, 6%, and 9% NaOH-treated fiber was found to be 506.2 ± 64.1, 380.8 ± 32.8, 338.7 ± 25.4, 296.0 ± 20.5, and 295.7 ± 42.9%; respectively (Fig. 3A). If cellulose fiber is soaked in water, the hydrogen bond between the fiber chain breaks and new hydrogen bond is formed between fiber-OH groups and water molecules leading to significant weight gain. On alkali treatment, the more hydrophilic components are removed resulting in increased water resistance or decreased water absorptivity [3]. Interestingly, the % weight loss (Fig. 2A) and % weight gain data (Fig. 3A) strongly negatively correlate ($r = -0.98$).

For completeness, the water uptake kinetics curves are also reported for selected samples (Fig. 3B). A typical water absorption kinetic curve, as observed for natural fibers [41, 42, 54], consisting of fast (at short immersion time) and slow water uptake (at longer immersion time) regimes is observed in all the samples.

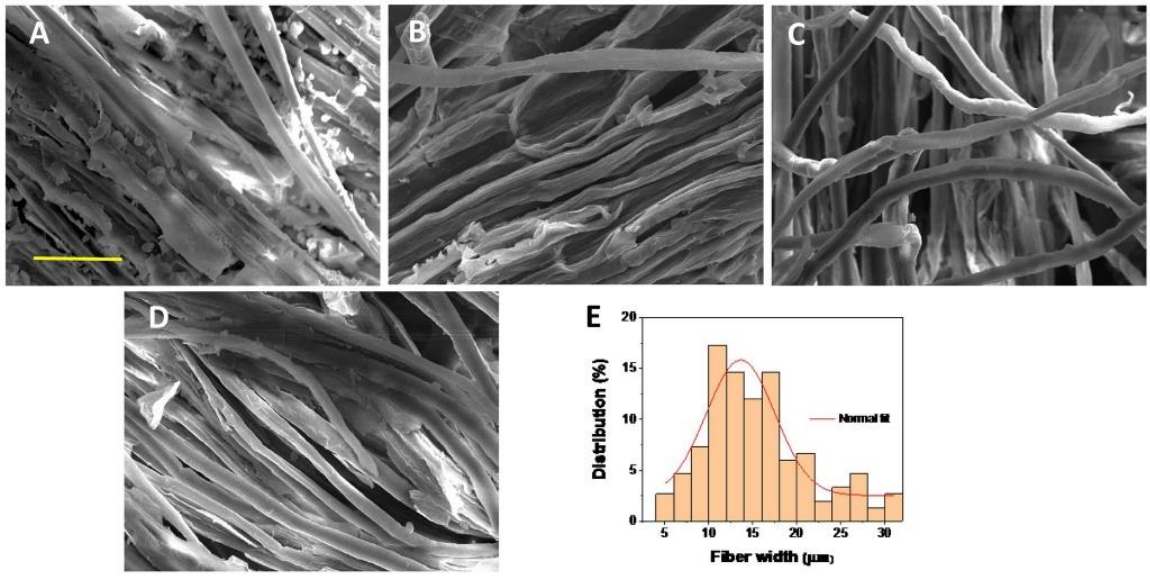

Fig. 5 SEM images and histogram showing the width of fiber. **A**, **B**, **C**, and **D** Representative SEM images for untreated, 3%, 6%, and 9% treated fiber samples, respectively. A scale bar of 50 μm shown in A also applies for B, C, and D. **E** A histogram plot ($n = 150$ and bin size 2 μm) with a normal distribution fit (solid line) to show the fiber width distribution in %

Literature studies have reported that the water absorption (as measured by % weight gain) depends on the origin (plant source and fiber location) or chemical composition of fiber, treatment condition, and water composition. In majority of studies, alkali-treated sample is reported to have improved water resistance or decreased weight gain [41, 42, 54, 55]. For examples, 1.4 times decrease in % weight gain (from 200 to 140%) was observed in 10% NaOH-treated abaca fiber [55], 2.5 times decrease (from 160 to 65%) was observed in 5% treated *Sterculia* fiber [41], and 1.3 times decrease (from ~ 850 to 630%) in 6% NaOH-treated Areca fiber [56]. Interestingly, increased water absorption is also reported in alkali-treated fiber. For examples, in 6% NaOH-treated cotton ~ 23 times increase (50% in untreated to 1160% in treated) and 1.5 increase in pineapple fiber (200% in untreated to 300% in treated) is reported. It is reasoned that alkali treatment removes hydrophobic waxy layer resulting increase in water uptake [56].

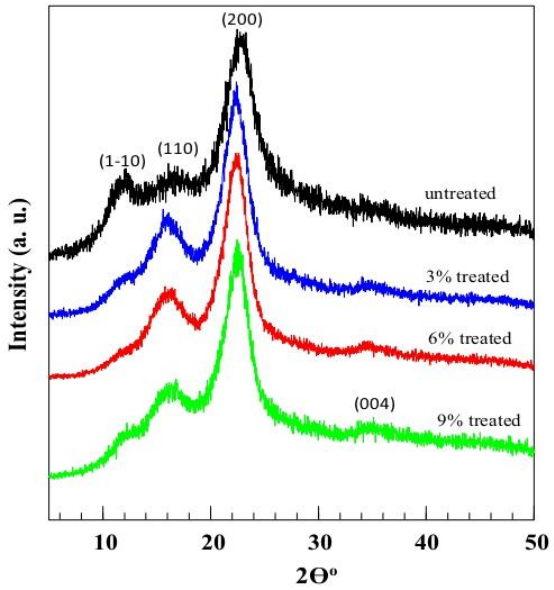

Fig. 6 XRD data of untreated and alkali-treated samples. For easy composition, data is overlaid vertically. The number within parentheses indicates the crystalline planes

3.3 FTIR study

The FTIR spectra of the fiber samples are very similar with a small difference in peak intensity, peak position, and shape of some specific bands (Fig. 4). A broad peak in the range of 3000–3600 cm^{-1} is assigned to the O–H stretching frequency of hydrogen-bonded networks in cellulose and hemicellulose [47, 57]. In alkali-treated samples, the shape of the band becomes more symmetric and narrower. This could be due to the disruption of hydrogen bonding between O–H groups of hemicellulose and cellulose resulting from partial loss of hemicellulose.

Table 2 XRD parameters for the fiber samples

Sample type	CI (%)	2Θ (°)	d_{200} (nm)	β (°)	D (nm)
Untreated	73	22.8	0.390	3.3	2.45
3% treated	76.2	22.3	0.398	2.7	3.00
6% treated	78.5	22.4	0.396	2.7	3.00
9% treated	75.25	22.5	0.395	2.9	2.79

A weak peak at 1730 cm^{-1} is attributed to ester or acetyl -C = O groups of (non-conjugated) hemicellulose or lignin [26, 29]. A characteristic peak at ~ 1260 cm^{-1} is attributed to the C-O stretching of acetyl groups of hemicellulose and cellulose [57]. These peaks are weaker in alkali-treated samples indicating removal of hemicellulose and lignin. These spectral changes are consistent with the weight loss data reported in Sect. 3.1. A characteristic peak ~ 1430 cm^{-1} attributed to $-CH_2$ bending vibration remains unchanged in the alkali-treated sample. This intact cellulose could help to preserve mechanical strength in the alkali-treated fiber [47, 58].

3.4 SEM imaging

The fiber surface of the untreated sample contains additional materials deposited on the surface (Fig. 5A). The additional mass could be non-cellulosic materials such as pectin, wax, inorganic minerals, hemicellulose, and lignin. Interestingly, in the alkali-treated samples surface impurities are removed and the fiber bundles separate into individual fibers. This observation is also consistent with the weight loss in the retting study, reduction of effective fiber bundle width, and weakening of hemicellulose and lignin-specific peaks in FTIR spectra reported in Sect. 3.1.

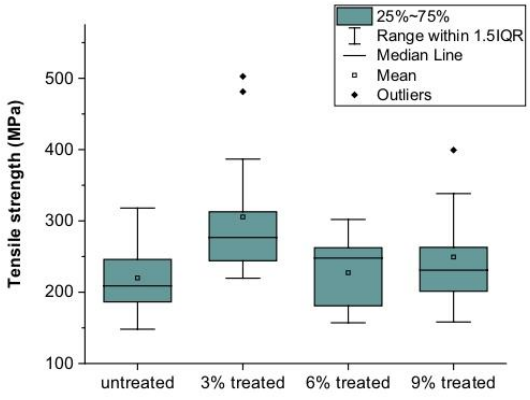

Fig. 7 Tensile strength data for the fiber samples. For easy comparison, mean, inter-quartile range and median values along with a few outliers ($n = 15$) are shown as a box and Whisker plot

Similar changes were reported in alkali-retted hemp [59], *Sterculia* [12], *Bauhinia* [41], kenaf [60], *M. oleifera* fruit fibers [48], *Carica papaya* bark fibers (5% NaOH [49], and water hyacinth plant fiber [50]. The single elementary fiber mean width and the width range ($n = 150$) measured from the 9% treated sample were found to be 15.4 ± 6 µm and 4.8–31.5 µm, respectively**.** A histogram plot showing the fiber width distribution is provided in Fig. 5E.

3.5 XRD study

The shape of the XRD profile for all the fiber samples resembles to that of a typical lignocellulose fiber (Fig. 6). Cellulose fiber in its natural form contains crystalline and amorphous domains [15, 61, 62]. The diffraction peaks at 2θ value at ~ 13° and ~ 16° originate from the crystalline planes (1–10) and (110), respectively. The strongest peak at ~ 22.5° originates from the (200) plane and a weak peak at ~ 35° from (004) planes of crystalline cellulose phase I, respectively [15, 61, 62]. To get a piece of preliminary information on crystallinity change on alkali retting, Segal's crystallinity index (CI) was calculated using Eq. (5).

$$CI = 100\left(\frac{I_{200}}{I_{200} + I_{am}}\right) \tag{5}$$

where I_{200} and I_{am} are the intensities of major crystalline peak and amorphous profile measured at 2θ values of ~ 22.5° and ~ 18.2°, respectively. The Segal's crystallinity index (CI) in untreated, 3%, 6%, and 9% alkali-treated samples was found to be 73%, 76.2%, 78.5%, and 75.2%, respectively. It is suggested that the removal of amorphous components such as hemicellulose and lignin mainly from the inter-fibrillar region can lead to the reorganization of cellulose chains and the increase in crystallinity index [12, 15, 37, 37, 47]. The same reasoning can explain the CI increase in alkali-treated samples. Increase in CI with alkali treatment is also reported in several other fiber types, for example, *M. oleifera* fruit fibers [48], *Carica papaya* bark fibers [49], water hyacinth fiber [50], and *Sterculia* fiber [12].

The full width at half maximum parameter (β, in radians) corresponding to the most intense peak corresponding to (200) plane was used to get crystallite size (D, nm) using the Scherrer equation [63].

$$D = \frac{\kappa\lambda}{\beta\cos\theta} \tag{6}$$

The κ factor of 0.94 and λ of 0.154 nm were used in the calculation. It is found that crystallite size increased by approximately 22% in both 3% and 6% alkali-treated samples and by 14% in the 9% alkali-treated sample (Table 2). The XRD data were further analyzed to get information on inter-planar spacing (d_{200}) (Eq. 7).

Table 3 Comparison of mechanical properties

Fiber	Treatment conditions	Tensile strength (MPa)	Elongation (%)
Lokta fiber (this study)	9% NaOH, RT, 1 h	249.3 ± 32.2	6–9
Jute fiber [47]	8% NaOH, RT, 1 h	350 ± 32.2	1–4
Carica papaya bark fibers [49]	5% NaOH, RT, 1 h	548 ± 14.6	1.83 ± 0.04
Borassus fruit fiber [37]	10% NaOH, RT, 0.5 h	160	34
Prosopis juliflora bark fiber [65]	Raw fiber	558 ± 13.4	1.77 ± 0.04
Cotton fiber [66]	Variable	200–400	6–8
Coir [66]	Variable	95–175	13.7–41
Flax [66]	-	500–1500	2.7–3.2
Bamboo fiber [67]	5% NaOH, RT, 24 h	222 ± 14.6	15.2 ± 0.04

$$n\lambda = 2d_{200}\sin\theta \tag{7}$$

In the calculation, $n = 1$ (first order diffraction), λ of 0.154 nm was used and θ was obtained from peak position of d_{200} (from XRD data). A small increase in inter-planar spacing (d_{200}) in alkali-treated samples could be due to micro-strains present on the crystallite surface [57, 64].

3.6 Mechanical strength

The tensile strength (MPa) data for the fiber samples is provided as a Box and Whisker plot (Fig. 7). The tensile strength for untreated, 3%, 6%, and 9% treated samples was found to be 219.9 ± 24.2 MPa, 305.5 ± 44.0 MPa, 227.3 ± 23.3 MPa, and 249.3 ± 32.2 MPa, respectively. The corresponding % elongation was found to be 8.5 ± 1.4, 7.0 ± 1.0, 8.0 ± 1.0, and 8.0 ± 1.1, respectively. This showed that tensile strength increases significantly on alkali treatment ($p < 0.01$). Literature studies report that tensile strength in alkali-treated samples, depending on treatment parameters and fiber type, is increased or decreased on retained [3, 19, 47, 59]. It is suggested that the removal of lignin and hemicellulose mainly from inter-fibrillar region decreases the internal constraint within cellulose chains and facilitates better organization. This could increase the tensile strength. The same reasoning could help to explain the tensile strength increase in Lokta fiber reported here. A small decrease in tensile strength at high alkali concentrations could be due to the formation of fiber surface defects.

The mechanical properties of natural fiber depend on fiber type and treatment conditions. Not all studies report the measurement parameters such as gauge length, testing speed, fiber diameter or width, and temperature and humidity. A comparison with few selected studies, which report very similar treatment conditions as this study, is provided in Table 3.

It is suggested that % elongation increases with microfibril angle (MFA) [65, 68]. For natural fiber, MFA ranges from 3 to 50°. Cotton is reported to have MFA of 20–30°, so it has higher % elongation (6–8%) than flax fiber (% elongation ~ 3%, MFA 10°). Lokta fiber has very similar % elongation as cotton fiber, and the MFA could be similar. It is found that fiber having low MFA and higher cellulose content can have high ultimate tensile strength [69]. The intermediate tensile strength of Lokta fiber could be due to high cellulose content and high MFA. Experimental measurement of microfibril angle, stress–strain curve, and SEM image of fiber surface at different levels of stress could provide more insight to the mechanical properties of the fibers.

3.7 Thermal analysis

The TGA and DTG data for selected fiber samples are reported in Fig. 8 and the insets, respectively. The TGA data for all samples show three distinct weight loss regions viz. T < 100 °C, 175–400 °C, and > 400 °C, as reported for

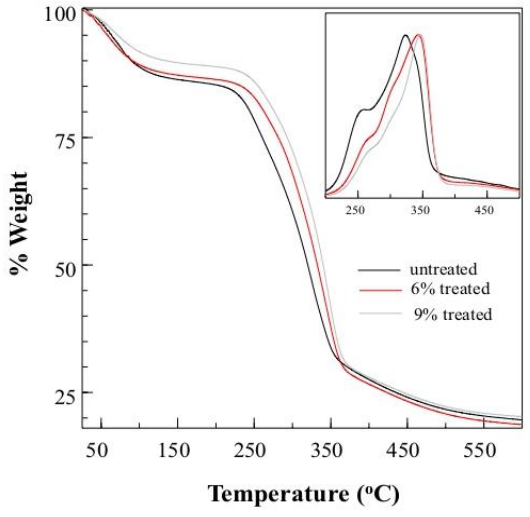

Fig. 8 Thermal analysis data. The main frame shows the TGA data for untreated, 6%, and 9% NaOH-treated samples. The inset shows the corresponding DTG data

Table 4 A summary of TGA data

Sample type	ΔT, °C	Mass loss, %	Maximum degradation temperature (T_{max}), °C	Residual mass or char at 600 °C, %
Untreated	26–100	11	325	18.9
	100–275	20		
	275–375	40		
	375–650	11.3		
6% treated	26–100	10	343	18.0
	100–275	12.6		
	275–375	47.5		
	375–650	10.7		
9% treated	26–100	8	347	19.7
	100–275	9.5		
	275–375	50.2		
	375–650	9.8		

typical lignocellulose biomass [48–50, 70]. For easy comparison, the % weight loss in different temperature windows is also provided in Table 4. In all samples, the initial weight at T < 100 °C is due to loss of volatile impurities and moisture. A small difference in weight loss in this region can be due to crystallinity change, differences in chemical composition, and the equilibrium moisture content.

The weight loss in the range of 200–300 °C is mainly due to the degradation of hemicellulose [70]. This region is more pronounced in DTG as a shoulder ~ 260 °C (Fig. 8 inset). Interestingly, the shoulder is stronger in the untreated sample suggesting higher hemicellulose content. This observation is consistent with chemical analysis, FTIR, and SEM data reported in earlier sections. The degradation of hemicellulose at lower temperatures than cellulose is linked to its amorphous nature and ease of de-polymerization [71].

The weight loss in the temperature range of 300–400 °C is mainly attributed to the cleavage of glycosidic linkage in cellulose [71]. This region appears as a sharp peak in DTG. The higher thermal stability of cellulose is due to well-organized long polymeric units. The maximum degradation temperature (T_{max}) for untreated, 6% treated, and 9% NaOH-treated samples was found to be 325 °C, 343 °C, and 347 °C, respectively (Table 4). This suggested that thermal stability is increased on alkali treatment. The increased thermal stability on alkali treatment could be linked to increased crystallinity and grain size. Increase in thermal stability on alkali treatment is also reported in other studies, for example increase from 321.1 to 346.6° in *Carica papaya* 5% NaOH-treated (1 h, RT) bark fibers [49] and 321 to 332° in 5% NaOH-treated (4 h, 80 °C) *Sterculia* fiber [12]. These results also indicate that alkali-treated sample has high thermal stability and can be used in the composite materials. Lignin degradation is reported to take place at a broad temperature range from 200 to 600 °C. This is attributed to high molecular mass having cross-linked structure [72]. The higher weight loss in the temperature ranges from 475 to 600 in the untreated sample could be due to higher lignin content.

A small difference is residual mass left could be due to difference in chemical composition and other impurities, for example inorganic minerals present. The residual mass ~ 600 °C is reported to increase or decrease [49] on alkali treatment. It is suggested that removal of hemicellulose can form more stable lignin–cellulose complex, which can result in increased residual char in alkali-treated sample [73]. This could explain an increase in residual char from 18.9% in untreated sample to 19.7% in 9% NaOH-treated sample. The residual mass around 600 °C is reported to be variable, for examples around 40% is reported in raw and alkali-treated *Acacia planifrons* bark fibers [74], 30–40% in raw and alkali-treated *Carica papaya* bark fibers [49], 25–28% in *Sterculia* fiber [12], 15–22% in jute fibers [73], 20–22% in Alfa stem fiber [20], 30–32% in water hyacinth fibers [50]. The low residual mass could suggest that Lokta fiber has low mineral impurities, and the biomass may be easy to process for making paper and biocomposite materials.

4 Conclusions

To summarize, several material properties of the untreated and 1%, 3%, 6%, and 9% NaOH-treated (w/v) Lokta fiber samples were systematically explored. The alkali treatment resulted in significant loss of extractives, lignin, and hemicellulose with increasing alkali concentration. This resulted in significant increase in cellulose content (from ~ 37 to 61%) in 9% NaOH-treated sample. The equilibrium moisture content and effective fiber width decreased significantly whereas fiber density, crystallinity index, and thermal stability increased on alkali treatment. These changes are due to the loss of lignin and hemicellulose from the fiber bundle, as shown by the evidence obtained from FTIR data and SEM images. The tensile strength for untreated, 3%, 6%, and 9% NaOH-treated fiber was found to be 219.9 ± 24.2 MPa, 305.5 ± 44.0 MPa, 227.3 ± 23.3 MPa, and 249.3 ± 32.2 MPa;

respectively. This showed that tensile strength increased significantly on alkali treatment ($p < 0.01$). The maximum degradation temperature (T_{max}) for untreated, 6% treated, and 9% NaOH-treated samples was found to be 325 °C, 343 °C, and 347 °C; respectively. This suggested that thermal stability is increased on alkali treatment. These findings will be important to optimize and understand the end properties of the Lokta fiber–based paper and composite materials. Experimental measurement of tensile curves and fracture analysis could provide more insight to the mechanical properties of the fibers. Additionally, a systematic study on material properties of Lokta fiber–derived paper and composite materials could be explored in future.

Acknowledgements The authors would like to acknowledge Dr. Zhiping Luo from Fayetteville State University for providing IMREL facility and Prof. Dr. Rameshwar Adhikari from Research Centre for Applied Science and Technology (RECAST), Tribhuvan University, Nepal for supporting in FTIR measurement.

Author contribution Conceptualization: [Bhanu Bhakta Neupane]; methodology: [Girja Mani Aryal, Krisha Prasad Kandel, Menuka Adhikari, Bhoj Gautam]; formal analysis and investigation: [Girja Mani Aryal, Menuka Adhikari, Hisila Dangol, Madan Poudel, Sushil Pokharel, Jianna Evans, Ramdeep Shrestha]; original draft preparation: [Girja Mani Aryal, Krishna Prasad Kandel]; preparing final paper: [Bhanu Bhakta Neupane, Bhoj Gautam, Menuka Adhikari]; funding acquisition: [Bhanu Bhakta Neupane, Bhoj Gautam]; supervision: [Bhanu Bhakta Neupane, Bhoj Gautam]. All authors have read and agreed to publish the current version of the manuscript.

Funding This work was supported by the University Grants Commission, Nepal (BBN # CRIG-78/79-S&T-02) and by National Science Foundation, USA (BG# EES 1900998).

Data availability The data that support the findings of this study are available from the corresponding authors [B. B. N and B. G.] upon reasonable request.

Declarations

Ethical approval Not applicable.

Competing interests The authors declare no competing interests.

References

1. Amara C, El Mahdi A, Medimagh R, Khwaldia K (2021) Nanocellulose-based composites for packaging applications. Curr Opin Green Sustain Chem 31:100512
2. Camargo PHC, Satyanarayana KG, Wypych F (2009) Nanocomposites: synthesis, structure, properties and new application opportunities. Mater Res 12:1–39
3. Chandrasekar M, Ishak MR, Sapuan SM et al (2017) A review on the characterisation of natural fibres and their composites after alkali treatment and water absorption. Plast Rubber Compos 46:119–136
4. Dufresne A (2008) Chapter 19 - cellulose-based composites and nanocomposites. In: Belgacem MN, Gandini A (eds) Monomers, Polymers and Composites from Renewable Resources. Elsevier, Amsterdam, pp 401–18
5. Liu W, Du H, Zhang M et al (2020) Bacterial cellulose-based composite scaffolds for biomedical applications: a review. ACS Sustain Chem Eng 8:7536–7562
6. Lobo FC, Franco AR, Fernandes EM, Reis RL (2021) An overview of the antimicrobial properties of lignocellulosic materials. Molecules 26:1749
7. Shavandi A, Hosseini S, Okoro OV et al (2020) 3D bioprinting of lignocellulosic biomaterials. Adv Healthc Mater 9:2001472
8. Sanjay MR, Madhu P, Jawaid M et al (2018) Characterization and properties of natural fiber polymer composites: a comprehensive review. J Clean Prod 172:566–581
9. Vinod A, Sanjay MR, Suchart S, Jyotishkumar P (2020) Renewable and sustainable biobased materials: an assessment on biofibers, biofilms, biopolymers and biocomposites. J Clean Prod 258:120978
10. Jagadeesh P, Puttegowda M, Thyavihalli Girijappa YG et al (2022) Effect of natural filler materials on fiber reinforced hybrid polymer composites: An Overview. J Nat Fibers 19:4132–4147
11. Bismarck A, Mishra S, Lampke T (2005) Plant fibers as reinforcement for green composites. Natural fibers, biopolymers, and biocomposites: CRC Press, pp 52–128
12. Kandel KP, Adhikari M, Kharel M et al (2022) Comparative study on material properties of wood-ash alkali and commercial alkali treated Sterculia fiber. Cellulose 29:5913–5922
13. Ververis C, Georghiou K, Christodoulakis N et al (2004) Fiber dimensions, lignin and cellulose content of various plant materials and their suitability for paper production. Ind Crops Prod 19:245–254
14. Fu S-Y, Lauke B (1996) Effects of fiber length and fiber orientation distributions on the tensile strength of short-fiber-reinforced polymers. Compos Sci Technol 56:1179–1190
15. Park S, Baker JO, Himmel ME et al (2010) Cellulose crystallinity index: measurement techniques and their impact on interpreting cellulase performance. Biotechnol Biofuels 3:1–10
16. Tanpichai S, Sampson WW, Eichhorn SJ (2012) Stress-transfer in microfibrillated cellulose reinforced poly (lactic acid) composites using Raman spectroscopy. Compos Part Appl Sci Manuf 43:1145–1152
17. Obame SV, Betené ADO, Naoh PM et al (2022) Characterization of the Neuropeltis acuminatas liana fiber treated as composite reinforcement. Results Mater 16:100327
18. Betené ADO, Batoum CS, Ndoumou Belinga RL et al (2023) Extraction and characterization of a novel tropical fibre *Megaphrynium macrostachyum* as a biosourced reinforcement for gypsum-based biocomposites. J Compos Mater 57:2543–2562
19. Hashim MY, Amin AM, Marwah OMF et al (2017) The effect of alkali treatment under various conditions on physical properties of kenaf fiber. J Phys Conf Ser 914:012030
20. Borchani KE, Carrot C, Jaziri M (2015) Untreated and alkali treated fibers from Alfa stem: effect of alkali treatment on structural, morphological and thermal features. Cellulose 22:1577–1589
21. Vardhini KJ, Murugan R, Rathinamoorthy R (2019) Effect of alkali treatment on physical properties of banana fibre. Indian J Fibre Text Res IJFTR 44:459–465
22. Km A, Nayeem J, Quadery AH et al (2018) Handmade paper from waste banana fibre. Bangladesh J Sci Ind Res 53:83–88
23. Aryal GM, Ware W, Han S et al (2021) Microscopic characterization of eco-friendly Lokta paper. Microsc Microanal 27:720–721
24. Aryal GM, Kandel KP, Bhattarai RK et al (2022) Material properties of traditional handmade paper samples fabricated from cellulosic fiber of Lokta bushes. ACS Omega 7:32717–32726
25. Elanthikkal S, Gopalakrishnapanicker U, Varghese S, Guthrie JT (2010) Cellulose microfibres produced from banana plant wastes: isolation and characterization. Carbohydr Polym 80:852–859

26. Haque MM, Hasan M, Islam MS, Ali ME (2009) Physico-mechanical properties of chemically treated palm and coir fiber reinforced polypropylene composites. Bioresour Technol 100:4903–4906
27. Booth I, Goodman AM, Grishanov SA, Harwood RJ (2004) A mechanical investigation of the retting process in dew-retted hemp (Cannabis sativa). Ann Appl Biol 145:51–58
28. Obi Reddy K, Uma Maheswari C, Shukla M, Muzenda E (2014) Preparation, chemical composition, characterization, and properties of Napier grass paper sheets. Sep Sci Technol 49:1527–1534
29. Tanpichai S, Witayakran S, Srimarut Y et al (2019) Porosity, density and mechanical properties of the paper of steam exploded bamboo microfibers controlled by nanofibrillated cellulose. J Mater Res Technol 8:3612–3622
30. Jabbari F, Babaeipour V, Bakhtiari S (2022) Bacterial cellulose-based composites for nerve tissue engineering. Int J Biol Macromol 217:120–130
31. Tanpichai S, Boonmahitthisud A, Soykeabkaew N, Ongthip L (2022) Review of the recent developments in all-cellulose nanocomposites: properties and applications. Carbohydr Polym 286:119192
32. Torres FG, Arroyo JJ, Troncoso OP (2019) Bacterial cellulose nanocomposites: an all-nano type of material. Mater Sci Eng C 98:1277–1293
33. Sitotaw YW, Habtu NG, Gebreyohannes AY et al (2021) Ball milling as an important pretreatment technique in lignocellulose biorefineries: a review. Biomass Convers Biorefinery. https://doi.org/10.1007/s13399-021-01800-7
34. Humphrey J, Navas-Alemán L (2010) Value chains, donor interventions and poverty reduction: a review of donor practice. IDS Research report 63. https://www.ids.ac.uk/download.php?file=files/dmfile/rr63.pdf. Accessed Jan 2024
35. Biggs S, Messerschmidt D (2005) Social responsibility in the growing handmade paper industry of Nepal. World Dev 33:1821–1843
36. Government of Nepal (2017) Nepal national center export strategy: handmade paper and paper products 2017–2021. International trade center, Government of Nepal, https://moics.gov.np/public/uploads/shares/strategy/Handmade_Paper__Paper_Products_compressed.pdf. Accessed Jan 2024
37. Boopathi L, Sampath PS, Mylsamy K (2012) Investigation of physical, chemical and mechanical properties of raw and alkali treated Borassus fruit fiber. Compos Part B Eng 43:3044–3052
38. Van de Weyenberg I, Truong TC, Vangrimde B, Verpoest I (2006) Improving the properties of UD flax fibre reinforced composites by applying an alkaline fibre treatment. Compos Part Appl Sci Manuf 37:1368–1376
39. Das AM, Ali AA, Hazarika MP (2014) Synthesis and characterization of cellulose acetate from rice husk: eco-friendly condition. Carbohydr Polym 112:342–349
40. Adeeyo OA, Oresegun OM, Oladimeji TE (2015) Compositional analysis of lignocellulosic materials: evaluation of an economically viable method suitable for woody and non-woody biomass. Am J Eng Res AJER 4:14–19
41. Kandel KP, Aryal GM, Neupane BB (2023) Kinetics of water sorption in single Sterculia and Bauhinia fibers at ambient temperature. Results Chem 5:100872
42. Espert A, Vilaplana F, Karlsson S (2004) Comparison of water absorption in natural cellulosic fibres from wood and one-year crops in polypropylene composites and its influence on their mechanical properties. Compos Part Appl Sci Manuf 35:1267–1276
43. Beakou A, Ntenga R, Lepetit J et al (2008) Physico-chemical and microstructural characterization of "Rhectophyllum camerunense" plant fiber. Compos Part Appl Sci Manuf 39:67–74
44. Truong M, Zhong W, Boyko S, Alcock M (2009) A comparative study on natural fibre density measurement. J Text Inst 100:525–529
45. ASTM (2004) ASTM D1776–04. American Society for Testing and Materials, West Conshohocken, Pennsylvania, USA, Standard practice for conditioning and testing textiles
46. Elmogahzy Y, Farag R (2018) Chapter 7-Tensile properties of cotton fibers: Importance, research, and limitations. In: Bunsell AR, editor. Handbook of Properties of Textile and Technical Fibers (Second Edition): Woodhead Publishing, p 223–273
47. Saha P, Manna S, Chowdhury SR et al (2010) Enhancement of tensile strength of lignocellulosic jute fibers by alkali-steam treatment. Bioresour Technol 101:3182–3187
48. Bharath KN, Madhu P, Gowda TGY et al (2020) Alkaline effect on characterization of discarded waste of Moringa oleifera fiber as a potential eco-friendly reinforcement for biocomposites. J Polym Environ 28:2823–2836
49. Saravanakumaar A, Senthilkumar A, Saravanakumar SS et al (2018) Impact of alkali treatment on physico-chemical, thermal, structural and tensile properties of *Carica papaya* bark fibers. Int J Polym Anal Charact 23:529–536
50. Sumrith N, Techawinyutham L, Sanjay MR et al (2020) Characterization of alkaline and silane treated fibers of 'water hyacinth plants' and reinforcement of 'water hyacinth fibers' with bioepoxy to develop fully biobased sustainable ecofriendly composites. J Polym Environ 28:2749–2760
51. Mwaikambo LY, Ansell MP (2002) Chemical modification of hemp, sisal, jute, and kapok fibers by alkalization. J Appl Polym Sci 84:2222–2234
52. Aziz SH, Ansell MP (2004) The effect of alkalization and fibre alignment on the mechanical and thermal properties of kenaf and hemp bast fibre composites: Part 1–polyester resin matrix. Compos Sci Technol 64:1219–1230
53. Modibbo UU, Aliyu BA, Nkafamiya II (2009) The effect of mercerization media on the physical properties of local plant bast fibres. Int J Phys Sci 4:698–704
54. Gouanvé F, Marais S, Bessadok A et al (2007) Kinetics of water sorption in flax and PET fibers. Eur Polym J 43:586–598
55. Punyamurthy R, Sampathkumar D, Srinivasa CV, Bennehalli B (2012) Effect of alkali treatment on water absorption of single cellulosic abaca fiber. BioResources 7:3515–3524
56. Begum HA, Tanni TR, Shahid MA (2021) Analysis of water absorption of different natural fibers. J Text Sci Technol 7:152–160
57. Sinha E, Rout SK (2008) Influence of fibre-surface treatment on structural, thermal and mechanical properties of jute. J Mater Sci 43:2590–2601
58. Sui G, Fuqua MA, Ulven CA, Zhong WH (2009) A plant fiber reinforced polymer composite prepared by a twin-screw extruder. Bioresour Technol 100:1246–1251
59. Liu H, You L, Jin H, Yu W (2013) Influence of alkali treatment on the structure and properties of hemp fibers. Fibers Polym 14:389–395
60. Fiore V, Di Bella G, Valenza A (2015) The effect of alkaline treatment on mechanical properties of kenaf fibers and their epoxy composites. Compos Part B Eng 68:14–21
61. French AD (2020) Increment in evolution of cellulose crystallinity analysis. Cellulose 27:5445–5448
62. Yao W, Weng Y, Catchmark JM (2020) Improved cellulose X-ray diffraction analysis using Fourier series modeling. Cellulose 27:5563–5579
63. Cullity B (1978) Elements of X-ray diffraction. Addision wisely Publishing Company Inc., London
64. Ioelovich M (2018) Determination of distortions and sizes of cellulose nanocrystallites. Res J Nanosci Eng 2:1–5
65. Saravanakumar SS, Kumaravel A, Nagarajan T et al (2013) Characterization of a novel natural cellulosic fiber from Prosopis juliflora bark. Carbohydr Polym 92:1928–1933
66. Seki Y, Sever K, Erden S et al (2012) Characterization of *Luffa cylindrica* fibers and the effect of water aging on the mechanical

properties of its composite with polyester. J Appl Polym Sci 123:2330–2337
67. Wong KJ, Yousif BF, Low KO (2010) The effects of alkali treatment on the interfacial adhesion of bamboo fibres. Proc Inst Mech Eng Part J Mater Des Appl 224:139–148
68. Reddy N, Yang Y (2005) Structure and properties of high quality natural cellulose fibers from cornstalks. Polymer 46:5494–5500
69. Petroudy SD (2017) Chapter 3-Physical and mechanical properties of natural fibers. In: Fan M, Fu F (eds) Advanced high strength natural fibre composites in construction. Woodhead Publishing, pp 59–83
70. Poletto M, Ornaghi HL, Zattera AJ (2014) Native cellulose: structure, characterization and thermal properties. Materials 7:6105–6119
71. Yang H, Yan R, Chen H et al (2006) In-depth investigation of biomass pyrolysis based on three major components: hemicellulose, cellulose and lignin. Energy Fuels 20:388–393
72. Kim H-S, Kim S, Kim H-J, Yang H-S (2006) Thermal properties of bio-flour-filled polyolefin composites with different compatibilizing agent type and content. Thermochim Acta 451:181–188
73. Ray D, Sarkar BK, Basak RK, Rana AK (2002) Study of the thermal behavior of alkali-treated jute fibers. J Appl Polym Sci 85:2594–2599
74. Senthamaraikannan P, Saravanakumar SS, Sanjay MR et al (2019) Physico-chemical and thermal properties of untreated and treated Acacia planifrons bark fibers for composite reinforcement. Mater Lett 240:221–224

Publisher's Note Springer Nature remains neutral with regard to jurisdictional claims in published maps and institutional affiliations.

Springer Nature or its licensor (e.g. a society or other partner) holds exclusive rights to this article under a publishing agreement with the author(s) or other rightsholder(s); author self-archiving of the accepted manuscript version of this article is solely governed by the terms of such publishing agreement and applicable law.

ACS OMEGA

http://pubs.acs.org/journal/acsodf

Article

Material Properties of Traditional Handmade Paper Samples Fabricated from Cellulosic Fiber of Lokta Bushes

Girja Mani Aryal, Krishna Prasad Kandel, Ram Kumar Bhattarai, Basant Giri, Menuka Adhikari, Alisha Ware, Shubo Han, Gibin George, Zhiping Luo, Bhoj Raj Gautam,* and Bhanu Bhakta Neupane*

Cite This: *ACS Omega* 2022, 7, 32717−32726

Read Online

ACCESS | Metrics & More | Article Recommendations | Supporting Information

ABSTRACT: Handmade papers (HPs) are fabricated from fibrous biomass of Lokta bushes and other plant species following traditional eco-friendly method in Nepal. Although HP fabricated from Lokta bushes is believed to be durable and resistant to bugs and molds, material properties of this paper are not reported in literature. In this study, we measured several material properties of 10 handmade Lokta paper samples collected from local enterprises and paper industries. The mean caliper, grammage, apparent density, equilibrium moisture content, Cobb 60, brightness, opacity, tensile strength, and tensile index values in the paper samples ranged from ∼90 to 700 μm, 50 to 150 g/m^2, 0.2 to 0.4 g/cm^3, 4 to 7%, 50 to 400 g/m^2, 56 to 67%, 83 to 98%, 30 to 2900 N/m, and 1 to 27 Nm/g, respectively. These properties suggested that the HPs are lightweight papers with intermediate to high strength. The tensile strength was found to be significantly higher along the length direction ($p < 0.05$). Characteristic features of cellulose, hemicellulose, and lignin were observed in FTIR spectra. The crystalline and amorphous phases were also identified in X-ray diffraction (XRD) data. Electron microscopy images revealed a nicely cross-linked network of intact fibers having almost parallel arrangement of microfibrils. These features could provide strength and durability to the paper samples. Understanding the material properties of HPs down to the sub-microscopic level may help improve the paper quality and find novel applications in the future.

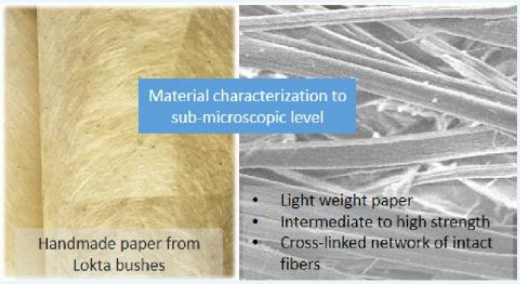

1. INTRODUCTION

Handmade paper (HP) making has been practiced across the globe since 105 AD.[1] It is believed that handmade paper making started, at least, in the 12th century AD in the western district of Baglung in Nepal.[2] In Nepal, HP is known as Nepali Kagaj. It is a traditional paper made from fibrous biomass of Lokta (*Daphne bholua* and *Daphne papyracea*) and Argeli (*Edgeworthia gardneri*) or their combinations. These plants are found at an elevation of 1600−4000 m in Nepal.[2−5] HP is believed to be a durable and bug- and mold-resistant paper and therefore is mostly used in official record keeping and religious texts.[3] Furthermore, a number of value-added products such as notebooks, photo albums, gift boxes and bags, and paper jewelries are fabricated from HP. The HP made from Lokta bushes is traditionally named Loka paper. However, any HP made from other plants is loosely termed as Lokta paper these days. There are ∼200 small- and medium-sized paper-making enterprises in Nepal, which support the livelihood of ∼55,000 families with an annual sell value of ∼$2.5 and ∼5.5 million in Nepal and abroad, respectively.[3]

HP making starts from harvesting stalks and manual removal of outer scaly bark. The long fiber mass is cut into small pieces and soaked in cold water for 6−12 h, and debris is removed manually. The biomass is boiled in water or ash solution for around 5−10 h. Next, the softened fiber biomass is beaten to make pulp and dispersed in water to make slurry. The slurry is poured in a wooden mesh frame or paper molds over a water tank, drained, and air-dried to obtain the paper sheet. In recent years, the hot water or ash solution digestion step of paper making is replaced by 4−5% hot alkali solution treatment for 3−10 h. Depending on the customers' need, additional steps such as chemical bleaching, calendaring, and machine glazing are performed.[3,4] The paper can be colored using traditional plant-based or commercial dyes if needed. Traditional HP making is considered an eco-friendly process since it requires low energy consumption, and little or no chemicals are used compared to the commercial paper-making process.

In recent years, several research groups are exploring the handmade paper making in laboratory settings. The paper sheets are fabricated from woody or non-woody parts of different plant species following mechanical and chemical methods of fiber

Received: July 12, 2022
Accepted: August 23, 2022
Published: September 1, 2022

ACS Publications

© 2022 The Authors. Published by American Chemical Society

https://doi.org/10.1021/acsomega.2c04398
ACS Omega 2022, 7, 32717−32726

processing or their combination.[6−11] A number of factors such as length and strength of individual fiber, organization of fiber, degree of cross-linking and bonding, chemical composition of fiber and processing parameters, extent of fibrillation, fines, and crill content determine the strength of a paper sheet.[12−18] The long fibers can form more contact points than short fibers, eventually leading to the paper of higher strength. However, the long fibers lead to the increased tendency to fiber entanglement and floc formation during processing.[14,19] The fiber aspect ratio, surface morphology, and chemical composition also affect the paper properties.[12] To understand the end properties of a paper sheet, it is particularly important to understand the material properties down to sub-microscopic levels.

Although HP fabricated from Lokta bushes is believed to be durable and resistant to bugs and molds, material properties of this paper are not reported in the literature. In this research, we determined the physical, optical, mechanical, and chemical properties of 10 HP samples collected from different paper enterprises of Nepal. A correlation between different parameters is provided, and the data are compared with other types of papers. We also compared the properties of paper sheet with raw Lokta fiber to understand the change in those properties during the paper-making process. Finally, we suggest few strategies to improve the HP quality and the potential applications of the HP Lokta paper.

2. MATERIALS AND METHODS

2.1. Materials. We collected 10 handmade Nepali paper samples, hereunder labeled from P1-10, from local paper enterprises directly. A total of 20 paper sheets (∼60 cm× 100 cm) made in the same lot were collected for each paper type. The samples were stored in an airtight container in dark until performing experiments.

Raw Lokta fiber was obtained from the fibrous inner bark of Lokta bushes collected from Baglung District of Nepal. The outer scaly bark was manually removed, and the fiber biomass was air-dried and then used for further study.

All the chemicals used in the study were purchased from Thermo Fisher Scientific India Pvt. Ltd and were used without further purification. All reagents were made in double-distilled water (pH = 7.1 ± 0.1 and conductivity 5 ± 1 μS).

2.2. Methods. *2.2.1. Measurement of Physical Properties.* We measured the thickness of a paper sheet (caliper) using a digital thickness micrometer (Hans Schmidt, D2000C) following the TAPPI T411 method.[20] Six independent measurements at different regions of the paper sheet were made.

Grammage or basic weight of the paper samples was measured following the TAPPI-410 method[21] under standard conditions of 23 °C temperature and 50% relative humidity (RH). Briefly, a paper sheet of 500 cm^2 was cut with a circular cutter, and its weight was taken (±0.001 g). Grammage (g/m^2) was obtained by taking the ratio of weight of paper (g) and its area (m^2). Six independent measurements were performed for each sample.

To measure the moisture content under ambient conditions, 2.000 g of the paper sample conditioned at 23 °C and 50% RH was placed in an oven (105 ± 2 °C) for 24 h. The sample was cooled in a non-hygroscopic desiccator and weighed. The difference in the weight before and after drying was used to calculate the moisture content of the paper. Three independent measurements were taken for each sample.

The Cobb 60 value was measured following the TAPPI-T441 method[22] for non-bibulous paper using a standard Cobb sizing tester. The excess water from the wetted specimen was removed by rolling a hand roller (10 kg) one back and one forward without applying additional pressure. The difference in weight of the paper after and before wetting was used to estimate the Cobb 60 value.

The opacity and brightness (ISO brightness) of the paper were determined using a standard brightness-opacity tester (UEC1018, India). Five paper specimens of size 5 mm × 5 mm were cut and put in the tester to determine the optical properties.

Tensile strength was determined under standard conditions of 23 °C and 50% RH using a tensile machine (UEC1005B, India) having a load capacity of 5−50 kg. Ten paper specimens of size 15 mm × 25 mm were cut for each paper. The cut piece was loaded in the tester to determine the strength along the length direction (LD) and cross direction (CD) of the wooden frame of paper molds. The tensile index (Nm/g) was calculated by dividing tensile strength of a paper (N/m) by its basic weight or grammage (g/m^2).

2.2.2. Determination of Chemical Composition. Lignin, cellulose, hemicellulose, and ash contents of the paper and fiber samples were determined gravimetrically following standard test methods.[23−26] To determine the cellulose content, 1.000 g of cellulose (oven-dried at 105 °C for 4 h and cooled in a non-hygroscopic desiccator) was treated with 5% NaOH (w/v) for 5 h (fiber to solution w/w ratio 1:30). The content was then cooled and neutralized with 10% H_2SO_4. The residual biomass was washed several times and treated for 5 h at room temperature with 2% H_2O_2 solution prepared in $NaHCO_3$−Na_2CO_3 buffer system of pH 9. The biomass was washed multiple times and dried at 105 °C until a constant weight was obtained. The weight difference was used to calculate cellulose content. Three independent measurements were made for each sample.

For the determination of lignin, 1.000 g of the extractive free paper sample was treated with 72% H_2SO_4 (sample to acid ratio 1:12.5 w/v) with careful shaking for 2 h. The top content was removed after several dilutions and washings. The residue was filtered and dried at 105 °C until a constant weight was obtained. The weight difference was used to calculate lignin content. Three independent measurements were made for each sample.

To determine the hemicellulose content, 1.000 g of the extractive free sample was boiled in 0.5 M NaOH for 4 h. The content was neutralized after several washings with distilled water and dried at 105 °C until a constant weight was obtained. The weight difference was used to calculate hemicellulose content. Three independent measurements were made for each sample.

To determine the ash content, 1.000 g of the moisture-free paper sample was burnt in an electric muffle furnace at 550 ± 10 °C. The weight difference was used to calculate ash content in percentage. Three independent measurements were made for each sample.

2.2.3. XRD, SEM, AFM, and FTIR Measurements. X-ray diffraction (XRD) data were collected in the 2θ range of 5−40° at a scan rate of 0.25°/min and a step size of 0.02° using a Rigaku Miniflex 600 X-ray diffractometer (operating at a 20 kV voltage and a 2 mA current). The X-ray source was the Cu Kα line (λ = 1.540 Å).

Scanning electron microscopy (SEM) images were collected using a field-emission electron probe microanalyzer (EPMA, JEOL JXA-8530F) with SDD X-ray energy-dispersive spectrometer (EDS). For each sample, four to six SEM images were collected at 100−5000× magnifications. Fiber width measurement was carried out using open-source software (ImageJ, NIH,

https://doi.org/10.1021/acsomega.2c04398
ACS Omega 2022, 7, 32717−32726

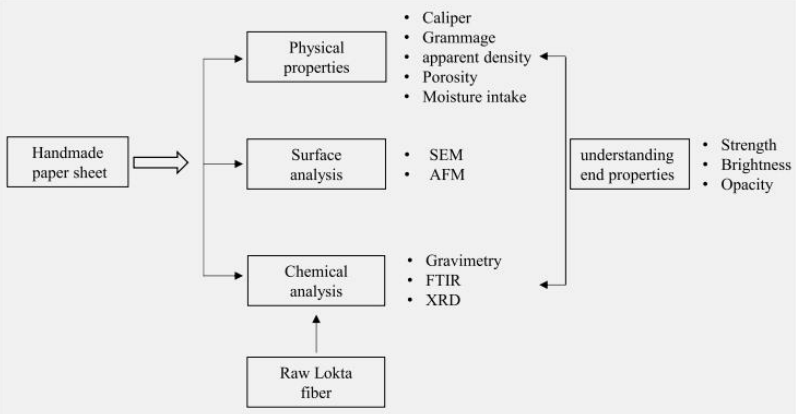

Figure 1. Schematic figure for the conceptual framework used in this work.

Table 1. Physical Properties of Paper Samples

paper	caliper (μm), n = 6	grammage (g/m^2), n = 6	apparent density (g/cm^3)	porosity (ε %)	moisture content (%), n = 3	Cobb 60 (g/m^2), n = 5
P1	207.2 ± 26.4	50.2 ± 2.4	0.25 ± 0.03	83.5 ± 2.3	4.3 ± 0.1	114.9 ± 14.0
P2	196.5 ± 11.1	74.7 ± 4.7	0.38 ± 0.03	74.4 ± 1.9	4.7 ± 0.3	154.2 ± 20.1
P3	462.5 ± 55.1	155.0 ± 11.7	0.34 ± 0.07	77.1 ± 4.5	5.3 ± 0.0	351.2 ± 14.0
P4	143.2 ± 2.8	47.7 ± 1.5	0.33 ± 0.01	77.6 ± 0.8	6.7 ± 0.8	96.4 ± 5.9
P5	158.0 ± 10.7	26.3 ± 1.9	0.17 ± 0.01	88.8 ± 1.1	5.8 ± 0.3	92.0 ± 9.1
P6	166.0 ± 13.2	54.6 ± 5.0	0.33 ± 0.02	77.7 ± 3.8	5.6 ± 1.2	128.5 ± 9.6
P7	274.8 ± 24.2	128.7 ± 5.3	0.47 ± 0.06	68.4 ± 3.2	6.±0.6	221.4 ± 10.4
P8	674.0 ± 110.7	128.9 ± 7.8	0.19 ± 0.05	86.9 ± 1.8	7.3 ± 0.4	411.4 ± 26.6
P9	91.8 ± 11.4	17.7 ± 2.4	0.20 ± 0.04	86.8 ± 2.8	5.9 ± 0.8	52.3 ± 4.6
P10	122.3 ± 8.3	28.7 ± 1.3	0.24 ± 0.01	84.2 ± 0.7	4.9 ± 0.5	63.1 ± 6.3

USA). Atomic force microscopy (AFM) was conducted using Agilent 5500.

The IR spectra were collected in the range of 4000−400 cm^{-1} in an attenuated total reflection (ATR) mode using a Fourier transform infrared spectrometer (FTIR) (ABB Bomen, MB100, Canada). The spectra were measured at the spectral resolution 4 cm^{-1}. To obtain a good signal-to-noise ratio, each reported spectrum is reported as an average of 16 optical scans. Prior to FTIR measurements, the paper samples were conditioned in standard atmosphere of 23 °C and 50% RH for 24 h and kept in a non-hygroscopic desiccator.

The basic idea or conceptual framework of this work is summarized in Figure 1.

3. RESULTS AND DISCUSSION

3.1. Basic Physical Properties. The basic physical parameters for all paper samples are provided in Table 1, and the individual data sets are provided in Tables S1−S3. The mean thickness values (caliper) for the paper samples ranged from ∼90 μm (P9) to 675 μm (P8). Similarly, grammage ranged from ∼20 g/m^2 (P9) to 150 (P3). A good positive correlation (r = 0.83) was observed between these two parameters. The wide variation in grammage indicates that these papers are intended for different purposes. Paper sheets having grammage at or below 50 are normally used for printing purpose, and the paper of higher grammage is used to design other value-added products such as photo albums and gift boxes.

We measured caliper with a digital micrometer having a resolution of 10 μm. For example, the caliper of sample P1 ranged from 180 to 254 μm (mean = 207.2 ± 26.4 μm). The large variation in caliper indicates that HP samples have non-uniform thickness. Handmade paper samples are generally fabricated following the chemical-mechanical method of fiber processing, which mostly results in long fiber (<1 mm). The long fibers have strong propensity to *floc* formation during the paper-making process, which results in thickness variation.[19,27]

We also calculated the apparent density (g/cm^3) of all the paper samples by taking the ratio of grammage (g/m^2) to thickness (μm). The apparent density ranged from ∼0.20 (P8 and P9) to 0.50 (P7) g/cm^3 (Table 1). Apparent density of paper also includes the volume occupied by air or open space in the paper. Therefore, apparent density is always lower than true density. The apparent density of machine-made and commercially available paper sheet has been reported to be higher (0.5−0.8 g/cm^3) than that of Lokta papers.[3,28] The low apparent density suggests that HPs are lightweight paper.

The apparent porosity of paper can be estimated from known density of paper network and cellulose.[29−32] In this work, apparent porosity was calculated using eq 1 (reprinted with permission from ref 29, copyright Elsevier 2012).

$$\varepsilon(\%) = \left[1 - \frac{\rho_{adp}}{\rho_{cf}}\right] \times 100 \quad (1)$$

where ρ_{adp} and ρ_{cf} are apparent density of the paper network and density of cellulose fiber, respectively. A cellulose fiber density of 1.49 g/cm^3 was used for the calculation.[33] Apparent porosity was found to be in the range of ∼69% (P7) to 89% (P5). A perfect negative correlation was observed between apparent density and

https://doi.org/10.1021/acsomega.2c04398
ACS Omega 2022, 7, 32717−32726

Table 2. Mechanical and Optical Properties of all the Paper Samples

	tensile strength, kN/m		tensile index, Nm/g				
samples	LD	CD	LD	CD	brightness	opacity	RBA
P1	0.6 ± 0.1	0.4 ± 0.1	12.7 ± 1.6	8.4 ± 1.3	66.8 ± 0.4	92.9 ± 0.5	0.028
P2	2.05 ± 0.1	1.9 ± 0.0	27.4 ± 1.1	25.4 ± 0.5	61.9 ± 0.7	97.1 ± 0.4	0.069
P3	2.02 ± 0.4	1.7 ± 0.1	13.0 ± 2.8	10.8 ± 0.8	65.1 ± 0.3	97.7 ± 0.2	0.052
P4	0.7 ± 0.0	0.6 ± 0.1	15.9 ± 0.5	12.1 ± 1.6	62.7 ± 0.5	95.3 ± 0.4	0.054
P5	0.03 ± 0.0	0.02 ± 0	1.2 ± 0.4	0.7 ± 0.1	61.8 ± 0.1	86.4 ± 2.2	0.013
P6	1.2 ± 0.1	1.08 ± 0.1	18.3 ± 1.2	16.9 ± 0.9	63.8 ± 0.7	95.4 ± 0.4	0.052
P7	2.9 ± 0.0	2.69 ± 0.1	22.4 ± 0.3	21.1 ± 1.0	61.4 ± 0.7	97.5 ± 0.3	0.103
P8	1.5 ± 0.0	1.25 ± 0.1	11.7 ± 0.4	9.7 ± 0.9	55.6 ± 0.3	97.8 ± 0.4	0.017
P9	0.3 ± 0.0	0.22 ± 0.0	14.3 ± 1.2	12.2 ± 0.9	59.6 ± 0.5	79.5 ± 3.4	0.019
P10	0.4 ± 0.0	0.34 ± 0.0	15.2 ± 1.1	11.4 ± 0.8	66.9 ± 0.4	87.4 ± 1.7	0.027

porosity ($r = -1$). In paper making, low apparent density (high porosity) arises due to the long and stiff fibers, insufficient refining, absence of fillers and fines, insufficient or no calendaring, and their combinations,[28] which could explain the low apparent density of handmade papers. Low apparent density in the range of 0.2−0.5 g/cm^3 was also reported in laboratory-made handmade paper samples.[6,10,11]

Equilibrium moisture content (EMC) of the paper samples ranged from ∼4.3% (P1) to 7.3% (P8). Similar values of moisture content were reported for cellulose-based paper sheet.[28] The Cobb 60 value is the most used parameter to measure the water absorption tendency of a paper sheet. Cobb 60 is the measurement of amount/weight of water absorbed in 60 s by 1 square meter of paper under 1 cm of water. The Cobb value depends on fiber chemical composition, fiber morphology and organization, and caliper. The Cobb sizing ranged from ∼50 (P9) to 410 g/m^2 in the samples we tested. The wide variation in Cobb 60 could be linked to the difference in chemical composition of the paper samples (reported in Table 3) and a small difference in fiber morphology and organization (SEM images in Figure 4). A Cobb 60 value of handmade paper shows strong positive correlation with the caliper ($r = +0.97$) and grammage ($r = +0.92$). It is possible that in thick and porous paper, the retained water could be difficult to remove with mechanical pressing, with a 10 kg roller in the experiment, leading to a high Cobb 60 value.

Table 3. Chemical Composition Data for the Paper Samples and Raw Lokta Fiber

samples	cellulose (%)	hemicellulose (%)	lignin (%)	ash (%)
P1	66.0 ± 1.7	23.5 ± 4.0	3.9 ± 0.5	7.8 ± 0.0
P2	67.4 ± 7.2	25.9 ± 0.4	5.7 ± 0.2	4.5 ± 0.7
P3	83.6 ± 6.5	11.4 ± 3	2.0 ± 0.5	3.5 ± 0.6
P4	81.7 ± 4.4	11.3 ± 4.0	2 ± 0.7	3.6 ± 0.5
P5	73.1 ± 2.8	19.5 ± 1.4	9.8 ± 0.3	7.7 ± 0.1
P6	80.4 ± 3.9	12.1 ± 2.2	5.4 ± 0.5	6.6 ± 0.4
P7	75.7 ± 3.8	14.1 ± 1.7	7.5 ± 0.7	3.5 ± 0.4
P8	71.4 ± 1.1	20.8 ± 0.3	9.3 ± 1.5	3.6 ± 0.1
P9	76.2 ± 1.8	18.2 ± 1.0	7.4 ± 0.5	7.1 ± 0.5
P10	75.7 ± 1.1	13.7 ± 2.1	7.9 ± 1.3	3.5 ± 0.6
raw fiber	36.8 ± 1.0	44.0 ± 1.0	19.2 ± 1.0	2.6 ± 0.2

3.2. Optical Properties. Brightness and opacity are the important optical parameters of paper. With blue light illumination, a yellowish paper reflects less light or absorbs more light. Therefore, higher brightness is the indicator of lower yellowness of paper. Brightness of the paper sample is determined by the degree of bleaching and surface smoothness. For bleached and gazed commercial printing paper, ISO brightness as high as 100% is reported.[28] The brightness of the paper samples ranged from 56% (P8) to 67% (P1 and P10) (Table 2 and Figure S1).

Brightness of paper and pulp samples depends on several parameters such as lignin and coloring impurity content and microscopic surface structures.[28] Relatively lower brightness values for the handmade paper samples could be due to unbleached pulp used in paper making and/or lower quality water and reagents used in the pulping process. The brightness and lignin content data for the paper samples (Tables 2 and 3) showed a fairly good negative correlation ($r = -0.51$).

Opacity measures the ability of paper to mask an object located on the back of the sheet. For double-sided printing, a high opacity paper is required to read the front page without being distracted by the characters or images on the back side and to avoid the strike through. In bulky paper sheet, microscopic air spaces or pores reflect more blue light, leading to high opacity.[28] In our study, opacity of the paper samples ranged from ∼83% (P9) to 98% (P2, P7, and P8) (Table 2). Higher opacity could be due to low apparent density or high porosity of the papers. We found a moderate positive correlation ($r = +0.68$) between opacity and apparent density.

3.3. Mechanical Properties. We measured tensile strength and tensile index of all the paper samples in two directions: along and across the length of the wooden frame or paper molds. For easy comparison hereunder, we label these directions LD and CD. In machine-made paper, there directions are commonly labeled as machine direction (MD) and cross direction (CD). The tensile strength along the LD ranged from 0.03 (P5) to 2.9 (P7) kN/m with the corresponding CD values ranged from 0.02 to 2.7 kN/m (Table 2 and Figure S1). In handmade paper making, pulp is added to a rectangular wooden mesh/frame (paper molds, size 40 cm × 60 cm) over the pool of water, and the slurry is gently dispersed by shaking the wooden frame along the length. This could result in partial alignment of fibers along the frame length and explain the observed difference in strength in two directions.

Tensile strength is the maximum stress applied per unit width (N/m or kN/m) of paper to break the paper strip. During printing and other applications such as preparation of gummed paper tape, a paper sheet can be subjected to different levels of stress. A paper having low tensile strength can lead to web breaking in these activities.[28] Moderately high values of tensile strength values indicate that web breaking during printing is less likely in the handmade paper samples reported here.

https://doi.org/10.1021/acsomega.2c04398
ACS Omega 2022, 7, 32717−32726

We also measured the tensile strength index, which is the grammage normalized tensile strength, values along LD and CD directions. Tensile index of the paper samples along the LD and CD ranged from 1.2 (P5) to 27.5 (P2) Nm/g and 0.7 (P5) to 25.4 (P2) Nm/g, respectively (Table 2). For all samples, the LD values are significantly higher than CD ($p < 0.05$) with an average LD: CD ratio of ~1.1 (P7) to 2 (P7). This indicates that the fiber orientation along two directions is different. An MD/CD ratio of ~1.5−5 is reported in machine-made paper.[28] This observation suggested that fiber orientation in handmade paper is lower than in machine-made paper.

Tensile strength of paper-based materials depends on several factors including strength of individual fiber, fiber length, and fiber-to-fiber contact and bonding. Considering a paper sheet as a multi-layered composite structure of two-dimensional fibrous networks not interwinded between layers, the amount of contact between two layers defined in terms of relative bonding area (RBA) can be calculated.[32,34] From the information on fractional porosity (ε) and number of fiber layers (n), which is defined as the ratio of caliper to fiber diameter, a rough estimate of RBA can be made.[32] The RBA values for all the paper samples are provided in Table 2. A fiber diameter of 10 μm was used in the estimation of RBA.

For fibers of the same length, coarseness, cross section perimeter, and bonding strength, the tensile strength of a fiber sheet is directly proportional to relative bonding area.[35,36] Microscopy images shown in the later section support the fact that the fiber morphology (length, width, and coarseness) is similar in the paper samples studied here. Interestingly, RBA values and measured tensile strength (Table 2) showed a fairly good positive correlation (r = +0.83) (Figure 2). Considering

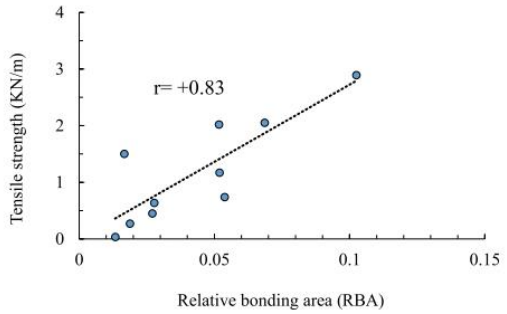

Figure 2. Plot of tensile strength versus relative bonding area. The dotted line is the liner fit to the measured data.

the abovementioned discussion, the lowest and highest tensile strength values for P5 and P7 could be due to the lowest and highest RBA values, respectively. Variation in tensile strength could be partly linked to variation in fiber-to-fiber bonding strength resulted from the difference in chemical composition (Table 3) in the paper sheets.

3.4. Chemical Analysis. We also measured cellulose, hemicellulose, lignin, and ash content in all the samples and in raw Lokta fiber (Table 3). The mean values (n = 3) for cellulose, hemicellulose, lignin, and ash content ranged from ~66 to 84, 11 to 26, 2 to 10, and 3 to 8%, respectively. As compared to paper samples, raw Lokta fiber showed a significantly high amount of lignin (~19%) and hemicellulose (~44%) and low amount of cellulose (~37%). In fiber processing, lignin and hemicellulose are partially removed, thereby resulting in a net increase in cellulose content.[26,37] This explains the higher amount of cellulose or lower lignin and hemicellulose observed in the paper samples. The difference in chemical composition in the paper samples could be due to variability in fiber processing and or different types of fibers used in making the paper samples.

3.5. FTIR and XRD Study. The FTIR data of all the paper samples and Lokta fiber are provided in Figure 3A. The spectra look similar in shape with a small difference in the relative peak intensities. We made the spectral assignments on the basis of literature-provided information.[30,38−41] The broad peak in the range of 3000−3600 cm^{-1} (with three weak peaks/shoulders) is attributed to the O−H stretching of cellulose. The weak peak ~2900 cm^{-1} is due to the aliphatic C−H stretching vibration in hemicellulose and cellulose.[38] Peak ~1735 cm^{-1} arises due to acetyl or ester C═O groups of hemicellulose or lignin,[30] and the peak ~1630 cm^{-1} originates from C═O stretching of conjugated lignin.[30,42] These peaks are relatively stronger in raw Lokta fiber. This observation suggested that hemicellulose and lignin are partially removed in pulping. A weak peak at 1250 cm^{-1} corresponds to C−O stretching of acetyl groups of hemicellulose and cellulose.[43] The peak is weaker in paper samples, suggesting that fiber processing during paper making resulted in removal of hemicellulose. These observations are consistent with the chemical analysis data reported in Table 3. A summary of the observed IR peaks and their interpretation is provided in Table 4.

Crystalline natural cellulose exists in two allomorphs I_α and I_β. I_β allomorph is reported to be thermodynamically more stable. Interestingly, characteristic peaks of crystalline cellulose I_β (weak peaks at ~710 and 3270 cm^{-1})[41,44,45] and amorphous cellulose (weak peak ~660 cm^{-1} and a weak broad shoulder ~3420 cm^{-1})[40] are also observed in all paper samples and raw fiber. We did not see the characteristic features for I_α in all the samples, which are reported to be ~3240 and 750 cm^{-1}.[44] The composition of I_α and I_β is reported to be species-dependent. Also, due to meta-stability of I_α, it could change to the I_β form during pulping.[41] Since I_α peaks are also absent in raw fiber, the later possibility could be ruled out.

The absorption intensity ratio of different IR bands is used to obtain information on hydrogen bond intensity (HBI) in cellulose-based samples.[46−49] Hydrogen bond intensity is related to the amount of bound water and structural flexibility. Generally, crystallinity decreases as HBI increases.[47] We used the absorption ratio of bands at ~3336 and 1320 cm^{-1} (A_{3336}/A_{1320}) to calculate HBI.[48,49] The HBI ranged from ~1.2 to 1.5 (Table 5). HBI depends on the type of fiber and fiber-processing parameters. Therefore, it is not surprising to see the observed differences in HBI in the samples. For reference, HBI in the range of 1.4−1.8 is reported for different cellulose samples.[47−49]

We also measured the XRD data of all the paper samples and raw fiber (Figure 3B). The peak at 2θ values of ~21.5 and ~15.5° originates from (200) and (1−10/110) planes of crystalline phase cellulose I, respectively.[50,51] A broad background underlying the peaks is attributed to the amorphous phase.[50,52] We also calculated the XRD crystallinity index (CI) following eq 2 (reprinted with permission from ref 26, copyright Springer Nature 2022).

$$\mathrm{CI} = \left(\frac{A_t - A_{am}}{A_t}\right) \times 100 \tag{2}$$

where A_t is the integrated intensity of both crystalline and amorphous phases and A_{am} is the intensity of amorphous phase

https://doi.org/10.1021/acsomega.2c04398
ACS Omega 2022, 7, 32717−32726

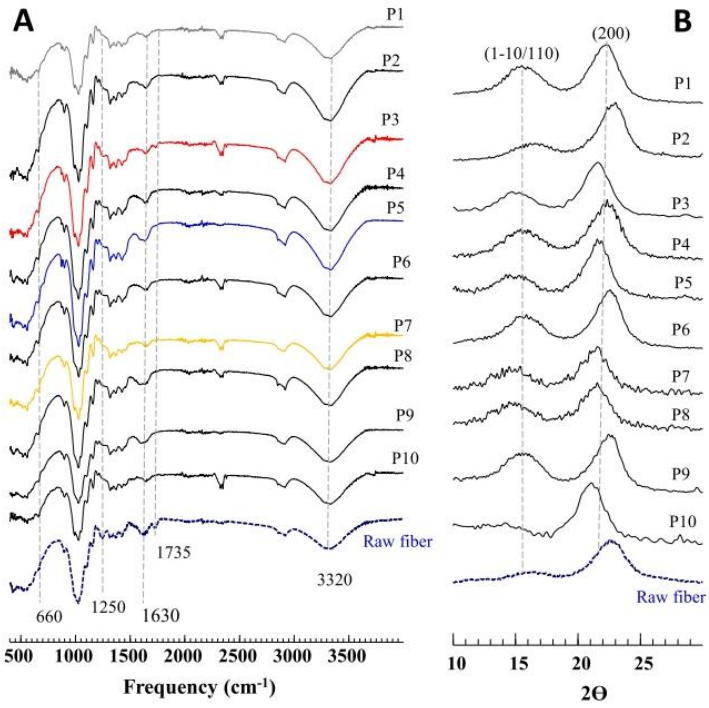

Figure 3. FTIR and XRD data. (A) FTIR data of paper samples P1−P10 and raw fiber. Spectra are overlaid vertically for easy compassion. Important peaks are indicated by dotted vertical lines. (B) XRD data of the paper samples. Reflection planes at 2θ values of ∼15.5 and 21.5° are indicated in parenthesis. For easy comparison, spectra are overlaid in the vertical direction.

Table 4. IR Peaks and Their Spectral Assignment[a]

peak position (cm^{-1})	relative intensity	assignment
3000−3600	S	O−H (symmetric) stretching of cellulose
2900	M	aliphatic C−H (asymmetric) stretching of cellulose and hemicellulose
2850	M	aliphatic C−H (symmetric) stretching of lignin and cellulose
2330, 2350	M	carbonate impurities
1735	W	C=O stretch (non-conjugated) hemicellulose and lignin
1630	M	C=O stretch (conjugated) lignin
1590	M	aromatic ring vibration and C=O stretch lignin
1510	W	aromatic ring vibration lignin
1465	W	C−H deformation lignin
1450	W	O−H in-plane bending cellulose and hemicellulose
1430	W	C−H in-plane deformation lignin
1370	M	C−H bending cellulose, hemicellulose, and lignin
1200	M	O−H bending of cellulose and hemicellulose
1250	W	C−O stretching of acetyl groups of hemicellulose and cellulose
1160	S	C−O−C asymmetrical stretching cellulose and hemicellulose
1030, 1000	S	C−O, C=C, and C−C−O stretching of lignin, cellulose, and hemicellulose
900, 875	M	glycosidic linkage hemicellulose and cellulose
710	W	O−H out of plane bending of crystalline cellulose I_β
660	W	O−H out of plane bending of amorphous cellulose

[a]S = strong, M = medium, and W = weak.

only. We carried out Gaussian fitting in the 2θ range of 10−30° to calculate A_t, A_{am}, and CI. The CI in the paper samples ranged from ∼62 to 85% (Table 4). In the raw fiber, CI was found to be 58.5%. The CI depends on the source of cellulose biomass and processing parameters, which explains the observed differences in the samples P1−P10. If a fiber is treated with alkali in the paper-making process, lignin is removed from the interfibrillar region, resulting in reorganization of the cellulose chain and an increase in the crystallinity index.[50,51] This explains the higher crystallinity index observed in all paper samples than in raw fiber. For reference, CI in the range 20−97% is reported for different cellulose samples.[47−49] We also found a good negative correlation between HBI and CI ($r = -0.83$). This observation is consistent with literature study.[47]

3.6. SEM Imaging of the Paper Samples. The representative SEM images of the paper samples are provided in Figure 4A−J. In the images, individual fibers are randomly arranged to form interwoven networks. The presence of long (>1 mm) and interconnected fibers provides strength to the paper sheet. It is interesting to find a few fibrillated, damaged, and curled fibers in images of paper samples P1, P2, and P10 (Figure 4A,B,J). Such fibers can be formed due to mechanical and chemical forces during fiber processing and paper making.

Fiber width is an important parameter to measure fiber intactness and strength of a paper sheet. A paper sheet having a large fraction of collapsed fiber can have lower strength.[12,28] We measured the fiber width in all the samples. The mean, minimum, and maximum fiber width values obtained from 100 measurements in each sample were found in the range of 9−11, 4−6, and 18−26 μm, respectively. The mean fiber width distribution was insignificant in all the samples ($p < 0.05$). As an

https://doi.org/10.1021/acsomega.2c04398
ACS Omega 2022, 7, 32717−32726

Table 5. Hydrogen Bonding Intensity (HBI) and CI of the Paper Samples

parameters	P1	P2	P3	P4	P5	P6	P7	P8	P9	P10
HBI	1.48	1.52	1.33	1.38	1.21	1.50	1.52	1.34	1.22	1.19
CI	70.7	65.4	72.9	62.4	83.8	72.6	62.2	70.2	83.6	84.5

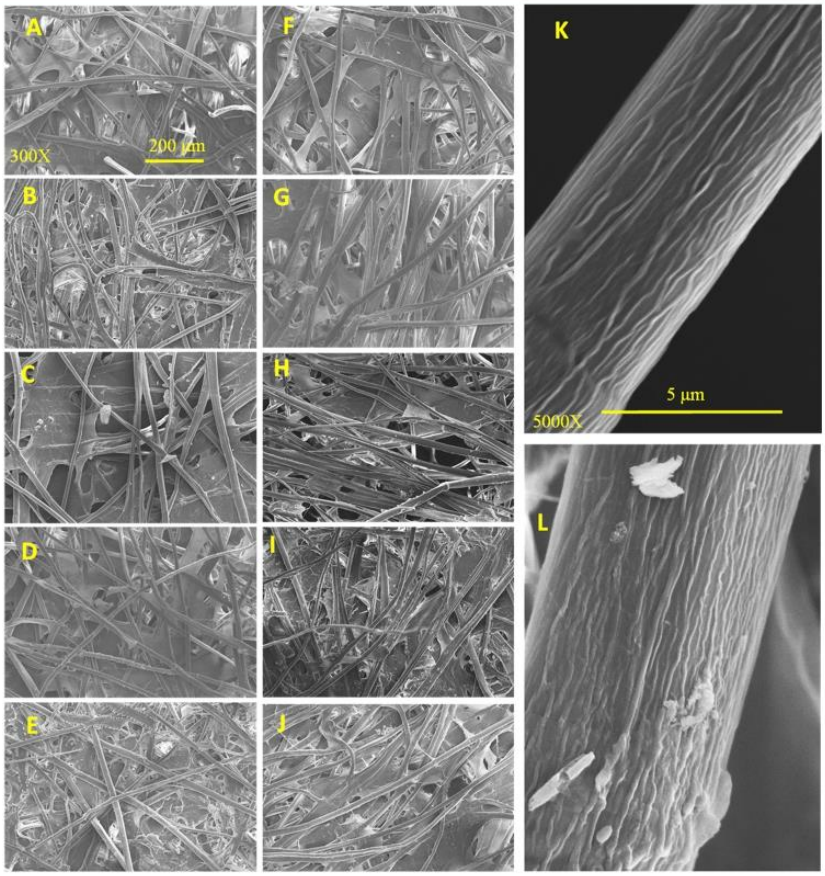

Figure 4. (A) SEM micrograph of the paper samples. (A–J) Images of paper samples P1–P10 taken at 300×, respectively. The scale bar of 200 μm shown in (A) also applies for (B–J). Images of individual fiber taken at 5000× for samples P3 (K) and P8 (L). The scale bar of 5 μm shown in (K) applies for (L).

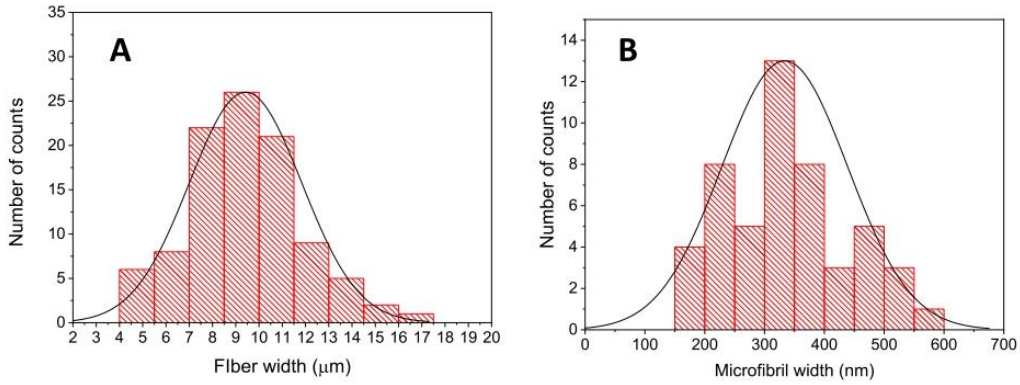

Figure 5. Fiber and microfibril width distribution. (A) Fiber width (n = 100) and (B) microfibril width distribution in P3 (n = 50). In both figures, the solid curve shows normal distribution.

https://doi.org/10.1021/acsomega.2c04398
ACS Omega 2022, 7, 32717−32726

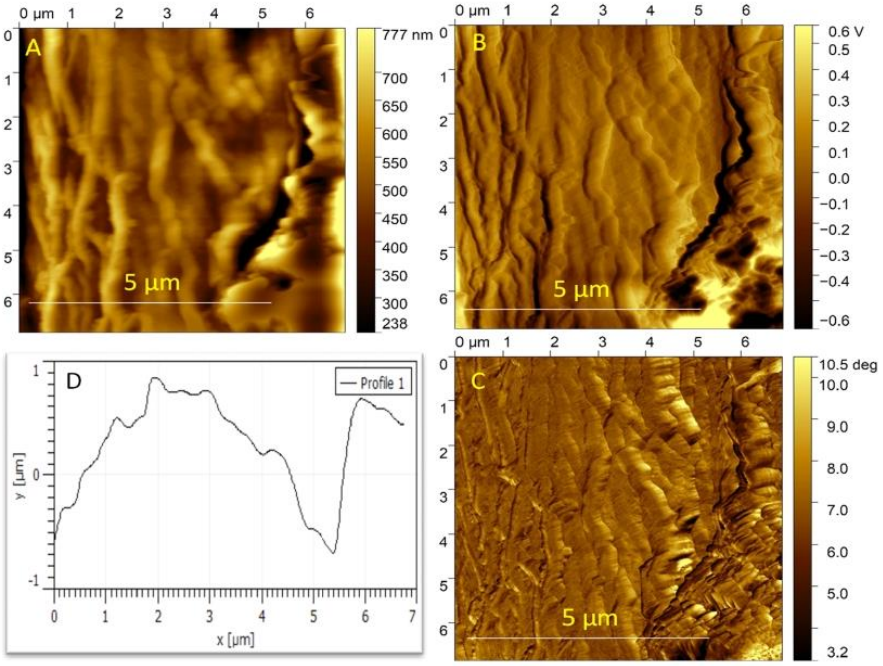

Figure 6. AFM topography (A), amplitude (B), and phase (C) images of small regions with a cellulose fiber and profile (D) along the line labeled in (A).

example, the fiber width distribution of sample P3 is provided in Figure 5A. During fiber processing, lumen or cell wall in some of the fibers can collapse to from ribbon-like flexible fibers. The collapsed fiber can have high apparent width.[14,53] Also, some of the fibers may not be separated or remain attached to form a bundle which can result in high apparent width. These reasonings explain observation of high apparent width ($\geq$20 μm) in some of the fibers. This fraction was found to be $\leq$5% in all the samples.

A zoomed-in image of individual fiber is provided in Figure 4K,L. It is interesting to see individual microfibrils that run almost straight along the lengths of fiber. We found mean microfibril width in the samples in the range of 250−450 nm (n = 50). As an example, the width distribution profile of sample P3 is provided in Figure 5B. The microfibrils are visible due to removal of gummy materials such as lignin and hemicellulose from the fiber surface during fiber processing. Almost parallel arrangement of the microfibrils (Figure 4K,L) can provide excellent strength to individual fiber and to the fiber web.

Tensile strength of a paper sheet depends partly on fiber surface roughness. Microscopic or sub-microscopic structures/roughness at the individual fiber level can lead to increased fiber−fiber bonding and increased strength.[12] To explore this, we carried out AFM imaging in a selected sample, the thinnest sample P9 (Figure 6A−D). The surface roughness and microfibrils are clearly visible in the images. A line profile on the topographic image shows a roughness of ~±700 nm (Figure 6D). These surface structures could be partly responsible for the paper strength.

3.7. Further Implications of the Research. Present study was intended to investigate material properties of HPs down to the sub-microscopic level and explains the observed difference in mechanical and optical properties. The paper samples had low apparent density (i.e., high porosity), thickness variation, and low brightness. Eco-friendly and low-cost strategies to improve these properties would be useful for handmade paper industries. Enzymatic bleaching of the pulp using locally isolated microbial cultures could be explored to increase the brightness. Calendaring of paper sheet by a locally designed handmade machine would be useful to improve high porosity and thickness variation issues.

In the future, handmade paper or raw Lokta fiber could be used as a starting material for the synthesis/fabrication of useful nanomaterials such as nanocellulose,[54−56] antimicrobial cellulose film,[57] and micro- and nanocomposite materials for chemical sensing and filtering applications.[58−60]

4. CONCLUSIONS

To summarize, we measured several physical and chemical parameters of 10 different Nepali handmade paper samples. The mean caliper, grammage, and apparent density values in the paper samples ranged from ~90 to 700 μm, 50 to 150 g/m^2, and 0.2 to 0.4 g/cm^3, respectively. The optical brightness, tensile strength, and tensile index values ranged from 56 to 67%, 30 to 2900 N/m, and 1 to 27 Nm/g, respectively. The tensile strength along the length direction (LD) was found to be significantly higher than in cross direction (CD) ($p < 0.05$). These properties suggested that HP is lightweight paper, having intermediate yellowness but medium to high tensile strength. In all the samples, characteristic features of crystalline and amorphous cellulose phases were observed both in FTIR and XRD data. SEM micrographs of the paper sheet revealed interconnecting networks of long cellulose fibers. Imaging of the individual fiber surface revealed almost parallel arrangement of microfibrils.

https://doi.org/10.1021/acsomega.2c04398
ACS Omega 2022, 7, 32717−32726

These properties explain the observed mechanical properties of the paper samples.

■ ASSOCIATED CONTENT

Supporting Information

The Supporting Information is available free of charge at https://pubs.acs.org/doi/10.1021/acsomega.2c04398.

Individual data sets (as measured) for caliper, grammage, tensile strength, tensile index, brightness, opacity, and chemical composition (PDF)

■ AUTHOR INFORMATION

Corresponding Authors

Bhoj Raj Gautam − *Department of Chemistry, Physics and Materials Science, Fayetteville State University, Fayetteville, North Carolina 28301, United States*; Email: bgautam@uncfsu.edu

Bhanu Bhakta Neupane − *Central Department of Chemistry, Tribhuvan University, Kathmandu 44613, Nepal*; orcid.org/0000-0003-0731-2552; Email: bbneupane@cdctu.edu.np

Authors

Girja Mani Aryal − *Central Department of Chemistry, Tribhuvan University, Kathmandu 44613, Nepal; Research Centre for Applied Science and Technology, Tribhuvan University, Kathmandu 44613, Nepal*

Krishna Prasad Kandel − *Central Department of Chemistry, Tribhuvan University, Kathmandu 44613, Nepal*

Ram Kumar Bhattarai − *Center for Analytical Sciences, Kathmandu Institute of Applied Sciences, Kathmandu 44600, Nepal*

Basant Giri − *Center for Analytical Sciences, Kathmandu Institute of Applied Sciences, Kathmandu 44600, Nepal*

Menuka Adhikari − *Department of Chemistry, Physics and Materials Science, Fayetteville State University, Fayetteville, North Carolina 28301, United States*

Alisha Ware − *Department of Chemistry, Physics and Materials Science, Fayetteville State University, Fayetteville, North Carolina 28301, United States*

Shubo Han − *Department of Chemistry, Physics and Materials Science, Fayetteville State University, Fayetteville, North Carolina 28301, United States*

Gibin George − *Department of Chemistry, Physics and Materials Science, Fayetteville State University, Fayetteville, North Carolina 28301, United States*

Zhiping Luo − *Department of Chemistry, Physics and Materials Science, Fayetteville State University, Fayetteville, North Carolina 28301, United States*; orcid.org/0000-0002-8264-6424

Complete contact information is available at: https://pubs.acs.org/10.1021/acsomega.2c04398

Notes

The authors declare no competing financial interest.

■ ACKNOWLEDGMENTS

This work was supported by the University Grants Commission, Nepal (to B.B.N. and K.P.K., grants # FRG-6/77-S&T-3 and PhD-76/77-S&T-10) and by NSF DMR 1827731 and EIR ECCS 1900837 (B.R.G., S.H. and Z.L.).

■ REFERENCES

(1) Hubbe, M. A.; Bowden, C. Handmade Paper: A Review of Its History, Craft, and Science. *BioResources* **2009**, *4*, 1736−1792.

(2) Biggs, S.; Messerschmidt, D. Social Responsibility in the Growing Handmade Paper Industry of Nepal. *World Dev.* **2005**, *33*, 1821−1843.

(3) ITC. *Nepal National Center Export Strategy: Handmade Paper and Paper Products 2017−2021*; International Trade Center, Government of Nepal, 2017; pp 1−124.

(4) Banjara, G. *Handmade Paper in Nepal: Upgrading with Value Chain Approach*; GTZ/PSP-RUFIN, 2007.

(5) Poudyal, A. Sustainability of Local Hand-Made Paper (Nepali Kagat) Enterprises: A Case Study of Dolakha District. *J. For. Livelihood* **2004**, *4*, 64−69.

(6) Mejouyo, P. W. H.; Nkemaja, E. D.; Beching, O. R.; Tagne, N. R.; Kana'a, T.; Njeugna, E. Physical and Tensile Properties of Handmade Sida Rhombifolia Paper. *Int. J. Biomater.* **2020**, *2020*, 1.

(7) Kumar, A.; Singh, B. P.; Jain, R. K.; Sharma, A. K. Banana Fibre (Musa Sapientum): A Suitable Raw Material for Handmade Paper Industry via Enzymatic Refining. *Int. J. Eng. Res.* **2013**, *2*, 1338−1350.

(8) Sottile, F.; Modica, A.; Rosselli, S.; Catania, C. A.; Cavallaro, G.; Lazzara, G.; Bruno, M. Hand-Made Paper Obtained by Green Procedure of Cladode Waste of Opuntia Ficus Indica (L.) Mill. from Sicily. *Nat. Prod. Res.* **2021**, *35*, 359−368.

(9) Arafat, Km.; Nayeem, J.; Quadery, A. H.; Quaiyyum, M. A.; Jahan, M. S. Handmade Paper from Waste Banana Fibre. *Bangladesh J. Sci. Ind. Res.* **2018**, *53*, 83−88.

(10) Reddy, K. O.; Uma Maheswari, C.; Shukla, M.; Muzenda, E. Preparation, Chemical Composition, Characterization, and Properties of Napier Grass Paper Sheets. *Sep. Sci. Technol.* **2014**, *49*, 1527−1534.

(11) Marrakchi, Z.; Khiari, R.; Oueslati, H.; Mauret, E.; Mhenni, F. Pulping and Papermaking Properties of Tunisian Alfa Stems (Stipa Tenacissima)—Effects of Refining Process. *Ind. Crops Prod.* **2011**, *34*, 1572−1582.

(12) Johansson, A. Correlations between Fibre Properties and Paper Properties. M.S. Thesis, 2011.

(13) Lundberg, M.; Norgren, M.; Edlund, H. Validation of Crill Measurements in a High-Yield Pulp Refining Process for Improved Fines Material Control. *Nord. Pulp Pap. Res. J.* **2018**, *33*, 200−209.

(14) Hubbe, M. A. Difficult Furnishes. *Proc. TAPPI* **1999**, *99*, 1353−1367.

(15) Larsson, P. T.; Lindström, T.; Carlsson, L. A.; Fellers, C. Fiber Length and Bonding Effects on Tensile Strength and Toughness of Kraft Paper. *J. Mater. Sci.* **2018**, *53*, 3006−3015.

(16) Fischer, W.; Mayr, M.; Spirk, S.; Reishofer, D.; Jagiello, L. A.; Schmiedt, R.; Colson, J.; Zankel, A.; Bauer, W. Pulp Fines—Characterization, Sheet Formation, and Comparison to Microfibrillated Cellulose. *Polymers* **2017**, *9*, 366.

(17) Boufi, S.; González, I.; Delgado-Aguilar, M.; Tarrès, Q.; Pèlach, M. À.; Mutjé, P. Nanofibrillated Cellulose as an Additive in Papermaking Process: A Review. *Carbohydr. Polym.* **2016**, *154*, 151−166.

(18) Motamedian, H. R.; Halilovic, A. E.; Kulachenko, A. Mechanisms of Strength and Stiffness Improvement of Paper after PFI Refining with a Focus on the Effect of Fines. *Cellulose* **2019**, *26*, 4099−4124.

(19) Beghello, L. Some Factors That Influence Fiber Flocculation. *Nord. Pulp Pap. Res. J.* **1998**, *13*, 274−279.

(20) TAPPI. *Thickness (Caliper) of Paper, Paperboard, and Combined Board*, 1997. T411 om-97.

(21) TAPPI. *Grammage of Paper and Paperboard (Weight per Unit Area)*, 2012. T410 om-08.

(22) TAPPI. *Water Absorptiveness of Sized (Non-Bibulous) Paper, Paperboard, and Corrugated Fiberboard (Cobb Test)*; TAPPI, 2012. T441 om-09.

(23) Das, A. M.; Ali, A. A.; Hazarika, M. P. Synthesis and Characterization of Cellulose Acetate from Rice Husk: Eco-Friendly Condition. *Carbohydr. Polym.* **2014**, *112*, 342−349.

(24) Ayeni, A. O.; Oresegun, O. M.; Oladimeji, T. E. Compositional Analysis of Lignocellulosic Materials: Evaluation of an Economically

Viable Method Suitable for Woody and Non-Woody Biomass. *Am. J. Eng. Res.* **2015**, *4*, 14−19.
(25) Boopathi, L.; Sampath, P. S.; Mylsamy, K. Investigation of Physical, Chemical and Mechanical Properties of Raw and Alkali Treated Borassus Fruit Fiber. *Composites, Part B* **2012**, *43*, 3044−3052.
(26) Kandel, K. P.; Adhikari, M.; Kharel, M.; Aryal, G. M.; Pandeya, S.; Joshi, M. K.; Dahal, B.; Gautam, B.; Neupane, B. B. Comparative Study on Material Properties of Wood-Ash Alkali and Commercial Alkali Treated Sterculia Fiber. *Cellulose* **2022**, *29*, 5913.
(27) Lundell, F.; Söderberg, L. D.; Alfredsson, P. H. Fluid Mechanics of Papermaking. *Annu. Rev. Fluid. Mech.* **2011**, *43*, 195−217.
(28) Bajpai, P. Paper and Its Properties. *Biermann's Handbook of Pulp and Paper: Paper and Board Making*; Elsevier, 2018; Vol. 2, pp 35−63.
(29) Tanpichai, S.; Sampson, W. W.; Eichhorn, S. J. Stress-Transfer in Microfibrillated Cellulose Reinforced Poly (Lactic Acid) Composites Using Raman Spectroscopy. *Composites, Part A* **2012**, *43*, 1145−1152.
(30) Tanpichai, S.; Witayakran, S.; Srimarut, Y.; Woraprayote, W.; Malila, Y. Porosity, Density and Mechanical Properties of the Paper of Steam Exploded Bamboo Microfibers Controlled by Nanofibrillated Cellulose. *J. Mater. Res. Technol.* **2019**, *8*, 3612−3622.
(31) Henriksson, M.; Berglund, L. A.; Isaksson, P.; Lindström, T.; Nishino, T. Cellulose Nanopaper Structures of High Toughness. *Biomacromolecules* **2008**, *9*, 1579−1585.
(32) Sampson, W. W. A Model for Fibre Contact in Planar Random Fibre Networks. *J. Mater. Sci.* **2004**, *39*, 2775−2781.
(33) Ehrnrooth, E. M. Change in Pulp Fibre Density with Acid-Chlorite Delignification. *J. Wood Chem. Technol.* **1984**, *4*, 91−109.
(34) Soszyński, R. M. Relative Bonded Area-A Different Approach. *Nord. Pulp Pap. Res. J.* **1995**, *10*, 150−151.
(35) Page, D. H. A. Theory for the Tensile Strength of Paper. *Tappi J.* **1969**, *52*, 674−681.
(36) Tao, J.; Liu, H. A Method to Determine Sheet Relative Bonded Area Using the Fiber Flexiblity Index. *Instrum. Sci. Technol.* **2011**, *39*, 161−172.
(37) Hashim, M. Y.; Amin, A. M.; Marwah, O. M. F.; Othman, M. H.; Yunus, M. R. M.; Chuan Huat, N. C. The Effect of Alkali Treatment under Various Conditions on Physical Properties of Kenaf Fiber. *J. Phys. Conf.*; IOP Publishing, 2017; Vol. *914*, p 012030. DOI: 10.1088/1742-6596/914/1/012030
(38) Poletto, M.; Ornaghi, H. L.; Zattera, A. J. Native Cellulose: Structure, Characterization and Thermal Properties. *Materials* **2014**, *7*, 6105−6119.
(39) Xu, F.; Yu, J.; Tesso, T.; Dowell, F.; Wang, D. Qualitative and Quantitative Analysis of Lignocellulosic Biomass Using Infrared Techniques: A Mini-Review. *Appl. Energy* **2013**, *104*, 801−809.
(40) Kondo, T.; Sawatari, C. A Fourier transform infra-red spectroscopic analysis of the character of hydrogen bonds in amorphous cellulose. *Polymer* **1996**, *37*, 393−399.
(41) Åkerholm, M.; Hinterstoisser, B.; Salmén, L. Characterization of the Crystalline Structure of Cellulose Using Static and Dynamic FT-IR Spectroscopy. *Carbohydr. Res.* **2004**, *339*, 569−578.
(42) Haque, M. M.; Hasan, M.; Islam, M. S.; Ali, M. E. Physico-Mechanical Properties of Chemically Treated Palm and Coir Fiber Reinforced Polypropylene Composites. *Bioresour. Technol.* **2009**, *100*, 4903−4906.
(43) Sinha, E.; Rout, S. K. Influence of Fibre-Surface Treatment on Structural, Thermal and Mechanical Properties of Jute. *J. Mater. Sci.* **2008**, *43*, 2590−2601.
(44) Sassi, J.-F.; Tekely, P.; Chanzy, H. Relative Susceptibility of the Iα and Iβ Phases of Cellulose towards Acetylation. *Cellulose* **2000**, *7*, 119−132.
(45) Sugiyama, J.; Persson, J.; Chanzy, H. Combined Infrared and Electron Diffraction Study of the Polymorphism of Native Celluloses. *Macromolecules* **1991**, *24*, 2461−2466.
(46) Xiao, L.-P.; Lin, Z.; Peng, W.-X.; Yuan, T.-Q.; Xu, F.; Li, N.-C.; Tao, Q.-S.; Xiang, H.; Sun, R.-C. Unraveling the Structural Characteristics of Lignin in Hydrothermal Pretreated Fibers and Manufactured Binderless Boards from Eucalyptus Grandis. *Sustainable Chem. Processes* **2014**, *2*, 9.
(47) Kljun, A.; Benians, T. A.; Goubet, F.; Meulewaeter, F.; Knox, J. P.; Blackburn, R. S. Comparative Analysis of Crystallinity Changes in Cellulose I Polymers Using ATR-FTIR, X-Ray Diffraction, and Carbohydrate-Binding Module Probes. *Biomacromolecules* **2011**, *12*, 4121−4126.
(48) Poletto, M.; Pistor, V.; Santana, R. M. C.; Zattera, A. J. Materials Produced from Plant Biomass: Part II: Evaluation of Crystallinity and Degradation Kinetics of Cellulose. *Mater. Res.* **2012**, *15*, 421−427.
(49) Oh, S. Y.; Yoo, D. I.; Shin, Y.; Seo, G. FTIR Analysis of Cellulose Treated with Sodium Hydroxide and Carbon Dioxide. *Carbohydr. Res.* **2005**, *340*, 417−428.
(50) Park, S.; Baker, J. O.; Himmel, M. E.; Parilla, P. A.; Johnson, D. K. Cellulose Crystallinity Index: Measurement Techniques and Their Impact on Interpreting Cellulase Performance. *Biotechnol. Biofuels* **2010**, *3*, 10.
(51) Saha, P.; Manna, S.; Chowdhury, S. R.; Sen, R.; Roy, D.; Adhikari, B. Enhancement of Tensile Strength of Lignocellulosic Jute Fibers by Alkali-Steam Treatment. *Bioresour. Technol.* **2010**, *101*, 3182−3187.
(52) Segal, L.; Creely, J. J.; Martin, A. E., Jr; Conrad, C. M. An Empirical Method for Estimating the Degree of Crystallinity of Native Cellulose Using the X-Ray Diffractometer. *Text. Res. J.* **1959**, *29*, 786−794.
(53) Aryal, G. M.; Aryal, B.; Kandel, K. P.; Neupane, B. B. Cellulose-Based Micro-Fibrous Materials Imaged with a Home-Built Smartphone Microscope. *Microsc. Res. Tech.* **2021**, *84*, 1794.
(54) Ilyas, R. A.; Sapuan, S. M.; Ishak, M. R.; Zainudin, E. S. Sugar Palm Nanofibrillated Cellulose (Arenga Pinnata (Wurmb.) Merr): Effect of Cycles on Their Yield, Physic-Chemical, Morphological and Thermal Behavior. *Int. J. Biol. Macromol.* **2019**, *123*, 379−388.
(55) Ilyas, R. A.; Sapuan, S. M.; Ishak, M. R. Isolation and Characterization of Nanocrystalline Cellulose from Sugar Palm Fibres (Arenga Pinnata). *Carbohydr. Polym.* **2018**, *181*, 1038−1051.
(56) Ilyas, R. A.; Sapuan, S. M.; Ishak, M. R.; Zainudin, E. S. Effect of Delignification on the Physical, Thermal, Chemical, and Structural Properties of Sugar Palm Fibre. *BioResources* **2017**, *12*, 8734−8754.
(57) Abral, H.; Ariksa, J.; Mahardika, M.; Handayani, D.; Aminah, I.; Sandrawati, N.; Pratama, A. B.; Fajri, N.; Sapuan, S. M.; Ilyas, R. A. Transparent and Antimicrobial Cellulose Film from Ginger Nanofiber. *Food Hydrocolloids* **2020**, *98*, 105266.
(58) Samy, M. M.; Mohamed, M. G.; Mansoure, T. H.; Meng, T. S.; Khan, M. A. R.; Liaw, C.-C.; Kuo, S.-W. Solid State Chemical Transformations through Ring-Opening Polymerization of Ferrocene-Based Conjugated Microporous Polymers in Host−Guest Complexes with Benzoxazine-Linked Cyclodextrin. *J. Taiwan Inst. Chem. Eng.* **2022**, *132*, 104110.
(59) Beckermann, G. W.; Pickering, K. L. Engineering and Evaluation of Hemp Fibre Reinforced Polypropylene Composites: Fibre Treatment and Matrix Modification. *Composites, Part A* **2008**, *39*, 979−988.
(60) Dufresne, A. Cellulose-Based Composites and Nanocomposites. *Monomers, Polymers and Composites from Renewable Resources*; Elsevier, 2008; pp 401−418.

https://doi.org/10.1021/acsomega.2c04398
ACS Omega 2022, 7, 32717−32726

Received: 16 September 2020 | Revised: 21 January 2021 | Accepted: 1 February 2021

DOI: 10.1002/jemt.23736

RESEARCH ARTICLE

MICROSCOPY RESEARCH & TECHNIQUE WILEY

Cellulose-based micro-fibrous materials imaged with a home-built smartphone microscope

Girja Mani Aryal[1,2] | Bishwa Aryal[1] | Krishna Prasad Kandel[1] | Bhanu Bhakta Neupane[1]

[1]Central Department of Chemistry, Tribhuvan University, Kathmandu, Nepal

[2]Research Centre for Applied Science and Technology, Tribhuvan University, Kathmandu, Nepal

Correspondence
Bhanu Bhakta Neupane, Central Department of Chemistry, Tribhuvan University, Kathmandu, Nepal.
Email: bbneupane@cdctu.edu.np

Funding information
University Grants Commission, Nepal, Grant# MRS-74/75/S&T-19

Review Editor: Paolo Bianchini

Abstract

Micro-fibrous materials are one of the highly explored materials and form a major component of composite materials. In resource-limited settings, an affordable and easy to implement method that can characterize such material would be important. In this study, we report on a smartphone microscopic system capable of imaging a sample in transmission mode. As a proof of concept, we implemented the method to image handmade paper samples–cellulosic micro-fibrous material of different thickness. With 1 mm diameter ball lens, individual cellulose fibers, fiber web, and microporous regions were resolved in the samples. Imaging performance of the microscopic system was also compared with a commercial bright field microscope. For thin samples, we found the image quality comparable to commercial system. Also, the diameter of cellulose fiber measured from both methods was found to be similar. We also used the system to image surfaces of a three ply surgical facemask. Finally, we explored the application of the system in the study of chemical induced fiber damage. This study suggested that the smartphone microscope system can be an affordable alternative in imaging thin micro-fibrous material in resource limited setting.

KEYWORDS
bright field microscope, contrast, handmade paper, micro-fibrous material, resolution

1 | INTRODUCTION

An imaging system helps to visualize small specimen or the details within the larger specimens which are not visible to naked eyes. Different versions of imaging techniques are available, such as far and near field optical, electron, and scanning probe. The choice of an imaging technique depends on the nature of sample, availability of resources, and the level of spatial details required. Optical microscopic systems are normally the method of choice for the study of soft and biological specimens at their native environments (Hell, 2007; Sawyer, Grubb, & Meyers, 2008; Stender et al., 2013; Xiong et al., 2013). Although super-resolution far field optical microscopic techniques provide significantly improved resolution (Hell, 2007; Iketaki, Watanabe, Bokor, & Fujii, 2006; Kuang, Zhao, & Wang, 2010; Li, Wu, & Chou, 2009; B. Neupane et al., 2015; Puthukodan, Murtezi, Jacak, & Klar, 2020), resolution of traditional optical microscopic systems is lower than that of electron microscopic methods. Nonetheless, different versions of conventional optical microscopic systems are being used in the characterization different fibrous materials (Choong, Yi, & Rutledge, 2015; Hayes & Gammon, 2010; Singh, Lim, & Manickavasagan, 2020). Electron and scanning probe microscopic techniques, depending on the nature of sample, can provide resolution from few nanometer to atomic scale, therefore these techniques are highly used in characterization of diverse materials including micro-fibrous materials (De Jonge & Ross, 2011; Hörber & Miles, 2003; Lee, Kim, Choi, Takeuchi, & Park, 2017; Venkateshaiah et al., 2020).

In recent years, smartphone microscopic systems are being explored as an affordable alternative to image and/or quantify specimens of few micrometer to few tenths of micrometer. Different

 © 2021 Wiley Periodicals LLC

design and imaging modalities are being explored (Ahmad Zahidi, Chung, Katariya, Liew, & Ng, 2019; Cybulski, Clements, & Prakash, 2014; Di Febo, Casas, & Antonini, 2021; Sung, Campa, & Shih, 2017; Switz, D'Ambrosio, & Fletcher, 2014; Vietz et al., 2019; Wei et al., 2017) and a number of biomedical applications of such systems are already reported, such as blood cell counting (Zeng et al., 2018), detection of parasites in different samples (Agbana et al., 2018; Bogoch et al., 2013; Koydemir et al., 2015), detection of sickle cell (Knowlton et al., 2015), and many more. Different version of digital microscopic systems are also being explored particularly in diagnostic applications (Araújo et al., 2019; Hedvat, 2010; Huisjes, van Solinge, Levin, van Wijk, & Riedl, 2018; Kratz et al., 2019). Apart from being affordable and easy to use, both smartphone and digital microscopic systems can be deployed for on-site applications and will find many interesting applications in future (Kanchi, Sabela, Mdluli, & Bisetty, 2018; Shan et al., 2019). It would be interesting to explore the material science applications of such system; for example, in the characterization of micro-porous and fibrous materials.

Composite materials are one of the highly explored materials. In such material, two or more domains having different properties are present in variable compositions to produce a material having properties unique from the constituent materials. The micro-fibrous material form an important component of many composite materials. The organization, shape and size of the fibrous phase is reported to affect the mechanical property and end application of composite materials (Amuthakkannan, Manikandan, Jappes, & Uthayakumar, 2013; Fu & Lauke, 1996; Sehaqui, Allais, Zhou, & Berglund, 2011; Takagi & Ichihara, 2004; Zimniewska & Wladyka-Przybylak, 2016). Paper- or sheet-based materials are the other important class of fibrous materials. These materials can be fabricated from woody or non woody portions of plants following mechanical or chemical processing (Bajpai, 2018). The end property of paper materials, such as tear index and tensile strength, depend on the fiber aspect ratio (length to width ratio), organization, fiber curl and kink, extent of external and internal fibrillation, and crill content in the pulp (Boufi et al., 2016; Fischer et al., 2017; Hubbe, 1999; Johansson, 2006; Larsson, Lindström, Carlsson, & Fellers, 2018; Lundberg, Norgren, & Edlund, 2018). These parameters depend largely on fiber processing protocol. For example, the fiber length in chemically processed pulp is higher than in mechanically processed pulp. The long fibers can form more contact points than short fibers and eventually lead to the paper of higher strength. However, the long fibers lead to the increased tendency to fiber entanglement and floc formation during processing (Hubbe, 1999).

Electron microscopic techniques are the current dominant methods used in morphological characterization of fibrous materials. These techniques are not easily available in resource limited settings. An affordable and easy to implement method that can provide preliminary information on the organization and size of fiber and distribution of micro-porous regions in the fibrous material would be important.

In this study, we developed and implemented smartphone microscopic method to image different micro-fibrous materials. We measured the imaging parameters of the microscope system and implemented it to the surface characterization of paper samples of different thickness. The imaging performance of the microscope was compared with a commercial bright field microscope. For both methods, image analysis was performed to get information on the size and organization of fiber in the samples. Finally, we also explored the application of the system in the study of chemical induced fiber damage.

2 | MATERIALS AND METHODS

The smartphone microscope system was designed following previously reported method (B. B. Neupane, Chaudhary, & Sharma, 2020) with some modification. The optical setup of the microscope is shown in Figure 1. The sapphire ball lens of 1, 2, and 4 mm diameter was purchased from Edmond Optics (unit price $20–25). To mount the lens, three aluminum plates (2 × 2 cm and thickness of 0.1, 0.1, and 0.05 cm) were obtained from local machine shop and a hole of ~0.8, 1.5, and ~ 3 mm diameter was made at the center so as to fit the respective ball lens. The ball lens were fixed on the hole with the help of transparent nail polish. The lens assembly was then mounted on the camera port of smartphone (3,120 × 4,160 pixels, screen size 12.2 × 6.7 cm) with the help of double sided transparent tape. For 2 and 4 mm ball lens, working distance between smartphone camera and ball lens assembly was adjusted by placing a thin piece of a paper cardboard having a hole of around 0.8 cm diameter at the center. The thickness of cardboard placed around 2 and 4 mm ball lenses was ~0.4 and 1 mm, respectively. A wooden box (15 × 15 × 15 cm) consisting a hole of ~0.5 cm on the top center (typically called as illuminating hole) was used as a sample stage. A commercially available white light emitting diode (LED) housed in the box was used for illumination. The optical system that consisted of: (a) a ball lens mounted to

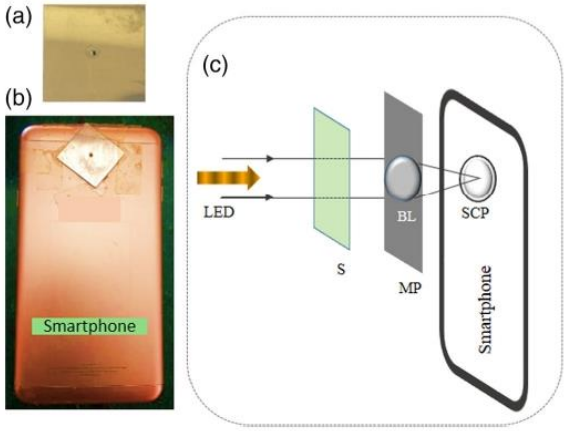

FIGURE 1 Basic components of a smartphone microscope and the optical setup. (a) A ball lens mounted to an aluminum substrate. (b) Ball lens assembly mounted to a smartphone. (c) Optical setup of the smartphone microscope. BL, ball lens; LED, light emitting diode; MP, mounting plate; S, sample; SCP, smartphone camera port [Color figure can be viewed at wileyonlinelibrary.com]

a smartphone, (b) sample stage, and (c) illumination source is collectively called the smartphone microscope (Figure 1).

To get information on the physical size of a specimen, the field of view (FOV) of an imaging system needs to be calibrated. We achieved this using a standard calibration slide having inter-grid distance of 10 μm (Generic). The slide was placed on the sample stage and image was captured with the smartphone–ball lens assembly. The number of pixels covered by the grids in the central focused region in the image were counted to get FOV in micrometer.

2.1 | Imaging of paper samples and a three ply surgical facemask

Ten different handmade paper samples were purchased from local markets. The samples are hereunder labeled as P1–P10. The thickness of samples, as measured by a micrometer screw gauge (least count 0.01 mm) was found to be ~420, 180, 30, 90, 125, 125, 100, 80, 40, and 80 μm, respectively. Handmade papers are made in local levels using raw cellulose fibers obtained from inner bark portion of Lokta (*Daphne papyracea* and *Daphne bholua*) or Argeli (*Edgeworthia gardener*) plants or their combination by Chemical pulping method. Traditionally, these papers are claimed to have high strength and durability (Banjara, 2007).

For imaging, a small piece of paper (~25 × 40 mm) was cut with scissors. The piece was then placed on the sample stage and imaged with the smartphone microscope. The autofocus option was disabled during imaging. Around 3–5 images were collected in the different regions of the paper. For comparison, the samples, unless stated, were also imaged at 40x with a commercial bright field microscope (#T490B-10MT, ×40–2000 Trinocular, Amscope). The microscope was equipped with a built in white LED, CMOS camera, and image acquisition software.

A commercially available three ply surgical facemask was obtained from local medical supplier. Small piece of mask was cut and three layers were separated. Three to five images of each layer was imaged both with smartphone and bright field imaging systems.

All the collected images were imported in the ImageJ software (NIH) and analyzed to get information such as fiber diameter, density, and organizations.

2.2 | Study on chemical induced fiber damage

The raw fiber was obtained from Lokta bushes and outer scaly bark was removed manually. Soxhlet extraction in acetone was carried to remove extractives. The fiber mass was dried in oven for 5 hours at 100 ± 5°C. Around 0.5 g of extractive free sample was treated with 6% NaOH (fiber to NaOH solution ratio 1:30) for 1 hr and washed several times with distilled water to remove the excess alkali. The treated fiber mass was oven dried for 5 hr at 100 ± 5°C. Another mercerized sample was prepared using 15% NaOH.

To assess the degree of fiber damage during treatment, iodine staining method was used (Young & Hindson, 1958). Briefly, few fiber bundles from each mercerized sample was stained with I_2 solution (0.5 g iodine, 1.5 g potassium iodide in 100 mL of distilled water) for 5 min in a glass slide. The excess iodine solution was removed. Triplicate slides were prepared for each sample type. The stained sample was then imaged with both optical microscopic systems and the color developed on the fiber was used to assess the degree of fiber damage.

3 | RESULTS AND DISCUSSION

3.1 | Measurement of optical parameters

FOV is one of the important parameters of an imaging system. Typically, it is the maximum area visible when looking though a camera (camera FOV) or eye piece (eyepiece FOV; Stender et al., 2013). The FOV of ball lens depends on diameter of ball lens, wavelength of illumination source, and refractive index of the ball lens material (Cybulski et al., 2014). It is to be noted that the ball lens has curved surface, so the rays coming from the outer regions of the lens are defocussed in the image plane. Because of this effect, only the central focused region of the image can be used for study. Also, FOV of ball lens can be affected by the smartphone camera attached to it. The effective FOV of 1, 2, and 4 mm ball lens microscope measured from the images (Figure 2a–c) was found to be ~240, 450, and 740 μm, respectively (Table 1). The ball lens has circular FOV and the reported value correspond to the diameter. In agreement with theory (Cybulski et al., 2014), the FOV increases with the increase of ball lens diameter.

An imaging system with higher FOV can visualize larger sample area per scan. However, to get good quality image (i.e., image having high spatial details), the resolution and contrast should be higher. Resolution is the measure of minimum distance of separation between two point objects at which the objects can be distinguished as separate objects (Gareau, Patel, & Rajadhyaksha, 2008; Stender et al., 2013). Contrast measures the intensity difference between specimen/region of interest and background (Peli, 1990). It is obvious in the images (Figure 2a–c) that the grid sharpness increases from 4 mm to 1 mm. Nonetheless, we measured the Michelson contrast (*MC*) or modulation, a commonly used parameter to define contrast in periodic structures, in the images. The *MC* (in %) was calculated as (Peli, 1990),

$$MC = \left(\frac{I_{max} - I_{min}}{I_{max} + I_{min}}\right) 100. \quad (1)$$

where, I_{max} and I_{min} are the maximum and minimum intensity. A line profile indicating I_{max} and I_{min} is provided in Figure 2d. Using target of 10 line pairs/mm (lp/mm), MC for 1, 2, 4 mm ball lens was found to be 28 ± 3, 26 ± 3, 26 ± 2%. For target of low frequency, in consistent

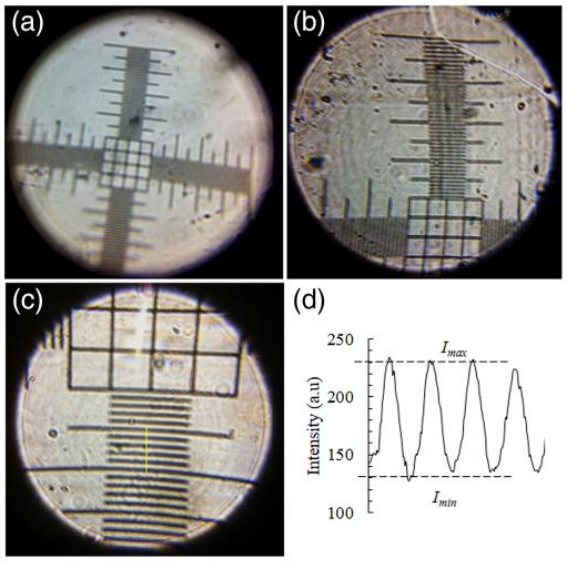

FIGURE 2 Measurement of field of view and contrast. Calibration slide imaged with a 4 mm (a), 2 mm (b), and 1 mm (c) ball lens. (d) A line profile of the calibration grid indicated by a yellow line in (c) [Color figure can be viewed at wileyonlinelibrary.com]

TABLE 1 Experimental optical parameter of ball lens microscope

Ball lens diameter (mm)	Diameter of the field of view (μm)	MC (%) at 100 lp/mm
1	240 ± 5	28 ± 1
2	450 ± 10	15 ± 3
4	740 ± 10	11 ± 1

with theory, the MC is virtually independent of ball lens diameter. If a target of 100 lp/mm was used, the *MC* for 1, 2 and 4 mm lens was found to be 28 ± 1%, 15 ± 3%, and 11 ± 1%, respectively. Since, 1 mm ball lens provided highest contrast even for high frequency target, the lens could provide better quality image than 2 and 4 mm lens.

To confirm this a thin paper sample (P10) was imaged with 4, 2, and 1 mm ball lens (Figure 3a-c). It is interesting to see the details in image increasing with decrease of ball lens diameter. In particular, individual cellulose fibers are well resolved in the image obtained with 1 mm lens microscope (Figure 3c).

3.2 | Imaging of the paper samples

Considering the best imaging performance among the ball lens, we imaged all the samples with the 1 mm lens. The representative images are provided in Figure 4a–j. For comparison, images collected with a commercial bright field microscope are also shown (Figures 4k–t). A close comparison of two sets of images reveal that, except for thick samples P1 and P2, smartphone images show fiber organization as good as commercial bright field microscope. In thick samples, enough photons do not reach the CMOS sensor of the smartphone camera. This could result in loss of image contrast and resolution. Since images were collected in transmittance mode, the bright patches of various size most likely represent pores or thin transparent regions in the sample. A close inspection of the images tells that: (a) the fibers are randomly oriented so as to form fiber web, (b) curled fiber are also visible in some samples, and (c) the distribution and size of pores is not uniform. Also, a rough estimation of fiber density, defined here as number of fibers per FOV (diameter of ~250 μm), can also be made from the images of thin samples. For example, the average fiber density for P10 obtained from smartphone and bright field microscope was found to be ~20 and 21, respectively.

All samples studied here were prepared by chemical pulping of raw fiber obtained from inner bark regions, that is, soft or non-woody parts of plants. It is known that chemical pulping yields longer fibers than mechanical pulping (Johansson, 2006; Larsson et al., 2018). This explains the observation of long fibers in all the samples (Figure 4a–j and k–t). It is generally accepted that long fiber can form more fiber joins and stronger network. The presence of long and cross linked fibers with less curl could provide high strength and durability to the paper.

With FOV calibrated, information on fiber diameter can also be obtained from the images. For example, the average diameter of fiber in P3 measured with a smartphone and commercial microscope was found to be 10 ± 2 μm and 11 ± 2 μm (n = 20), respectively. In both methods, diameter in the range of 8–14 μm was observed. It is known that the cellulose fiber diameter varies with type and size of plant and fiber processing parameters (Sfiligoj Smole, Hribernik, Stana Kleinschek, & Kreže, 2013; Trache et al., 2020; Ververis, Georghiou, Christodoulakis, Santas, & Santas, 2004). Also during processing the fiber wall can collapse resulting in ribbon like flexible fiber. Such collapsed fiber will have higher apparent diameter (Hubbe, 1999). The observed variation in fiber diameter could be due to presence of fibers of different plant origin and or ribbon like fibers formed during fiber processing.

For completeness, we also imaged a paper sheet made by mechanical pulping. The paper had thickness comparable to P10. The surface morphology of paper, as revealed both in smartphone (Figure 5a) and bright field microscopic image (Figure 5b), is very different from the chemically pulped paper of similar thickness (i.e., P10). Particularly, individual fibers are not well resolved and surface porosity is low. This difference could be due to high fiber density (compact sheet) due to presence of short fibers and secondary fines formed during fiber processing.

3.3 | Imaging of a three ply surgical facemask

We also implemented the microscope for the surface characterization of most commonly used three ply and SMS type (spun bonded–melt blown–spun bonded) surgical facemask. By design, the outermost hydrophobic layer (coded blue) is made to protect the user from watery muco-salivary droplets, the middle layer (M layer) to filter fine particles, and the innermost layer to absorb exhaled droplets and

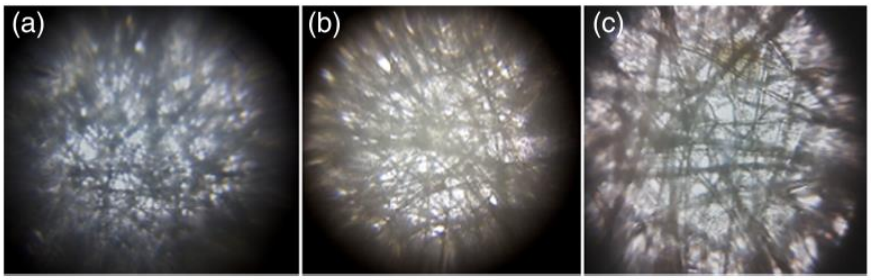

FIGURE 3 Imaging performance of different ball lens. Image of a paper sample (P10) collected with smartphone consisting of 4 mm (a), 2 mm (b), and 1 mm (c) ball lens [Color figure can be viewed at wileyonlinelibrary.com]

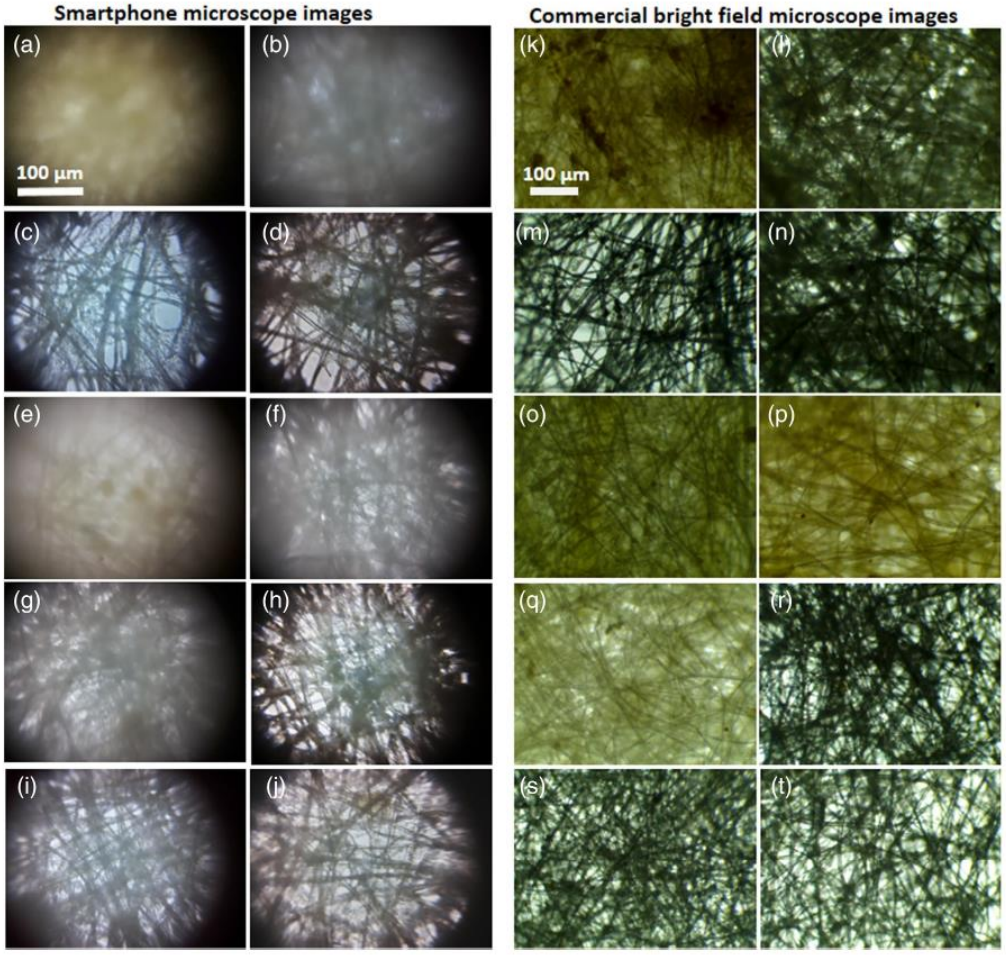

FIGURE 4 Optical image of handmade paper samples. (a–j) Image of the samples P1–P10 taken with the smartphone microscope. (k–t) Image of the respective samples taken with a commercial bright field microscope. The thickness of samples (P1–P10) was around ~420, 180, 30, 90, 125, 125, 100, 80, 40, and 80 µm, respectively. A scale bar of 100 µm shown in A and K applies to the images (b–j) and (k–t), respectively [Color figure can be viewed at wileyonlinelibrary.com]

moisture thereby decreasing dampness and increasing user comfort (Chua, 2020). It would be interesting to explore structure–function relation of the mask layers. The optical microscopic images reveal that the outer (Figure 5c,f) and inner layers (Figure 5e,h) have larger fibers, low fiber density, and are porous. These observation suggest that these layers can provide barrier protection to coarse particles only. In the middle layer, as evident in Figure 5d,g, fibers are smaller and tightly packed to result low porosity. These properties along with

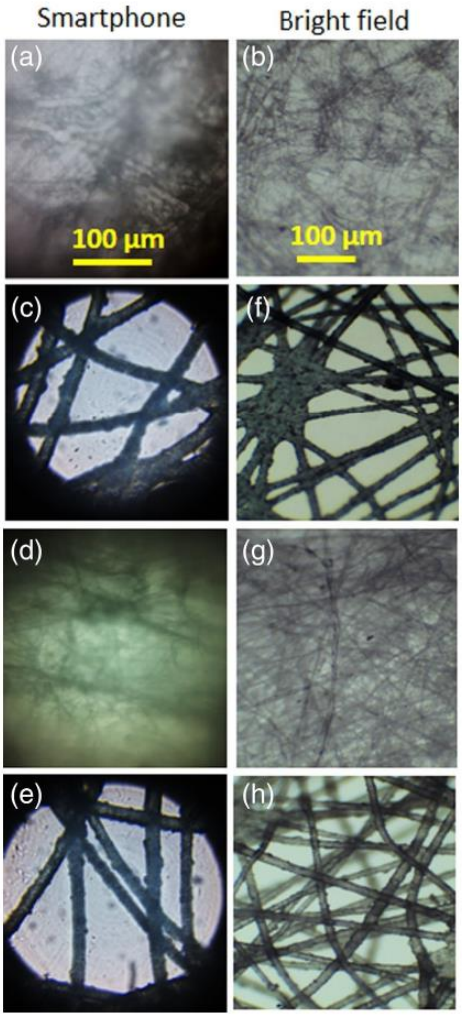

FIGURE 5 Surface images of mechanically pulped paper and a three ply surgical facemask. (a) Representative surface image of a mechanically pulped paper imaged with a smartphone and (b) bright field microscope. The images of inner S layer, middle M layer, and outer S layer of a three ply surgical facemask taken with a smartphone microscope are respectively shown in (c), (d), and (e). The corresponding images taken with bright field microscope are shown in (f), (g), and (h). The scale bar shown in (a) also applies for images (c), (d), and (e). Similarly, the scale bar shown in B also applies for images (f), (g), and (h) [Color figure can be viewed at wileyonlinelibrary.com]

presence of electrostatic charge (electret filter) can even filter fine particles.

3.4 | Study on chemical induced fiber damage

Iodine staining is one of the methods of choice to assess the degree of fiber damage at different level of fiber processing. A light yellow coloration in the optical images is indicative of intact fiber (Young & Hindson, 1958). We collected the images of 6 and 15% NaOH treated and I_2 stained Lokta fiber samples both with smartphone and bright field microscope (Figures 6a–d). The 6% NaOH treated samples showed light yellow coloration and 15% NaOH treated fiber sample appeared light to dark gray. The difference in coloration could arise due to different level of iodine adsorption on the fiber surface. It is reported that harsh alkali treatment leads to increased fibrillation and or increased surface damage which could provide more surface area for I_2 adsorption and eventually to color difference (Chandrasekar, Ishak, Sapuan, Leman, & Jawaid, 2017; Zafeiropoulos, 2008). This explains why the fiber treated with 15% NaOH appears to have different color from the 6% NaOH treated.

Above observations suggest that the smartphone microscope can be an affordable and easy to implement alternative in characterization of cellulose-based micro-fibrous material. Although, the method presented here is limited to thin samples, still there are range of materials and processes that could be imaged and characterized with the system; such as (a) surface porosity of adsorbent materials, (b) microscopic defects and porosity in membrane filters, (c) cracks and their formation in ceramic materials, (d) morphological characterization of suspended particulate matters, (e) filler distribution in composite materials and many more. Another interesting application could be the study of dust mite droppings that are known to cause allergic problems when lodged in bed coverings (Höfer, Berner-Dannenmann, Marquardt, & Hammer, 2019).

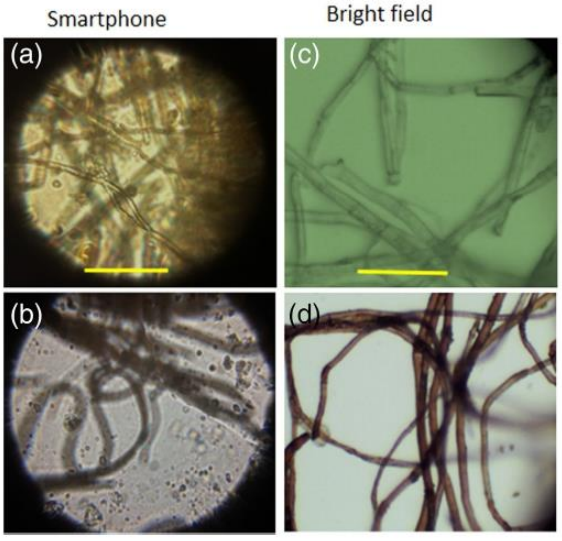

FIGURE 6 Images of chemically treated and iodine stained fiber samples. Smartphone microscopic images of the fiber sample with 6% (a) and (b) 15% NaOH treatment. The corresponding images taken with a bright field microscope is shown in (c) and (d), respectively. Bright field images were taken at 100X [Color figure can be viewed at wileyonlinelibrary.com]

It is to be noted that the FOV provided by smartphone microscope is lower than that of commercial microscope; circular FOV ~240 μm diameter for smartphone microscope versus rectangular FOV of 750 × 1,000 μm for bright field. It means, smaller sample area can be imaged per scan with the smartphone microscope. Another issue is the smaller working distance of the ball lens. This demands that during imaging the lens should be virtually touching the sample surface.

4 | CONCLUSIONS

To summarize, we developed and implemented a smartphone based microscopic system in the characterization of range of fibrous materials. We found that the image quality increases with decrease of ball lens diameter. Using a ball lens of 1 mm diameter, information on fiber organization, fiber diameter, and micro-porous regions in different paper samples can be obtained. For thin sample, the image quality is found to be as good as that of commercial bright field microscope. We also explored the application of the system in the study of chemical induced fiber damage. Our study suggested that the smartphone microscope can be an affordable and easy to implement alternative in characterization of cellulose-based micro-fibrous material. Our future work would be the development of a smartphone based software application that can collect and process the images and provide digital information to the user.

ACKNOWLEDGMENTS

BA acknowledges University Grants Commission (UGC), Nepal for proving thesis support grant to do the research. We also acknowledge center for analytical sciences at Kathmandu Institute of Applied Sciences (KIAS) for proving access to commercial bright field microscope.

CONFLICT OF INTEREST

Authors have no conflict of interest relevant to this article.

DATA AVAILABILITY STATEMENT

The data that support the findings of this study are available from the corresponding author upon reasonable request.

ORCID

Bhanu Bhakta Neupane https://orcid.org/0000-0003-0731-2552

REFERENCES

Agbana, T. E., Diehl, J.-C., van Pul, F., Khan, S. M., Patlan, V., Verhaegen, M., & Vdovin, G. (2018). Imaging & identification of malaria parasites using cellphone microscope with a ball lens. *PLoS One*, *13* (10), e0205020.

Ahmad Zahidi, A. A., Chung, D. C., Katariya, M., Liew, O. W., & Ng, T. W. (2019). Living specimens under field immobilization and smartphone microscopic observation. *Microscopy Research and Technique*, *82*(10), 1741–1747.

Amuthakkannan, P., Manikandan, V., Jappes, J. W., & Uthayakumar, M. (2013). Effect of fibre length and fibre content on mechanical properties of short basalt fibre reinforced polymer matrix composites. *Materials Physics and Mechanics*, *16*(2), 107–117.

Araújo, A. L. D., Arboleda, L. P. A., Palmier, N. R., Fonseca, J. M., de Pauli Paglioni, M., Gomes-Silva, W., … Speight, P. M. (2019). The performance of digital microscopy for primary diagnosis in human pathology: A systematic review. *Virchows Archiv*, *474*(3), 269–287.

Bajpai, P. (2018). Brief description of the pulp and papermaking process. In *Biotechnology for pulp and paper processing* (pp. 9–26). New York, USA: Springer.

Banjara, G. (2007). *Handmade paper in Nepal: Upgrading with value chain approach*. Kathmandu, Nepal: GTZ/PSP-RUFIN.

Bogoch, I. I., Andrews, J. R., Speich, B., Utzinger, J., Ame, S. M., Ali, S. M., & Keiser, J. (2013). Mobile phone microscopy for the diagnosis of soil-transmitted helminth infections: A proof-of-concept study. *The American Journal of Tropical Medicine and Hygiene*, *88*(4), 626–629.

Boufi, S., González, I., Delgado-Aguilar, M., Tarrès, Q., Pèlach, M. À., & Mutjé, P. (2016). Nanofibrillated cellulose as an additive in papermaking process: A review. *Carbohydrate Polymers*, *154*, 151–166.

Chandrasekar, M., Ishak, M. R., Sapuan, S. M., Leman, Z., & Jawaid, M. (2017). A review on the characterisation of natural fibres and their composites after alkali treatment and water absorption. *Plastics, Rubber and Composites*, *46*(3), 119–136.

Choong, L. T., Yi, P., & Rutledge, G. C. (2015). Three-dimensional imaging of electrospun fiber mats using confocal laser scanning microscopy and digital image analysis. *Journal of Materials Science*, *50*(8), 3014–3030.

Chua, M. H., Cheng, W., Goh, S. S., Kong, J., Li, B., Lim, J. Y., … Yang, L. (2020). Face masks in the new COVID-19 normal: materials, testing, and perspectives. *Research*, *2020*, 1–40.

Cybulski, J. S., Clements, J., & Prakash, M. (2014). Foldscope: Origami-based paper microscope. *PLoS One*, *9*(6), e98781.

De Jonge, N., & Ross, F. M. (2011). Electron microscopy of specimens in liquid. *Nature Nanotechnology*, *6*(11), 695–704.

Di Febo, R., Casas, L., & Antonini, A. (2021). A smartphone-based petrographic microscope. *Microscopy Research and Technique*. https://doi.org/10.1002/jemt.23697

Fischer, W. J., Mayr, M., Spirk, S., Reishofer, D., Jagiello, L. A., Schmiedt, R., … Bauer, W. (2017). Pulp fines—Characterization, sheet formation, and comparison to microfibrillated cellulose. *Polymers*, *9*(8), 366.

Fu, S.-Y., & Lauke, B. (1996). Effects of fiber length and fiber orientation distributions on the tensile strength of short-fiber-reinforced polymers. *Composites Science and Technology*, *56*(10), 1179–1190.

Gareau, D. S., Patel, Y. G., & Rajadhyaksha, M. (2008). Basic principles of reflectance confocal microscopy. In *Reflectance confocal microscopy of cutaneous tumors* (pp. 13–18). Florida, USA: CRC Press.

Hayes, B. S., & Gammon, L. M. (2010). *Optical microscopy of fiber-reinforced composites*. Ohio, USA: ASM international.

Hedvat, C. V. (2010). Digital microscopy: Past, present, and future. *Archives of Pathology and Laboratory Medicine*, *134*(11), 1666–1670.

Hell, S. W. (2007). Far-field optical nanoscopy. *Science (New York, N.Y.)*, *316*(5828), 1153–1158. https://doi.org/10.1126/science.1137395

Höfer, D., Berner-Dannenmann, N., Marquardt, C., & Hammer, T. (2019). Resistance of commercial bed covers against Faecal pellets of house dust mites: Behaviour of seams and zippers. *Journal of Textile Science and Technology*, *5*(02), 27–37.

Hörber, J. K. H., & Miles, M. J. (2003). Scanning probe evolution in biology. *Science*, *302*(5647), 1002–1005.

Hubbe, M. A. (1999). Difficult furnishes. *Proceedings of TAPPI*, *99*, 1353–1367.

Huisjes, R., van Solinge, W. W., Levin, M. D., van Wijk, R., & Riedl, J. A. (2018). Digital microscopy as a screening tool for the diagnosis of hereditary hemolytic anemia. *International Journal of Laboratory Hematology*, *40*(2), 159–168.

Iketaki, Y., Watanabe, T., Bokor, N., & Fujii, M. (2006). Construction of super-resolution microscope based on cw laser light source. *Review of Scientific Instruments*, *77*(6), 063112.

Kanchi, S., Sabela, M. I., Mdluli, P. S., & Bisetty, K. (2018). Smartphone based bioanalytical and diagnosis applications: A review. *Biosensors and Bioelectronics*, *102*, 136–149.

Knowlton, S. M., Sencan, I., Aytar, Y., Khoory, J., Heeney, M. M., Ghiran, I. C., & Tasoglu, S. (2015). Sickle cell detection using a smartphone. *Scientific Reports*, *5*, 15022.

Koydemir, H. C., Gorocs, Z., Tseng, D., Cortazar, B., Feng, S., Chan, R. Y. L., … Ozcan, A. (2015). Rapid imaging, detection and quantification of *Giardia lamblia* cysts using mobile-phone based fluorescent microscopy and machine learning. *Lab on a Chip*, *15*(5), 1284–1293.

Kratz, A., Lee, S., Zini, G., Riedl, J. A., Hur, M., Machin, S., & Haematology, I. C. for S. (2019). Digital morphology analyzers in hematology: ICSH review and recommendations. *International Journal of Laboratory Hematology*, *41*(4), 437–447.

Kuang, C., Zhao, W., & Wang, G. (2010). Far-field optical nanoscopy based on continuous wave laser stimulated emission depletion. *Review of Scientific Instruments*, *81*(5), 053709.

Larsson, P. T., Lindström, T., Carlsson, L. A., & Fellers, C. (2018). Fiber length and bonding effects on tensile strength and toughness of kraft paper. *Journal of Materials Science*, *53*(4), 3006–3015.

Lee, W. C., Kim, B. H., Choi, S., Takeuchi, S., & Park, J. (2017). Liquid cell electron microscopy of nanoparticle self-assembly driven by solvent drying. *The Journal of Physical Chemistry Letters*, *8*(3), 647–654.

Li, Q., Wu, S. S., & Chou, K. C. (2009). Subdiffraction-limit two-photon fluorescence microscopy for GFP-tagged cell imaging. *Biophysical Journal*, *97*(12), 3224–3228.

Lundberg, M., Norgren, M., & Edlund, H. (2018). Validation of crill measurements in a high-yield pulp refining process for improved fines material control. *Nordic Pulp & Paper Research Journal*, *33*(2), 200–209.

Neupane, B., Jin, T., Mellor, L., Loboa, E., Ligler, F., & Wang, G. (2015). Continuous-wave stimulated emission depletion microscope for imaging Actin cytoskeleton in fixed and live cells. *Sensors*, *15*(9), 24178–24190.

Neupane, B. B., Chaudhary, R. K., & Sharma, A. (2020). A smartphone microscopic method for rapid screening of cloth facemask fabrics during pandemics. *PeerJ*, *8*, e9647.

Peli, E. (1990). Contrast in complex images. *Journal of the Optical Society of America*, *7*(10), 2032–2040.

Puthukodan, S., Murtezi, E., Jacak, J., & Klar, T. A. (2020). Localization STED (LocSTED) microscopy with 15 nm resolution. *Nanophotonics*, *9*, 783–792.

Sawyer, L., Grubb, D. T., & Meyers, G. F. (2008). *Polymer microscopy*. Berlin, Germany: Springer Science & Business Media.

Sehaqui, H., Allais, M., Zhou, Q., & Berglund, L. A. (2011). Wood cellulose biocomposites with fibrous structures at micro-and nanoscale. *Composites Science and Technology*, *71*(3), 382–387.

Sfiligoj Smole, M., Hribernik, S., Stana Kleinschek, K., & Kreže, T. (2013). Plant fibres for textile and technical applications. *Advances in Agrophysical Research*, 369–398. IntechOpen, London, UK.

Shan, Y., Wang, B., Huang, H., Jian, D., Wu, X., Xue, L., … Liu, F. (2019). On-site quantitative Hg2+ measurements based on selective and sensitive fluorescence biosensor and miniaturized smartphone fluorescence microscope. *Biosensors and Bioelectronics*, *132*, 238–247.

Singh, S. S., Lim, L.-T., & Manickavasagan, A. (2020). Imaging and spectroscopic techniques for microstructural and compositional analysis of lignocellulosic materials: A review. *Biomass Conversion and Biorefinery*, 1–19. https://doi.org/10.1007/s13399-020-01075-4.

Stender, A. S., Marchuk, K., Liu, C., Sander, S., Meyer, M. W., Smith, E. A., … Cheng, J.-X. (2013). Single cell optical imaging and spectroscopy. *Chemical Reviews*, *113*(4), 2469–2527.

Sung, Y., Campa, F., & Shih, W.-C. (2017). Open-source do-it-yourself multi-color fluorescence smartphone microscopy. *Biomedical Optics Express*, *8*(11), 5075–5086.

Switz, N. A., D'Ambrosio, M. V., & Fletcher, D. A. (2014). Low-cost mobile phone microscopy with a reversed mobile phone camera lens. *PLoS One*, *9*(5), e95330.

Takagi, H., & Ichihara, Y. (2004). Effect of fiber length on mechanical properties of "green" composites using a starch-based resin and short bamboo fibers. *JSME International Journal Series A Solid Mechanics and Material Engineering*, *47*(4), 551–555.

Trache, D., Tarchoun, A. F., Derradji, M., Hamidon, T. S., Masruchin, N., Brosse, N., & Hussin, M. H. (2020). Nanocellulose: From fundamentals to advanced applications. *Frontiers in Chemistry*, *8*, 392.

Venkateshaiah, A., Padil, V. V., Nagalakshmaiah, M., Waclawek, S., Černík, M., & Varma, R. S. (2020). Microscopic techniques for the analysis of micro and nanostructures of biopolymers and their derivatives. *Polymers*, *12*(3), 512.

Ververis, C., Georghiou, K., Christodoulakis, N., Santas, P., & Santas, R. (2004). Fiber dimensions, lignin and cellulose content of various plant materials and their suitability for paper production. *Industrial Crops and Products*, *19*(3), 245–254.

Vietz, C., Schütte, M. L., Wei, Q., Richter, L., Lalkens, B., Ozcan, A., … Acuna, G. P. (2019). Benchmarking smartphone fluorescence-based microscopy with DNA origami Nanobeads: Reducing the gap toward single-molecule sensitivity. *ACS Omega*, *4*(1), 637–642.

Wathen, R. (2006). Studies on fiber strength and its effect on paper properties. *KCL Communications* (Vol. 11, pp. 1–98). Espoo, Finland: KCL.

Wei, Q., Acuna, G., Kim, S., Vietz, C., Tseng, D., Chae, J., … Ozcan, A. (2017). Plasmonics enhanced smartphone fluorescence microscopy. *Scientific Reports*, *7*(1), 2124.

Xiong, B., Zhou, R., Hao, J., Jia, Y., He, Y., & Yeung, E. S. (2013). Highly sensitive sulphide mapping in live cells by kinetic spectral analysis of single au-Ag core-shell nanoparticles. *Nature Communications*, *4*(1), 1–9.

Young, F. S., & Hindson, W. R. (1958). 40—The identification of damage to lignified fibres a new microscopical test using iodine and sulphuric acid. *Journal of the Textile Institute Transactions*, *49*(11), T554–T560.

Zafeiropoulos, N. E. (2008). Engineering the fibre–matrix interface in natural-fibre composites. In *Properties and performance of natural-fibre composites* (pp. 127–162). Amsterdam, The Netherlands: Elsevier.

Zeng, Y., Jin, K., Li, J., Liu, J., Li, J., Li, T., & Li, S. (2018). A low cost and portable smartphone microscopic device for cell counting. *Sensors and Actuators A: Physical*, *274*, 57–63.

Zimniewska, M., & Wladyka-Przybylak, M. (2016). Natural fibers for composite applications. In *Fibrous and textile materials for composite applications* (pp. 171–204). Berlin, Germany: Springer.

How to cite this article: Aryal GM, Aryal B, Kandel KP, Neupane BB. Cellulose-based micro-fibrous materials imaged with a home-built smartphone microscope. *Microsc Res Tech*. 2021;1–8. https://doi.org/10.1002/jemt.23736

doi:10.1017/S1431927621002932
Microsc. Microanal. 27 (Suppl 1), 2021
© Microscopy Society of America 2021

Microscopic Characterization of Eco-friendly Lokta Paper

Girja Mani Aryal[1], Washat Ware[2], Shubo Han[3], Gibin George[2], Zhiping Luo[3], Krishna Prasad Kandel[1], Bhoj Gautam[2] and Bhanu Neupane[1]

[1]Tribhuvan University, Kathmandu, Nepal, [2]Fayetteville State University, Fayetteville, North Carolina, United States, [3]Fayetteville State University, FAYETTEVILLE, North Carolina, United States

Lokta paper is a handmade paper indigenous to Nepal. The paper is made from inner fibrous bark of Lokta bushes; evergreen shrubs that grow in Himalayan forests ranging from 1600 to 4000 m. Because of its durability and resistance to bugs and moulds, the paper in its original or modified from is being used in official documents, calligraphy, holy books, packaging materials, and even to make paper bills [1]. The paper is fabricated in local levels following the traditional eco–friendly method of fiber processing. Firstly, outer scaly bark from raw fiber is manually removed and cut to small pieces and soaked in cold water for 5−6 hours. The biomass is boiled in water for around 5−10 hours and then washed with ash or alkali solution. The softened fiber biomass is beaten to make pulp and then dispersed to make slurry. The slurry is poured in a wooden mesh frame or paper moulds over a water tank. The frame is then drained and air dried to get paper sheet. Depending on the demand, the paper can be colored using natural dyes obtained from different plants and or patterned for artistic purposes. A systematic characterization of lokta paper sheet from material perspective, which helps to explain it novel properties, is missing in literature. In this work, we studied fiber organization, morphology and elemental distribution in lokta paper sheet with the help of scanning electron microscope (SEM) coupled to an electron probe micro analyzer (EPMA). For SEM imaging the paper sample was sputter coated with carbon and imaged in a JEOL field–emission JXA−8530F EPMA equipped with an SDD X-ray energy-dispersive spectrometer (EDS). Finally, we also did atomic force microscopy (AFM) imaging in tapping mode to explore surface roughness and structural details in the sample at nanoscopic level. AFM was performed at ambient condition in tapping mode. Finally, the X–ray diffraction (XRD) data were collected at Braggs' angle 2θ ranging from 5 to 40° by a X-ray diffractometer. The Cu Kα line (λ=1.540A°) was used as X–ray source. The SEM micrographs of lokta paper imaged at different magnification is shown are figure 1A-D. The micrographs show that in the paper the cellulosic fibers are randomly oriented so as to form densely packed interwoven networks (Figure 1 and B). It is known that strength of paper sheet is largely determined by strength of individual fiber and degree of cross linking within the individual fibers. The presence of long interconnecting fibers having no or low curl could provide durability and strength to the paper sheet. With further zooming individual fiber surface can be imaged (Figure 1C and D). We found fiber diameter in the range of 10−14 micrometer. In most of the fibers, individual micro–fibrils that run straight along the length of fiber are clearly visible (yellow dotted regions in Figure C and D). In some fibers gummy material is found attached on the surface (white dotted region in Figure 1C. The micro–fibrils are visible due to removal of gummy materials such as lignin and hemicellulose from the fiber surface during processing. We found micro–fibril diameter and spacing in the range of 100−350 nm and 100−500 nm, respectively. The almost parallel arrangement of micro–fibril could provide excellent strength to individual fiber and to the paper sheet. The observation of micro-fibrils is also reported in fiber processed form other plant types and biomass [2, 3]. In a cellulose fiber amorphous and crystalline phases are known to exist in different proportions but these phases are not visible in SEM images. However, we observed the contribution from two cellulose forms in the XRD data (Figure 1E). The peak at 2Θ values of ~16° and 22° originate from the crystalline planes (101) and (002), respectively. A broad background underlying the crystalline peaks originates form the amorphous regions [4].

g/10.1017/S1431927621002932 Published online by Cambridge University Press

We also did the EPMA analysis in the micro–regions labeled + in Figure 1A. We found C and O as the major elements along with other minor elements Ca, Fe, and Cl heterogeneously distributed in the paper. The elements C and O come from the cellulosic biomass, Ca could come from unwashed alkali or impurities in water, and Fe and Cl could come from water impurities. Figure 2 shows the AFM phase and topographic images of lokta paper. It is interesting to see the crystalline or quasi–crystalline regions on the surface (white boxes in figure 2A). These regions could be lignin and or other foreign materials precipitated on the fiber surface. The distinct stripes having cross section of ~200−300 nm indicate the micro–fibril on the fiber. We see the roughness at the level of ~±100 nm (figure 2B) which roughly corresponds to the height form top of a micro–fibril to the cleft adjacent to it. The measurement of force–distance curve that can provide the information on the elastic modulus in the different regions on individual fiber (fiber strength) could be subject of further study [5].

*Correspondence: bbneupane@cctu.edu.np, bgautam@uncfsu.edu

Acknowledgements: This work was supported by NSF PREM program DMR 1827731, EIR (ECCS-1900837), and DOD W911NF-09-1-0011.

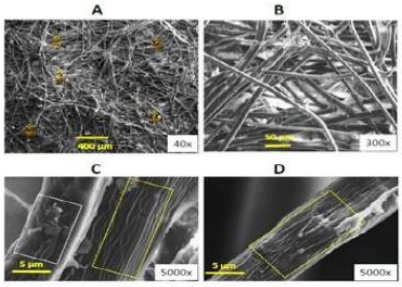

Figure 1. (A) SEM micrograph of the Lokta paper sheet measured at magnification of 40x, (B) 300x, (C) and (D) 5000x. Scale bar in A, B, C and D is 400, 50, 5, 5 µm, respectively.

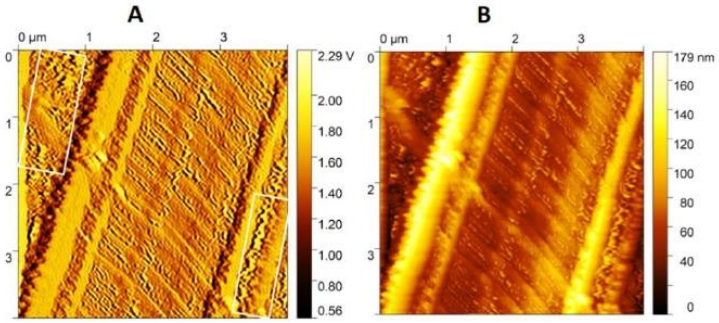

Figure 2. (A) Phase and (B) topographic AFM images of a small regions with a cellulose fiber.

References

[1] G. B. Banjara, German Technical Cooperation (GTZ), Handmade Paper in Nepal (2007).
[2] H. Sosiati et. al., International Conference on Physics 2014 (ICP 2014), p. 12
[3] H. Zhao et. al., Carbohydrate Polymers, 68 (2007), p. 235.
[4] S. Park, et. al, Biotechnology for Biofuels, 10 (2010), p. 1-10.
[5] R. R. Lahiji et. al., Lagmuir, 26(2010), p. 4480.

g/10.1017/S1431927621002932 Published online by Cambridge University Press